Modifikation bekannter immunmodulierender Substanzklassen mit Makroliden zum therapeutischen Einsatz in onkologischen und Autoimmunmodellen

Dissertation

der Mathematisch-Naturwissenschaftlichen Fakultät

der Eberhard Karls Universität Tübingen

zur Erlangung des Grades eines

Doktors der Naturwissenschaften

(Dr. rer. nat.)

vorgelegt von

Simon Straß

aus Stuttgart

Tübingen

2023

Gedruckt mit Genehmigung der Mathematisch-Naturwissenschaftlichen Fakultät der Eberhard Karls Universität Tübingen.

Tag der mündlichen Qualifikation:	26.07.2023
Dekan:	Prof. Dr. Thilo Stehle
1. Berichterstatter/-in:	Prof. Dr. Stefan Laufer
2. Berichterstatter/-in:	Prof. Dr. Michael Lämmerhofer

Die vorliegende Arbeit wurde im Zeitraum vom 01.12.2016 bis 19.05.2023 unter der Betreuung von Prof. Dr. Stefan A. Laufer in den Laboren der Synovo GmbH in Tübingen angefertigt.

Inhaltsverzeichnis

Abkürzungsverzeichnis

ADME	Absorption, Distribution, Metabolismus und Elimination
AUC	*Area under the curve*
BALB/c	*Bagg albino*
CCL	Chemokin-Ligand
c_{max}	Maximale Konzentration
CXCL	Motif Chemokin-Ligand
DMF	Dimethylfumarat
EAE	*Experimental Autoimmune Encephalomyelitis*
FA	Ameisensäure
FFAR	*Free fatty acid receptor*
GM-CSF	Granulozyten-Makrophagen-Kolonie-stimulierende Faktor
GPR109A	G-Protein-gekoppelte Rezeptor 109A
GSH	Glutathion
HCA_2	*Hydroxycarboxylic acid receptor 2*
HPLC-MS/MS	*Liquid chromatography–mass spectrometry*
hTLR	Humaner Toll-like Rezeptor
IFNα	Interferon alpha
IKK	*Inhibitory κB Kinase*
IL	Interleukin
IRAK	*Interleukin-1 receptor-associated* Kinase
IRF	*Interferon regulatory factors*
LPS	Lipopolysaccharid
mDC	Myeloide dendritische Zellen
MEF	Monoethylfumarat
MHK	Minimale Hem-Konzentration
MMF	Monomethylfumarat
MS	Multiple Sklerose
MSU	Mononatriumurat
MyD88	Myeloide Differenzierungs-Primärantwort 88
NF-κB	Nuclear factor kappa-light-chain-enhancer of activated B cells

NLRs	NOD-like Rezeptoren
NMR	*Nuclear magnetic resonance*
PAMPs	*Pathogen-associated molecular patterns*
PBMC	Periphere mononukleäre Blutzellen
pDC	Plasmazytoide dendritische Zellen
PRR	*Pattern Recognition Receptor*
PRRs	*Pattern Recognitions* Rezeptoren
qPCR	*Real-time polymerase chain reaction*
RNA	Ribonukleinsäure
RT	Raumtemperatur
SCFA	Kurzkettige Fettsäuren
sICAM-1	Lösliches Interzelluläres Zelladhäsionsmolekül 1
TFA	Trifluoressigsäure
THF	Tetrahydrofuran
TIR	Toll/IL-1 Rezeptor
TLRs	*Toll-like* Rezeptoren
TNFR	*Tumor necrosis factor receptor*
TNFα	Tumornekrosefaktor α
TRAF6	*Tumor necrosis factor receptor (TNFR)-associated factor 6*
TRAM	*TRIF-related adapter molecule*
TRIF	*TIR-domain-containing adapter-inducing interferon-β*

1. Zusammenfassung

Diese Arbeit setzt sich aus vier Teilbereichen zusammen, welche durch ihre Fragestellungen im Zusammenhang stehen und in jeweils einer Publikation endeten. Zentral ist dabei vor allem die Idee, *Small Molecules*, welche ein intrazelluläres Ziel (vornehmlich Rezeptoren) besitzen, pharmakokinetisch verfügbar zu machen und in höherer Konzentration in relevante Zellkompartimente zu akkumulieren. Dafür wurden makrolidische Grundstrukturen, in der Regel aufgebaut auf Azithromycin, verwendet und dienten als Trägermolekül. Die Eigenschaften dieser Azithromycin-Moleküle beruhten auf ihren bekannten Fähigkeiten metabolisch stabil und säureresistent zu sein und gleichzeitig in einem hohen Maße in Gewebe und Immunzellen zu akkumulieren. Dazu wurden an die Hydroxygruppen in den Positionen 11, 2‘ und 4“ des Azithromycins über eine Esterbindung kurzkettige Fettsäuren (Propionat oder Butyrat) bzw. Methylfumarat gekoppelt.

Kurzkettige Fettsäuren bzw. SCFAs sind wasserlösliche Carbonsäuren mit weniger als sechs Kohlenstoffatomen. Sie entstehen größtenteils durch bakterielle Fermentation von Ballaststoffen im Darm und sind anaerobe Stoffwechsel-Endprodukte. Neben der Nutzung als Energiequelle für Epithelzellen sind sie wichtig für die Kommunikation zwischen dem Darmmikrobiom und dem Immunsystem des Wirts. Eine ballaststoffarme Ernährung und damit eine geringere Menge an SCFAs wird in Zusammenhang mit verschiedenen Autoimmunerkrankungen gebracht. Die Regulierung des Immunsystems läuft hierbei über *free fatty acid* Rezeptoren (FFAR2 und FFAR3), welche unter anderem lysosomal in Immunzellen vorkommen. Um diese Rezeptoren spezifisch anzusprechen, wurden 11-2‘-4“-Triester von Propionat und Butyrat mit Azithromycin synthetisiert und auf ihre pharmakologischen Eigenschaften untersucht. Für die genauere Evaluierung der Verteilung und der Stabilität dieser Substanzen wurden zusätzlich alle möglichen Hydrolyseprodukte synthetisiert (je drei Diester und drei Monoester für beide Fettsäurederivate). Es wurden anschließend pharmakologische Studien in Mäusen durchgeführt, welche zeigen konnten, dass diese makrolidischen SCFA-Derivate schnell aufgenommen werden und sehr gut in Gewebe penetrieren können. Es konnte weiterhin gezeigt werden, dass diese Substanzen spezifisch in definierten Geweben unterschiedlich hydrolysiert werden. Abweichend von zunächst gemessenen *in vitro* Stabilitäten zeigte sich *in vivo*, dass bestimmte Darmabschnitte

(Jejunum und teilweise Duodenum) und Lebergewebe in der Lage sind die eigentlich stabilere 4“-Esterbindung zu spalten.

In vergleichbarer Weise sollten die Derivate der Fumarate angegangen werden. Dimethylfumarat findet Verwendung als anti-inflammatorisches Medikament bei Psoriasis und Multipler Sklerose. Der genau Wirkmechanismus ist nicht geklärt, jedoch wird vermutet, dass entweder die Michael-Addition der Doppelbindung der Fumarate an Thiole (häufig Glutathion) oder die agonistische Bindung an den G-gekoppelten Rezeptor GPR109A von zentraler Bedeutung sind. Die Kopplung von Methylfumarat an Azithromycin (in Positionen 2‘ und/oder 4“) sollte eine bessere intrazelluläre Verfügbarkeit erreichen und damit sowohl Glutathion (oder möglicherweise andere Thiol-tragende Stoffe), als auch den lysosomalen GPR109A ansprechen. Es konnte gezeigt werden, dass eine äußerst schnelle Reaktion mit Glutathion in *in vitro* und *in situ* stattfindet und dort auch eine effektive anti-inflammatorische Reaktion auslöst (etwa 25fach geringere Konzentration notwendig als im Vergleich DMF um TNFα und IL-1β signifikant zu reduzieren). Dies trifft vor allem auf Substanzen mit 4“-Fumaraten zu, welche ein stabiles und nachweisbares Produkt mit Glutathion eingehen konnten. In Psoriasis Mausmodellen zeigten sich jedoch die Verbindungen mit den leichter hydrolysierbaren 2‘-Estern als wirksamer. Sie waren in der Lage in niedrigen Konzentrationsbereichen (0,06 bis 0,12 mg/kg) Creme-induzierte Hautveränderungen abzumildern und die Genexpression von pro-inflammatorischen Zytokinen (TNFα, IL-17A, IL-17F, IL-6, IL-1β, NLRP3 und IL-23A) zu verringern. Diese Daten deuten daher darauf hin, dass *in vivo* relevante Mechanismen auf die Interaktion mit GPR109A angewiesen sind.

Die endosomalen Toll-like Rezeptoren (TLR)7 und 8 spielen eine zentrale Rolle in der Erkennung von viralen Infektionen und sind damit ein wichtiger Teil der angeborenen Immunantwort. Neben den natürlich vorkommenden einzelsträngigen RNAs sind vor allem Imidazoquinoline (z.B. Imiquimod oder Resiquimod) als Agonisten bekannt. Nachteilig an diesen synthetischen Agonisten sind ihre starken Nebenwirkungen bei systemischer Anwendung. Dies liegt vermutlich an einer schnellen Metabolisierung und Eliminierung der Substanzen und damit einhergehend niedrigen AUC (*area under the curve*) und höherer maximaler Konzentration, was zu einer scharf ansteigenden und schlecht verträglichen Zytokin Freisetzung führt. Die in dieser Arbeit vorgestellten TLR7/8-Agonisten nutzen das bekannte Bindungsmotiv aus den Imidazoquinolinen und binden dies über nicht-hydrolysierbare Amidbindungen an Azithromycin. Durch die dadurch veränderten

pharmakokinetischen Eigenschaften wurden bessere AUC und eine geringere maximale Konzentration erreicht. Die Leitsubstanzen induzieren die Sekretion von IFNα aus menschlichen Leukozyten im gleichen Bereich wie Resiquimod, induzieren aber mindestens 10-mal weniger TNFα in diesem System. Dies ließ sich im Mausmodell reproduzieren, in welchem TLR8 keine bekannte Aktivität gegenüber *Small Molecules* zeigt. Die neuen Substanzen zeigten, unabhängig ob gekoppelt an ein Makrolid oder als ungebundenes sekundäres Amin, eine längere Exposition als Resiquimod und damit auch eine veränderte Kinetik in der Freisetzung proinflammatorischer Zytokine. Diese Ergebnisse könnten Probleme bei der Verträglichkeit lindern und geben Einblicke in die TLR7/8-Aktivierung dieser Substanzklasse.

Ein weiterer Teil dieser Arbeit war die Untersuchung und Weiterentwicklung von Creme-induzierten Psoriasis Mausmodellen. Es handelt sich dabei um eine bei Mäusen, meist durch die Applikation von Aldara® ausgelöste, lokale Hautveränderung, welche sich durch Rötung, Schuppen und Verdickung optisch äußert und eine Ausschüttung von pro-inflammatorischen Zytokinen bewirkt. Aldara® wird eigentlich zur Behandlung von Basalzell-Hautkrebs, aktinischer Keratose und Feigwarzen und kutanen Warzen verwendet und enthält Imiquimod als Wirkstoff, welcher im Mausmodell auch als Induktionsstoff publiziert ist. Es zeigte sich jedoch, dass die Induktion auch stark abhängig ist von dem zugesetzten Hilfsstoff Isostearinsäure. Im Mausmodell konnte gezeigt werden, dass Cremeformulierungen, welche Isostearinsäure beinhalteten innerhalb von 2 Tage zu einer lokalen Hautentzündung geführt haben, während Imiquimod-haltige Cremes bis zu 5 Tage für eine Hautreaktion benötigten. Es konnte weiter gezeigt werden, dass Isostearinsäure vermutlich über eine Inflammasom-Aktivierung die Ausschüttung von proinflammatorischen Zytokinen begünstigt hat. Insgesamt zeigten die Daten, dass Psoriasis-ähnliche Hautreaktionen bei Mäusen stärker von Isostearinsäure angetrieben werden, als allgemein berichtet wird, was bei der Verwendung dieses Mausmodells zwingend mitbeachtet werden muss.

2. Abstract

This work is composed of four sub-areas, which are broadly interrelated and each of which resulted in a publication. The central idea was to make small molecules, which have an intracellular target (primarily receptors), pharmacologically available and to accumulate them in high concentrations in the relevant cell compartments. For this purpose, basic macrolidic structures, usually built on azithromycin, were used and acted as the carrier molecule. The properties of these azithromycin derivatives were based on their known ability to be metabolically stable, acid-resistant, and to accumulate to a high degree in tissue and immune cells. Therefore, short-chain fatty acids (propionate or butyrate) or methyl fumarate were coupled to the hydroxy groups in positions 11, 2' and 4" of azithromycin via an ester bond.

Short-chain fatty acids or SCFAs are water-soluble carboxylic acids with less than six carbon atoms. They are largely formed by bacterial fermentation of dietary fiber in the intestine and are anaerobic metabolic end products. In addition to being used as an energy source for epithelial cells, they are important for communication between the gut microbiome and the host immune system. A diet low in fiber and thus lower in SCFAs has been linked to various autoimmune diseases. The free fatty acid receptors (FFAR2 and FFAR3) are part of the immune system and can be found lysosomally in immune cells. In order to specifically target these receptors, 11-2'-4" triester of propionate and butyrate were coupled to azithromycin and investigated for their pharmacological properties. In order to evaluate the distribution and stability of these compounds in detail, all possible hydrolysis products were additionally synthesized (three diesters and three monoesters, each for both fatty acid derivatives). Subsequently, pharmacological studies were carried out in mice, which showed that these macrolide SCFA derivatives are rapidly absorbed and can penetrate tissues very well. It was further shown that these substances are specifically hydrolyzed differently in defined tissues. Deviating from the initially measured *in vitro* stabilities, it was shown *in vivo* that certain intestinal sections (jejunum and partially duodenum) and liver tissue are able to cleave the more stable 4"-ester bond.

In a similar way, the derivatives of fumarates were addressed. Dimethyl fumarate has use as an anti-inflammatory drug against psoriasis and multiple sclerosis. The exact mechanism of action is not fully understood, but either a Michael addition of the double bond of the fumarates to thiols (often glutathione) or agonistic binding to the G-coupled receptor GPR109A is thought to be central to this. The coupling of methyl fumarate to azithromycin (in

positions 2' and/or 4") should achieve better intracellular availability, thus targeting both glutathione and the lysosomal GPR109A. What was demonstrated is an extremely fast response to glutathione in *in vitro* and *in situ* experiments and also an effective anti-inflammatory response (about 25-fold lower concentration needed than in comparison to DMF for significant reduction of TNFα and IL-1β) by the compounds with 4"-fumarates, which were able to form a stable and detectable product with glutathione. However, in psoriasis mouse models, low doses (0.06 bis 0.12 mg/kg) of the compounds with the more readily hydrolyzable 2'-esters were shown to be more effective. They were able to attenuate cream-induced skin lesions and reduce gene expression of pro-inflammatory cytokines (TNFα, IL-17A, IL-17F, IL-6, IL-1β, NLRP3, and IL-23A). These data suggest that relevant *in vivo* mechanisms rely on interactions with GPR109A.

The endosomal Toll-like receptors TLR7 and 8 play a central role in the recognition of viral infections and are an important part of the innate immune response. In addition to naturally occurring single-stranded RNAs, imidazoquinolines (e.g., Imiquimod or Resiquimod) are the most well-known agonists. Disadvantages of these synthetic agonists are their strong side effects when used systemically. This is likely due to rapid metabolization and elimination of the compounds, with consequently low AUC (area under the curve) and higher peak concentrations, resulting in a sharply increasing and poorly tolerated release of cytokines. The TLR7/8 agonists presented in this work utilize the known binding motif from the imidazoquinolines and link this to azithromycin via a non-hydrolyzable amide bond. The resulting changes in pharmacokinetic properties resulted in a better AUC and lower peak concentration. The lead compounds induced IFNα secretion from human leukocytes in the same range as Resiquimod, but induced at least 10-fold less TNFα in this system. This could be reproduced in a mouse model, in which TLR8 shows no known activity toward small molecules. The new compounds, whether coupled to a macrolide or as an unbound secondary amine, showed longer exposure than Resiquimod and thus altered kinetics in the release of proinflammatory cytokines. These results may alleviate tolerability issues and provide insight into TLR7/8 activation of this class of compounds.

Additionally, in the course of this work, the cream-induced psoriasis mouse model was investigated. For this model local skin change in mice is triggered by the application of Aldara®, which visually manifests itself as rubor, scaling and thickening and causes a release of pro-inflammatory cytokines. Aldara® was originally used for the treatment of basal cell skin cancer,

actinic keratosis and cutaneous warts and contains imiquimod as the active ingredient, which is also published as an inducer in this murine psoriasis model. However, it was shown that the induction is also strongly dependent on the excipient isostearic acid. In our mouse model, we showed that cream formulations containing isostearic acid induced local skin inflammation within 2 days, while creams containing imiquimod required up to 5 days for a skin reaction. Isostearic acid was further shown to promote the release of proinflammatory cytokines via inflammasome activation. Overall, the data show that psoriasis-like skin reactions in mice are driven more strongly by isostearic acid than is commonly reported, an important point to consider when using this mouse model.

3. Liste der Publikationen der Dissertation

Eine aktuelle Übersicht der Publikation des Autors kann unter folgender ORCID ID eingesehen werden:

0000-0003-3803-6976

In der vorliegenden Dissertation werden die Ergebnisse aus den folgenden Publikationen dargestellt:

Straß, S., Schwamborn, A., Keppler, M., Cloos, N., Guezguez, J., Guse, J. H., Burnet, M., & Laufer, S. (2021). Synthesis, Characterization, and in vivo Distribution of Intracellular Delivered Macrolide Short-Chain Fatty Acid Derivatives. *ChemMedChem*, *16*(14), 2254–2269. https://doi.org/10.1002/cmdc.202100139

Straß, S. Geiger, J., Cloos, N., Späth, N., Geiger, S., Schwamborn, A., De Oliveira, L., Martorelli, M., Guse, J.-H., Sandri, T. L., Burnet, M., & Laufer, S. (2023). Immune cell targeted Fumaric Esters support a role of GPR109A as a primary target of Monomethyl Fumarate *in vivo*. https://doi.org/10.1007/s10787-023-01186-0

Straß, S., Geiger, J., Martorelli, M., Geiger, S., Cloos, N., Keppler, M., Fischer, T., Riexinger, L., Schwamborn, A., Guezguez, J., Späth, N., Cruces, S., Guse, J.-H., Sandri, T. L., Burnet, M., & Laufer, S. (2023). Isostearic acid is an active component of imiquimod formulations used to induce psoriaform disease models. *Inflammopharmacology*. https://doi.org/10.1007/s10787-023-01175-3

Keppler, M., **Straß, S.** (geteilte Erstautorenschaft), Sophia Geiger, Tina Fischer, Nadja Späth, Thilo Weinstein, Anna Schwamborn, Jamil Guezguez, Jan Hinrich Guse, Stefan Laufer, Michael Burnet (2023). Imidazoquinolines with improved pharmacokinetic properties induce a high IFNα to TNFα ratio *in vitro* and *in vivo.* Eingereicht am 17.02.2023 in *Frontiers in Immunology*. Sonderausgabe zum Thema "*The Role of Toll-like Receptors and their Related Signaling Pathways in Viral Infection and Inflammation*"

Weitere Publikationen, deren Ergebnisse nicht oder nicht direkt in die vorliegende Dissertation eingeflossen sind:

Laux, J., Martorelli, M., **Straß, S.**, Schollmeyer, D., Burnet, M., & Laufer, S. (2023, eingereicht in *ACS Pharmacology & Transl. Sc.).* Inherent fluorescence demonstrates immunotropic properties for novel Janus kinase 3 inhibitors.

Keppler, M., **Straß, S**., Bäuerlein, C., Guse, J.-H., Eggers, M., Reisser, M., Burnet, M. (2022). *Novel Imidazoquinolines with Immunostimulatory Effects.* Patent application number 63/476,786

Saris, A., Qin, W., van Linge, C. C. A., Reijnders, T. D. Y., Florquin, S., Burnet, M., **Straß, S.**, de Vos, A. F., & van der Poll, T. (2022). The Azithromycin Pro-Drug CSY5669 Boosts Bacterial Killing While Attenuating Lung Inflammation Associated with Pneumonia Caused by Methicillin-Resistant Staphylococcus aureus. *Antimicrobial Agents and Chemotherapy*, 66(9), e0229821. https://doi.org/10.1128/aac.02298-21

Pietrzik, N., Burnet, M. W., Bäuerlein, C., Eggers, M., Guse, J.-H., Hahn, U., & **Straß, S.** (2018). *Novel Anti-infective and Anti-inflammatory Compounds*. Patent WO2018/161039 A1

Konferenzbeiträge:

Straß, S., Cloos, N., Heinzel, C., Keppler, M., Guse, J., Burnet, M., & Laufer, S. (2020). *Effect of Lysosomal SCFA Delivery on Immune Response*. Crohn's & Colitis Congress, Austin, USA.

Laux, J., **Straß, S.**, Martorelli, M., Späth, N., Fischer, T., Schwamborn, A., Guse, J., Burnet, M., Laufer, S. (2022). *Modification of Azithromycin: Synthesis of SCFA Donors, covalently linked Macrolide Conjugates and non-antibiotic Immunomodulators*. Frontiers in Medicinal Chemistry, Freiburg, Deutschland.

Straß, S., Fischer, T., Schwamborn, A., Späth, N., Dengler, M., Guezguez, J., Guse, J., Burnet, M., Laufer, S. (2022). *Design of Novel Intracellular Macrolide SCFA Donors*. World Congress on Inflammation, Rom, Italien.

Keppler, M., Geiger, S., **Straß, S.**, Pokoj, C., Burnet, M. (2023). *Novel Imidazoquinolines with improved pharmacokinetic properties.* Cancer Immunotherapy Meeting CIMT, Mainz, Deutschland.

4. Einleitung

Eine zentrale Herausforderung bei der Entwicklung neuer Medikamente stellt die Pharmakokinetik dar. Die Einnahme durch PatientInnen soll möglichst komfortabel sein, jedoch muss gleichzeitig der applizierte Stoff das Target gut erreichen und die notwendige Stabilität aufweisen, um so eine Wirksamkeit zu haben. Das halbsynthetische Makrolid Azithromycin verbindet diese Eigenschaften.

4.1. Azithromycin

Makrolide sind eine Klasse von Verbindungen, welche natürlich oder semisynthetisch vorkommen und aus einem Lactonring mit 14 bis 16 Atomen bestehen und mindestens einen Zucker beinhalten [1]. Azithromycin (9-deoxy-9a-aza-9a-methyl-9a-homoerythromycin A, Abbildung 1) entstand aus der Erweiterung des Lactonrings von Erythromycin, dem ursprünglich in der Natur vorkommenden Makrolid, an der Position 9 durch die Einführung einer Methylaminogruppe und war damit der erste Vertreter der Klasse der Azalide [2]. Durch die zweite Aminogruppe wird im Vergleich zu Erythromycin eine bessere Stabilität bei sauren pH-Werten und eine vorteilhaftere Pharmakokinetik erreicht, welche Azithromycin einen breiten Einsatz als Antibiotikum verschaffte [1,3].

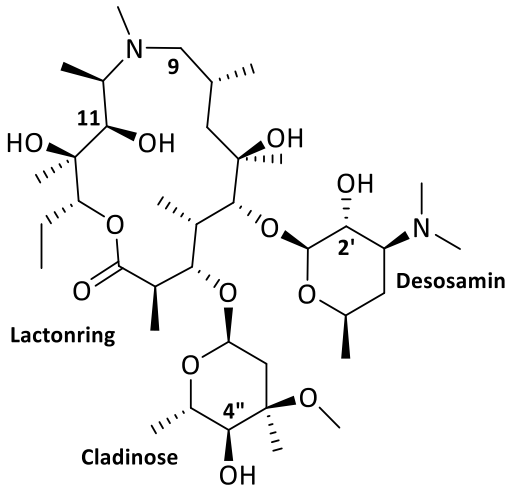

Abbildung 1. Struktur von Azithromycin mit den beiden Zuckern Desosamin und Cladinose am zentralen Lactonring. Nummeriert sind die Positionen, welche für die Synthesen von Interesse waren. Erstellt mit ChemDraw 20.1.

4.1.1 Pharmakokinetik und lysosomale Aufnahme

Azithromycin wird nach oraler Gabe sehr schnell resorbiert und in Gewebe verteilt. Vorzugsweise sind dies Lunge, Leber, Milz und Haut. Azithromycin erreicht so ein Gewebe zu Serum Verhältnis vom 10- bis 100-fachen, wohingegen Erythromycin einen Faktor von etwa 0,5 bis 5 erreicht [4]. Über dieses Gewebe ist eine langsame Rückführung in den Blutkreislauf

vorhanden, wodurch eine lange Wirksamkeit erreicht wird. Noch 12 bis 48 Stunden nach Gabe einer Einzeldosis (500 mg) wurden noch Konzentrationen (1 bis 9 mg/kg) in Gewebe erreicht, die oberhalb der MHK_{90} (Minimale Hemm-Konzentration für 90% der Bakterienstämme) lagen [5]. Die Eliminierung erfolgt primär biliär mit den Faeces, zu einem kleinen Teil auch über den Urin [5].

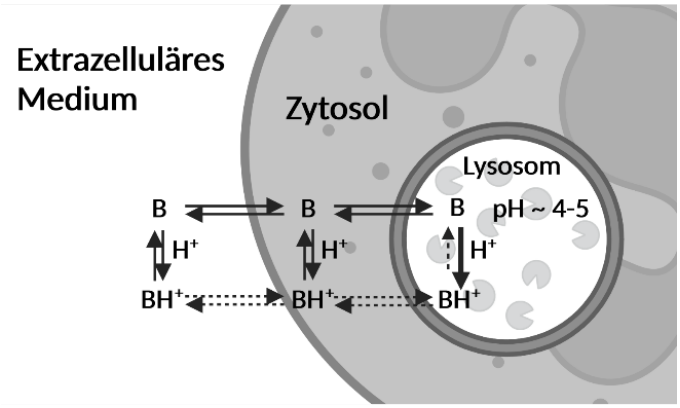

Abbildung 2. Subzelluläre Verteilung von schwachen Basen (in diesem Fall von makrolidbasierten Wirkstoffen) zwischen extrazellulärem Medium, Zytosol und saurem Lysosom. Erstellt mit Biorender. Angepasst aus [6] und JULA.

In vitro Studien zeigten eine subzelluläre Verteilung von Azithromycin in Lysosomen, intrazelluläre Vesikel zum Verdau von Materialien bei saurem pH-Wert [7]. Die Aufnahme in Zellen erfolgt über einen kurzen Zeitraum und erreicht einen Faktor von über 200 im Vergleich zum extrazellulären Medium [3,8]. Dies geschieht in der Regel durch einen passiven Influx in die sauren Kompartimente, eine anschließende Protonierung der Substanzen und dadurch einen sehr geringen Anteil an Efflux und eine langsame Rückverteilung (Abbildung 2). Dieser Effekt ist typisch für schwache Basen, wie zum Beispiel Makrolide.

Lysosomale Kompartimente zeichnen sich aus durch ihre Fähigkeit zellfremdes und zelleigenes Material zu verdauen. Dies geschieht durch die dort im sauren pH-Bereich aktiven Enzyme (Proteasen, Lipasen und Nukleasen), welche eingeschlossene Pathogene wie Bakterien und Viren verdauen. Beim Verdau freigesetzte Moleküle und Strukturmotive, welche als pathogen-assoziierte molekulare Muster (PAMPs) bezeichnet werden, können durch Rezeptoren innerhalb der Zelle erkannt werden. Sogenannte *Pattern Recognition* Rezeptoren (PRRs) sind ein zentraler Teil der angeborenen Immunantwort und kommen sowohl an Zelloberfläche, als auch intrazellulär vor. Zu den intrazellulären Rezeptoren gehören *NOD-like* Rezeptoren (NLRs), einige *Toll-like* Rezeptoren (TLR7, 8 und 9), aber auch bei der Phagozytose eingeschlossene membranständige Rezeptoren, wie kurzkettigen Carbonsäure Rezeptoren *free fatty acid receptor 2* (FFAR2), FFAR3 und GPR109A [9,10]. Anhand dieser Rezeptoren erkennen Immunzellen potentielle Pathogene oder deren Strukturmotive.

Ein Beispiel dafür ist GPR109A ein G-Protein-gekoppelte Membranrezeptor, welcher Niacin, Buttersäure und Monomethylfumarat (MMF) als endogene Agonisten binden kann und von Keratinozyten und Immunzellen, insbesondere von Neutrophilen und Makrophagen, exprimiert wird [11]. Eine Aktivierung von GPR109A steht im Zusammenhang mit dem anti-inflammatorischen und protektivem Schutz von DMF in MS und bei Psoriasis [11,12]. Des Weiteren führt die Aktivierung zur Ausschüttung von gefäßerweiternden Prostaglandinen, was eine Erklärung für das häufig auftretende *Flushing* (Erröten) ist [12].

FFAR2 und FFAR3 gehören ebenfalls zur Klasse der G-Protein-gekoppelten Rezeptoren (auch bekannt unter den Namen GPR43 für FFAR2 bzw. GPR41 für FFAR3), wobei beide stark in Immunzellen exprimiert werden. Zusätzlich kommt FFAR2 in Fettgewebe, Ileum und Colon vor. FFAR3 ist ebenfalls in Fettgewebe, aber auch in Milz und anderem immunrelevantem Gewebe exprimiert [13–15]. Dabei spielen sie eine Rolle unter anderem in der Hemmung von Entzündungsprozessen und der Krebsbildung, der Stärkung verschiedener Elemente der Dickdarmbarriere und bei der Verringerung von oxidativem Stress [16]. Eine Aktivierung von FFAR2 und 3 führt unter anderem zu einer Verringerung der Chemokine bzw. Zytokine Chemokin-Ligand (CCL)1, CCL2, GM-CSF (Granulozyten-Makrophagen-Kolonie-stimulierender Faktor), IL-1α, IL-1β und sICAM-1 (lösliches Interzelluläres Zelladhäsionsmolekül 1) [17].

Als ein zentraler Teil der angeborenen Immunität sind Toll-like Rezeptoren in der Lage unterschiedliche Pathogene anhand spezifischer Muster (daher auch Teil der Klasse der Mustererkennungsrezeptoren; *Pattern Recognition Receptors* (PRR)) zu erkennen. Sie konnten in allen Wirbeltieren, aber auch in einfachen Organismen (ursprüngliche Entdeckung in *Drosophila melanogaster* als Toll-Rezeptoren [18]), nachgewiesen werden. Dabei sind zum Beispiel in Menschen zehn und in Mäusen 12 Subtypen bekannt [19]. Diese können grob in zwei Gruppen eingeteilt werden: die an der Zelloberfläche vorkommenden, beispielsweise beim Menschen TLR1/2/4/5/6/10 und die intrazellulären, in diesem Fall TLR3/7/8/9. Die endosomal-vorkommenden TLR7 und 8 spielen dabei eine zentrale Rolle in der Erkennung von viralen und bakteriellen Infektionen [20,21]. Hierbei sind einzelsträngige Ribonukleinsäuren (RNA) die natürlichen Liganden, während synthetisch vor allem Imiquimod (TLR7) und Resiquimod (TLR7/8) als Vertreter der Imidazoquinoline bekannt sind [20,22,23]. TLR7 ist stark in plasmazytoiden dendritischen Zellen (pDC) exprimiert, wohingegen TLR8 eher in Monozyten, Makrophagen und myeloiden dendritischen Zellen (mDC) vorkommt [24,25].

Bei der Reaktion auf Pathogene durch das angeborene Immunsystem, in diesem Fall mittels TLRs, spielen vor allem die beiden Transkriptionsfaktoren *Nuclear factor kappa-light-chain-enhancer of activated B cells* (NF-κB) und IRF-Familie (*interferon regulatory factors*) (siehe Abbildung 3) [26,27]. Eine NF-κB Aktivierung kann dabei entweder durch den klassischen kanonischen oder den nicht-kanonischen, alternativen Signalweg stattfinden, wobei der kanonische Signalweg über die PRRs (*Pattern Recognition Receptors*) abläuft und der nicht-kanonische mehr dem adaptiven Immunsystem zugeschrieben wird. Für die Regulierung der kanonischen NF-κB Kaskade ist der *Inhibitory κB Kinase* (IKK)-Komplex notwendig, welcher hier vornehmlich über IKKβ und IKKγ abläuft [26,28]. Die humane IRF-Familie besteht aus neun Mitgliedern, welche zentral an der Expression von Interferonen beteiligt ist [29]. Dabei sind IRF3/5/7 die wichtigsten Vertreter für die Regulierung der Typ I Interferone, wobei IRF5, ähnlich zu NF-κB, auch die pro-inflammatorische Zytokin Expression beeinflusst [26]. Die am C-Terminus der TLRs ständige Toll/IL-1 Rezeptor (TIR) Domäne bindet Adapter- und Brückenproteine, wie myeloide Differenzierungs-Primärantwort 88 (MyD88), *TIR-domain-containing adapter-inducing interferon-β* (TRIF) oder *TRIF-related adapter molecule* (TRAM) und ist verantwortlich für das *Downstream Signalling* [26,30]. Dabei sind, abgesehen von TLR3, alle TLRs abhängig von MyD88, welches wiederum für die Translokation von NF-κB und IRF in den Zellkern verantwortlich ist. MyD88 bildet mit der *Interleukin-1 receptor-associated* Kinase (IRAK; 1/2/4) ein Myddosom, in welchem IRAK1/2 phosphoryliert werden. Dadurch wird eine Konformationsänderung ausgelöst, welche dazu führt, dass TRAF6 (*tumor necrosis factor receptor (TNFR)-associated factor 6*) an das Mydosome bindet [26]. IRAK1 führt zur Aktivierung von IRF7. IRAK2 und TRAF6 können NF-κB aktivieren, wobei TRAF6 hier zunächst den IKK-Komplex aktiviert. TRAF6 ist des Weiteren in der Lage mit IRF5 und IRF7 zu interagieren und deren Aktivierung auszulösen, was eine Genexpression von Typ I IFN (IRF5 und IRF7) bzw. pro-inflammatorischen Zytokinen (IRF5) zur Folge hat [26].

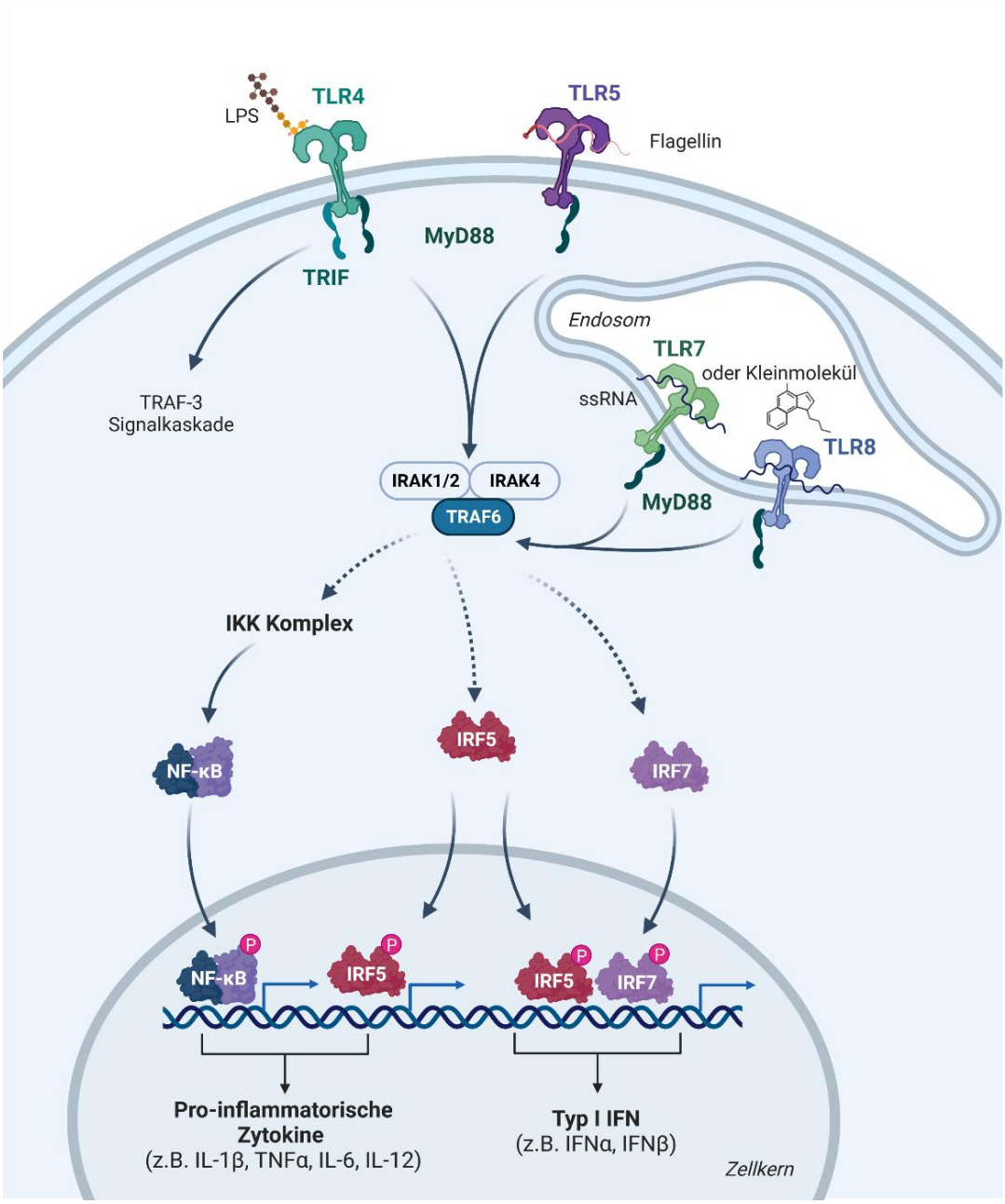

Abbildung 3. Signalwege und Lokalisierung verschiedener TLRs, wobei TLR1/2/4/5/6/10 in der Zellmembran vorkommen und TLR3/7/8/9 intrazellulär liegen. TLR7/8 werden dabei von ssRNA bzw. *Small Molecules* (Klasse der Imidazoquinoline) angesprochen. MyD88 bildet dabei das Adapterprotein am Rezeptor (für alle TLRs, außer TLR3). IRAK1/2/4 und TRAF6 bilden ein Mydosome, welches im phosphorylierten Zustand (IRAK1/2) NF-κB aktiviert. Aktivierung der Transkriptionsfaktoren NF-κB und der IRF-Familie führt zur Expression von pro-inflammatorischen Zytokinen bzw. Typ I Interferonen. Erstellt mit Biorender aus Vorlage von N. Odoard und nach A. Kusiak [26,31].

4.1.2 Antiinflammatorische Eigenschaften von Makroliden

Obwohl Azithromycin primär als Antibiotikum eingesetzt wird und über Wirksamkeit gegen *Streptococcus pneumoniae, Mycoplasma pneumoniae, Haemophilus influenzae, Moraxella catarrhalis, Chlamydia pneumoniae* und *Legionella pneumophila* verfügt [3], hat es darüber hinaus jedoch über weitere Eigenschaften. So ist publiziert, dass die Applikation von Azithromycin zu einer antiinflammatorischen Reaktion führt. Im Lipopolysaccharid (LPS) induzierten Model für Sepsis in Mäusen führte die Applikation von Azithromycin zu einer Verringerung von proinflammatorischen Zytokinen wie Interleukin (IL)-6, IL-1ß und Tumornekrosefaktor α (TNFα) [32]. Diese Effekte lassen sich jedoch nicht auf eine direkte Immunsuppression reduzieren, es kommt dagegen vielmehr zu einer immunmodulatorischen Reaktion. Dabei ist Azithromycin unter anderem in der Lage, das Gleichgewicht von pro-inflammatorischen M1 Makrophagen hin zu M2 Makrophagen zu verschieben [1,33,34].

Es konnte weiterhin gezeigt werden, dass Azithromycin die Phagozytose-Eigenschaften von apoptotischen Zellen durch Alveolar Makrophagen wiederherstellen kann [35,36]. Die Gabe von Azithromycin zeigte sich als hilfreich in Bronchiolitis obliterans, zystischer Fibrose und diffuser Panbronchiolitis [1]. Eine Gabe über einen längeren Zeitraum führt jedoch zur möglichen Ausbildung von Resistenzen in Bakterien und ist daher unvorteilhaft. Als möglicher Lösungsansatz würden sich hier nicht-antibiotische Derivate von Azithromycin anbieten, welche jedoch weiterhin immunmodulatorische Eigenschaften besitzen [36–38].

4.1.3 Verwendung von Makroliden als *Prodrug*

Mit den Eigenschaften der guten Pharmakokinetik, schnellen Aufnahme und hoher Stabilität eignet sich Azithromycin als Trägermolekül für Wirkstoffe. Dabei gilt zu beachten, dass die ursprünglichen Eigenschaften von Azithromycin erhalten bleiben. Dies bezieht sich vor allem auf die pharmakologischen Eigenschaften. Chemisch gut zugänglich und als Synthese beschrieben ist vor allem die Modifikation der Hydroxygruppe in der 2‘-Position [39]. Ähnlich dazu können auch Reaktionen an den Positionen 4“ und 11 vorgenommen werden [40]. Dort ist zum Beispiel eine Bindung über einen Ester möglich, welcher idealerweise über Hydrolyse im Zielsystem wieder verfügbar gemacht werden kann. Zusätzlich zu Estersynthesen in diesen Positionen, werden in dieser Arbeit auch Modifikationen am Amin des Desosamines vorgenommen, welche keiner Hydrolyse unterliegen, jedoch die pharmakologischen Eigenschaften nicht außerordentlich verändern.

4.2. Kurzkettige Carbonsäuren

Kurzkettige Fettsäuren sind Carbonsäuren mit bis zu sechs Kohlenstoffatomen (Abbildung 4 links und mittig). Es sind stechend bis unangenehm riechende, bei Raumtemperatur flüssige, Substanzen mit einem hohen Siedepunkt. Durch die Carboxygruppe(n) ist diese Stoffgruppe sehr gut wasserlöslich. Ein verlängerte Alkylkette verstärkt den lyophilen Charakter, womit die Wasserlöslichkeit abnimmt.

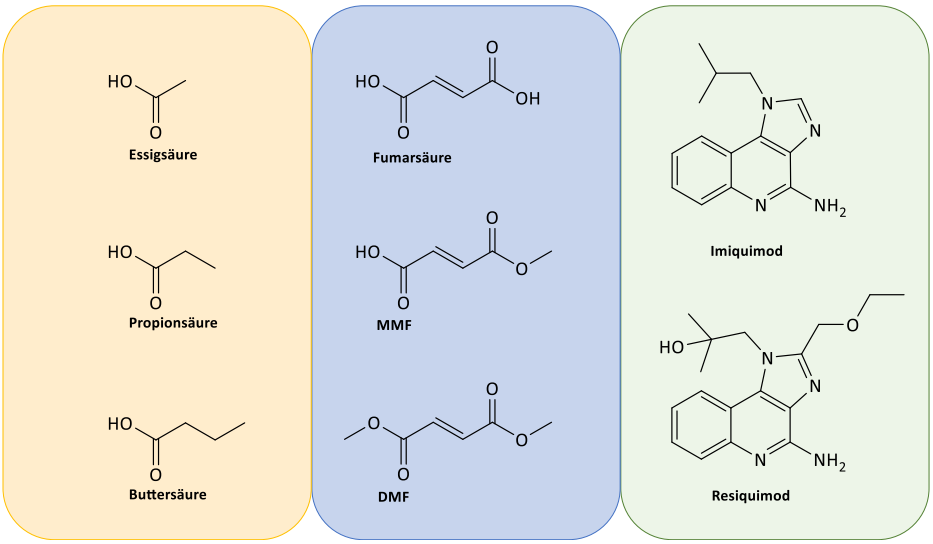

Abbildung 4. Klassische kleinmolekulare Agonisten für aufgeführte intrazellulären Rezeptoren. Gelb: Kurzkettige Fettsäuren (FFAR2/3, GPR109A). Blau: Fumarsäure und (Di-)Methylester (GPR109A). Grün: TLR7 bzw. TLR7/8 Agonisten aus der Klasse der Imidazoquinoline.

4.2.1 SCFA

Kurzkettige Fettsäuren (SCFA; meist bezogen auf Acetat, Propionat und Butyrat; Abbildung 4 links) sind Monocarbonsäuren mit weniger als sechs Kohlenstoffatomen. In Lebewesen entstehen sie größtenteils durch bakterielle Fermentation von Ballaststoffen im Darm und sind anaerobe Stoffwechsel-Endprodukte. Im humanen Dickdarm können SCFA hohe Konzentrationen erreichen (Acetat 64 mM, Propionat 27 mM, Butyrat 25 mM), wobei die Menge abhängig ist von verschiedenen Faktoren, wie zum Beispiel Ernährung und Mikrobiom. Diese SCFAs dienen dort hauptsächlich als Energiequelle für die Darmepithelzellen, spielen aber auch eine Rolle bei der Kommunikation zwischen dem Mikrobiom und dem Immunsystem des Darmepithels. Diese Kommunikation findet dabei unter anderem über die Fettsäurerezeptoren FFAR2 und FFAR3 oder über GPR109A statt [41,42]. Dabei ist FFAR2 sensitiv für Acetat und Propionat, wohingegen FFAR3 eine höhere Affinität für Propionat, Butyrat und Valerat besitzt [13,43]. Beide Rezeptoren werden von Immunzellen exprimiert und kommen in einer Vielzahl von Gewebe vor [13,44]. Neben Nikotinsäure und Fumaraten wird GPR109a auch

durch Butyrat aktiviert und wird vor allem auf Zellen des Fettgewebes, aber auch auf Neutrophilen und Makrophagen exprimiert [45].

Lokal im Darm können diese kurzkettigen Fettsäuren zu einer verbesserten Epithelbarriere beitragen und einen regulatorischen Einfluss auf das Immunsystem nehmen [41,46]. Dies wird relevant in Bezug auf verschiedene Autoimmunerkrankungen wie Asthma, Allergien oder chronisch-entzündliche Darmerkrankungen (*inflammatory bowel* disease (IBD); häufigste Vertreter hierbei sind Morbus Crohn und Colitis ulcerosa). Hier kann ein Mangel an SCFAs zu einer Verschlimmerung dieser Krankheiten führen [16,47]. Man geht davon aus, dass die Umstellung der Ernährung in westlichen/entwickelten Ländern und die damit einhergehende Verringerung der Aufnahme von Ballaststoffen (durchschnittlich circa 16 g pro Tag, statt der empfohlenen 25 bis 38 g pro Tag) mit dem Anstieg von Autoimmunerkrankungen korreliert [47,48]. Dabei spielt die Menge an SCFAs, neben ω-3-Fettsäuren, eine zentrale Rolle [48]. Eine geringe Zufuhr von Ballaststoffen kann zu einer Dysbiose des Darmmikrobioms (z.B. Abnahme von Butyrate-produzierenden Bakterien *Roseburia hominis* und *Eaecalibacterium prausnitizi*), einer schlechten intestinalen Barrierefunktion und einer damit einhergehenden fehlregulierten Immunantwort führen [49–51]. Eine intakte Immunantwort ist ein wichtiger Faktor bei entzündlichen Darmerkrankungen.

Der Ursprung einer IBD ist nicht vollständig geklärt, jedoch geht man davon aus, dass eine genetische Prädisposition (z.B. Durchlässigkeit der Epithelbarriere) zugrunde liegt, welche in Kombination mit gewissen Umweltfaktoren, einer Dysbiose im Darmmikrobiom und einer übersteuerten Immunantwort zu einer chronischen Darmentzündung führen kann [52,53]. Auslösend ist hierbei vermutlich TNFα, welches wiederum zu einer Hochregulierung von anderen Entzündungsmediatoren (IL-1, IL-6) führt (Medikation durch anti-TNFα Antikörper wie z.B. Adalimumab, Etanercept und Infliximab) [54]. Im gesunden Zustand verhindert die Epithelbarriere ein Übertreten von Bakterien und anderen Mikroorganismen und sorgt für die Passage von Wasser, Elektrolyten und Nährstoffen [55]. Durch eine Rückbildung der Mukusschicht und einer geringeren Dichte der Diffusionsbarriere in den Zellzwischenräumen (*tight junctions*) entsteht eine höhere Permeabilität und damit einhergehend der mögliche Übertritt von Bakterien in die *Lamina Propia* (siehe Abbildung 5).

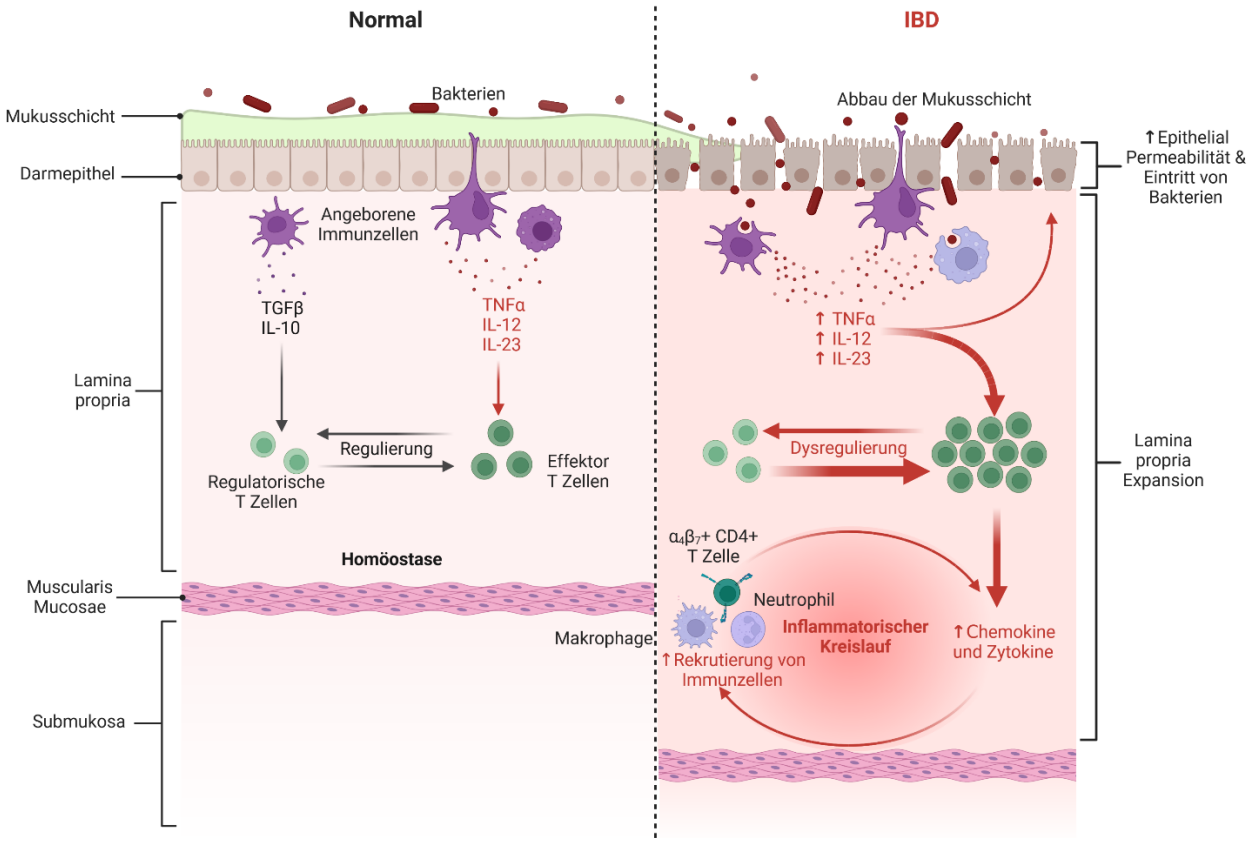

Abbildung 5. Immunregulierung und Epithelbarriere in gesunder Darmumgebung (links) und in IBD (rechts). Die schützende Mukusschicht und eine geringe Enge der *Tight Junctions* zwischen den Zellen führt zu einer erhöhten Permeabilität der Epithelzellschicht und einem Übertritt von Bakterien. Dies in Kombination mit einer genetischen Prädisposition können zu einer Dysregulierung des Immunsystems führen und so einen inflammatorischen Kreislauf von erhöhten Chemokinen und Zytokinen und einer Rekrutierung von Immunzellen führen. Übernommen und angepasst aus Biorender.

Zur Behandlung stehen neben der Anwendung von Antikörpern auch *Small Molecules* zur Verfügung. Eine häufige Anwendung findet hierbei zum Beispiel Sulfasalazin, eine entzündungshemmende Verbindung bestehend aus dem Sulfonamid Sulfapyridin und 5-Aminosalicylsäure. Es konnte auch gezeigt werden, dass die Supplementierung von hohen Dosen an Butyrat oder Propionat eine Linderung der Symptome zur Folge hat. Durch Geruch und Formulierungsproblemen ist die Anwendung jedoch limitiert [16,56,57]. In dieser Arbeit wurde jedoch versucht mit Hilfe von Makrolid Derivaten kurzkettige Fettsäuren in relevantem Gewebe bzw. in die dazugehörigen Immunzellen verfügbar zu machen. Dazu wurden die Fettsäuren an Hydroxygruppen in den Positionen 11, 2‘ und 4“ des Azithromycins über eine Esterbindung gebunden. Als zentrale Moleküle wurden hierbei die Triester von Propionat bzw. Butyrat ausgewählt, da diese die größten Mengen an SCFAs in relevanten Zellkompartimenten bereitstellen konnten und die dortigen Fettsäurerezeptoren eine Sensitivität aufweisen. Zur genauen Analyse der Stabilität, Verteilung und Metabolisierung dieser Substanzen wurden zusätzlich alle Di- und Monoester dieser Substanzen synthetisiert und charakterisiert. Darüber hinaus wurden jedoch weitere Substanzen (siehe Tabelle 1) hergestellt, charakterisiert und

teilweise auf ihre Eigenschaften in zellbasierten Assays und in Mausmodellen getestet. So wurden mögliche Kandidaten gesucht, welche Eigenschaften aufwiesen, welche möglicherweise einen Nutzen in der Behandlung von IBD haben. So zeigten sich zum Beispiel die Ester von Propionat und Butyrat als vielversprechend und sollen weitergehend untersucht werden [58].

Tabelle 1. Im Laufe dieser Arbeit synthetisierte kurzkettige Fettsäure-Ester auf Basis von Azithromycin. * Ketolid Derivat von Azithromycin, ohne Cladinose. Auch publiziert unter CSY0073 [38]. ** Nicht-antibiotisches Azithromycin-Derivat mit Morpholingruppe in 3‘ Position, anstatt Dimethylamin.

Seitenkette	Basis	Pos. 11	2'	4''
Butyryl	Azithromycin		x	
Butyryl	Azithromycin	x	x	
Butyryl	Azithromycin	x	x	x
Butyryl	Azithromycin	x		
Butyryl	Azithromycin	x		x
Butyryl	Azithromycin			x
Butyryl	Azithromycin		x	x
Butyryl	Ketolid-Azithromycin*		x	
Propionyl	Azithromycin		x	
Propionyl	Azithromycin	x	x	
Propionyl	Azithromycin	x	x	x
Propionyl	Azithromycin	x		
Propionyl	Azithromycin	x		x
Propionyl	Azithromycin			x
Propionyl	Azithromycin		x	x
Acetyl	Azithromycin		x	
Iso-Butyryl	Azithromycin		x	
2-Acetoxypropionyl	Azithromycin		x	
Pivaloyl	Azithromycin		x	
Niacin	Azithromycin		x	
Cyclobutylcarbonsäure	Azithromycin		x	
Cyclopropylcarbonsäure	Azithromycin		x	
Methoxyacetyl	Azithromycin		x	
3-Hydroxybutyryl	Azithromycin		x	
Pyrazincarbonsäure	Azithromycin		x	
Monomethylsuccinyl	Azithromycin		x	
Hippursäure	Azithromycin		x	
Phenylthiocarbamat	Azithromycin		x	
Monomethylfumaryl	Azithromycin		x	
Monomethylfumaryl	Azithromycin		x	x
Monomethylfumaryl	Azithromycin			x
Monomethylfumaryl	Ketolid-Azithromycin*		x	
Monomethylfumaryl	Morpholin-Azithromycin**		x	
Monomethylfumaryl	Morpholin-Azithromycin**		x	x
Monomethylfumaryl	Morpholin-Azithromycin**	x	x	

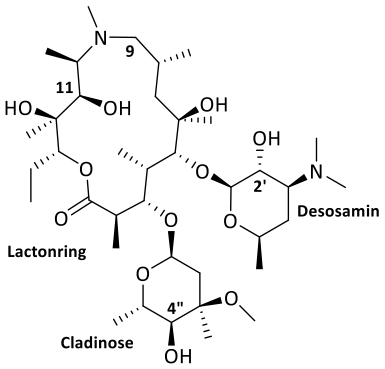

Abbildung 6. Struktur von Azithromycin mit den beiden Zuckern Desosamin und Cladinose am zentralen Lactonring. Nummeriert sind die Positionen, welche für die Synthesen von Interesse waren. Erstellt mit ChemDraw 20.1.

4.2.2 Fumarate

Fumarate (Abbildung 4 Mitte) sind Ester der ungesättigten Dicarbonsäure Fumarsäure. Fumarate werden schon seit Mitte der 1990er zur Behandlung von Psoriasis eingesetzt. Unter dem Namen Fumaderm® wird eine Mischung aus Dimethylfumarat (DMF), Monoethyl Fumarat (MEF) als Ca^{2+}, Mg^{2+} und Zn^{2+} Salz eingesetzt [59]. In neuerer Zeit finden Fumarate auch Anwendung zur Behandlung von Multipler Sklerose (MS). Dies trifft auf die Ester DMF (vermarktet als Tecfidera®), Diroximelfumarat (vermarktet als Vumerity®) und MMF (vermarktet als Bafiertam®) zu [60–62]. Diese Medikamente wirken alle mechanistisch an der gleichen Stelle. So sind diese Substanzen alle darauf ausgelegt nach Applikation MMF systemisch verfügbar zu machen (DMF und Diroximel Fumarat nach Hydrolyse und MMF direkt), welches der aktive Metabolit ist [62].

Genaue Aufklärung über den Mechanismus von MMF gibt es noch nicht, jedoch ist bekannt, dass MMF ein Agonist für GPR109A (auch *Hydroxycarboxylic acid receptor 2* (HCA_2)) ist, DMF hingegen nicht [63]. Studien konnten zeigen, dass die Aktivierung von GPR109A durch MMF eines der zentralen Mechanismen in der Behandlung von MS ist und die Wirksamkeit im Mausmodel EAE (*Experimental Autoimmune Encephalomyelitis*) nachweisen [11,64]. Eine Bindung führt zur Reduktion von proinflammatorischen Zytokinen und einer verringerten Anzahl an Neutrophil Adhäsion, Migration und Rekrutierung [65–67].

Alternativ zum ersten Mechanismus steht die kovalente Bindung der Thiol-Gruppe von Glutathion (GSH) an die Doppelbindung von Fumarsäureestern (Michael Reaktion; jedoch zum großen Teil limitiert auf DMF oder andere Diester der Fumarsäure) und eine damit einhergehende antientzündliche, immunsuppressive und zytoprotektive Eigenschaft [68–71]. Diese Reaktion ist jedoch nicht limitiert auf GSH allein und kann auch mit anderen Cysteinen oder Thiol-tragenden Stoffen passieren. Durch die schnelle Hydrolyse von DMF nach oraler Applikation ist der vermutlich aktive Metabolit MMF der zentrale Wirkstoff [66].

Neben dem Einsatz als Medikament gegen MS finden Fumarate Anwendung gegen mittlere bis schwere Psoriasis. In Patienten und Patientinnen mit Psoriasis konnte gezeigt werden, dass die orale Gabe von Fumarsäureestern zu einer Verschiebung von proinflammatorischen T-Helferzellen (Th) 1 und Th17, hin zu anti-entzündlichen Th2 Zelltypen begünstigt. Dies ging einher mit der Reduktion von IL-17A, IL-1ß, IL-22, IL-36α und IL-36γ [72,73]. Psoriasis ist eine chronische Hautentzündung und Autoimmunerkrankung, welche sich durch sichtbare und schmerzhafte Entzündung und Hyperproliferation der Haut manifestiert und bei etwa 1-2%

der Menschen auftritt [74]. Klinische Anzeichen sind eine lokale Verdickung der Epidermis durch Hyperproliferation von Keratinozyten, ein reduziertes bzw. fehlendes *Stratum granulosum* (Hypogranulosis), lokale Rötung der Haut aufgrund einer Erweiterung der Blutgefäße, Akkumulierung von Neutrophilen im *Stratum corneum* (Munro-Abszesse) und die Infiltration von CD4+, CD8+ und antigenpräsentierenden dendritischen Zellen in Dermis und Epidermis. Eine Heilung ist bisher noch nicht möglich, jedoch beinhalten Behandlungen unter anderem topische, systemische und Photo-Therapie. Das zentrale Ziel einer Therapie besteht dabei darin, die psoriatische Entzündung zu verringern, ohne das Immunsystem generell zu unterdrücken. In dieser Hinsicht hat die Einführung der auf IL-17 und IL-23 gerichteten Therapie zu einer erheblichen Verbesserung der Lebensqualität geführt.

Die Suche nach verbesserten Therapien für Psoriasis erfordert Modelle, welche die Krankheitsmechanismen in ihrer Form nachbilden können und in der Lage sind ähnliche Symptome hervorzurufen. Van der Fits *et al.* schlugen 2009 erstmals ein Mausmodell für Psoriasis vor, welches auf der wiederholten topischen Applikation von Imiquimod (pro-inflammatorische Reaktion durch Aktivierung von TLR7) in Form von Aldara® basiert [75]. Dies führt zu einer pro-inflammatorischen Reaktion und einer lokalen Hautveränderung, welche der akuten Phase der Psoriasis beim Menschen ähnelt. Auf Grund der geringen Kosten, einfachen Anwendung und schnellen Etablierung wird dieses Modell in der Praxis häufig angewandt [76]. Es muss jedoch betrachtet werden, dass die Induktion limitierende Faktoren hat. So wirkt unter anderem IMQ auch systemisch und verursacht Splenomegalie, Lymphadenopathie und möglicherweise erhöhte systemische Zytokine und ist wahrscheinlich auch ein Adenosinrezeptor-Inhibitor [75–78]. Walter *et al.* (2013) zeigten, dass Isostearinsäure (25% von Aldara®) *in vitro* und *in vivo* ebenfalls proinflammatorische Effekte hervorrufen konnte und daher ein wichtiger Faktor in der Entwicklung der Krankheitsmechanismen und Symptomen ist [79]. In einer, im Zuge dieser Arbeit angefertigten, Publikation wurde weiter auf die funktionelle Rolle von Isostearinsäure im beschriebenen murinen Psoriasis Modell eingegangen.

Die im Zuge dieser Arbeit publizierten neuen Derivate basieren auf Estern von MMF mit Azithromycin in dessen 2‘ und/oder 4“ Position (siehe Tabelle 1, unten). Zusätzlich wurde als Negativkontrolle zu den Fumaraten ein 2‘-Monomethylsuccinylester von Azithromycin synthetisiert. Im Laufe der Anfertigung der Publikation zeigte, dass die Fumarat-Substanzen nützliche anti-entzündliche Effekte hatten, jedoch mögliche antibiotische Effekte von

hydrolysiertem Azithromycin zu bakteriellen Resistenzen führen könnten, wurde weitergehend eine Klasse an nicht-antibiotischen Fumarat-Makrolid-Derivaten entwickelt (siehe ebenfalls Tabelle 1, unten). Diese basieren entweder auf CSY0073, einem Ketolid von Azithromycin, welches ohne Cladinose keine antibiotischen Eigenschaften besitzt [38,80] oder auf Azithromycin-Derivaten, welche eine Variation in der 3‘-Stelle aufweisen. Hierbei wurde über eine Epoxid-Zwischenstufe [81] das Dimethylamin durch ein Morpholin ersetzt. Diese strukturelle Veränderung verhindert die Bindung an bakterielle Ribosomen und damit eine direkte antibiotische Wirkung (Daten nicht gezeigt). Die weitergehenden Eigenschaften sind jedoch mit Azithromycin vergleichbar. Daten aus pharmakokinetischen Studien (nicht publiziert) zeigten ähnliche Verteilungen, Stabilität und Aufnahme dieser Substanzen.

Die Azithromycin-Fumarate wurden auch in anderen Krankheitsmodellen, abgesehen von den in den Publikationen aufgeführten Mausmodellen (Creme-induzierte Psoriasis und Mononatriumurat (MSU) Gicht Modell), getestet. So zeigte sich in IBD eine deutliche Verschlechterung der Symptome, des Körpergewichts und der Länge des Colons am finalen Studientag im Vergleich zur Vehikel-Gruppe und zur Kontroll-Gruppe (Ciclosporin 25 mg/kg). Dies konnte sowohl für DMF (30 mg/kg), als auch 2‘-Monomethylfumarat-Azithromycin (0,1 mg/kg) festgestellt werden, auch wenn das für DMF bisher anders publiziert wurde [82,83]. Dies könnte ein Hinweis auf die starken immunregulierenden Eigenschaften dieser Substanzklasse sein, welche dazu führte, dass das Immunsystem zwar unterdrückt, aber dadurch ein bakterielles Infektionsgeschehen toleriert wurde. Des Weiteren konnte im EAE-Modell zwar eine Wirksamkeit von DMF (100 mg/kg) gezeigt werden, jedoch waren die verwendeten makrolidischen Fumarat-Derivate (2‘-Monomethylfumarat-Azithromycin 0,05 und 0,1 mg/kg und 2‘-4“-Monomethylfumarat-Azithromycin 0,025 und 0,05 mg/kg) wirkungslos und zeigten keine Verbesserung der Symptome im Vergleich zur Vehikel-Gruppe, was vermutlich am Makrolid-Gerüst liegt, welches ein Durchdringen der Blut-Hirn-Schranke verhindert [84].

4.3. Imidazoquinoline

Imiquimod und Resiquimod sind TLR7 bzw. TLR7/8 Agonisten (Abbildung 4, rechts), welche beide der Klasse der Imidazoquinoline angehören. Diese sind trizyklische niedermolekulare Verbindungen mit meist anti-viralen bzw. immunstimulierenden Eigenschaften und eine damit einhergehende Induktion von proinflammatorischen Zytokinen (Interferon alpha (IFNα), TNFα, IL-12 und andere) [85]. Ihre Bindungsstelle befindet sich dabei konserviert im selben Motiv, wobei der Aminoquinolyl Teil über Stacking planar Wasserstoffbrückenbindungen in der Rezeptortasche eingeht. Die Butylseitenkette des Resiquimods bildet dabei hydrophobe Wechselwirkungen in einer Seitentasche aus, wobei die Kettenlänge von vier Atomen am günstigsten für die Bindung ist (siehe Abbildung 7) [83,86–88]. Eine Modifikation mit Heteroatomen (Sauerstoff im Fall von Resiquimod) kann zu einer leicht verbesserten Affinität führen [87,88]. Diese Seitenkette ist bei Imiquimod nicht vorhanden.

Während Resiquimod zwar potenter wirkt, ist Imiquimod als einziges als Medikament zugelassen. Klinische Anwendung findet Imiquimod in der Behandlung von Basalzellenkarzinomen oder Genitalwarzen. Jedoch beides nur in topischer Anwendung, da systemisch angewendet starke Nebenwirkungen zu erwarten sind. Dies ist im Besonderen für Resiquimod zu beachten. Zwar zeigten sich gute Effekte in der dermalen Applikation zur Behandlung von Genitalherpes in einer Phase II Studie, diese konnten sich jedoch in Phase III nicht bestätigen. Weiterhin zeigte sich in der oralen Anwendung bei chronischer Hepatitis C zwar eine Reduktion der Virustiter, aber gleichzeitig führten schon geringe Dosen zu starken Nebenwirkungen, welche häufig als grippeähnliche Symptome beschrieben wurden [89–91]. Diese Effekte treten vermutlich auf Grund von einer sehr steilen Dosis-Wirkungs-Kurve, einer kurzen Halbwertszeit und schlechten Eigenschaften in der Gewebeverteilung und einer damit einhergehenden höheren Dosis auf. Ziel war es daher das therapeutische Fenster dieser Substanzen zu vergrößern und die pharmakokinetischen Eigenschaften zu verbessern und gleichzeitig die immunstimulierenden Eigenschaften beizubehalten. Der Ansatz in dieser Arbeit beruhte dabei auf die Kopplung von bekannten Imidazoquinolin Motiven (siehe Abbildung 8) über Linkermoleküle an ein makrolidisches Grundgerüst und der miteinhergehenden besseren Pharmakokinetik und damit Aufnahme in Gewebe und Immunzellen.

Es zeigte sich im Laufe der Untersuchung der neuen Strukturen jedoch, dass schon die Imidazoquinol-Linker-Moleküle (ohne Makrolid) eine erheblich höhere Stabilität und bessere Pharmakokinetik aufwiesen, wie das die Vergleichssubstanzen Imiquimod und Resiquimod zeigten. Daher wurden die Charakterisierung und die Untersuchung sowohl von Makrolid-gekoppelten TLR-Agonisten, als auch der freien Agonisten weiter untersucht. Dabei zeigten sich darüber hinaus jedoch auch eine Verschiebung der Zytokin Antwort auf die Stimulation mit den beschriebenen TLR-Agonisten im Vergleich zu Resiquimod und Imiquimod, wobei sich die Affinität der Substanzen bezüglich ihrer Rezeptoren eher in Richtung TLR7, statt TLR8, verschiebt. Wobei die Rezeptor Affinität jedoch vermutlich eine untergeordnete Rolle spielt und im Vordergrund hierbei eher die Pharmakokinetik bzw. die spezifische Verteilung in lysosomale Zellkompartimente ist.

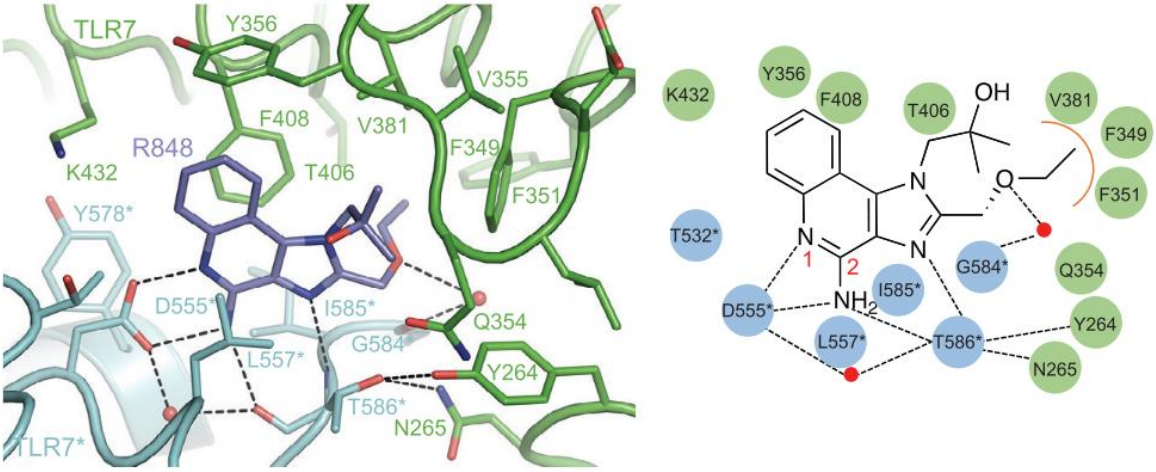

Abbildung 7. Links, vergrößerte Ansicht *Mm*TLR7-Resiquimod Bindung. Rechts, schematische Darstellung der Wechselwirkungen zwischen Resiquimod und TLR7. Der orangefarbene Bogen zeigt hydrophobe Interaktionen zwischen der Ethoxymethylgruppe von Resiquimod und TLR7. Die roten Kreise stellen Wassermoleküle dar. Wasserstoffbrücken sind durch die Strichlinien gekennzeichnet. Übernommen von Zhang *et al*. [88].

Die Synthesevorschriften für die TLR-Agonisten, welche in dieser Arbeit synthetisiert und später publiziert wurden, basieren vor allem auf Publikationen von Shukla *et al.*, weichen jedoch an einigen Stellen ab [92]. So war die Substitutionsreaktion des Chlors durch ein Amin in Schritt 6 (Abbildung 8, von S1.6 zu S1.7) nicht exakt nachzubearbeiten, da keine Mikrowellen-Apparatur zur Verfügung stand. Alternativ wurden andere Synthesewege, mit anderen Reaktionsbedingungen, Lösemitteln oder Ausgangsstoffen versucht (siehe Tabelle 2), wobei die meisten dieser Ansätze zu keiner Reaktion, falschen Produkten oder Nebenprodukten geführten haben. Schlussendlich wurde über den Zwischenschritt des Einführens von Hydrazin in den aromatischen Ring und die anschließende Reduktion mit Zink eine funktionierende

Synthese mit guter Ausbeute gefunden, welche von Kayamar *et al.* auch beschrieben wurde [93].

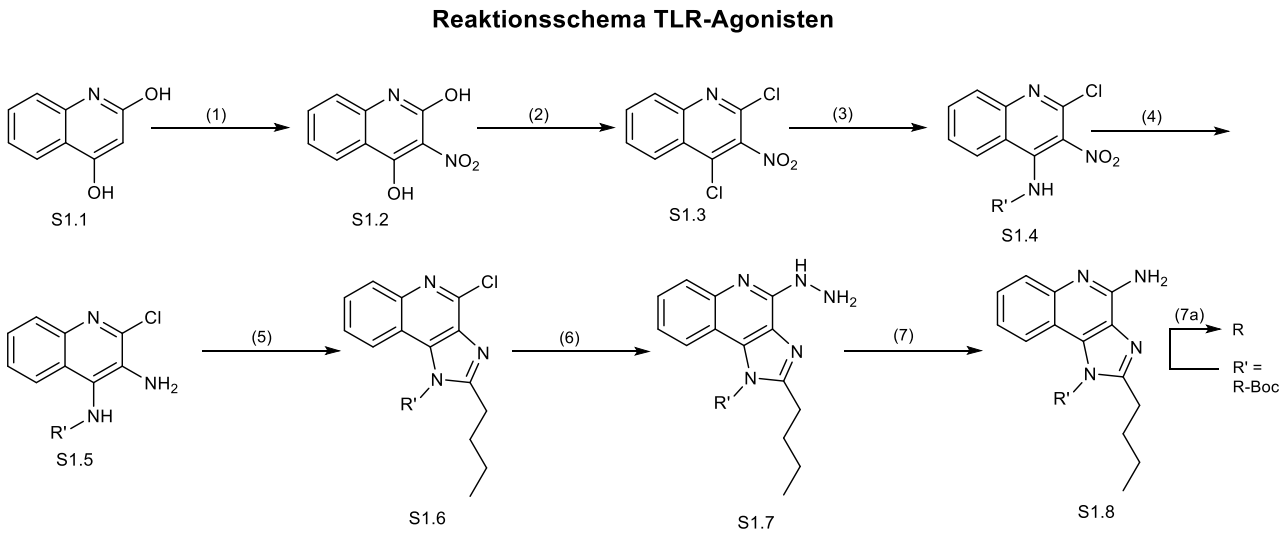

Abbildung 8. Zusammenfassung der Reaktionsschritte (genaue Synthesevorschrift befindet sich in Abschnitt 9 bzw. in Anhang zur Publikation aus Abschnitt 9) und verwendeten Reagenzien: (1) HNO_3, (2) $PhP(=O)Cl_2$, (3) H_2N-R', 45°C, (4) H_2/Pd oder Na_2S2O_4, (5) $C_4H_9C(OCH_3)_3$, Δ, (6) N_2H_4/H_2O, Δ, (7) Zn/TFA/EtOH, (7a) DCM/TFA; Hydrolyse von Boc Schutzgruppe, falls vorhanden. R kann sein: 2-(4-Piperidinyl)-Ethyl, (4-Piperidinyl)-Methyl, 2-[2-(2-Aminoethoxy)Ethoxy]-Ethyl. R' ist 2-[2-(2-Hydroxyethoxy)-Ethoxy]Ethyl (liegt als Pentanoat vor in S1.4 bis S1.7).

Die Anwendung dieser neuen Substanzen soll dabei im Bereich der antiviralen bzw. onkologischen Gebieten liegen. Durch die beobachtete Verschiebung des TNFα/IFN-Verhältnisses in Richtung Typ I IFN ist eine Anwendung in der Behandlung von Virusinfektionen und als Ersatztherapie zur direkten Gabe von rekombinantem IFNα angedacht. Dabei könnte die verringerte Ausschüttung von TNFα zu einer verbesserten Verträglichkeit führen.

Tabelle 2. Auflistung verschiedener Reaktionsansätze für die Substitutionsreaktion am Aromaten in den synthetisierten TLR-Agonisten in Schritt S1.6 in Abbildung 8. RT steht für Raumtemperatur, FA für Ameisensäure, THF für Tetrahydrofuran und TFA für Trifluoressigsäure.

Testreagenz	Lösemittel	Zusätze	Temp [C°]	Produkte	Ausbeute
NH_3	Methanol	$AgNO_3$	60	Silber-Edukt-Komplex	-
Formamid	-	K_2CO_3	170	Foramid-Produkt, Dimerisierung	gering
Trifluoracetamid	-	K_2CO_3	120	Produkt-Boc, Produkt-TFA, Dimer	gering
Aetamid	-	K_2CO_3	150	Produkt-Acetamid, Dimer	gering, viel Dimer
Trifluoracetamid	-	K_2CO_3	120	Divers	-
Trifluoracetamid	-	K_2CO_3	120	Produkt-Boc, etwas Produkt-TFA	TFA-Addukt
Trifluoracetamid	Isobutanol	K_2CO_3	120	Isobutanol-Addukt	-
Trifluoracetamid	Toluol	K_2CO_3	120	etwas Produkt, viel Dimer	ca. 30%
Trifluoracetamid	Dioxan	K_2CO_3	120	kein Produkt, viel Edukt und Dimer	-
Bistrifluoracetamid	-	K_2CO_3	100	Substitution mit -OH und Addition von TFA	-
Harnstoff	-	-	160	Produkt-Harnstoff und Dimer	ca. 50%
Trifluoracetamid	-	K_2CO_3	150	Produkt-TFA und Dimer	ca. 50%
NH_4Cl	Methanol	1% FA, ZnCl2	RT	keine Reaktion	-
NH_4Cl	Ethanol	1% FA, ZnCl2	80	keine Reaktion	-
Piperidin	-	-	RT	schnelle Reaktion mit sekundärem Amin	-
NH_3 in Dioxan	-	-	RT	keine Reaktion	-
Dibenzylamin	-	-	70	keine Reaktion	-
Urotropin	-	-	80	keine Reaktion	-
Trifluoressigsäure und TFAA	-	-	RT	Polymerisation	-
Isoindole	-	-	RT	keine Reaktion	-
Trifluoracetamid	-	K_2CO_3	130	keine Reaktion	-
NH_3 in Dioxan	THF	Cu I	RT	keine Reaktion	-
Biuret	Wasser	K_2CO_3	100	keine Reaktion	-
Biuret	Nitrobenzol	K_2CO_3	150	keine Reaktion	-
Morpholin	-	-	RT	schnelle Reaktion mit sekundärem Amin	-
Dimethylamin	DMSO	-	RT	schnelle Reaktion mit sekundärem Amin	-
Dibenzylamin	Dioxan	-	RT	keine Reaktion	-
Hydroxylamin in Wasser	Ethanol	$NaHCO_3$	RT	keine Reaktion	-
Hydrazin in Wasser	Ethanol	-	RT	Reaktion	Voll umgesetzt
NH_3 mit Formaldehyd	Wasser/Ethanol	-	RT	keine Reaktion	-
Hydrazin in Wasser	Ethanol	-	80 °C	Reaktion	Voll umgesetzt

5. Zielsetzung

Da sich intrazellulär in Immunzellen wichtige Rezeptoren für die Immunantwort befinden, welche dort Verdauprodukte von Bakterien (z. B. SCFAs) oder Abbauprodukte aus Lysosomen (z. B. virale Partikel, wie RNA) detektieren, war das Ziel, Substanzen zu entwickeln, welche sich dort akkumulieren und diese Rezeptoren ansprechen können. Daher wurden basierend auf Azithromycin mehrere Klassen an neuartigen Syntheseprodukten entwickelt, welche entweder durch Hydrolyse lokal Liganden freisetzen können beziehungsweise makrolidische Substanzen, welche durch nicht-hydrolisierbare Linkermoleküle Agonisten tragen können.

Im Detail behandelt diese Arbeit Esterverbindungen von Azithromycin und SCFAs bzw. Fumarsäure Derivaten in den Positionen 11, 2‘ und/oder 4“ und amidische Strukturen von Azithromycin Derivaten über einen Linker mit TLR-Agonisten. Ziel war es, die pharmakokinetischen Eigenschaften von Azithromycin beizubehalten und die gelinkten Substanzen subzellulär verfügbar zu machen. Ein Schwerpunkt der Arbeit liegt dabei auf der Synthese und der Charakterisierung dieser Substanzen und deren genauer Dekorationsmuster mittels (2D-)NMR und MS/MS-Analyse. Zur genauen Bestimmung der Subtanzeigenschaften wurden Analysen zur Stabilität, Toxizität, Metabolismus, zelluläre Aufnahme und Pharmakokinetik gemacht.

Für die kurzkettigen Fettsäuren wurde hierbei der Fokus auf Propionat und Butyrate gelegt, da deren Relevanz in der Immunfunktion größer ist, als bei anderen SCFAs (z.B. Acetat). Als Zielsubstanzen wurden die dreifach substituierten 11-2‘-4“-Ester von Fettsäure und Azithromycin gewählt, um je mehrere Äquivalente SCFA lysosomal verfügbar zu machen. Ziel war es diese Substanzen genau zu charakterisieren und auf ihre Eigenschaften bezüglich Stabilität und Pharmakokinetik zu untersuchen. Dazu wurden zusätzlich alle möglichen Hydrolyseprodukte synthetisiert (je drei Diester und drei Monoester für beide Fettsäurederivate) und jeweils die Strukturaufklärung durchgeführt.

Ähnlich vorgegangen wurde für die Fumarsäure Derivate. Durch die Kopplung über eine Estergruppe sollte die Aufnahme und Verteilung von Monomethylfumarat in lysosomale Zellkompartimente verbessert werden. Dabei stand die Betrachtung der unterschiedlichen Hydrolysegeschwindigkeiten der Produkte (2‘- gegenüber 4“-Estern) und die Evaluierung deren Nutzen in Bezug auf Psoriasis und einem möglichen besseren Verständnis des Wirkmechanismus von Fumaraten im Generellen im Fokus.

Es wurde weitergehend auch untersucht inwiefern sich verschiedene Inhaltsstoffe aus Aldara® auf die Induktion von Psoriasis-ähnlichen Hautveränderungen im Mausmodell auswirken. Dies wurde dafür genutzt, ein besseres Verständnis darüber zu gewinnen, inwiefern die Wirkmechanismen getesteter Substanzen eine Verbesserung in humaner Psoriasis erreichen können. Ziel war dabei die Evaluierung verschiedener Bestandteile der Creme und deren Einfluss auf die Induktion der Krankheitssymptome und wie sich dies in der Anwendung und Analyse im Tiermodell nutzen lässt.

Zuletzt wurde auf Basis von bekannten Imidazoquinolin-Strukturen neue TLR7- bzw. TLR7/8-Agonisten synthetisier. Über einen Linker, welcher außerhalb des bekannten Bindungsmotivs liegt, sollte über eine amidische Kopplung an Azithromycin eine verbesserte ADME (Absorption, Distribution, Metabolismus und Elimination) erreicht werden. Bisherige Imidazoquinoline scheiterten an zu starken Nebenwirkungen in der systemischen Anwendung und finden maximal als topisches Arzneimittel (Imiquimod) Anwendung. Durch das Makrolid sollten die pharmakologischen Eigenschaften dahingehend angepasst werden, dass eine schnellere Verteilung in Gewebe und subzelluläre Kompartimente erreicht werden, mit dem Ziel einer geringeren Belastung für PatientInnen.

6. Zusammenfassung der Ergebnisse

Als Signalmoleküle können SCFAs in lysosomalen Kompartimenten starke immunregulierende Wirkungen haben. Sie dienen dort als Signalmoleküle für das Vorhandensein von anaeroben Organismen und indizieren dem Immunsystem eine mögliche Infektion. Um die Eigenschaften der lysosomalen SCFAs besser zu verstehen, wurde in dieser Arbeit („Synthesis, Characterization, and *in vivo* Distribution of Intracellular Delivered Macrolide Short-Chain Fatty Acid Derivatives“) spezifisch die Pharmakokinetik durch Kopplung an Azithromycin (Pos. 11, 2‘ und 4“) modifiziert. Durch die Synthese aller Zwischenmetaboliten und die dazugehörige Strukturaufklärung konnten Aussagen über Pharmakokinetik, Stabilität, Hydrolyse und Metabolismus *in vitro* und *in vivo* gemacht werden. Die Substanzen werden durch einen niedrigen pH-Wert stabilisiert. Die Butyratderivate erwiesen sich als stabiler als die Derivate der Propionate. Tri-Ester waren stabiler als Di- oder Mono-Ester. Die Estergruppen waren *in vivo* stabiler als vorher durch *in vitro* Versuche beobachtet und die Hydrolyse der einzelnen Positionen war organspezifisch. Die beobachteten Konzentrationen und Verteilungen stehen

im Einklang mit pharmakodynamischen Wirkungen und sind in ihrer Pharmakokinetik vergleichbar mit Azithromycin.

Dimethyl- und Monomethylfumarat sind Methylester der ungesättigten Dicarbonsäure Fumarsäure. Es wird vermutet, dass die Wirkung von DMF auf einer Michael-Addition an Thiole beruht und so immunmodulatorisch wirkt. Eine andere Hypothese besagt, dass MMF, das Hydrolyseprodukt von DMF, ein Ligand für den Fettsäurerezeptor GPR109A ist, welcher auch in den Lysosomen von Immunzellen zu finden ist. In dieser Arbeit („Immune cell targeted Fumaric Esters support a role of GPR109A as a primary target of Monomethyl Fumarate *in vivo*“) wurden Ester von MMF und von Azithromycin abgeleitete Makrolide hergestellt, welche durch lysosomales *Trapping* in Immunzellen angereichert werden sollten. Die neuen Substanzen waren Ester von Azithromycin in dessen 2‘- und 4“-Positionen. In *in vitro* Versuchen zeigten die Substanzen mit 4“-Estern eine deutliche Reduktion von proinflammatorischen Zytokinen (25fach im Vergleich zu DMF). Die 2'-Ester des MMF waren, wie MMF, *in vitro* inaktiv. Die 4''-Ester formten *in situ* schnell Glutathion-Konjugate, während die 2'-Konjugate nicht mit Thiolen reagierten, jedoch über die Zeit hydrolysierten und MMF in diesen Zellen freisetzten. Anschließend wurde getestet, wie die Substanzen *in vivo* im Psoriasis Mausmodell funktionieren. Hierbei zeigte sich, dass die 2'-Ester am aktivsten waren und die Hautveränderungen, das Körpergewicht und die Zytokin Werte sich im Vergleich zu Kontrollgruppen verbessert zeigten. Im Gegensatz dazu waren die 4“-Ester hier weniger aktiv. Diese Daten deuten darauf hin, dass *in vivo* relevante Mechanismen auf die Freisetzung von MMF abzielen. Im Gegensatz dazu dürften die mit der Konjugation von GSH *in vitro* verbundenen Wirkungen *in vivo* nicht so wirksam sein, da die verwendete Dosis viel niedriger ist und freie Thiole in deutlich höherer Konzentration *in vivo* vorkommen.

Als Wirkstoff in Aldara® wird der TLR7-Agonist Imiquimod eingesetzt, welcher immunstimulierende Eigenschaften besitzt. In der Forschung dient Aldara® zur Induktion einer Hautentzündung bei Mäusen, welche die humane Psoriasis nachahmen soll. Die vorliegende Arbeit („Isostearic acid is an active component of imiquimod formulations used to induce psoriaform disease models. Inflammopharmacology“) beschäftigt sich mit der Beobachtung, dass die Stimulation nicht ausschließlich auf Imiquimod zurückzuführen ist, sondern auch von anderen Komponenten abhängt. Um die Mechanismen genauer zu untersuchen, wurden verschiedene Induktionscremes präpariert und in einem Mausmodell dermal appliziert. Es zeigte sich, dass Cremeformulierungen, welche Isostearinsäure beinhalteten, innerhalb von 2

Tage zu einer lokalen Hautentzündung führten, während Imiquimod-haltige Cremes bis zu 5 Tage für eine Hautreaktion benötigten. Es konnte weiter gezeigt werden, dass Isostearinsäure über eine Aktivierung des Inflammasoms die Ausschüttung von proinflammatorischen Zytokinen begünstigt. Obwohl Imiquimod leicht verstoffwechselt und eliminiert wird und daher in Plasma und Leber kaum bzw. nicht detektiert werden konnte, zeigten sich hohe Konzentrationen in verschiedenen Hautproben. Die Daten in dieser Publikation deuten darauf hin, dass Psoriasis-ähnliche Hautreaktionen bei Mäusen stärker von Isostearinsäure angetrieben werden, als allgemein berichtet wird. Dies ist in der Betrachtung der Ergebnisse aus solchen Creme-induzierten Studien mit einzubeziehen und muss bei der Evaluierung von Testsubstanzen mitbeachtet werden.

Der klinische Einsatz von synthetischen TLR-Agonisten ist auf die dermale Anwendung beschränkt, da eine systemische Anwendung von TLR-Agonisten, zu starken Nebenwirkungen führt. Zugrundeliegend sind dabei vermutlich ungünstige pharmakologische Eigenschaften, die sich aus schneller Metabolisierung und Eliminierung zusammensetzen. Der Ansatz in dieser Arbeit („Imidazoquinolines with improved pharmacokinetic properties induce a high IFNα to TNFα ratio *in vitro* and *in vivo*“) war die Entwicklung und Synthese von neuartigen TLR7/8-Agonisten auf Basis von bekannten Imidazoquinolin-Kernstrukturen und einem Makrolidträgermolekül. Dadurch sollten verbesserte pharmakologische Eigenschaften, mit verlängerter AUC und geringerem c_{max}, erreicht werden. Unsere Verbindungen zeigten hierbei eine hTLR7/8-agonistische Aktivität und eine maximale hTLR7-Aktivierung zwischen 40 und 80% von Resiquimod. Unsere Leitkandidaten induzieren die Sekretion von IFNα aus menschlichen Leukozyten im gleichen Bereich wie Resiquimod, induzieren aber mindestens 10-mal weniger TNFα im selben System. Dies deutet auf einen höhere agonistische Spezifität auf hTLR7 hin. Diese Ergebnisse ließen sich im Mausmodell reproduzieren. Die neuen Substanzen zeigten, unabhängig ob gekoppelt an ein Makrolid oder als ungebundenes sekundäres Amin, eine längere Exposition als Resiquimod und damit auch eine veränderte Kinetik in der Freisetzung proinflammatorischer Zytokine und sind wahrscheinlich eine Folge der veränderten Pharmakokinetik und Stabilität.

7. "Synthesis, Characterization, and *in vivo* Distribution of Intracellular Delivered Macrolide Short-Chain Fatty Acid Derivatives"

Straß, S., Schwamborn, A., Keppler, M., Cloos, N., Guezguez, J., Guse, J. H., Burnet, M., & Laufer, S. (2021). Synthesis, Characterization, and in vivo Distribution of Intracellular Delivered Macrolide Short-Chain Fatty Acid Derivatives. *ChemMedChem*, *16*(14), 2254–2269. https://doi.org/10.1002/cmdc.202100139 (für *Supporting Information* siehe Anhang)

Eigenanteil an Publikation

Die Idee zur Synthese der gelisteten Stoffe wurde von Dr. Burnet, Dr. Guse und mir ausgearbeitet. Alle aufgeführten Synthesen wurden von mir durchgeführt. Die Aufnahme der NMR-Spektren erfolgte durch die Uni Tübingen über die Arbeitsgruppe Laufer. Die Auswertung der Spektren, die Charakterisierung und die Strukturaufklärung wurde von mir, unter Anleitung von Dr. Guse, durchgeführt. Die pharmakokinetischen Studien wurden von Frau Cloos und mir geplant. Die Ausführung wurde dann in Zusammenarbeit mit dem Tierstall der Synovo GmbH durchgeführt. Die Aufarbeitung, Analyse und Messung der Proben aus den Studien, sowie der Proben aus den Stabilitäten wurde von Frau Schwamborn, Herrn Keppler und mir getätigt. Die Entwicklung der dabei verwendeten HPLC-MS/MS Methode geht auf die Arbeiten von Dr. Guezguez, Frau Schwamborn und mir zurück. Die schriftliche Ausarbeitung und Visualisierung erfolgten durch mich. Prof. Laufer wirkte bei der Arbeit unterstützend und betreuend. Dr. Burnet, Dr. Guse und Prof. Laufer haben das Manuskript überprüft und korrigiert.

ChemMedChem | Full Papers doi.org/10.1002/cmdc.202100139 | Chemistry Europe, European Chemical Societies Publishing

Synthesis, Characterization, and in vivo Distribution of Intracellular Delivered Macrolide Short-Chain Fatty Acid Derivatives

Simon Straß,[a, b] Anna Schwamborn,[b] Manuel Keppler,[b] Natascha Cloos,[b] Jamil Guezguez,[b] Jan-Hinrich Guse,[b] Michael Burnet,*[b] and Stefan Laufer[a]

Short-chain fatty acids (SCFAs) have a range of effects in metabolism and immune regulation. We have observed that delivery of SCFAs to lysosomes has potent immune regulatory effects, possibly as a surrogate signal for the presence of anaerobic organisms. To better understand the pharmacology of lysosomal SCFA donors, we investigated the distribution and metabolism of propionate and butyrate donors. Each analog (**1a** and **2a**) can donate three SCFA equivalents via ester hydrolysis through six intermediate metabolites. The compounds are stabilized by low pH, and stability in cells is usually higher than in medium, but is cell-type specific. Butyrate derivatives were found to be more stable than propionates. Triesters were more stable than di- or mono-esters. The donors were surprisingly stable in vivo, and hydrolysis of each position was organ specific. Jejunum and liver caused rapid loss of 4″ esters. The gut metabolite pattern by i.v. differed from that of p.o. application, suggesting luminal and apical enzyme effects in the gut epithelium. Central organs could de-esterify the 11-position. Levels in lung relative to other organs were higher by p.o. than via i.v., suggesting that delivery route can influence the observed pharmacology and that gut metabolites distribute differently. The donors were largely eliminated by 24 h, following near linear decline in organs. The observed levels and distribution were found to be consistent with pharmacodynamic effects, particularly in the gut.

Introduction

Short chain fatty acids (SCFAs; most commonly acetate, propionate and butyrate) are water-soluble carboxylic acids with less than six carbons. They derive largely from bacterial fermentation of dietary fiber in the gut and are anaerobic metabolic end products. In the human colon concentrations of these SCFAs can reach mM-levels (acetate 64 mM, propionate 27 mM, butyrate 25 mM).[1] These SCFAs are a source of energy for colonocytes but they also act as mediators in the communication between the intestinal microbiome and the immune system present behind the intestinal epithelium.[2]

Both colonocytes and monocytes express SCFA receptors. Free fatty acid receptor 2 (FFAR2 or GPR43) interacts mainly with acetate and propionate, whilst the free fatty acid receptor 3 (FFAR3 or GPR41) has higher affinity for propionate, butyrate, and valerate.[1] FFAR2 and 3 are highly expressed in immune cells. FFAR2 is also expressed in adipose tissue, distal ileum and colon, while FFAR3 is preferentially expressed in adipose tissue, spleen and immune tissue.[1] FFAR2 is reported in the context of inflammatory and immune response, whilst FFAR3 has been associated with metabolic disorders.[3,4]

Butyrate is a known inhibitor of histone deacetylases (HDAC), a group of enzymes involved in gene regulation through their repressive influence on transcription. This inhibition leads to a suppression of nuclear factor kappa B (NF-κB) translocation.[5] The G protein-coupled receptor 109a (GPR109a or HCA2) is a receptor for niacin, but also butyrate.[6] GPR109a is primarily expressed on adipocytes, but also neutrophils and macrophages. Activation of GPR109a leads to recruitment of β-arrestins and regulation of vascular inflammation in atherosclerosis.[3,7] Olfactory receptor 78 (Olfr78) also uses SCFAs as ligands, particularly acetate and propionate.[8] Olfr78 is expressed in smooth muscle cells of the vasculature and kidney. It plays an important role in regulation of blood pressure.[8] SCFAs can regulate tissue inflammation but their effect depends on the type and concentration of the SCFA as well as the species and type of immune cell which in turn correlates with the expression pattern of receptors (FFAR2, FFAR3, GPR109 A and Olfr78).[9,10] The SCFA receptors have a range of disease associations including inflammatory bowel disease (IBD), diabetes, obesity, colon cancer, arthritis, colitis, hypertension, and asthma,[11] making them candidate pharmacological targets, albeit, targets that potentially require agonism instead of inhibition.

The role of SCFAs in inflammatory bowel diseases (Crohn's disease (CD) and ulcerative colitis (UC)) in particular has been demonstrated via studies on dysbiosis of the gut

[a] S. Straß, Prof. S. Laufer
Pharmaceutical Chemistry, Institute for Pharmaceutical Sciences
Eberhard-Karls-Universität Tübingen
Auf der Morgenstelle 8
72076 Tübingen (Germany)
[b] S. Straß, A. Schwamborn, M. Keppler, N. Cloos, J. Guezguez, J.-H. Guse, M. Burnet
Synovo GmbH
Paul-Ehrlich Straße 15
72076 Tübingen (Germany)
E-mail: michael.burnet@synovo.com

Supporting information for this article is available on the WWW under https://doi.org/10.1002/cmdc.202100139

ChemMedChem | Full Papers doi.org/10.1002/cmdc.202100139 | Chemistry Europe European Chemical Societies Publishing

microbiome.[5,12–15] These studies suggest that insufficient SCFA from the gut lumen leads to loss of barrier function and inappropriate immune activation.[12] These effects appear to be primarily mediated by lack of propionate and butyrate, whilst acetate appears to be less critical.

Application of either propionate or butyrate to treat IBD has been attempted, however, both require high doses and have problems of smell and formulation to reach necessary stable concentrations in the colon.[12] FFAR2 and 3, for example, need concentrations above 0.5 mM (EC_{50}) for their activation.[16] This could, in theory be obtained with a combination of a high fiber diet and a butyrogenic microbiome, yet, these appear to be absent in many patients. Therapy of dysbiosis has been proposed via fecal transplant, probiotic preparations and dietary modification.[17–21] Nevertheless, these types of therapies are difficult to standardize and effects can be largely transient. While the technology for widespread therapy with microorganisms is developing, a simplified small molecule approach that simulates a healthy microbiome may be one means to use knowledge and to mimic the microbiome in the treatment of gut disorders. The substances we describe here are active in the range of 0.1 mg/kg and are thus much more efficient than free SCFAs.[22,23]

Sensing of SCFAs appears to take place at several levels. Colonocytes have surface receptors which appear to regulate tight junction formation and density. Resident monocytes likewise express surface receptors,[16] however, staining patterns suggested the possible intracellular or lysosomal location of FFAR3 in monocytes.[24] We hypothesized that intracellular and lysosomal receptors may assist a monocyte or other phagocytotic cells in sensing danger signal and that SCFAs detected in the lysosome could indicate that an anaerobic organism has been encountered. This, for example, seems to be the case in Acne where propionic acid released by *Propionibacterium acnes* causes strong local immune stimulation.[25] Containment of the gut microbiome is a major role for the immune system. Similarly, anaerobic infections are particularly difficult for the immune system to contain (toxins, poor vascular access, low pH, and lack of oxygen limiting energy metabolism and production of reactive oxygen species). Given the predominance of anaerobes in the gut and the role of immune cells in preventing peritonitis, such sensors may be beneficial in orchestrating an enhanced response to bacterial invasions of the gut epithelium. That SCFAs are readily soluble, volatile and diffuse easily makes them suitable as a form of signal to immune cells that anaerobes are present or have been engulfed. In particular, the possible intra-cellular presence of SCFA receptors supported a putative role in immune stimulus and danger signal sensing post-phagocytosis.[24]

In dysbiosis, the lack of SCFAs appears to both render the gut epithelium more porous and to down-regulate innate immune surveillance. This, in turn, seems to lead to a risk of bacterial translocation, leaky gut, colitis and potentially other immune regulatory disorders.[26,27]

To test the idea that intracellular sensing of SCFAs may be beneficial, we designed compounds that could preferentially deliver SCFAs to intracellular compartments, notably the phagolysosome.

To this end we used Azithromycin (9-deoxy-9a-aza-9a-methyl-9a-homoerythromycin A), a 15-membered ring macrolide, as a carrier with tropism to the lysosome. Azithromycin was first developed in 1979 as a derivative of erythromycin with an additional nitrogen in the core macrolide ring. This influences its pharmacokinetic characteristics (higher tissue distribution and longer elimination half-life)[28] and provides better stability in acidic environment.[29] Azithromycin is also known for its ability to accumulate into the phagolysosomes of immune cells[30] perhaps explaining its activity against intracellular pathogens like *Chlamydia pneumoniae* and *Legionella pneumophila*. Apart from its antibacterial properties it also shows immunomodulating effects in e.g. diffuse panbronchiolitis, cystic fibrosis and bronchiolitis obliterans syndrome.[29] Azithromycin showed significant anti-inflammatory effects for example in lipopolysaccharide (LPS) induced sepsis in mice by inhibiting the pro-inflammatory cytokines interleukin (IL)-6, IL-1β and tumor necrosis factor α (TNFα).[31]

Various groups have shown that Azithromycin is able to concentrate into immune cells (Intracellular/Extracellular concentration (I/E)) many-fold over plasma concentrations and thereby, to be targeted towards inflammation sites where immune cells accumulate.[32–34] I/E ranges from 35 to 200 in macrophages (within respectively 3 h and 24 h) and from 80 to over 500 in polymorphonuclear leukocytes (PMNs) within respectively 2 h to 3 h.[32,35–38] The proposed explanation is that Azithromycin is an amphiphilic base that is trapped in acidic compartments and negatively charged sites inside cells (lysosome, phagolysosome) due to its two amine groups that become positively charged at lower pH.[39] This transport is regulated by pH, temperature and extra- as well as intracellular concentration of the macrolide. While this effect is wide spread amongst lipophilic amine drugs, it is particularly strong for Azithromycin despite the five hydroxy groups that it bears. After a single dose of Azithromycin, tissue to serum concentration ratios exceeded 100.[40]

Because of these properties, we used Azithromycin (and its analogs) as a carrier for SCFA esters and synthesized new macrolides with propionate and butyrate at the 11, 2′ and 4″ positions. These compounds serve as Azithromycin pro-drugs that also deliver SCFAs into immune cells to activate the FFA2/3 receptors.

Since SCFA esters are not able to interact with the targeted receptors, any activation would be dependent on hydrolysis. Similarly, targeted effects would depend on retention of known Azithromycin distribution in the body. To determine how such tri-esters behave, we investigated their stability and metabolism in cultured immune cells, human whole blood and via pharmacokinetic studies in mice. Given that the position of hydrolysis impacts known effects of Azithromycin, we prepared possible metabolites of the macrolides (Table 1 and Figure 1) with different substitution patterns of fatty acids.

ChemMedChem | Full Papers doi.org/10.1002/cmdc.202100139 | Chemistry Europe European Chemical Societies Publishing

Table 1. Substitution pattern of Azithromycin derivatives, with lead substances **1a** and **2a**.

Compound	11-Pos.	2′-Pos.	4″-Pos.	MW [g/mol]
1a	butyrate	butyrate	butyrate	959
1b	butyrate	OH	OH	819
1c	OH	butyrate	OH	819
1d	OH	OH	butyrate	819
1e	butyrate	butyrate	OH	889
1f	butyrate	OH	butyrate	889
1g	OH	butyrate	butyrate	889
2a	propionate	propionate	propionate	917
2b	propionate	OH	OH	805
2c	OH	propionate	OH	805
2d	OH	OH	propionate	805
2e	propionate	propionate	OH	861
2f	propionate	OH	propionate	861
2g	OH	propionate	propionate	861
3[a]	OH	OH	OH	749

[a] This entry represents Azithromycin.

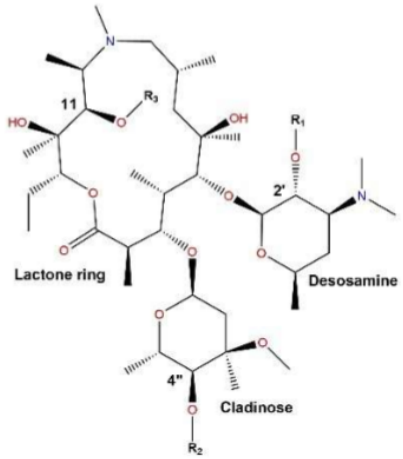

Figure 1. General structure. R_1 to R_3 are defined in Table 1.

Results and Discussion

Synthesis

The substitution pattern of core macrolide with ester groups can be found in Table 1. The syntheses of **1a** and **2a** were carried out by esterification of the hydroxy groups of Azithromycin (3) in position 11, 2′ and 4″ with butyric anhydride respectively propionic anhydride. For **1c** and **2c** Azithromycin was dissolved in dichloromethane (DCM) and butyrate anhydride respectively propionate anhydride was added. **1d** and **2d** were achieved by converting the 4″ position with respectively butyryl chloride or propionyl chloride into their esters. **1f** and **2f** have a decorated hydroxy group in position 11 and 4″. This pattern was carried out by dissolving respectively **1a** and **2a** in methanol and thus solvate the ester function in 2′ position. The compounds **1b** and **2b** were obtained by dissolving respectively **1e** or **2e** in methanol and thus hydrolyzing ester function in 2′ position. For compounds **1g** and **2g** Azithromycin was decorated with esters in positions 2′ and 4″ in each case with butyryl chloride or propionyl chloride. For compounds **1b** to **1f** and **2b** to **2f** the synthesis was not optimized, since they were only required as metabolite standards of **1a** and **2a**.

Analytics

To demonstrate the substitution pattern of the products we used MS/MS (Table 2 and Figure 2B) and nuclear magnetic resonance (NMR). Three fragmentation patterns are apparent: first a cleavage of the cladinose sugar occurs; second, the loss of desosamine; third, while the core lactone ring remains stable, there is elimination of a water.[41–43] Depending on the substitution position fragments vary in the mass of the bound esters demonstrating the different substitution patterns of the molecules. These observations support the proposed position of the esters.

NMR studies were performed to identify all substances and to show the specific shift of ester groups in the positions 11, 2′ and 4″ of the molecules. All NMR spectra were compared with Azithromycin and can be found in the Supporting Information. NMR data of Azithromycin has been published elsewhere.[44,45] The chemical shifts (^{1}H and ^{13}C) for each substance can be found in the experimental section. Additional to ^{1}H and ^{13}C NMR, Heteronuclear single-quantum correlation spectroscopy (HSQC) and H–H correlation spectroscopy (H–H–COSY) were performed for **1a** and **2a** (and **1b**, **1c**, **1f**) to check proposed structures. With HSQC it was possible to carry out an assignment of the crucial protons in position around the newly formed esters (Figure 2A for **1a**). ^{1}H NMR studies show for **1a** and **2a** chemical shifts for position 11, 2′ and 4″ downfield compared to **3**. For compounds **1b**–**1g** and **2b**–**2g** this could also be shown. Using the example of **1a**, the proton bound to

Table 2. Specific MS/MS fragmentation patterns. M^+ peak and Frag 1 to 4 show m/z ratio.

Compound	$[M+H]^+$	Frag 1	Frag 2	Frag 3	Frag 4
1a	959	731	713	468	–
1b	819	661	643	468	–
1c	819	661	643, 228	398	–
1d	819	591	573	434, 416	–
1e	889	731	713, 228	468	–
1f	889	661	643	486	–
1g	889	661	643, 228	398	–
2a	917	703	685	454	–
2b	805	647	629, 490	472	454
2c	805	647, 214	629	416, 398	–
2d	805	591	573, 434	416	–
2e	861	703	685	454	–
2f	861	647	629, 490	472	454
2g	861	647	629, 214	398	–

ChemMedChem | Full Papers doi.org/10.1002/cmdc.202100139 | Chemistry Europe European Chemical Societies Publishing

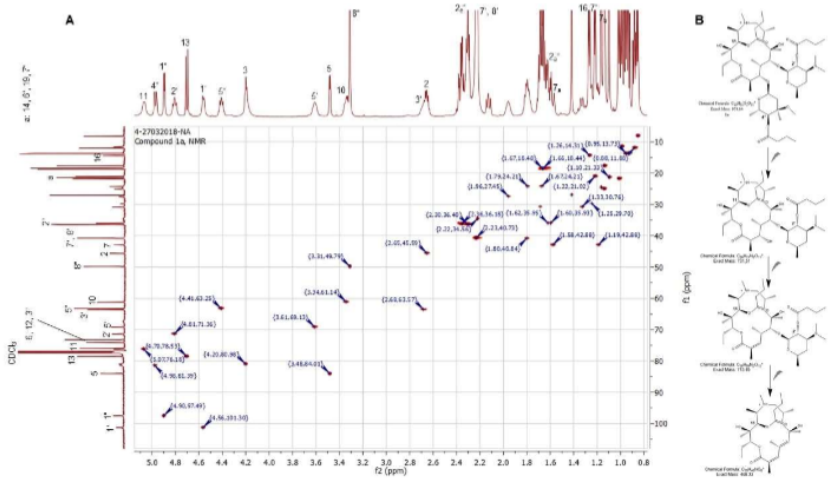

Figure 2. HSQC NMR (**A**) and MS/MS fragmentation pattern (**B**) of compound **1 a. A** shows correlation of ^{1}H NMR spectra (horizontal) with ^{13}C NMR spectra (vertical) of tri-butyrate ester **1 a**. Found peaks were assigned and correlations between ^{1}H and ^{13}C could confirm hypothesized structure. **B** shows MS/MS fragmentation confirming the assumed structure of **1 a**.

carbon 11 was shifted from 3.68 ppm in **3** to 5.06 ppm in **1 a**. The proximal proton of carbon 10 was also shifted downfield (from 2.69 ppm to 3.34 ppm). The 2′ proton shifted from 3.24 ppm to 4.81 ppm as did those of carbons 1′ (4.44 ppm to 4.56 ppm) and 3′ (2.48 ppm to 2.68 ppm). The proton bound to the 4″ carbon is at 3.03 ppm in **3** and at 4.70 ppm in **1 a** and that at 5″ is shifted from 4.08 ppm (**3**) to 4.41 ppm (**1 a**). Similar shifts can be observed for **2 a** (this also applies to all other compounds).

Esterification of the 11 position in the macrolide ring caused greater changes in the NMR spectra (correlated and non-correlated) then with esterification of 2′ or 4″. This suggests that derivatization of 11 position causes bigger changes in the stereo chemistry of the macrolide ring.

Stability studies

Esters are well known to hydrolyze chemically, or via esterases or lipases, and our earlier work had demonstrated the lability of the 2′ esters.[22,23] To ensure that the compounds could be prepared and stored in a stable form we investigated their stability in solution under various conditions and to support analysis of possible pharmacokinetic studies. In particular, the 2′ position of Azithromycin interacts with the bacterial ribosome.[46] If it is esterified, it is not a direct inhibitor of the ribosome.[47,48] If it is de-esterified, it is potentially a direct antibacterial substance.

In addition to the issue of the delivery of a potential known antibiotic, the rate and site at which the esters are cleaved will determine the effective dose of SCFA at each organ or cell-type. To this end, it is important to know where and how the ester bonds are hydrolyzed and thus how and at what rate the SCFAs are released. Hydrolysis depends on various factors, like temperature, pH, enzyme activity, solvent, membrane partition, solvent exposure, lipophilicity, or steric hindrance. Lipophilicity by propionate and butyrate esters are known to vary with chain length, with slightly faster hydrolysis in propionate derivatives.[49,50] However, differences between the positions of the ester bonds on the macrolide have a greater impact on lipophilicity or steric effects. The positions 2′ and 11 are 2-aminoalkylesters, which can undergo facilitated hydrolysis by intramolecular catalysis of the amino group.[51,52] Enzyme activity and pH vary significantly, depending on the *in vivo* compartment. pH stability data for the 2′ esters **1 c** and **2 c** (most labile position) are shown in Table 3. Stability was measured at pH

Table 3. Half-life values [h] for derivates in different pH values at 4°C.

Compound	pH 4	5	6	7	8
1 c	>100	>100	79.6	18.9	6.9
2 c	>100	>100	30.9	10.2	2.2

ChemMedChem | Full Papers doi.org/10.1002/cmdc.202100139 | Chemistry Europe European Chemical Societies Publishing

values of 4, 5, 6, 7 and 8 up to 24 hours. Samples were injected directly from buffered solutions (either acetate or phosphate buffer solutions) into HPLC-ELSD system at 4 °C. At acidic pH values the substances are stable. Increasing the pH made them more sensitive to hydrolysis, with hydrolysis proceeding most rapidly at pH 8. Overall, the hydrolysis rates of **1c** and **2c** are similar with slightly lower half-life values for the propionate derivative (**2c**) which is consistent with literature.[49,50]

Cell stability testing was performed with **1a** and **2a** in human whole blood and cultured U937cells over 24 h at 37 °C. Samples were collected at various times after substance application and mixed with six volumes of acetonitrile (with 0.1% of formic acid) to precipitate protein and lyse cells. The supernatant was collected, and the identity and concentration of metabolites measured via HPLC-MS/MS. Results are shown as half-life values in Table 4.

The hydrolysis kinetics can be divided into two groups. The first group (11 and 4'' esters) does not hydrolyze within 24 h (**1b**, **1d**, **1f**, **2b**, **2d**, **2f**). The second group undergoes first order hydrolysis at the 2' ester over 1–6 h (**1c**, **1e**, **1g**, **2a**, **2c**, **2e**, **2g**).

The loss of the 2' ester was accompanied by the appearance of the hydrolysis product. The lability of the 2' position may be due to two possible mechanisms (relevant also to the 11 esters); 2-aminoalkylesters can undergo specific hydrolysis reactions through intramolecular catalysis of the amino group. In one form, the amino group catalyzes the hydrolysis by a water molecule. The nitrogen coordinates one proton of water and the oxygen attacks the carbonyl-C to cleave the ester.[51] Alternatively, an intramolecular attack of the nitrogen on the carbonyl-C forms a five-membered ring intermediate, which then shifts to form an amide.[52] This is then hydrolyzed by water.

At the 11 position, the hydrolysis is retarded, but can still occur to a certain extent (see Supporting Information Compound **1b**, **1f**, **2b**, **2f**). Although it is, like the 2' position, an ester function of a 2-aminoalcohol, the deceleration of hydrolysis can be explained by steric hindrance of the relatively inflexible lactone ring. The amino group is therefore less suitable for catalysis.

Table 4. In vitro half-life values [h] for derivates in U937 cells, human whole blood, RPMI medium.

Compound	Whole blood	U937	RPMI
1a	>100	12.6	>100
1b	>100	>100	60.8
1c	5.1	3.0	1.6
1d	>100	>100	>100
1e	11.5	3.1	1.5
1f	>100	>100	50.8
1g	6.0	0.6	0.5
2a	2.7	2.2	1.1
2b	>100	>100	>100
2c	1.9	1.0	1.0
2d	>100	>100	>100
2e	2.6	1.9	1.0
2f	>100	>100	34.9
2g	3.2	1.5	1.0

In contrast to pH buffered solutions, stability in cells and media is complicated by a range of factors including: partition to acidic compartments, binding to serum proteins, insertion into membranes, binding to plastic, fixation on positive polymers (heparin, chondroitin sulfate), binding to nucleic acids (e.g. ribosomes) and other negatively charged sites, and the presence of hydrolytic enzymes (lipases, esterases etc.). Based on both published data[53] and our own studies with fluorescent analogs (not shown), the main effects in cells are due to partition to acidic compartments and membrane insertion.

Paradoxically, in contact with cells, most compounds exhibit greater stability than in medium. Given that lower pH is also stabilizing, and that the compounds are known to insert to membranes, these data are consistent with partition to the lysosomes and other negatively charged structures of the cells reported for macrolides.[54]

The hydrolysis rate of the tri-propionate, **2a**, is slower than for other 2' propionate ester derivatives (**2c**, **2e**, **2g**). This effect is more pronounced in cultured cells and whole blood than it is in medium. This might be explained by the higher hydrophobicity of the tri-ester (see table of cLogP values in Supporting Information) increasing membrane partition and higher accumulation into the membranes of acidic compartments and thus stabilization of the 2' position.

Similarly, the butyrate esters are more hydrophobic and more stable: **1a** is more stable than the other 2' butyrate ester derivatives (**1c**, **1e**, **1g**). Also, **1a** seems to be more stable in RPMI medium and human whole blood (Table 4 and figures in Supporting Information) but is hydrolyzed in U937 cells within 12.6 hours. We propose that these effects are due to a combination of increased hydrophobicity promoting binding to serum protein and cell-specific hydrolytic activity.

Differences of hydrolysis rates between **1a** and **2a** can be partly explained by deactivation due to the longer carbon chain in the butyrate but are bigger than expected. Given that the tributyrate (**1a**) is at least 4× less soluble than **2a** (data in Supporting Information), and that it has a cLogP ca. 2-units higher, we propose that **1a** is likely more protected from water due to affinity for hydrophobic sites.

In summary, solution stability, and stability in media and cell systems all indicate that stability increases as the number of esterified sites increases, and with increasing carbon chain length.

These data show that despite having fragile esters, the model compounds are sufficiently stable for use *in vivo* and that these properties are improved with higher degrees of substitution.

Pharmacokinetics

To understand the metabolism of these substances, we have prepared a set of models and diagrams of the pathways apparent in murine and cellular pharmacokinetics. These are found in Figures 3 and 5 and in the Supporting Information.

Briefly, the butyrate derivatives are both more stable and more intestinally bound than the propionates. The 2' ester is

ChemMedChem | Full Papers doi.org/10.1002/cmdc.202100139 | Chemistry Europe European Chemical Societies Publishing

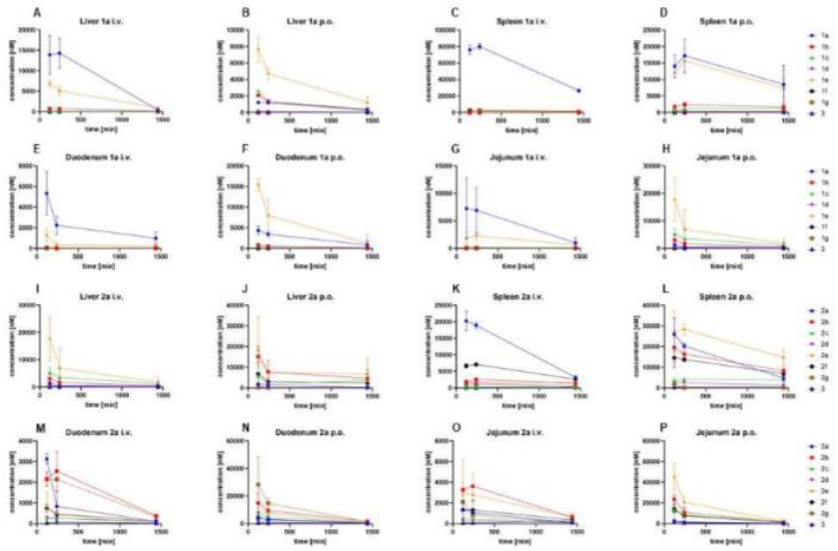

Figure 3. Comparison of pharmacokinetic data (BALB/c mice, female, 17 weeks old, n = 3) of lead substances **1a** and **2a** in different organs via oral (10 mg/kg) or intravenous (2 mg/kg) route. **A**–**H**: Oral vs. intravenous application of **1a** and possible metabolites (**1b**–**1g**, **3**) in different organs (remaining organ data in Supporting Information). I–P: Oral vs. intravenous application of **2a** and possible metabolites (**2b**–**2g**, **3**) in different organs (remaining organ data in Supporting Information).

surprisingly stable and appears to transit the gut largely intact. The intestine and the liver are also able to selectively de-esterify the 4″ position. We propose that this is an enzymatic reaction.

Once the 4″ is cleaved, the remnant di-esters are generally less stable. Paradoxically, the cleavage of the 11 position is often faster than the 2′ once the substance is in tissue.

These general observations indicate that the propionate tri-ester is more systemic and has a high capacity to deliver SCFAs while the butyrate is more gut specific. To the issue of delivery of the active antibacterial Azithromycin, very little was detected suggesting that no or low antibacterial effect could be expected. With respect to the gut microbiome, Azithromycin and 2′ OH-analogs were essentially absent from the gut or the gut washes.

The propionate and butyrate tri-esters are candidate immune and metabolic modulatory drugs. To fulfill the requirements for activity in these classes of disease, adequate properties of formulation, uptake, distribution and elimination are required.

Pharmacokinetics were investigated in mice to determine the distribution and metabolism of **1a** and **2a**. One area of intended application of the substances is IBD where the lysosomal delivery of SCFAs should stimulate both gut epithelium and associated lamina propria immune cells.[22,55] This use implies that oral administration should provide availability in the intestine and that the drugs should be metabolized there to provide tissue with the desired SCFAs.

Azithromycin itself is a relatively metabolically stable drug. It was originally prepared with the objective of reducing the rate of cladinose loss in the upper gastrointestinal (GI) tract and to limit binding to hERG (human ether-a-go-go-related gene implicated in long-Qt effects). In contrast, the derivatives are intended to hydrolyze. Azithromycin has high bioavailability and a high volume of distribution. Within blood, a significant portion is associated with leukocytes, however, the large part is associated with tissue. To ensure adequate assessment of exposure, we determined substance levels in whole blood (to include leukocytes) and tissues where macrolides are known to accumulate (spleen, liver, gut; see Figure 3). The possible metabolites for **1a** are **3** and **1b** to **1g**. For **2a** metabolites are **3** and **2b** to **2g**.

Pharmacokinetic studies were performed in female mice (BALB/c, 17 weeks) with tail blood sampling after 0.5, 1, 2, 4, 8 and 24 h. Organs and organ flushes (heart blood, liver, lung, spleen, kidney, brain, eye, bile, duodenum, jejunum, ileum, cecum, colon) were collected after 2 h, 4 h and 24 h. We

compared oral (p.o.; 10 mg/kg) with intravenous (i.v.; 2 mg/kg) application to determine bioavailability. Drug levels were determined with HPLC-MS/MS (Sci-ex API4500 coupled with an Agilent 1260 HPLC).

Classical approaches to calculate bioavailability are complicated by the very high volumes of distribution of the substances and the wide range of metabolites. To this end, we have calculated overall organ loads for the routes at various times (see also Supporting Information). To facilitate calculations, all values are expressed in nM, to ensure that levels of metabolites can be compared irrespective of molecular weight, and to allow comparison with in vitro activity studies.

Pharmacokinetics of 1a

Blood concentration decreased rapidly after i.v. and p.o. treatment. This is explained by fast distribution to tissue.[40] After 4 h blood concentrations were almost at baseline (p.o. 2 h). T_{max} of **1a** p.o. was 15 min and i.v. 30 minutes (precipitation after i.v. application can be ruled out).

In both p.o. and i.v. applications, the major analyte found in blood is **1a**, only minor amounts of the 4″OH were detected. Concentration values are similar, although the dose p.o. was five times higher (10 mg/kg p.o. vs. 2 mg/kg i.v.). This can be explained by high distribution to tissue after oral application (intestine and liver) before entering the blood compartment (intestinal flush values were generally low). After oral application as a solution (0.5% citric acid), **1a** must pass the gastrointestinal tract via, chylomicrons, lymph or blood or via the liver to enter the systemic circulation. In this process, it is exposed to different pH values in the stomach and intestine. Gastric pH in the mouse is moderate (pH 4), which stabilizes the esters (no enteric protection was applied) and is not sufficiently acidic to cleave the cladinose (a minor reaction in the human stomach). The small intestine of fasted mice has a pH of 5.0–5.2 and the colon a mean pH value of 4.4–4.7.[56] These pH levels are more acidic then in the human gut and could explain the quite slow hydrolysis rates observed in gut compartments. On the other hand, enzymes like trypsin, chymotrypsin, pepsin or various lipases could hydrolyze esters regardless of the pH values found there.[57]

Following i.v. and p.o. administration **1a** undergoes different metabolism patterns. Following i.v. application **1a** is stable with low levels of **1e**, (11-2′-DiBut). After oral administered **1a** is rapidly converted to **1e**, the 4″ de-esterification product. **1e** is the major substance detected in intestines and liver. It is also produced in the isolated mouse intestine in vitro. **1e** was also apparent in kidney, spleen, eye, brain, and lung at around the same amount as **1a**. Other metabolites are at lower levels. The main metabolite in in vitro stability studies, **1f** (11-4″-DiBut) was only found in minor concentrations in some organs (i.e. eye).

These data suggest that the tri-butyrate reaches the systemic circulation, but that in the liver and intestine, there is significant 4″ de-butyrylation activity. Given that the 4″ cleavage product is not apparent in organs like spleen or kidney following i.v. application, it is likely that where it is present p.o., it is derived from the gut or the liver. The dominance of the **1e** in the liver p.o. and its presence, i.v., suggests that it is also generated in the liver.

Intestines: Following i.v. application, the tri-butyrate **1a** was the dominant analyte in all intestine samples. **1e** was apparent in jejunum and ileum. In contrast, following p.o. application, **1e** was always dominant. The Jejunum and ileum had the most complex metabolite patterns. Jejunum had more **1c** (2′ ester) remaining, whereas, ileum had more **1b** (11-ester). This may reflect, in part, differing pH. In both cecum and colon, **1e** was dominant with some **1b** in cecum.

These data suggest two aspects of intestinal metabolism. The first is that contact to the intestine via lumen and mucosa results in more cleavage and that this is highest in jejunum and ileum. Transfer of **1a** to intestine from the blood following i.v. application is associated with much lower cleavage in terms of % total macrolide. This could be due to the overall higher levels (up to 10 μM), or it could be due to the presence of the enzyme responsible for cleaving the 4″ ester in the luminal secretions. Alternatively, it is possible that the enzymes present in the apical side of enterocytes differ from those in the basal membrane, and that contact to the luminal side following p.o. application changes the pattern observed.

As the stability results indicated that the ester bond at 4″-position is very stable, it is proposed that the cleavage is catalyzed by enzyme(s).

There are luminal, gut wall or mucosal enzymes in the GI tract which could contribute to the pre-systemic metabolism of a drug.[58] It might be that some of these enzymes can cleave the ester bond at the 4″-position better than those at the other positions, as these may not be as accessible to the enzymes due to steric or membrane binding effects.

While 4″ hydrolysis takes place in the liver following i.v. application, further transport to systemic circulation appears largely absent given that these organs have high levels of tri-ester but little or no amounts **1e**, the 4″ cleavage product.

To test whether the substances are hydrolyzed in gut compartments, various gut segments were removed from female BALB/c mice and incubated with compound. After 4 h, samples were taken and analyzed by HPLC-MS/MS.

The results of gut stability testing showed distinct hydrolysis pattern for different sections (Figure 4). The low pH value of stomach stabilizes the ester bonds and **1a** is largely not hydrolyzed (small amounts of **1g** can be found). Duodenum and ileum show minor hydrolyzation of **1a** to **1e**, **1f** and **1g**. Jejunum has the least amount of **1a** remaining and the highest concentration of **1e** and small amounts of **1b** and **1f**. Cecum and colon have higher tissue levels of **1c**, which was not found in luminal content or other compartments. These results suggest that the gut, and in particular, the jejunum, is responsible for metabolism following oral application.

To determine whether the enzyme responsible is luminal or tissue bound we assayed luminal contents separately for hydrolytic activity. These data suggest that hydrolysis is both luminal and tissue bound, that it is sensitive to competition from triglycerides, and is thus likely due to a secreted enzyme such as a pancreatic lipase.

ChemMedChem | Full Papers doi.org/10.1002/cmdc.202100139 | Chemistry Europe European Chemical Societies Publishing

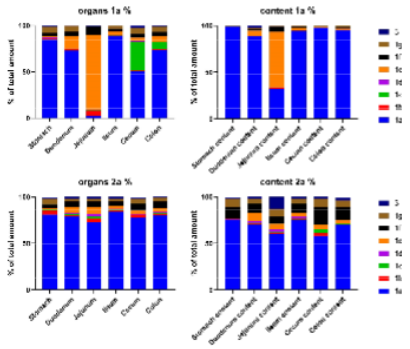

Figure 4. Gut compartments incubated with **1a** or **2a** for 4 h at 37 °C. Results show % metabolites to total amount of detected analyte concentration. Organs % displays tissue concentration of analytes in gut compartments. Content % displays concentration of analytes in intestinal fluids.

Contrary to many assumptions on ester fate, pH values in gut compartments were more stabilizing to the substances. The presence of diet and or tissue appeared to stabilize the substances on application.

Pharmacokinetics of 2a

The general observations for **1a** were also apparent as trends for **2a**, however, there were differences. The tri-propionate analog **2a** was more labile, generated more diverse products, was more systemic and lead to higher organ loads.

Blood concentration values decrease rapidly after i.v. and p.o. treatment. After 4 h blood concentrations almost declined to baseline. The C_{max} of **2a** p.o. was at 15 min, and at 30 min i.v. Following, p.o. applications, metabolites **2e**, **2f**, and **2b** were dominant. In i.v. treated mice **2f** was prominent.

Given that the patterns of metabolism for the propionate derivatives were more complex, they will be described in detail. All time courses of metabolite production are recorded in the Supporting Information.

Liver: Following i.v. treatment, the dominant liver metabolite is the 4″ position cleavage product **2e**. In blood, and other major organs, **2e** is relatively minor. This suggests that **2e** is formed in the liver and that it is not re-exported to other tissues at high rates. Cleavage of the 2′ position in liver appears to be faster given that the 11 position ester **2b** is the next most prominent product. Nonetheless, 2′ ester **2c** is also apparent suggesting an approximate 2-fold faster hydrolysis of 2′ vs. 11 position in the liver. The situation in the liver following p.o. application is much more complicated given that there is considerable conversion of the tri-ester in each gut segment. Thus, the liver content is almost certainly a function of both gut metabolites, and locally generated metabolites. **2a** is very low in the liver following oral application. Instead **2e** (2′, 11 ester) and **2b** (11 ester) predominate. That **2b** levels are similar to **2e** p.o., in contrast to the i.v. pattern, suggests that gut derived metabolites contribute to the overall liver pattern of metabolites.

Intestine: i.v. and p.o. application resulted in different patterns of **2a** metabolism in the gut that were more pronounced than those reported for **1a**. These were time and position dependent. To interpret time effects, it is important to bear in mind that the transit time of the mouse gut is of the order of 6 to 7 hours.[61]

At 120 min following i.v. application, **2a** was still dominant in the upper GI – duodenum, and in the colon. In other parts of the intestine, **2b** (11 prop) dominates at all times. The ileum appears to have the highest concentration of 2a and metabolites following i.v. application (ca. 3-fold higher total macrolide than other tissue) suggesting a tissue specific affinity for this class of substance. Detectable amounts of most analytes are present in the intestine at 24 h suggesting that they leave the tissue relatively slowly despite the food throughput.

In contrast, levels from p.o. application were uniformly higher consistent with the 5× higher dose and the quasi-topical application to the gut. At 120 min, the upper intestine had levels in the order of 10–15× higher total macrolides (150 μM) vs. i.v. and 10-fold the colon levels. By 24 h levels had declined in all tissues in the same proportion suggesting that remobilization along the intestine after uptake is limited.

Dominant metabolites varied along the intestine following p.o. application. In duodenum, **2g** (2′, 4″ prop) was most present. In jejunum, **2e** (2′, 11 prop) was dominant, in ileum and cecum, **2b** (11 prop) was the main product, while in colon it was **2e** and then **2b**. The lack of apparent mobility and the differing metabolites suggests that many are formed in the tissues and are not transported along the gut. To check this possibility in detail, the fluids resulting from the rinsing of the intestinal samples were also analyzed. In general, these were 4–5-fold less concentrated than the corresponding tissue sample. The luminal metabolite profile was generally not the same as the tissue profile (data not shown).

Spleen: Following i.v. application, **2a** appeared converted primarily to **2f** (11,4″ prop) which in turn appeared to convert to **2b** (11 props) with **2d** (4″ prop) at lower levels. Following p.o. application, the **2a** was present in similar amounts to **2e** (2′, 11 prop) which was apparently then converted to **2b** (11 prop) or **2c** (2′ prop). Another product, **2f** (11 4″ prop) was likely derived from **2a** in situ.

Kidney: Following i.v. application, **2a** appeared to convert to **2f** (11 4″ prop), preferentially to **2b** (11 prop) or then **2d** (4″ prop). Following p.o., the dominant metabolite was **2e** (2′ 11 prop), which converted equally to **2b** (11 prop) and **2c** (2′ prop). The other main metabolite, **2f** (11 4″ prop) could either derive from **2a** in situ or from other organs.

Eye: Following i.v. application the dominant metabolites in the eye are **2f** (11 4″ prop), **2b** (11 prop) and **2d** (4″ prop). Following p.o. the metabolites are dominated by **2b** (11 prop) followed by **2e** (2′ 11 prop), **2f** (11 4″ prop) with **2g** (4″ prop)

ChemMedChem | Full Papers doi.org/10.1002/cmdc.202100139 | Chemistry Europe European Chemical Societies Publishing

rising over time. The eye contains lysosomes with different properties to others in the body (degradation of visual pigments) and has a different pH in the vitreous.[62] These factors may explain the distinct metabolite profile in the eye.

Brain: Following i.v. application, the brain contains similar amounts of **2a** and **2f** (11 4" prop), suggesting that cleavage of 2' esters may occur in the brain. Following p.o. application, **2b** (11 prop), **2f** (11 4" prop), and **2e** (2' 11 prop) are similarly present, suggesting some transport of intestinal metabolites to the brain. Macrolides are generally considered not to cross the blood brain barrier due to their size and polar surface area.[63] These more hydrophobic derivatives may be more amenable to non-specific hydrophobic uptake routes. Given current interest in the gut brain axis, the delivery of SCFAs to microglia and astrocytes, or the stimulation of central lysosomes may also be beneficial and is being pursued by our group.[2,64]

Lung: Following i.v. application the order of prevalence of lung metabolites was **2f** (11 4" prop), **2b** (11 prop), **2a** (2' 11 4" prop), **2d** (4" prop), **2e** (2' 11 prop) and **2g** (4" prop). Following p.o. application, it was **2b** (11 prop) **2e** (2' 11 prop) and **2f** (11 4" prop).

These data suggest that also in the lung, gut or liver metabolites may be present following oral application changing the dominant metabolite. These distinctions are of interest because substances of this class appear to stimulate host defense functions in myeloid cells.[65,66] Lung tissue is exposed to pathogens and lung infection is a possible area of use of such substances. Levels in the lung following p.o. application were about half those of spleen, liver or kidney as opposed to approximately one fifth in i.v. application. These data suggest that the various esters have different partition properties in tissues and that the pattern of metabolites in the intestine influences tissue distribution.

The results of the gut stability testing for **2a** (Figure 4) showed no distinct hydrolysis pattern. The overall major compound detected was 2a and the major metabolites were 11 4" propionate **2f** and 2' 4" propionate **2g**. This leads to the assumption that the propionate ester is hydrolyzed nonspecifically in the gut compartments.

SCFA delivery

A key goal of this study was to determine the ability of the substances to deliver SCFAs to target cells and tissues. Using organ concentrations and the assumption that the large parts of the metabolites were generated locally, we arrived at an estimate of effective average tissue concentrations of 28–70 μM butyrate per hour delivered orally and 9–18 μM per hour via i.v. application. Free propionate delivered per hour orally can reach 142–388 μM per hour and i.v. 92–107 μM per hour.

These free SCFAs are mainly released in lysosomal compartments. Since these compartments only make up around 1–5% of the total volume of an immune cell, it is likely that any

Figure 5. Schematic representation of the different routes of metabolism of **1a** (left) and **2a** (right) in the intestinal segments after oral administration. The arrows shown represent relative amounts of the detected substances within an intestinal section. Whilst **1a** is relatively stable and hydrolyses mainly in the intestine at the 4" position, **2a** shows a much greater and broader hydrolysis behaviour.

ChemMedChem | Full Papers doi.org/10.1002/cmdc.202100139 | Chemistry Europe European Chemical Societies Publishing

receptor in these membranes will be exposed to higher concentrations than the average tissue concentration.

For example, the lung had an apparent macrolide load of 30 μM at 2 h with 66% of the original SFA still present suggesting that 10 μM SCFA had been delivered. This corresponds to a lysosomal concentration of ca. 1 mM, or 0,5 mM/h. This is in a range sufficient to activate FFAR2/3 if it is present in or near the lysosome.[16]

A similar calculation for the jejunum yields ca. 120 μM macrolides at 2 h, again ca. 66% SCFA still present, or 40 μM SCFA delivered corresponding to ca. 4 mM in the putative lysosomes or 2 mM/h. The exact lysosomal volume varies and the sensitivity of the putative intracellular receptors is not known. Nonetheless, these data suggest that in the dose range employed in vivo (0.1 to 3 μmol/kg), there will be sufficient SCFA delivered to the lysosome to yield transient interaction with the receptors.

Conclusion

Macrolides such as Azithromycin can be adapted to carry SCFAs. The multi-esterified macrolides are able to deliver SCFAs to cytoplasmic compartments in immune and epithelial cells and to mimic signaling processes as they release SCFAs. The cytoplasmic and lysosomal delivery of SCFAs probably simulates the presence of anaerobic bacteria and acts as a mild immune stimulant.

These tri-esters exhibit similar general pharmacokinetics to those of Azithromycin but vary in the patterns of metabolite formation and distribution depending on route of administration and tissue in which they are absorbed (figure 5 and figure 6).

In a general sense, the esters would be expected to hydrolyze chemically in all settings, however, this is not the case. The 4'' ester appears to require enzymatic cleavage. The 2' and 11 esters were more labile to chemical hydrolysis in solution but were much less labile in biological matrices. Both acidic compartments and membranes probably protect the esters *in vivo* and in cells.

Butyrate derivatives were more hydrophobic, less soluble, less distributed and less labile than corresponding propionate derivatives. While both the tri-butyrate (**1a**) and tri-propionate (**2a**) had similar properties, the propionates were associated with higher uptake, metabolic diversity and systemic distribution than the butyrates.

While it is expected that delivery of butyrates and propionates may signal similarly in some circumstances, differences in distribution, affinity for FFARs and rate of donation may all cause the molecules to have different profiles in disease settings.

While we have used Azithromycin as a carrier for this study, there are other macrolides that are not anti-bacterial molecules that are able to perform the same task as Azithromycin. Thus, although Azithromycin itself was only observed at very low levels, this may be an issue in resistance management and its use in therapies of this kind may be seen as impractical. Thus, we have prepared analogs that are not be directly antibacterial and that fulfill the same properties and effects as substances reported here.

The therapeutic goal of the compounds described here is to modulate barrier function and the immune response by simulating the presence of anaerobic organisms in the lysosomal compartment. The pharmacokinetic data suggest that for both propionate and butyrate derivatives, the effect will be systemic but that butyrates will be more active in the gut relative to other organs. The amounts, the rate of de-esterification and the distribution suggest that they can both deliver sustained pulses of intracellular/lysosomal SCFAs in a range adequate to activate receptors. These observations provide a rationale for the reported activity of this compound class.

Experimental Section

Synthesis

All reagents and solvents were purchased from commercial sources and used as received. Reaction progress was monitored with mass spectra (Finnigan LCQ Deca XP MAX, Software Xcalibur 2.0.7 SP1) and via TLC (Merck TLC Silica gel 60 F254). Spots were visualized with Hanessian's stain, based on a Cerium Molybdate solution and heat. ^{1}H-NMR spectra were recorded with a Bruker Avance 400 (400 MHz) or Bruker (300 MHz). ^{13}C-NMR spectra were recorded with a Bruker or Bruker (75 MHz). Spectra were recorded in $CDCl_3$ solution and chemical shifts (ppm) were referenced to solvent. Coupling constants (*J*) are given in Hz. Solvents were evaporated with rotary evaporator (RV8 IKA, KNF SC 920) operating at reduced pressure. Flash chromatography was carried out with Interchim puriFlash 5.020 with Interchim PF-15SIHP–F0040 or PF-50SIHP–F0040 columns. Purity studies were performed with HPLC set up from Varian (ProStar) and ELS detection (Sedere Sedex 80). Mobile phase: water (0.05% formic acid)/methanol (0.05% formic acid). Stationary phase: Dr. Maisch ReproSil-Pur 120 C18-AQ, 5 μm, 75×3 mm. HRMS measurements were made using a Bruker maXis 4G ESI-TOF from Daltonik [JL1], using ESI+ mode and the following settings: Capillary voltage 4.5 kV, source temperature 200 °C, gas flow 6 l/min, nebulizer gas pressure 1.2 bar, end plate offset −0.5 kV and an m/z range of 100 to 1350 m/z.

1a (2S,3S,4R,6R)-6-(((2R,3R,4R,5R,8R,10R,11R,12S,13S,14R)-4-(butyryloxy)-11-(((2S,3R,4R,6R)-3-(butyryloxy)-4-(dimethylamino)-6-methyltetrahydro-2H-pyran-2-yl)oxy)-2-ethyl-3,10-dihydroxy-3,5,6,8,10,12,14-heptamethyl-15-oxo-1-oxa-6-azacyclopentadecan-13-yl)oxy)-4-methoxy-2,4-dimethyltetrahydro-2H-pyran-3-yl butyrate, ^{1}H NMR (600 MHz, $CDCl_3$) δ 5.07 (d, *J*=6.2 Hz, 1H), 4.97 (d, *J*=8.9 Hz, 1H), 4.90 (d, *J*=4.6 Hz, 1H), 4.81 (t, 1H), 4.70 (d, *J*=9.8 Hz, 1H), 4.56 (d, *J*=7.0 Hz, 1H), 4.41 (dq, *J*=12.5, 6.1 Hz, 1H), 4.20 (t, *J*=5.0 Hz, 2H), 3.61 (s, 1H), 3.48 (d, *J*=4.4 Hz, 1H), 3.38–3.33 (m, 1H), 3.31 (s, 3H), 2.65 (dt, *J*=13.9, 7.1 Hz, 2H), 2.39–2.33 (m, 3H), 2.31 (q, *J*=13.4, 6.3 Hz, 5H), 2.23 (d, *J*=7.4 Hz, 7H), 2.13 (t, 1H), 1.96 (s, 1H), 1.85–1.75 (m, 3H), 1.72–1.55 (m, 10H), 1.42 (s, 2H), 1.33 (dd, *J*=24.2, 12.3 Hz, 1H), 1.27 (d, *J*=7.2 Hz, 3H), 1.22 (d, *J*=6.1 Hz, 3H), 1.18–1.13 (m, 8H), 1.10 (s, 3H), 1.03–0.84 (m, *J*=26.9, 19.5, 13.4, 6.6 Hz, 23H), ^{13}C NMR (151 MHz, $CDCl_3$) δ 176.39, 173.51, 173.19, 172.73, 101.29, 97.49, 84.03, 81.01, 78.56, 77.37, 77.16, 76.95, 76.21, 75.94, 74.11, 73.20, 71.39, 69.17, 63.61, 63.30, 61.19, 49.86, 45.66, 42.95, 40.79, 36.51, 36.48, 36.36, 36.02, 30.85, 29.83, 27.55, 27.05, 25.08, 24.30, 21.82, 21.43, 21.12, 18.73, 18.49, 18.45, 17.70, 14.42, 13.89, 13.84, 13.65, 12.00, 11.60, 8.20, HRMS *m/z* calcd for $C_{50}H_{91}N_2O_{15}^+$:

ChemMedChem | Full Papers doi.org/10.1002/cmdc.202100139 | Chemistry Europe European Chemical Societies Publishing

959.64140, found: 959.64079, colorless solid, yield 2580 mg (33.6%), purity 99.7% via HPLC-ELSD, **3** (6.0 g, 8.0 mmol) was dissolved in butyric acid subsequently 3 eq of butyric anhydride was added. Solution was stirred at room temperature (RT). Progress was detected via TLC and MS. After four days a catalytic amount 4-dimethylaminopyridine (DMAP) and 3 eq butyric anhydride was added. Work up was done after five days, when sufficient product was detected. To extract product liquid-liquid extraction was performed. First with citric acid solution (5%, 3x), then citric acid solution was washed with ethyl acetate. Acidic solution was neutralized with sodium carbonate and macrolide transferred into organic phase (ethyl acetate) with liquid-liquid extraction three times. Organic phases were combined and washed with brine/water two times, dried with sodium sulphate and solvent evaporated. Afterwards residue was purified by flash chromatography (stationary phase: silica gel, 2.5 µm, Ø = 3 cm, h = 14 cm, mobile phase: cyclohexane/acetone with triethylamine) to carry out white solid powder. As a side product in the purification step 2000 mg of **1e** was obtained.

1b (2S,3R,4R,6R)-2-(((2R,3R,4R,5R,8R,10R,11R,12S,13S,14R)-4-(butyryloxy)-2-ethyl-3,10-dihydroxy-13-(((2R,4R,5S,6S)-5-hydroxy-4-methoxy-4,6-dimethyltetrahydro-2H-pyran-2-yl)oxy)-3,5,6,8,10,12,14-heptamethyl-15-oxo-1-oxa-6-azacyclopentadecan-11-yl)oxy)-4-(dimethylamino)-6-methyltetrahydro-2H-pyran-3-yl butyrate, ^{1}H NMR (300 MHz, $CDCl_3$) δ 7.26 (s, 1H), 5.04 (d, J = 9.4 Hz, 1H), 4.98 (dd, J = 9.9, 2.9 Hz, 1H), 4.88 (d, J = 4.5 Hz, 1H), 4.35 (d, J = 7.3 Hz, 1H), 4.21 (t, 1H), 4.08 (td, J = 12.4, 6.1 Hz, 1H), 3.59 (dd, J = 9.4, 6.1 Hz, 2H), 3.50 (d, J = 2.9 Hz, 1H), 3.46–3.37 (m, 1H), 3.33 (dd, J = 7.3, 2.7 Hz, 1H), 3.28 (d, J = 5.1 Hz, 3H), 3.05–2.95 (m, 1H), 2.66–2.50 (m, 2H), 2.37–2.26 (m, 9H), 2.24 (s, 3H), 2.20–2.09 (m, 1H), 1.99 (d, J = 22.9 Hz, 2H), 1.84–1.72 (m, 2H), 1.66 (dd, J = 14.8, 7.3 Hz, 3H), 1.59–1.47 (m, 2H), 1.34 (d, J = 13.8 Hz, 1H), 1.29 (s, 3H), 1.26 (s, 3H), 1.24 (s, 3H), 1.22 (s, 2H), 1.20 (s, 2H), 1.20 (s, 3H), 1.18 (s, 3H), 1.11 (d, J = 7.1 Hz, 3H), 1.06 (d, J = 6.5 Hz, 3H), 0.96 (t, J = 7.4 Hz, 3H), 0.91 (s, 1H), 0.88 (s, 3H), 0.85 (s, 2H), ^{13}C NMR (75 MHz, $CDCl_3$) δ 176.07, 173.21, 105.48, 97.32, 80.11, 78.05, 77.58, 77.16, 76.74, 75.91, 75.80, 74.07, 72.90, 70.62, 69.83, 65.90, 65.14, 61.42, 49.52, 46.01, 43.33, 41.07, 40.55, 36.46, 35.30, 29.27, 28.47, 25.56, 24.27, 21.74, 21.53, 21.19, 18.45, 18.09, 14.16, 13.88, 11.93, 11.75, 8.50, HRMS *m/z* calcd for $C_{42}H_{79}N_2O_{13}^+$: 819.55767, found: 819.55840, white solid, yield 100 mg (35.2%), purity 98.5% via HPLC-ELSD, **1e** (200 mg, 0.23 mmol) was dissolved in methanol and stirred at room temperature. After two days solvents were evaporated. The residue was purified by flash chromatography (stationary phase: silica gel, 2.5 µm, Ø = 3 cm, h = 14 cm, mobile phase: cyclohexane/chloroform/isopropanol/ammonia in methanol) to carry out white solid powder.

1c (2S,3R,4R,6R)-4-(dimethylamino)-2-(((2R,3S,4R,5R,8R,10R,11R,12S,13S,14R)-2-ethyl-3,4,10-trihydroxy-13-(((2R,4R,5S,6S)-5-hydroxy-4-methoxy-4,6-dimethyltetrahydro-2H-pyran-2-yl)oxy)-3,5,6,8,10,12,14-heptamethyl-15-oxo-1-oxa-6-azacyclopentadecan-11-yl)oxy)-6-methyltetrahydro-2H-pyran-3-yl butyrate, ^{1}H NMR (600 MHz, $CDCl_3$) δ 5.10 (d, J = 4.7 Hz, 1H), 4.78 (dd, J = 10.5, 7.6 Hz, 1H), 4.69 (dd, J = 9.7, 2.2 Hz, 1H), 4.54 (d, J = 7.5 Hz, 1H), 4.22 (dd, J = 4.3, 1.9 Hz, 1H), 4.04 (dq, J = 9.2, 6.3 Hz, 1H), 3.68 (s, 1H), 3.58 (d, J = 7.1 Hz, 1H), 3.54–3.47 (m, 1H), 3.36 (s, 3H), 3.34–3.28 (m, 1H), 3.03 (d, J = 9.3 Hz, 1H), 2.75–2.68 (m, 2H), 2.65 (d, J = 9.4 Hz, 1H), 2.51 (d, J = 10.1 Hz, 1H), 2.37–2.27 (m, 5H), 2.25 (d, J = 4.5 Hz, 6H), 2.22 (dd, J = 15.8, 7.6 Hz, 2H), 2.07 (s, 1H), 1.98 (d, J = 7.5 Hz, 1H), 1.94–1.84 (m, 2H), 1.73 (d, J = 12.5 Hz, 1H), 1.70–1.61 (m, 4H), 1.61–1.55 (m, 1H), 1.50–1.41 (m, 1H), 1.32 (d, J = 6.3 Hz, 3H), 1.30 (s, 3H), 1.25 (s, 3H), 1.22 (d, 3H), 1.19 (d, J = 7.5 Hz, 3H), 1.17 (s, 1H), 1.09 (d, J = 6.7 Hz, 3H), 1.06 (s, 3H), 0.98–0.92 (m, 5H), 0.90 (dd, J = 9.9, 5.7 Hz, 4H), 0.87 (dd, J = 7.7, 1.5 Hz, 6H), ^{13}C NMR (151 MHz, $CDCl_3$) δ 178.53, 177.23, 172.70, 172.56, 101.53, 100.75, 94.77, 83.19, 78.29, 78.13, 77.95, 77.54, 77.37, 77.16, 76.95, 74.42, 74.28, 73.93, 73.76, 73.19, 72.96, 71.51, 71.26, 70.15, 69.33, 68.33, 65.80, 65.74, 63.88, 63.51, 62.72, 49.53, 49.49, 45.33, 42.12, 42.03, 40.64, 36.62, 36.60, 36.46, 35.36, 34.92, 30.83, 30.59, 27.46, 26.77, 22.09, 21.77, 21.44, 21.36, 21.04, 18.64, 18.45, 18.41, 18.35, 16.37, 14.92, 14.30, 13.90, 13.88, 13.69, 11.99, 11.39, 9.08, 8.19, 7.63, HRMS *m/z* calcd for $C_{42}H_{79}N_2O_{13}^+$: 819.55767, found: 819.55847, white solid, yield 966 mg (22.1%), purity 99.7% via HPLC-ELSD, 3 (4000 mg, 5.34 mmol) was dissolved in DCM. To this solution 1 eq of triethylamine was added. Afterwards 2.2 eq of butyric anhydride was added dropwise. Solution was stirred at room temperature. Reaction was monitored via TLC and MS. Work up was done after two days, when sufficient product was detected. To extract product liquid-liquid extraction was performed. First with citric acid solution (5%, 3x), then citric acid solution was washed with ethyl acetate. Acidic solution was neutralized with sodium carbonate and macrolide transferred into organic phase (ethyl acetate) with liquid-liquid extraction three times. Organic phases were combined and washed with brine/water two times, dried with sodium sulphate and solvent evaporated. To obtained residue was purified by flash chromatography (stationary phase: Interchim C18, 2.5 µm, Ø = 2.5 cm, h = 14 cm, mobile phase: water/methanol with formic acid) to carry out white solid powder.

1d (2S,3S,4R,6R)-6-(((2R,3S,4R,5R,8R,10R,11R,12S,13S,14R)-11-(((2S,3R,4R,6R)-4-(dimethylamino)-3-hydroxy-6-methyltetrahydro-2H-pyran-2-yl)oxy)-2-ethyl-3,4,10-trihydroxy-3,5,6,8,10,12,14-heptamethyl-15-oxo-1-oxa-6-azacyclopentadecan-13-yl)oxy)-4-methoxy-2,4-dimethyltetrahydro-2H-pyran-3-yl butyrate, ^{1}H NMR (600 MHz, $CDCl_3$) δ 5.19 (d, J = 4.9 Hz, 1H), 5.05 (d, J = 4.8 Hz, 1H), 4.69 (dd, J = 9.8, 2.5 Hz, 2H), 4.56 (d, J = 7.4 Hz, 1H), 4.42 (dt, J = 12.5, 6.2 Hz, 1H), 4.25 (dd, J = 3.8, 2.0 Hz, 1H), 3.82–3.76 (m, 1H), 3.68 (d, J = 4.7 Hz, 1H), 3.61 (d, J = 7.2 Hz, 1H), 3.39 (s, 1H), 3.31 (s, 3H), 3.23 (dd, J = 10.2, 7.4 Hz, 1H), 2.98 (s, 1H), 2.75 (ddd, J = 14.9, 7.4, 4.0 Hz, 2H), 2.68 (dd, J = 13.5, 6.6 Hz, 2H), 2.56–2.52 (m, 2H), 2.39 (d, J = 15.2 Hz, 1H), 2.37–2.31 (m, J = 15.3, 7.7 Hz, 1H), 2.30 (d, J = 1.9 Hz, 7H), 2.29–2.24 (m, 1H), 2.04 (d, J = 11.4 Hz, 1H), 2.02–1.95 (m, 2H), 1.89 (dtd, J = 10.2, 7.6, 2.6 Hz, 1H), 1.76 (d, J = 14.7 Hz, 1H), 1.71–1.60 (m, 4H), 1.45 (ddd, J = 14.5, 9.8, 7.3 Hz, 1H), 1.42 (s, 6H), 1.29 (s, 3H), 1.19 (dd, J = 6.7, 3.2 Hz, 6H), 1.16 (d, J = 6.2 Hz, 3H), 1.09 (d, J = 5.9 Hz, 6H), 1.08 (s, 1H), 1.05 (d, J = 7.6 Hz, 3H), 0.96 (t, J = 7.4 Hz, 3H), 0.90–0.89 (m, 3H), 0.88 (d, J = 7.5 Hz, 2H), ^{13}C NMR (151 MHz, $CDCl_3$) δ 179.08, 173.37, 102.52, 94.80, 83.37, 78.69, 77.83, 77.58, 77.37, 77.16, 76.95, 74.37, 73.76, 73.07, 71.11, 70.25, 67.99, 65.70, 63.22, 62.64, 49.57, 46.07, 45.34, 42.34, 40.49, 36.37, 35.09, 29.08, 27.69, 27.04, 26.92, 22.09, 21.94, 21.44, 18.61, 17.93, 16.32, 14.68, 13.85, 11.40, 9.18, 7.48, HRMS *m/z* calcd for $C_{42}H_{79}N_2O_{13}^+$: 819.55767, found: 819.55803, white solid, yield 1540 mg (50.3%), purity 98.7% via HPLC-ELSD, **3** (3.0 g; 4.0 mmol) was dissolved in pyridine subsequently 4 eq of butyryl chloride was added to the ice cold solution dropwise. Solution was stirred at room temperature (RT). Progress was detected via TLC and MS. Work up was done after two days, when sufficient product was detected. To extract product liquid-liquid extraction was performed. First with citric acid solution (5%, 3x), then citric acid solution was washed with ethyl acetate. Acidic solution was neutralized with sodium carbonate and macrolide transferred into organic phase (ethyl acetate) with liquid-liquid extraction three times. Organic phases were combined and washed with brine/water two times, dried with sodium sulphate and solvent evaporated. Afterwards residue was purified by flash chromatography (stationary phase: silica gel, 2.5 µm, Ø = 3 cm, h = 14 cm, mobile phase: cyclohexane/acetone with triethylamine) to carry out white solid powder. As a side product in the purification step 1400 mg of **1g** was obtained.

1e (2S,3R,4R,6R)-2-(((2R,3R,4R,5R,8R,10R,11R,12S,13S,14R)-4-(butyryloxy)-2-ethyl-3,10-dihydroxy-13-(((2R,4R,5S,6S)-5-hydroxy-4-meth-

oxy-4,6-dimethyltetrahydro-2H-pyran-2-yl)oxy)-3,5,6,8,10,12,14-heptamethyl-15-oxo-1-oxa-6-azacyclopentadecan-11-yl)oxy)-4-(dimethylamino)-6-methyltetrahydro-2H-pyran-3-yl butyrate, ^{1}H NMR (600 MHz, $CDCl_3$) δ 5.08 (d, J=8.5 Hz, 1H), 4.98 (d, J=8.6 Hz, 1H), 4.82 (dd, J=19.6, 6.7 Hz, 2H), 4.51 (d, J=7.5 Hz, 1H), 4.21 (t, J=4.8 Hz, 1H), 4.03 (dq, J=12.6, 6.2 Hz, 1H), 3.57 (dd, J=10.2, 5.7 Hz, 1H), 3.48 (d, J=4.7 Hz, 1H), 3.39–3.32 (m, 1H), 3.30 (d, J=7.6 Hz, 3H), 3.01 (t, J=9.9 Hz, 1H), 2.65 (dd, J=12.5, 6.7 Hz, 2H), 2.36–2.27 (m, 7H), 2.27–2.19 (m, 9H), 2.14 (dd, J=20.9, 11.7 Hz, 1H), 1.96 (s, 1H), 1.84–1.74 (m, 3H), 1.74–1.57 (m, 8H), 1.53 (dd, J=15.1, 4.8 Hz, 1H), 1.42 (s, 2H), 1.30 (d, J=6.3 Hz, 3H), 1.27 (d, J=7.2 Hz, 3H), 1.25–1.22 (m, 6H), 1.16 (d, J=3.5 Hz, 6H), 1.02 (d, J=6.5 Hz, 3H), 0.97 (dd, J=13.8, 6.4 Hz, 6H), 0.94 (t, J=6.5 Hz, 3H), 0.89 (d, J=7.3 Hz, 2H), 0.87–0.85 (m, 4H), ^{1}H NMR (600 MHz, $CDCl_3$) δ 7.26, 5.09, 5.08, 4.98, 4.97, 4.84, 4.84, 4.81, 4.80, 4.52, 4.51, 4.21, 4.21, 4.20, 4.05, 4.04, 4.03, 4.03, 4.01, 4.00, 3.67, 3.58, 3.57, 3.56, 3.55, 3.48, 3.47, 3.38, 3.36, 3.35, 3.35, 3.34, 3.32, 3.31, 3.30, 3.03, 3.01, 3.00, 2.67, 2.65, 2.64, 2.63, 2.38, 2.35, 2.34, 2.32, 2.31, 2.30, 2.29, 2.28, 2.26, 2.24, 2.22, 2.17, 2.15, 2.14, 2.12, 2.09, 2.07, 1.96, 1.80, 1.79, 1.78, 1.72, 1.71, 1.70, 1.68, 1.67, 1.66, 1.65, 1.65, 1.64, 1.64, 1.63, 1.63, 1.63, 1.62, 1.61, 1.61, 1.58, 1.56, 1.55, 1.54, 1.53, 1.52, 1.42, 1.41, 1.39, 1.37, 1.35, 1.33, 1.30, 1.29, 1.27, 1.26, 1.25, 1.24, 1.23, 1.22, 1.20, 1.19, 1.16, 1.16, 1.14, 1.12, 1.12, 1.11, 1.10, 1.08, 1.06, 1.06, 1.05, 1.04, 1.02, 1.01, 0.98, 0.97, 0.96, 0.95, 0.95, 0.94, 0.93, 0.91, 0.90, 0.88, 0.87, 0.86, 0.85, 0.83, 0.06, HRMS *m/z* calcd for $C_{46}H_{85}N_2O_{14}^+$: 889.59953, found: 889.60014, white solid, yield 2000 mg (28.1%), purity 95.6% via HPLC-ELSD$_u$ as side product in synthesis of **1a**.

1f (2S,3S,4R,6R)-6-(((2R,3R,4R,5R,8R,10R,11R,12S,13S,14R)-4-(butyryloxy)-11-(((2S,3R,4R,6R)-4-(dimethylamino)-3-hydroxy-6-methyltetrahydro-2H-pyran-2-yl)oxy)-2-ethyl-3,10-dihydroxy-3,5,6,8,10,12,14-heptamethyl-15-oxo-1-oxa-6-azacyclopentadecan-13-yl)oxy)-4-methoxy-2,4-dimethyltetrahydro-2H-pyran-3-yl butyrate, ^{1}H NMR (600 MHz, $CDCl_3$) δ 5.05 (d, J=9.2 Hz, 1H), 4.96 (dd, J=10.4, 2.4 Hz, 1H), 4.93 (d, J=4.8 Hz, 1H), 4.69 (dd, J=9.8, 5.3 Hz, 1H), 4.45 (tt, J=10.3, 5.1 Hz, 2H), 4.37 (d, J=7.3 Hz, 1H), 4.22 (t, 1H), 3.65–3.57 (m, 2H), 3.47 (d, J=2.2 Hz, 1H), 3.42 (d, J=7.3 Hz, 1H), 3.31 (t, J=5.2 Hz, 1H), 3.30 (s, 3H), 2.65–2.56 (m, 2H), 2.36 (ddd, J=15.7, 12.3, 8.2 Hz, 3H), 2.30 (dd, J=9.5, 5.0 Hz, 9H), 2.24 (s, 3H), 2.16 (dd, J=12.3, 8.2 Hz, 1H), 1.67 (pd, J=7.4, 2.5 Hz, 6H), 1.63–1.59 (m, 1H), 1.53 (d, J=13.7 Hz, 1H), 1.42 (s, 3H), 1.28 (d, J=7.4 Hz, 4H), 1.22 (d, J=6.1 Hz, 3H), 1.17 (d, J=3.0 Hz, 6H), 1.12 (dd, J=6.7, 3.5 Hz, 6H), 1.09 (s, 3H), 1.05 (d, J=6.6 Hz, 3H), 0.95 (dd, J=14.2, 7.3 Hz, 7H), 0.89–0.85 (m, 7H), ^{13}C NMR (151 MHz, $CDCl_3$) δ 176.20, 173.54, 173.15, 105.18, 102.49, 97.39, 94.82, 86.73, 81.46, 80.05, 78.69, 78.48, 77.85, 77.57, 77.37, 77.16, 76.95, 75.87, 75.82, 74.38, 73.84, 73.75, 73.20, 73.07, 71.11, 70.60, 69.70, 67.98, 65.69, 65.07, 63.44, 63.21, 61.44, 49.96, 49.56, 46.04, 45.95, 43.69, 41.21, 40.55, 36.45, 36.36, 36.31, 36.05, 35.10, 29.40, 28.54, 28.31, 27.04, 26.91, 25.20, 24.34, 22.09, 21.92, 21.58, 21.43, 21.33, 21.21, 18.72, 18.60, 18.44, 17.93, 17.41, 16.31, 14.71, 14.34, 13.88, 13.85, 13.82, 11.97, 11.40, 8.45, HRMS *m/z* calcd for $C_{46}H_{85}N_2O_{14}^+$: 889.59953, found: 889.59950, white solid, yield 222 mg (34.2%), purity 96.7% via HPLC-ELSD, **1a** (700 mg, 0.73 mmol) was dissolved in methanol and stirred at room temperature for three days. Solvents were evaporated to obtain white powder. Residue was purified via column chromatography (solid phase: silica gel 60–200 μm, mobile phase: chloroform/isopropanol/ammonia in methanol) to carry out white solid powder.

1g (2S,3S,4R,6R)-6-(((2R,3S,4R,5R,8R,10R,11R,12S,13S,14R)-11-(((2S,3R,4R,6R)-3-(butyryloxy)-4-(dimethylamino)-6-methyltetrahydro-2H-pyran-2-yl)oxy)-2-ethyl-3,4,10-trihydroxy-3,5,6,8,10,12,14-heptamethyl-15-oxo-1-oxa-6-azacyclopentadecan-13-yl)oxy)-4-methoxy-2,4-dimethyltetrahydro-2H-pyran-3-yl butyrate, ^{1}H NMR (300 MHz, $CDCl_3$) δ 5.03 (d, J=4.7 Hz, 1H), 4.75–4.56 (m, 4H), 4.32 (dd, J=9.7, 6.2 Hz, 1H), 4.20 (d, J=6.3 Hz, 1H), 4.14 (d, J=3.7 Hz, 1H), 3.69 (dd, J=9.7, 5.8 Hz, 1H), 3.58 (d, J=5.6 Hz, 1H), 3.51 (d, J=6.6 Hz, 1H), 3.28 (s, 3H), 2.76–2.68 (m, 2H), 2.60 (dt, J=12.2, 6.2 Hz, 2H), 2.42 (d, J=10.2 Hz, 1H), 2.36–2.26 (m, 3H), 2.24 (s, 3H), 2.19 (s, 6H), 2.02–1.80 (m, 4H), 1.65–1.53 (m, 7H), 1.36 (s, 4H), 1.21 (s, 3H), 1.17–1.07 (m, 11H), 1.02 (dd, J=11.7, 4.7 Hz, 9H), 0.90 (dt, J=7.4, 3.7 Hz, 6H), 0.86–0.81 (m, 9H), ^{13}C NMR (75 MHz, $CDCl_3$) δ 178.64, 173.33, 172.53, 149.75, 124.07, 100.34, 95.19, 83.40, 78.65, 78.37, 77.70, 77.58, 77.36, 77.16, 76.74, 74.54, 74.45, 73.72, 73.07, 71.85, 70.28, 67.51, 63.79, 63.22, 62.27, 49.41, 45.06, 42.06, 41.27, 40.83, 36.73, 36.58, 36.38, 35.29, 30.79, 27.39, 27.03, 26.79, 21.99, 21.73, 21.44, 21.28, 18.61, 18.49, 18.02, 16.27, 15.24, 13.84, 13.64, 11.35, 9.26, 7.67, HRMS *m/z* calcd for $C_{46}H_{85}N_2O_{14}^+$: 889.59953, found: 889.60009, white solid, yield 1400 mg (19.6%), purity 98.2% via HPLC-ELSD, as side product in synthesis of **1d**.

2a (2S,3R,4S,6R)-4-(dimethylamino)-2-(((2R,3R,4R,5R,8R,10R,11R,12S,13S,14R)-2-ethyl-3,10-dihydroxy-13-(((2R,4R,5S,6S)-4-methoxy-4,6-dimethyl-5-(propionyloxy)tetrahydro-2H-pyran-2-yl)oxy)-3,5,6,8,10,12,14-heptamethyl-15-oxo-4-(propionyloxy)-1-oxa-6-azacyclopentadecan-11-yl)oxy)-6-methyltetrahydro-2H-pyran-3-yl propionate, ^{1}H NMR (300 MHz, $CDCl_3$) δ 5.05 (d, J=8.6 Hz, 1H), 4.96 (dd, J=10.3, 2.3 Hz, 1H), 4.88 (d, J=4.5 Hz, 1H), 4.80 (dd, J=10.4, 7.7 Hz, 1H), 4.69 (d, J=9.8 Hz, 1H), 4.54 (d, J=7.5 Hz, 1H), 4.39 (dd, J=9.7, 6.3 Hz, 1H), 4.18 (t, J=5.2 Hz, 1H), 3.60 (dd, J=9.8, 5.8 Hz, 1H), 3.46 (d, J=4.3 Hz, 1H), 3.34 (d, J=9.0 Hz, 1H), 3.30 (s, 3H), 2.75–2.58 (m, 2H), 2.44–2.28 (m, 8H), 2.22 (d, J=4.5 Hz, 8H), 2.18–2.04 (m, 2H), 1.95 (s, 1H), 1.84–1.54 (m, 6H), 1.29–1.03 (m, 30H), 0.99 (dd, J=8.7, 7.1 Hz, 6H), 0.86 (dd, J=11.6, 6.9 Hz, 7H), ^{13}C NMR (75 MHz, $CDCl_3$) δ 176.37, 174.36, 173.93, 173.55, 101.30, 97.51, 84.04, 78.58, 77.58, 77.37, 77.16, 76.74, 76.24, 75.93, 74.05, 73.18, 71.51, 69.14, 63.52, 63.27, 61.16, 49.83, 45.62, 42.97, 40.83, 35.98, 31.14, 27.86, 27.71, 24.97, 24.27, 21.78, 21.36, 21.07, 17.62, 14.44, 11.95, 11.51, 9.44, 9.25, 9.21, 8.11, HRMS *m/z* calcd for $C_{47}H_{85}N_2O_{15}^+$: 917.59445, found: 917.59477, white solid, yield 1449 mg (23.7%), purity 97.9% via HPLC-ELSD, **3** (5000 mg, 6.67 mmol) was dissolved in DCM, 1.1 eq pyridine was added and then cooled with ice. Afterwards 1.1 eq propionic anhydride was added dropwise to the solution. Solution was stirred at room temperature and reaction monitored via TLC and MS. After 12 h 1.1 eq of pyridine and propionic anhydride was added. This was repeated after a week and 12 days. After three weeks solution was washed with saturated sodium bicarbonate solution, water and brine (each 3x), dried with sodium sulphate and solvent evaporated. Residue was purified via column chromatography (solid phase: silica gel 60–200 μm, mobile phase: chloroform/isopropanol/ammonia in methanol) to carry out white solid powder. As a side product in the purification step 1870 mg of **2e** was obtained.

2b (2R,3R,4R,5R,8R,10R,11R,12S,13S,14R)-11-(((2S,3R,4S,6R)-4-(dimethylamino)-3-hydroxy-6-methyltetrahydro-2H-pyran-2-yl)oxy)-2-ethyl-3,10-dihydroxy-13-(((2R,4R,5S,6S)-5-hydroxy-4-methoxy-4,6-dimethyltetrahydro-2H-pyran-2-yl)oxy)-3,5,6,8,10,12,14-heptamethyl-15-oxo-1-oxa-6-azacyclopentadecan-4-yl propionate, ^{1}H NMR (300 MHz, $CDCl_3$) δ 4.98 (d, J=9.4 Hz, 1H), 4.92 (d, J=9.9 Hz, 1H), 4.82 (d, J=4.5 Hz, 1H), 4.29 (d, J=7.3 Hz, 1H), 4.19–4.12 (m, 1H), 4.02 (td, J=12.5, 6.2 Hz, 1H), 3.61 (d, J=9.7 Hz, 1H), 3.53 (dd, J=10.7, 6.2 Hz, 1H), 3.45 (s, 1H), 3.39–3.32 (m, 1H), 3.30–3.24 (m, 1H), 3.21 (s, 3H), 3.17 (s, 1H), 2.94 (d, J=9.3 Hz, 1H), 2.60–2.43 (m, 3H), 2.29 (dd, J=15.2, 7.6 Hz, 3H), 2.23 (s, 7H), 2.18 (s, 3H), 2.16–2.05 (m, 2H), 1.90 (d, J=6.8 Hz, 1H), 1.74 (d, J=4.5 Hz, 1H), 1.70 (d, J=2.9 Hz, 1H), 1.63 (dd, J=15.5, 9.7 Hz, 2H), 1.53–1.41 (m, 2H), 1.26 (d, J=5.5 Hz, 1H), 1.22 (d, J=6.4 Hz, 5H), 1.17 (d, J=6.3 Hz, 4H), 1.14 (s, 5H), 1.11 (d, J=7.3 Hz, 6H), 1.08–1.02 (m, 5H), 1.00 (d, J=6.4 Hz, 3H), 0.82 (t, J=7.5 Hz, 6H), ^{13}C NMR (75 MHz, $CDCl_3$) δ 176.10, 173.97, 105.44, 97.26, 87.09, 81.31, 80.02, 78.03, 77.58, 77.16, 76.74, 75.90, 75.86, 74.06, 72.89, 70.61, 69.83, 65.88, 65.13, 61.41, 49.51, 45.97, 43.33, 41.09, 40.53, 35.27, 29.22, 28.43, 27.86, 25.53, 24.26,

21.72, 21.54, 21.18, 18.08, 14.15, 11.91, 11.72, 9.27, 8.44, HRMS *m/z* calcd for $C_{41}H_{77}N_2O_{13}^+$: 805.54202, found: 805.54560, white solid, yield 214 mg (40.8%), purity 96.4% via HPLC-ELSD, **2e** (560 mg, 0.65 mmol) was dissolved in methanol and stirred at room temperature. Reaction was monitored via TLC and MS. After two days solvents were evaporated. Afterwards residue was purified by flash chromatography (stationary phase: silica gel, 2.5 μm, Ø = 3 cm, h = 14 cm, mobile phase: cyclohexane/chloroform/isopropanol/ammonia in methanol) to carry out white solid powder.

2c (2S,3R,4R,6R)-4-(dimethylamino)-2-(((2R,3S,4R,5R,8R,10R,11R,12S,13S,14R)-2-ethyl-3,4,10-trihydroxy-13-(((2R,4R,5S,6S)-5-hydroxy-4-methoxy-4,6-dimethyltetrahydro-2H-pyran-2-yl)oxy)-3,5,6,8,10,12,14-heptamethyl-15-oxo-1-oxa-6-azacyclopentadecan-11-yl)oxy)-6-methyltetrahydro-2H-pyran-3-yl propionate, ^{1}H NMR (300 MHz, $CDCl_3$) δ 5.09 (d, *J* = 4.4 Hz, 1H), 4.81 (dd, *J* = 10.4, 7.5 Hz, 1H), 4.72 (d, *J* = 7.9 Hz, 1H), 4.55 (d, *J* = 7.5 Hz, 1H), 4.20 (d, *J* = 2.2 Hz, 1H), 4.02 (dd, *J* = 9.1, 6.3 Hz, 1H), 3.70 (s, 1H), 3.57 (d, *J* = 6.9 Hz, 3H), 3.35 (s, 2H), 3.33–3.24 (m, 1H), 3.04 (d, *J* = 9.2 Hz, 1H), 2.87–2.61 (m, 4H), 2.55 (d, *J* = 11.2 Hz, 1H), 2.44–2.35 (m, *J* = 11.5 Hz, 4H), 2.31 (s, 7H), 2.28–2.18 (m, 3H), 2.00 (s, 1H), 1.94–1.73 (m, 3H), 1.70–1.53 (m, 2H), 1.31 (d, *J* = 4.4 Hz, 6H), 1.27–1.00 (m, 22H), 0.98–0.72 (m, 9H), ^{13}C NMR (75 MHz, $CDCl_3$) δ 178.36, 173.48, 100.66, 94.79, 83.22, 78.18, 77.58, 77.16, 76.74, 74.42, 74.06, 73.19, 71.22, 69.79, 68.19, 65.82, 63.85, 49.51, 45.39, 42.14, 40.60, 36.54, 34.85, 30.93, 28.03, 27.30, 26.63, 22.21, 21.73, 21.50, 21.27, 18.31, 16.49, 14.85, 11.37, 9.08, 7.89, HRMS *m/z* calcd for $C_{41}H_{77}N_2O_{13}^+$: 805.54202, found: 805.54290, white solid, yield 3467 mg (62.2%), purity 94.0% via HPLC-ELSD, **3** (5.2 g, 6.9 mmol) was dissolved in dichloromethane. Afterwards the solution was cooled with ice and 1.2 eq of pyridine was added, followed by 1.1 eq of propionic anhydride. Solution was stirred at room temperature overnight. Reaction was monitored via TLC and MS. Work up was done after two days, when sufficient product was detected. To extract product liquid-liquid extraction was performed. DCM solution was worked up with a saturated solution of ammonium chloride three times, followed by water three times. Organic phase was then dried with sodium sulphate and solvent evaporated to carry out white solid powder.

2d (2S,3S,4R,6R)-6-(((2R,3S,4R,5R,8R,10R,11R,12S,13S,14R)-11-(((2S,3R,4R,6R)-4-(dimethylamino)-3-hydroxy-6-methyltetrahydro-2H-pyran-2-yl)oxy)-2-ethyl-3,4,10-trihydroxy-3,5,6,8,10,12,14-heptamethyl-15-oxo-1-oxa-6-azacyclopentadecan-13-yl)oxy)-4-methoxy-2,4-dimethyltetrahydro-2H-pyran-3-yl propionate, ^{1}H NMR (300 MHz, $CDCl_3$) δ 5.16 (d, *J* = 4.7 Hz, 1H), 4.74 (s, 1H), 4.68 (d, *J* = 9.8 Hz, 2H), 4.55 (d, *J* = 7.4 Hz, 1H), 4.49–4.34 (m, 1H), 4.29–4.23 (m, 1H), 3.78 (dd, *J* = 9.1, 6.0 Hz, 1H), 3.67 (d, *J* = 4.0 Hz, 1H), 3.62 (d, *J* = 7.1 Hz, 1H), 3.46 (q, *J* = 7.0 Hz, 1H), 3.38 (s, 1H), 3.31 (s, 3H), 3.22 (dd, *J* = 10.1, 7.4 Hz, 2H), 2.89 (s, 1H), 2.81–2.73 (m, 1H), 2.68 (dd, *J* = 13.7, 6.9 Hz, 1H), 2.51 (d, *J* = 9.9 Hz, 2H), 2.44–2.32 (m, 3H), 2.30 (s, 3H), 2.29 (s, 5H), 2.24 (s, 1H), 2.10–1.93 (m, 3H), 1.88 (ddd, *J* = 14.3, 7.7, 2.6 Hz, 1H), 1.76 (d, *J* = 14.7 Hz, 1H), 1.68–1.57 (m, 2H), 1.29 (s, 3H), 1.20–1.18 (m, 4H), 1.16 (d, *J* = 3.6 Hz, 5H), 1.13 (d, *J* = 1.2 Hz, 3H), 1.06 (m, *J* = 10.5, 6.4 Hz, 14H), 0.88 (t, *J* = 6.7 Hz, 6H), ^{13}C NMR (75 MHz, $CDCl_3$) δ 178.96, 174.23, 102.50, 94.91, 83.37, 78.79, 77.98, 77.58, 77.16, 76.74, 74.42, 74.01, 73.73, 73.06, 71.14, 70.25, 68.00, 65.67, 63.18, 62.50, 49.57, 45.25, 42.37, 42.06, 40.48, 36.46, 35.16, 29.00, 27.72, 27.61, 26.91, 22.08, 21.91, 21.39, 17.95, 16.29, 14.83, 11.39, 9.38, 9.24, 7.57, HRMS *m/z* calcd for $C_{41}H_{77}N_2O_{13}^+$: 805.54202, found: 805.54319, white solid, yield 320 mg (72.9%), purity 96.0% via HPLC-ELSD, **2a** (500 mg, 0.55 mmol) was dissolved in methanol and stirred at room temperature. Reaction was monitored via TLC and MS. After eight days solvents were evaporated to obtain white solid powder.

2e (2S,3R,4R,6R)-4-(dimethylamino)-2-(((2R,3R,4R,5R,8R,10R,11R,12S,13S,14R)-2-ethyl-3,10-dihydroxy-13-(((2R,4R,5S,6S)-5-hydroxy-4-methoxy-4,6-dimethyltetrahydro-2H-pyran-2-yl)oxy)-3,5,6,8,10,12,14-heptamethyl-15-oxo-4-(propionyloxy)-1-oxa-6-azacyclopentadecan-11-yl)oxy)-6-methyltetrahydro-2H-pyran-3-yl propionate, ^{1}H NMR (300 MHz, $CDCl_3$) δ 5.07 (d, *J* = 8.8 Hz, 1H), 4.96 (dd, *J* = 10.2, 2.4 Hz, 1H), 4.82 (d, *J* = 6.0 Hz, 1H), 4.79 (d, *J* = 7.7 Hz, 1H), 4.49 (d, *J* = 7.6 Hz, 1H), 4.18 (t, *J* = 5.1 Hz, 1H), 4.01 (dq, *J* = 12.6, 6.3 Hz, 1H), 3.61–3.50 (m, 1H), 3.45 (d, *J* = 4.7 Hz, 1H), 3.34 (d, *J* = 6.6 Hz, 1H), 3.28 (s, 3H), 3.00 (t, *J* = 9.6 Hz, 1H), 2.74–2.55 (m, 2H), 2.40–2.25 (m, 7H), 2.23 (s, 6H), 2.21 (s, 3H), 2.17–2.07 (m, 2H), 1.95 (s, 1H), 1.85–1.46 (m, *J* = 38.4, 20.2, 14.8, 6.0 Hz, 6H), 1.39–1.19 (m, 12H), 1.18–1.07 (m, 14H), 1.01 (d, *J* = 6.5 Hz, 3H), 0.96 (d, *J* = 7.0 Hz, 3H), 0.91–0.80 (m, *J* = 11.7, 6.9 Hz, 7H), ^{13}C NMR (75 MHz, $CDCl_3$) δ 176.34, 173.99, 173.51, 101.66, 97.44, 84.53, 81.41, 81.06, 78.10, 77.58, 77.37, 77.16, 76.74, 76.11, 75.94, 74.15, 72.93, 71.44, 69.39, 65.77, 63.61, 61.17, 49.52, 45.72, 42.78, 40.83, 35.35, 30.97, 27.86, 27.45, 25.13, 24.29, 21.77, 21.01, 18.37, 14.38, 11.97, 11.48, 9.26, 9.19, 8.09,HRMS *m/z* calcd for $C_{44}H_{81}N_2O_{14}^+$: 861.56823, found: 861.56943, white solid, yield 1870 mg (32.5%), purity 96.0% via HPLC-ELSD, as side product in synthesis of **2a**.

2f (2R,3R,4R,5R,8R,10R,11R,12S,13S,14R)-11-(((2S,3R,4S,6R)-4-(dimethylamino)-3-hydroxy-6-methyltetrahydro-2H-pyran-2-yl)oxy)-2-ethyl-3,10-dihydroxy-13-(((2R,4R,5S,6S)-4-methoxy-4,6-dimethyl-5-(propionyloxy)tetrahydro-2H-pyran-2-yl)oxy)-3,5,6,8,10,12,14-heptamethyl-15-oxo-1-oxa-6-azacyclopentadecan-4-yl propionate, ^{1}H NMR (300 MHz, $CDCl_3$) δ 5.04 (d, *J* = 9.4 Hz, 1H), 5.00–4.94 (m, 1H), 4.93 (d, *J* = 5.0 Hz, 1H), 4.70 (d, *J* = 9.8 Hz, 1H), 4.46 (dq, *J* = 12.5, 6.2 Hz, 1H), 4.37 (d, *J* = 7.3 Hz, 1H), 4.26–4.18 (m, 1H), 3.68–3.52 (m, *J* = 9.3, 6.1 Hz, 2H), 3.47 (d, *J* = 2.3 Hz, 1H), 3.46–3.38 (m, 1H), 3.35–3.25 (m, 4H), 2.68–2.49 (m, *J* = 25.4, 11.3, 8.3 Hz, 2H), 2.44–2.30 (m, 5H), 2.28 (s, 6H), 2.24 (s, 3H), 2.20–2.11 (m, 2H), 1.99–1.92 (m, 1H), 1.89–1.47 (m, 6H), 1.29–1.03 (m, 34H), 0.87 (t, *J* = 7.6 Hz, 6H), ^{13}C NMR (75 MHz, $CDCl_3$) δ 176.20, 174.42, 173.92, 105.17, 97.35, 86.62, 81.41, 80.00, 78.58, 77.58, 77.16, 76.74, 75.87, 73.84, 73.22, 70.61, 69.71, 65.07, 63.42, 61.43, 49.96, 45.90, 43.69, 41.22, 40.52, 36.05, 29.30, 28.31, 27.86, 27.70, 25.17, 24.34, 21.58, 21.30, 21.22, 17.38, 14.33, 11.95, 9.46, 9.27, 8.38, HRMS *m/z* calcd for $C_{44}H_{81}N_2O_{14}^+$: 861.56823, found: 861.56904, white solid, yield 312 mg (68.5%), purity 99.7% via HPLC-ELSD, **2a** (485 mg, 0.53 mmol) was dissolved in methanol and stirred at room temperature. Reaction was monitored via TLC and MS. After two days solvents were evaporated and residue purified by flash chromatography (stationary phase: silica gel, 2.5 μm, Ø = 3 cm, h = 14 cm, mobile phase: cyclohexane/chloroform/isopropanol/ammonia in methanol) to carry out white solid powder.

2g (2S,3R,4S,6R)-4-(dimethylamino)-2-(((2R,3S,4R,5R,8R,10R,11R,12S,13S,14R)-2-ethyl-3,4,10-trihydroxy-13-(((2R,4R,5S,6S)-4-methoxy-4,6-dimethyl-5-(propionyloxy)tetrahydro-2H-pyran-2-yl)oxy)-3,5,6,8,10,12,14-heptamethyl-15-oxo-1-oxa-6-azacyclopentadecan-11-yl)oxy)-6-methyltetrahydro-2H-pyran-3-yl propionate, ^{1}H NMR (300 MHz, $CDCl_3$) δ 5.11 (d, *J* = 4.7 Hz, 1H), 5.00 (s, 1H), 4.80–4.55 (m, 4H), 4.41–4.26 (m, *J* = 12.3, 5.9 Hz, 1H), 4.18–4.11 (m, 1H), 3.71 (dd, *J* = 9.3, 5.9 Hz, 1H), 3.59 (s, 1H), 3.48 (d, *J* = 6.9 Hz, 1H), 3.30 (s, 2H), 2.95 (s, 1H), 2.72–2.55 (m, 3H), 2.46 (d, *J* = 9.9 Hz, 1H), 2.38–2.25 (m, 5H), 2.24 (s, 4H), 2.20 (s, 3H), 2.03–1.79 (m, *J* = 10.1, 7.7, 6.6 Hz, 4H), 1.71–1.52 (m, *J* = 18.0, 11.8, 6.8 Hz, 4H), 1.47–1.27 (m, 3H), 1.21 (t, *J* = 7.0 Hz, 6H), 1.17–0.98 (m, 24H), 0.89–0.77 (m, 9H), ^{13}C NMR (75 MHz, $CDCl_3$) δ 178.74, 174.03, 173.18, 100.31, 94.65, 83.02, 78.53, 77.51, 77.09, 76.66, 74.17, 73.64, 72.94, 71.74, 70.13, 67.33, 63.63, 63.07, 62.46, 49.25, 45.11, 41.95, 41.83, 40.72, 36.16, 34.93, 31.07, 29.64, 27.93, 27.55, 27.45, 26.65, 21.87, 21.56, 21.24, 17.74, 16.16, 14.55, 11.21, 9.21, 9.04, 8.82, 7.28, HRMS *m/z* calcd for $C_{44}H_{81}N_2O_{14}^+$: 861.56823, found: 861.56871, white solid, yield 215 mg (100%), purity 95.1% via HPLC-ELSD, **2d** (200 mg, 0.25 mmol) was dissolved in dichloromethane. To this solution 1.1 eq pyridine was added, followed by 1.1 eq propionic

ChemMedChem | Full Papers doi.org/10.1002/cmdc.202100139 | Chemistry Europe European Chemical Societies Publishing

anhydride. Solution was stirred at room temperature and progress was monitored via TLC and MS. Work up was done after two days, when sufficient product was detected. To extract product liquid-liquid extraction was performed. First with citric acid solution (5%, 3x), then citric acid solution was washed with ethyl acetate. Acidic solution was neutralized with sodium carbonate and macrolide transferred into organic phase (ethyl acetate) with liquid-liquid extraction three times. Organic phases were combined and washed with brine/water two times, dried with sodium sulphate and solvent evaporated to carry out white solid powder.

3 Azithromycin (2R,3S,4R,5R,8R,10R,11R,12S,13S,14R)-11-(((2S,3R,4R,6R)-4-(dimethylamino)-3-hydroxy-6-methyltetrahydro-2H-pyran-2-yl)oxy)-2-ethyl-3,4,10-trihydroxy-13-(((2R,4R,5S,6S)-5-hydroxy-4-methoxy-4,6-dimethyltetrahydro-2H-pyran-2-yl)oxy)-3,5,6,8,10,12,14-heptamethyl-1-oxa-6-azacyclopentadecan-15-one, ^{1}H NMR (600 MHz, $CDCl_3$) δ 5.21 (s, 1H), 5.17 (d, J = 4.7 Hz, 1H), 4.69 (dd, J = 9.8, 2.5 Hz, 1H), 4.44 (d, J = 7.3 Hz, 1H), 4.27 (dd, J = 3.5, 1.9 Hz, 1H), 4.08 (dq, J = 9.5, 6.2 Hz, 1H), 3.68 (s, 1H), 3.63 (d, J = 7.4 Hz, 1H), 3.55–3.47 (m, 1H), 3.37 (d, J = 2.1 Hz, 1H), 3.34 (s, 3H), 3.24 (dt, J = 13.5, 6.7 Hz, 1H), 3.03 (t, J = 9.6 Hz, 2H), 3.00–2.83 (m, 2H), 2.73 (dq, J = 11.1, 3.7 Hz, 1H), 2.69 (dd, J = 13.8, 7.0 Hz, 1H), 2.54 (d, J = 10.3 Hz, 1H), 2.50–2.44 (m, 1H), 2.35 (d, J = 15.3 Hz, 1H), 2.31 (s, 9H), 2.15 (t, J = 9.1 Hz, 1H), 2.08–1.94 (m, 3H), 1.89 (dqd, J = 15.1, 7.6, 2.6 Hz, 1H), 1.77 (d, J = 14.6 Hz, 1H), 1.70 (d, J = 12.5 Hz, 1H), 1.58 (dd, J = 15.2, 5.0 Hz, 1H), 1.45 (ddt, J = 14.2, 9.5, 7.2 Hz, 1H), 1.34–1.30 (m, 6H), 1.26–1.23 (m, 4H), 1.22 (d, J = 6.1 Hz, 3H), 1.18 (d, J = 7.5 Hz, 3H), 1.08 (d, J = 5.3 Hz, 6H), 1.03 (d, J = 7.6 Hz, 3H), 0.92–0.85 (m, 6H), ^{13}C NMR (151 MHz, $CDCl_3$) δ 179.06, 103.01, 94.61, 83.52, 78.28, 77.79, 77.59, 77.37, 77.16, 76.95, 74.34, 73.82, 73.63, 73.13, 70.97, 70.21, 68.85, 66.04, 65.75, 62.70, 49.60, 45.49, 42.51, 42.40, 40.53, 36.33, 34.81, 29.10, 27.72, 26.90, 22.12, 21.74, 21.48, 21.45, 18.33, 16.37, 14.69, 11.39, 9.12, 7.41.

Analytics

Purity testing was performed with a Varian ProStar210 system coupled to SEDEX LT-ELSD 80 LT and using a Dr. Maisch ReproSil-Pur120 C_{18}-Aq column (75 × 3 mm, 5 μm). The mobile phase was composed of water containing 0.05% formic acid (eluent A) and methanol containing 0.05% formic acid (eluent B). Gradient used was: 5% B for 5 min, to 100% B in 20 min, 100% B for 4 min, to 5% B in 1 min, 5% B for 5 min. Flow rate was set to 1.3 ml/min. Nitrogen gas in ELSD was used for the nebulization and evaporation of the mobile phase. Pressure was set at 3.3 bar and the drift tube temperature of the ELSD was 75 °C. UV detection was set to $\lambda = 254$ nm. For pH stability studies buffers consisted of sodium acetate for the pH-range of 4–5 and phosphate buffer made of sodium hydrogen phosphate and potassium dihydrogen phosphate for the pH-range of 6–8. Concentrations of sodium acetate and phosphate buffers were 250 mM. A defined aliquot substance was added from DMSO stock solutions (100 mM) to the buffer and mixed for a final concentration of 1 mM. The final DMSO concentration of the solution was 1%. Concentrations were measured with an Agilent 1100 system coupled to SEDEX LT-ELSD 80 LT and using a Dr. Maisch ReproSil-Pur120 C_{18}-Aq column (75 × 3 mm, 5 μm). The mobile phase was composed of water containing 0.05% formic acid (eluent A) and acetonitrile containing 0.05% formic acid (eluent B). Gradient used was: 5% B for 3 min, to 95% B in 15 min, then again 5% B for 5 min. Flow rate was set to 1.5 ml/min. Nitrogen gas in ELSD was used for the nebulization and evaporation of the mobile phase. Pressure was set at 3.3 bar and the drift tube temperature of the ELSD was 75 °C. Stability testing in cells, whole blood and medium was performed with an Agilent 1290 Infinity system coupled to a triple quadrupole Sciex API 4000 LC/MS/MS detector. A Dr. Maisch ReproSil-Pur120 C_{18}-Aq column (3 × 75 mm, 5 μm) was used for the separation of possible metabolites. The mobile phase was composed of water containing 0.1% formic acid (eluent A) and acetonitrile containing 0.1% formic acid (eluent B). Gradient used was: 5% B for 1 min, to 100% B in 4 min, 100% B for 3 min, to 5% B in 1 min, 5% for 4 min. MS tunes can be found in the Supporting Information.

Solubility testing was performed in water with 500 mM DMSO stocks of **1a** or **2a** at room temperature. DMSO concentration was kept at 0.1%. Volume of water was kept at 1 mL. After pipetting solution was vigorously mixed and checked for precipitation after 5 min.

Bioanalytics

Cell lines were cultured in 175 cm^2 cell culture flasks at 37 °C in a humidified atmosphere of 5% CO_2. Cell densities were determined with an automated cell counter (Luna II). Cells were cultured in RPMI 1640 medium with 10% heat inactivated foetal bovine serum and were sub-cultured once a cell density of $> 1 \times 10^6$ cells/mL was reached. Medium was changed by replacing it by fresh RPMI 1640 medium with 10% FBS. Human whole blood was obtained from healthy volunteers. Whole human peripheral blood was collected in a sterile tube containing Li-heparin as anticoagulant. Aliquots of whole blood were kept in an incubator at 37 °C. For stability testing U937 cells were diluted wit RPMI 1640 medium with 10% heat inactivated foetal bovine serum until a concentration of 5×10^6 cells/mL was reached. Whole blood was not further diluted. The reactions were initiated by the addition of the test compounds (from 10 mM DMSO stock) to 1 mL of cell suspension to yield a final compound concentration of 15 μM and a maximum DMSO concentration of 0.15%. The assay was performed in an incubator at 37 °C. 50 μL of cell suspension were taken after 0, 0.25, 0.5, 1, 2, 4, 6, and 24 hours and extracted in 300 μL of acetonitrile with 0.1% formic acid and immediately frozen at −25 °C. Right before HPLC-MS/MS analysis the samples were centrifuged for 10 minutes at 10 000 rpm and the supernatant was transferred into HPLC-vials. Quantification was done by HPLC-MS/MS.

Pharmacokinetics

All protocols were approved by the Institutional Animal Care and Ethics Committee and performed under German law (License 35/9185.81-7/SYN-11/18). Mice (BALB/c, female, 17 weeks old) were purchased from Janvier Labs. Animals were acclimatized for at least one week with normal chow and drinking water *ad libitum* before the start of the experiment. Animals were grouped (n = 3) in standard cages at room temperature and euthanized with carbon dioxide. Treatments were administered oral or intravenous. For i.v. stock solutions were prepared in DMSO and diluted with BALB/c serum (2 mg/kg, 10% DMSO end concentration). For oral route treatment was dissolved in 0.5% citric acid (10 mg/kg). Organs were collected after 2, 4 and 24 h. Whole blood was collected from tail after 15 and 30 min, 1, 2, 4, 8 and 24 h. Collected samples were frozen in liquid nitrogen and stored at −25 °C until further processing. Frozen organ samples were thawed, digested with Proteinase K (1:1, supplied from VWR, diluted 1:40 in phosphate buffer 20 mM) for 1 h at 50 °C and homogenized (FastPrep-24 5G, MP Biomedicals). Three volumes of acetonitrile were added, solution was again homogenized, centrifuged (10 min at 14,000 rpm, Eppendorf Centrifuge 5417R) and supernatant taken for HPLC-MS/MS analysis. Blood samples were thawed, acetonitrile (three volumes) was added and solution was sonicated for 5 min. Supernatant was taken after centrifugation (10 min at 14,000 rpm, Eppendorf Centrifuge 5417R) and analysed via HPLC-MS/MS.

Gut stability

All protocols were approved by the Institutional Animal Care and Ethics Committee and performed under German law. Mice (BALB/c, female, 17 weeks old) were purchased from Janvier Labs. Animals were acclimatized for at least one week with normal chow and drinking water *ad libitum* before the start of the experiment. Animals were euthanized with carbon dioxide and the digestive system was removed. Surgical sewing material was used to separate the different gut compartments (stomach, duodenum, jejunum, ileum, cecum, colon). Each compartment was injected with 100 µL of a 5 µM solution (in 0.05% citric acid) of compound. Compartments were incubated in 0.9% saline with 20 g/L glucose at 37 °C. After 4 h samples of each compartment and its content were collected. Organs were digested with proteinase K (1:1, supplied from VWR, diluted 1:40 in phosphate buffer 20 mM to end concentration of 1 mg/mL proteinase) for 1 h at 50 °C and homogenized (FastPrep-24 5G, MP Biomedicals). Three volumes of acetonitrile were added, solution was again homogenized, centrifuged (10 min at 14,000 rpm, Eppendorf Centrifuge 5417R) and supernatant taken for HPLC-MS/MS analysis. Content samples were diluted with three volumes of acetonitrile, sonicated for 5 min and supernatant was taken after centrifugation (10 min at 14.rpm, Eppendorf Centrifuge 5417R) and analysed via HPLC-MS/MS. Possible influences on hydrolysis rate in gut were determined in content of jejunum and duodenum taken from mice (three C57BL/6 males, 20 weeks old, pooled). Content was collected through rinsing of fluids from either jejunum or duodenum and diluted with phosphate buffer (1:1 for duodenum content and 1:2 for jejunum content) and divided into six samples. First was treated with sodium azide (0.1%), second sample was incubated with bis(4-nitrophenyl)-phosphate (BNPP; 10 µM), third sample was incubated with plant oil (5%), fourth sample was incubated on ice, fifths sample was centrifuged (5 min at 14,000 rpm, Eppendorf Centrifuge 5417R) and supernatant was taken, last sample was not treated. Each sample was incubated for 4 h at 37 °C (except sample stored on ice). Samples were then diluted with three volumes of acetonitrile, sonicated for 5 min and supernatant was taken after centrifugation (10 min at 14.rpm, Eppendorf Centrifuge 5417R) and analysed via HPLC-MS/MS.

Statistics

Any statistical and half-life calculations were made with GraphPad Prism. Means are shown with standard deviation or standard error.

Acknowledgements

We would like to thank colleagues from Synovo GmbH and the University of Tübingen who assisted in this research. Special thanks to the members of the in vivo facility and the team of the analytics/bioanalytics department at both institutions.

Keywords: short-chain fatty acids · lysosomal trapping · dietary fiber · IBD · SCFA donor

[1] B. T. Layden, A. R. Angueira, M. Brodsky, V. Durai, W. L. Lowe, *Transl. Res.* **2013**, *161*, 131–140.
[2] B. Dalile, L. Van Oudenhove, B. Vervliet, K. Verbeke, *Nat. Rev. Gastroenterol. Hepatol.* **2019**, *16*, 461–478.
[3] M. Li, B. van Esch, P. Henricks, *Eur. J. Pharmacol.* **2018**, *831*, 52–59.
[4] T. Ulven, *Front. Endocrinol.* **2012**, *3*, 111.
[5] H. M. Hamer, D. Jonkers, K. Venema, S. Vanhoutvin, F. J. Troost, R. J. Brummer, *Aliment. Pharmacol. Ther.* **2008**, *27*, 104–119.
[6] N. Singh, A. Gurav, S. Sivaprakasam, E. Brady, R. Padia, H. Shi, M. Thangaraju, P. D. Prasad, S. Manicassamy, D. H. Munn, J. R. Lee, S. Offermanns, V. Ganapathy, *Immunity* **2014**, *40*, 128–139.
[7] J. T. Chai, J. E. Digby, R. P. Choudhury, *Curr. Atheroscler. Rep.* **2013**, *15*, DOI 10.1007/s11883-013-0325-9.
[8] J. L. Pluznick, R. J. Protzko, H. Gevorgyan, Z. Peterlin, A. Sipos, J. Han, I. Brunet, L. X. Wan, F. Rey, T. Wang, S. J. Firestein, M. Yanagisawa, J. I. Gordon, A. Eichmann, J. Peti-Peterdi, M. J. Caplan, *Proc. Natl. Acad. Sci. USA* **2013**, *110*, 4410–4415.
[9] K. Meijer, P. De Vos, M. G. Priebe, *Curr. Opin. Clin. Nutr. Metab. Care* **2010**, DOI 10.1097/MCO.0b013e32833eebe5.
[10] M. Li, B. C. A. M. van Esch, G. T. M. Wagenaar, J. Garssen, G. Folkerts, P. A. J. Henricks, *Eur. J. Pharmacol.* **2018**, DOI 10.1016/j.ejphar.2018.05.003.
[11] Z. Ang, D. Xiong, M. Wu, J. L. Ding, *FASEB J.* **2018**, *32*, 289–303.
[12] A. Geirnaert, M. Calatayud, C. Grootaert, D. Laukens, S. Devriese, G. Smagghe, M. De Vos, N. Boon, T. Van De Wiele, *Sci. Rep.* **2017**, *7*, 1–14.
[13] W. N. D'Souza, J. Douangpanya, S. Mu, P. Jaeckel, M. Zhang, J. R. Maxwell, J. B. Rottman, K. Labitzke, A. Willee, H. Beckmann, Y. Wang, Y. Li, R. Schwandner, J. A. Johnston, J. E. Towne, H. Hsu, *PLoS One* **2017**, *12*, 1–15.
[14] L. Macia, J. Tan, A. T. Vieira, K. Leach, D. Stanley, S. Luong, M. Maruya, C. Ian McKenzie, A. Hijikata, C. Wong, L. Binge, A. N. Thorburn, N. Chevalier, C. Ang, E. Marino, R. Robert, S. Offermanns, M. M. Teixeira, R. J. Moore, R. A. Flavell, S. Fagarasan, C. R. Mackay, *Nat. Commun.* **2015**, *6*, DOI 10.1038/ncomms7734.
[15] P. Gonçalves, J. R. Araújo, J. P. Di Santo, *Inflamm. Bowel. Dis.* **2018**, *24*, 558–572.
[16] Z. Ang, D. Xiong, M. Wu, J. L. Ding, *FASEB J.* **2018**, *32*, 289–303.
[17] M. El-Salhy, J. Valeur, T. Hausken, J. Gunnar Hatlebakk, *Neurogastroenterol. Motil.* **2020**, DOI 10.1111/nmo.13983.
[18] J. Lee, V. R. Venna, D. J. Durgan, H. Shi, J. Hudobenko, N. Putluri, J. Petrosino, L. D. McCullough, R. M. Bryan, *Gut Microbes* **2020**, *12*, 1–14.
[19] J. Tan, C. McKenzie, P. J. Vuillermin, G. Goverse, C. G. Vinuesa, R. E. Mebius, L. Macia, C. R. Mackay, *Cell Rep.* **2016**, *15*, 2809–2824.
[20] F. Bishehsari, P. A. Engen, N. Z. Preite, Y. E. Tuncil, A. Naqib, M. Shaikh, M. Rossi, S. Wilber, S. J. Green, B. R. Hamaker, K. Khazaie, R. M. Voigt, C. B. Forsyth, A. Keshavarzian, *Genes* **2018**, *9*, DOI 10.3390/genes9020102.
[21] L. Wang, J. Zhang, Z. Guo, L. Kwok, C. Ma, W. Zhang, Q. Lv, W. Huang, H. Zhang, *Nutrition* **2014**, *30*, 776–783.e1.
[22] S. Strass, C. Heinzel, N. Cloos, M. Keppler, J. Guse, M. Burnet, S. Laufer, *Gastroenterology* **2020**, *158*, S20.
[23] M. W. Burnet, N. Pietrzik, C. Baeuerlein, M. Eggers, J.-H. Guse, U. Hahn, S. Strass, *Novel Anti-Infective and Anti-Inflammatory Compounds* **2018**, US20200262857.
[24] Z. Ang, J. Z. Er, N. S. Tan, J. Lu, Y. C. Liou, J. Grosse, J. L. Ding, *Sci. Rep.* **2016**, *6*, 1–15.
[25] G. Tax, E. Urbán, Z. Palotás, R. Puskás, Z. Kónya, T. Bíró, L. Kemény, K. Szabó, *Acta Derm.-Venereol.* **2016**, *96*, 43–49.
[26] J. E. Harbison, A. J. Roth-Schulze, L. C. Giles, C. D. Tran, K. M. Ngui, M. A. Penno, R. L. Thomson, J. M. Wentworth, P. G. Colman, M. E. Craig, G. Morahan, A. T. Papenfuss, S. C. Barry, L. C. Harrison, J. J. Couper, *Pediatr. Diabetes* **2019**, *20*, 574–583.
[27] J. de la Cuesta-Zuluaga, N. T. Mueller, R. Álvarez-Quintero, E. P. Velásquez-Mejía, J. A. Sierra, V. Corrales-Agudelo, J. A. Carmona, J. M. Abad, J. S. Escobar, *Nutrients* **2019**, *11*, DOI 10.3390/nu11010051.
[28] K. Togami, S. Chono, K. Morimoto, *Biopharm. Drug Dispos.* **2011**, DOI 10.1002/bdd.767.
[29] M. Bosnar, M. Dominis-Kramarić, K. Nujić, D. Stupin Polančec, N. Marjanović, I. Glojnarić, V. Eraković Haber, *Int. Immunopharmacol.* **2013**, *15*, 498–504.
[30] M. B. Carlier, I. García-Luque, J. P. Montenez, P. M. Tulkens, J. Piret, *Int. J. Tissue React.* **1994**, *16*, 211–220.
[31] M. Bosnar, B. Bošnjak, S. Čužić, B. Hrvačić, N. Marjanović, I. Glojnarić, O. Čulić, M. J. Parnham, V. E. Haber, *J. Pharmacol. Exp. Ther.* **2009**, *331*, 104 LP-113.
[32] M. T. Labro, *Clin. Microbiol. Infect.* **1996**, *1*, DOI 10.1111/j.1469-0691.1996.tb00588.x.
[33] W. Schönfeld, H. A. Krist, *Macrolide Antibiotics*, Birkhäuser Basel, Basel, **2002**.
[34] J. A. Retsema, J. M. Bergeron, D. Girard, W. B. Milisen, A. E. Girard, *J. Antimicrob. Chemother.* **1993**, *31*, 5–16.

[35] M. Bosnar, Ž. Kelnerić, V. Munić, V. Eraković, M. J. Parnham, *Antimicrob. Agents Chemother.* **2005**, DOI 10.1128/AAC.49.6.2372-2377.2005.
[36] R. P. Gladue, G. M. Bright, R. E. Isaacson, M. F. Newborg, *Antimicrob. Agents Chemother.* **1989**, *33*, 277–282.
[37] G. L. Mandell, E. Coleman, *Antimicrob. Agents Chemother.* **2001**, *45*, 1794–1798.
[38] J. Blais, D. Beauchamp, S. Chamberland, *J. Antimicrob. Chemother.* **1994**, *34*, 371–382.
[39] K. Togami, S. Chono, K. Morimoto, *Subcellular Distribution of Azithromycin and Clarithromycin in Rat Alveolar Macrophages (NR8383) in Vitro*, **2013**.
[40] R. M. Shepard, F. C. Falkner, *J. Antimicrob. Chemother.* **1990**, *25*, 49–60.
[41] B. Barrett, V. Bořek-Dohalský, P. Fejt, S. Vaingátová, J. Huclová, B. Němec, I. Jelínek, *Anal. Bioanal. Chem.* **2005**, *383*, 210–217.
[42] D. Debremaeker, D. Visky, H. K. Chepkwony, A. Van Schepdael, E. Roets, J. Hoogmartens, *Rapid Commun. Mass Spectrom.* **2003**, *17*, 342–350.
[43] Y. Jin, Y. Xu, J. Zhou, Z. Zhou, J. Wang, *Rapid Commun. Mass Spectrom.* **2020**, *34*, DOI 10.1002/rcm.8772.
[44] J. Barber, *Magn. Reson. Chem.* **1991**, *29*, 740–743.
[45] R. J. Brennan, J. Barber, *Magn. Reson. Chem.* **1992**, *30*, 327–333.
[46] M. J. Parnham, V. E. Haber, E. J. Giamarellos-Bourboulis, G. Perletti, G. M. Verleden, R. Vos, *Pharmacol. Ther.* **2014**, *143*, 225–245.
[47] C. Ma, Z. Liu, H. Song, R. Jiang, F. He, S. Ma, *J. Antibiot.* **2010**, *63*, 3–8.
[48] A. N. Tevyashova, A. M. Korolev, E. P. Mirchink, E. B. Isakova, I. A. Osterman, *J. Antibiot.* **2019**, 22–33.
[49] S. V. Anantakrishnan, *Proc. Indian Acad. Sci. Sect. A* **1952**, *36*, 338–341.
[50] T. H. Fife, *J. Am. Chem. Soc.* **1965**, *87*, 4597–4600.
[51] H. Bundgaard, A. Buur, S. C. Chang, V. H. L. Lee, *Int. J. Pharm.* **1986**, *33*, 15–26.
[52] J. A. Zaslowsky, E. Fisher, *J. Phys. Chem.* **1963**, *67*, 959–961.
[53] M. Matijašić, V. Munić Kos, K. Nujić, S. Čužić, J. Padovan, G. Kragol, S. Alihodžić, B. Mildner, D. Verbanac, V. Eraković Haber, *Pharmacol. Res.* **2012**, DOI 10.1016/j.phrs.2012.06.001.
[54] H. Derendorf, *Int. J. Antimicrob. Agents* **2020**, *55*, 106007.
[55] Y. Feng, Y. Wang, P. Wang, Y. Huang, F. Wang, *Cell. Physiol. Biochem.* **2018**, *49*, 190–205.
[56] E. L. McConnell, A. W. Basit, S. Murdan, *J. Pharm. Pharmacol.* **2008**, *60*, 63–70.
[57] L. A. Lokshina, V. N. Orekhovich, V. A. Sklyankina, *Nature* **1964**, *204*, 580–580.
[58] Y. N. Gavhane, A. V. Yadav, *Saudi Pharm. J.* **2012**, *20*, 331–344.
[59] J. L. Davis, S. Y. Gardner, S. L. Jones, B. A. Schwabenton, M. G. Papich, *J. Vet. Pharmacol. Ther.* **2002**, *25*, 99–104.
[60] M. Filist, K. Buś-Kwaśnik, H. Ksycińska, P. J. Rudzki, *J. Pharm. Biomed. Anal.* **2014**, *100*, 184–189.
[61] P. Padmanabhan, J. Grosse, A. B. M. A. Asad, G. K. Radda, X. Golay, *EJNMMI Res.* **2013**, *3*, 1.
[62] D. Sinha, M. Valapala, P. Shang, S. Hose, R. Grebe, G. A. Lutty, J. S. Zigler, K. Kaarniranta, J. T. Handa, *Exp. Eye Res.* **2016**, *144*, 46–53.
[63] T. Gaillard, J. Dormoi, M. Madamet, B. Pradines, *Malar. J.* **2016**, *15*, 1–11.
[64] Y. P. Silva, A. Bernardi, R. L. Frozza, *Frontiers in Endocrinology* **2020**, *11*, 1–14.
[65] R. Corrêa-Oliveira, J. L. Fachi, A. Vieira, F. T. Sato, M. A. R. Vinolo, *Clin. Transl. Immunol.* **2016**, DOI 10.1038/cti.2016.17.
[66] J. Schulthess, S. Pandey, M. Capitani, K. Rue-Albrecht, I. Arnold, F. Franchini, A. Chomka, N. Ilott, D. Johnston, E. Pires, J. McCullagh, S. N. Sansom, C. V. Arancibia-Cárcamo, H. H. Uhlig, F. Powrie, *Immunity* **2019**, 1–14.

Manuscript received: February 26, 2021
Accepted manuscript online: March 31, 2021
Version of record online: May 11, 2021

8. „Immune cell targeted Fumaric Esters support a role of GPR109A as a primary target of Monomethyl Fumarate *in vivo*“

Straß, S. Geiger, J., Cloos, N., Späth, N., Geiger, S., Schwamborn, A., De Oliveira, L., Martorelli, M., Guse, J.-H., Sandri, T. L., Burnet, M., & Laufer, S. (2023). Immune cell targeted Fumaric Esters support a role of GPR109A as a primary target of Monomethyl Fumarate *in vivo*. *Inflammopharmacology.* https://doi.org/10.1007/s10787-023-01186-0 (für *Supporting Information* siehe Anhang).

Eigenanteil an Publikation

Die Idee zur Synthese der gelisteten Stoffe wurde von Dr. Burnet, Dr. Guse und mir ausgearbeitet. Alle aufgeführten Synthesen wurden von mir durchgeführt. Die Aufnahme der NMR-Spektren erfolgte durch die Uni Tübingen über die Arbeitsgruppe Laufer. Die Auswertung der Spektren, die Charakterisierung und die Strukturaufklärung wurde von mir durchgeführt. Frau J. Geiger, Frau Späth, Frau S. Geiger, Frau Martorelli und ich waren verantwortlich für die Struktur und Ausführung der *in vitro* Experimente und die Aufarbeitung von anfallenden Proben für die Analyse. *In vivo* Experimente wurden von Dr. de Oliveira da Cuhna, Dr. Burnet, Frau J. Geiger, Frau Cloos und mir geplant und durchgeführt. Die Aufarbeitung, Analyse und Messung der Proben aus den Studien, sowie der Proben aus den Stabilitäten und die Entwicklung der Methode für die HPLC-MS/MS wurde von Frau Schwamborn und mir getätigt. Die qPCR-Analyse wurde von Frau J. Geiger und Dr. Lucas Sandri geplant und durchgeführt. Die schriftliche Ausarbeitung und Visualisierung erfolgten durch mich. Alle AutorInnen haben das Manuskript überprüft und korrigiert. Prof. Laufer wirkte bei der Arbeit unterstützend und beratend.

Inflammopharmacology
https://doi.org/10.1007/s10787-023-01186-0

Inflammopharmacology

ORIGINAL ARTICLE

Immune cell targeted fumaric esters support a role of GPR109A as a primary target of monomethyl fumarate in vivo

Simon Straß[1,2] · Johanna Geiger[2] · Natascha Cloos[2] · Nadja Späth[2] · Sophia Geiger[2] · Anna Schwamborn[2] · Luciano De Oliveira da Cunha[2] · Mariella Martorelli[1,2] · Jan-Hinrich Guse[2] · Thaisa Lucas Sandri[2,3] · Michael Burnet[2] · Stefan Laufer[1]

Received: 2 December 2022 / Accepted: 19 February 2023

Abstract
Dimethyl fumarate (DMF) is approved as a treatment for multiple sclerosis (MS), however, its mode of action remains unclear. One hypothesis proposes that Michael addition to thiols by DMF, notably glutathione is immunomodulatory. The alternative proposes that monomethyl fumarate (MMF), the hydrolysis product of DMF, is a ligand to the fatty acid receptor GPR109A found in the lysosomes of immune cells. We prepared esters of MMF and macrolides derived from azithromycin, which were tropic to immune cells by virtue of lysosomal trapping. We tested the effects of these substances in an assay of response to Lipopolysaccharide (LPS) in freshly isolated human peripheral blood mononuclear cells (PBMCs). In this system, we observed that the 4″ ester of MMF (compound 2 and 3) reduced levels of Interleukins (IL)-1β, IL-12 and tumor necrosis factor alpha (TNFα) significantly at a concentration of 1 µM, while DMF required about 25 µM for the same effect. The 2′ esters of MMF (compound 1 and 2) were, like MMF itself, inactive in vitro. The 4″ ester formed glutathione conjugates rapidly while the 2′ conjugates did not react with thiols but did hydrolyze slowly to release MMF in these cells. We then tested the substances in vivo using the imiquimod/isostearate model of psoriasis where the 2′ ester was the most active at 0.06–0.12 mg/kg (approximately 0.1 µmol/kg), improving skin score, body weight and cytokine levels (TNFα, IL-17A, IL-17F, IL-6, IL-1β, NLRP3 and IL-23A). In contrast, the thiol reactive 4″ ester was less active than the 2′ ester while DMF was ca. 300-fold less active. The thiol reactive 4″ ester was not easily recovered from either plasma or organs while the 2′ ester exhibited conventional uptake and elimination. The 2′ ester also reduced levels of IL-6 in acute monosodium urate (MSU) induced inflammation. These data suggest that mechanisms that are relevant in vivo center on the release of MMF. Given that GPR109A is localized to the lysosome, and that lysosomal trapping increases 2′ ester activity by > 300 fold, these data suggest that GPR109A may be the main target in vivo. In contrast, the effects associated with glutathione (GSH) conjugation in vitro are unlikely to be as effective in vivo due to the much lower dose in use which cannot titrate the more concentrated thiols. These data support the case for GPR109A modulation in autoimmune diseases.

Keywords Psoriasis · Fumarates · Macrolides · GPR109A · Lysosomal Trapping

Introduction

Fumaric esters are anti-inflammatory drugs used as therapeutic treatments against psoriasis and multiple sclerosis (MS). Fumaderm® is a mixture of dimethyl fumarate (DMF) and monoethyl fumarate (MEF) in the mixed Ca^{2+}, Mg^{2+} and Zn^{2+} (Gillard et al. 2015; Linker and Gold 2013) salt forms. It was first approved in 1994 and since then is solely licensed in Germany. DMF oral therapy was approved by the Food and Drug Administration (FDA) in the United States in 2004 as Tecfidera® against MS (Linker and Gold 2013). A new form to be commercialized

✉ Michael Burnet
michael.burnet@synovo.com

1 Pharmaceutical Chemistry, Institute for Pharmaceutical Sciences, Eberhard Karls University Tübingen, Tübingen, Germany

2 Synovo GmbH, Tübingen, Germany

3 Institute of Tropical Medicine, Eberhard Karls University Tübingen, Tübingen, Germany

Published online: 01 April 2023

as Skilarence® contains DMF and XP23829 (prodrug for monomethyl fumarate (MMF)). These fumarates have anti-inflammatory, cytoprotective, and immunomodulatory properties, however the underlying mechanisms of action are still not fully understood. So far, it is known that fumarates are able to inhibit the up-regulation of the nuclear factor kappa B (NF-κB) pathway (McGuire et al. 2016). This impacts not only cell differentiation and apoptosis, but also lowers levels of inflammatory cytokines and adhesion molecules and leads to a shift from proinflammatory T helper cells (Th) 1 and Th17 to an anti-inflammatory Th2 response (Mills et al. 2018). DMF or MEF treatment also activates the nuclear factor erythroid 2-related factor 2 (Nrf2) pathway and thus regulation of cytoprotective mechanisms. Higher levels of Nrf2 are associated with reduced oxidative stress and cellular antioxidant responses (Brennan et al. 2015; Helwa et al. 2017; Liu et al. 2016a). The degree of oxidative cell stress is positively associated with the severity of psoriasis (Kadam et al. 2010; Pleńkowska et al. 2020). DMF also conjugates to GSH via Michael addition, causing intracellular depletion of GSH at higher doses under physiological conditions (Xu et al. 2018). The product is a 2-(*S*-glutathionyl)-succinic dimethyl ester and is specific to DMF but not MMF. Its formation is associated with anti-inflammatory, immunosuppressive and cytoprotective responses (Brennan et al. 2015; Schmidt et al. 2007; Sullivan et al. 2013; Ghoreschi et al. 2011; Zheng 2015). The reaction between GSH and fumaric esters can also take place with other thiols like cysteine or thiol containing proteins such as glyceraldehyde 3-phosphate dehydrogenase (GAPDH), an enzyme in the aerobic glycolytic pathway. With this, fumaric esters thus inhibit GAPDH activity (Kornberg et al. 2018; Angiari and O'Neill 2018; Park et al. 2019).

The G protein-coupled receptor GPR109A, a receptor for nicotinic acid, is also activated by MMF leading to reduced neutrophil adhesion, migration and recruitment (Gillard et al. 2015; Mrowietz et al. 2018). In neutrophils, nicotinic acid stimulation also leads to apoptosis via a cAMP driven mechanism (Kostylina et al. 2008). GPR109A is also implicated in nicotinic acid mediated skin proliferation and it is highly expressed in epidermal keratinocytes (Bermudez et al. 2011). Activation of GPR109A results in its transport to the endosome where it remains trapped while associated with its agonist ligand (Li et al. 2010). The endosome is often acidified in neutrophils, which may lead to an acidic ligand diffusing out of the endosome. Activation of GPR109A by nicotinic acid and beta-hydroxy butyrate leads to suppression of inflammatory cytokine production in retinal cells suggesting that anti-inflammatory effects of its activation may be more general than in neutrophils alone (Gambhir et al. 2012). Many of these observations are thought to support activity in MS.

In respect of GPR109A, DMF is the prodrug for the active metabolite and GPR109A ligand MMF. DMF, being neutral, is able to diffuse through cell membranes, whilst MMF, being a free acid, is hindered in passive diffusion (Mrowietz et al. 2018). After oral administration of DMF, a large proportion is rapidly hydrolyzed to MMF (Linker and Gold 2013; Mills et al. 2018; Helwa et al. 2017; Miglio et al. 2015) and the rest to the DMF-GSH-conjugate. It is not clear whether this form of DMF is further active in vivo. The reaction is reversible, but its metabolite the mercapturic acid of DMF is detected in urine (Wollina 2011). These data suggest that the dominant circulating product of DMF after oral application in vivo is MMF (Mrowietz et al. 2018).

Based on these data, we hypothesized that if MMF were preferentially directed to myeloid cells like neutrophils it should exert a more potent anti-inflammatory effect (Fig. 1B). To test this concept, we synthesized a set of new compounds (**1–3** listed in Fig. 1A) designed to deliver the active metabolite MMF to immune cells/inflammation sites. This was done by coupling MMF to the macrolide Azithromycin. Azithromycin is known to be able to accumulate rapidly in tissue and immune cells (Bosnar et al. 2005; Carryn et al. 2003; Togami et al. 2013). It is proposed that the reason for the accumulation is acid trapping to the lysosomes, facilitated by the two amphiphilic amines. Bosnar et al. (2005) showed specific uptake of Azithromycin into immune cells which we confirmed in a previous study demonstrating beneficial distribution patterns (spleen, liver and lung) for anti-inflammatory effect after oral application (Straß et al. 2021). Although some previous studies showed a possible effect of Azithromycin in psoriasis, our focus was on understanding the efficacy of fumarates. While Azithromycin has robust general anti-inflammatory properties, these are mainly reported at much higher systemic doses (e.g. 5–10 mg/kg) whereas we seek more potent effects in the range of 0.1 mg/kg per oral (p.o.) in murine models (Huang and Shieh 2016; Saxena and Dogra 2010; Balloy et al. 2014). As a general rule, our previous data suggest that lipophilic amphiphiles like Azithromycin can have anti-inflammatory effects on the gut from 1 µmol/kg and systemic effects from 10 to 100 µmol/kg, which are doses sufficient to inhibit the lysosomal phospholipases (Burnet et al. 2015).

Our novel set of compounds and data provide a new means to investigate the mode of action of fumarates. In particular, we set out to answer, whether their effect is more related to interactions with GSH or possibly with the endosomal/lysosomal receptor GPR109A (Li et al. 2010).

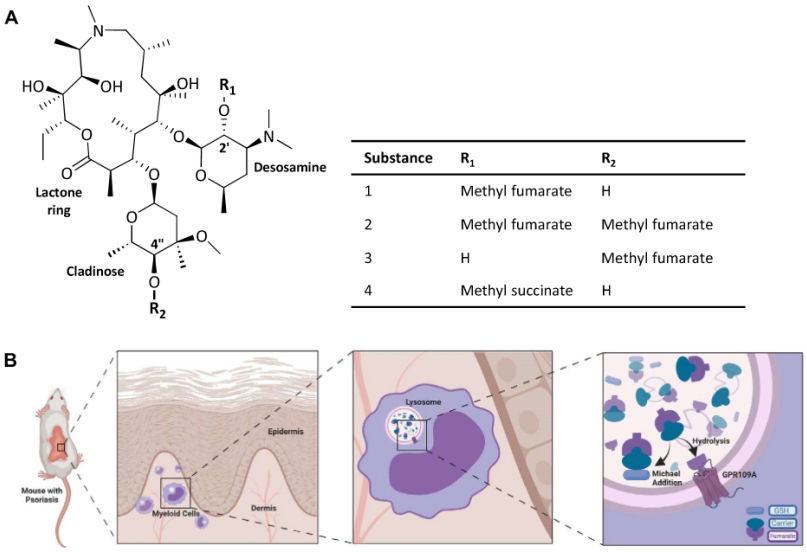

Substance	R_1	R_2
1	Methyl fumarate	H
2	Methyl fumarate	Methyl fumarate
3	H	Methyl fumarate
4	Methyl succinate	H

Fig. 1 **A** Macrolide core structure with possible reaction sites R_1 and R_2. Synthesized substances with side chains listed in table. **B** Psoriatic mouse skin and accumulation of macrolidic derivatives into lysosomal compartments of myeloid cells at the site of inflammation and interaction with possible targets (GSH, GPR109A). Adapted from BioRender (2022) "Arm with Rash and Callout"

Materials and methods

Synthesis

We synthesized three new fumarate macrolide compounds (**1–3**) and to avoid/control for non-specific effects of the carrier construct, we prepared a reference substance based on Azithromycin esterified with methyl succinate (**4**) to be used as a comparator to the active compounds in in vitro studies. This comparator substance (**4**) replicates many of the properties of the fumarate esters but does not possess the double bond that can react with GSH and is not reported to interact with GPR109A. All chemicals were purchased from commercial sources and used as received. Reaction monitoring was performed via mass spectrometry (Finnigan LCQ Deca XP MAX, Software Xcalibur 2.0.7 SP1) and thin layer chromatography (TLC; Merck TLC Silica gel 60 F254). TLC spots were detected with Hanessian's stain, based on a Cerium Molybdate solution and heat (through heat gun for approximately 30 s). Nuclear magnetic resonance (NMR) spectra were recorded with a Bruker Avance 400 (400 MHz) or Bruker Avance III (300 MHz). Substances were dissolved in $CDCl_3$ and chemical shifts (ppm) were referenced to $CHCl_3$/Tetramethylsilane. Coupling constants (J) are given in Hz. After reaction steps solvents were evaporated with rotary evaporator (RV8 IKA, KNF SC 920) under vacuum (at, if not stated differently, 35–40 °C). To purify substances flash chromatography was performed (Interchim puriFlash 5.020 with Interchim PF-15SIHP-F0040 or PF-50SIHP-F0040 columns). Purity of reaction products was determined via high performance liquid chromatography (HPLC) Varian (ProStar) and evaporative light scattering (ELS) detection (Sedere Sedex 80). Mobile phases contained water (0.05% formic acid) and methanol (0.05% formic acid) as gradients. Stationary phase was ReproSil-Pur 120 C_{18}-AQ, 5 µm, 75 × 3 mm (Dr. Maisch). High resolution mass spectra were recorded with a Bruker maXis 4G ESI-TOF from Daltonik [JL1], using ESI^+ mode with following settings: Capillary voltage 4.5 kV, source temperature 200 °C, gas flow 6 L/min, nebulizer gas pressure 1.2 bar, end plate offset – 0.5 kV and an m/z range of 100–1350.

Compound 1 (2S,3R,4S,6R)-4-(dimethylamino)-2-(((2R,3S,4R,5R,8R,10R,11R,12S,13S,14R)-2-ethyl-3,4,10-trihydroxy-13-(((2R,4R,5S,6S)-5-hydroxy-4-methoxy-4,6-dimethyltetrahydro-2H-pyran-2-yl)oxy)-3,5,6,8,10,12,14-heptamethyl-15-oxo-1-oxa-6-azacyclopentadecan-11-yl)oxy)-6-methyltetrahydro-2H-pyran-3-yl methyl fumarate, ^{1}H NMR (400 MHz, $CDCl_3$) δ 6.83 (d, J = 1.9 Hz, 2H), 5.02 (d, J = 4.5 Hz, 1H), 4.85 (dd, J = 10.6, 7.5 Hz, 1H), 4.65 (d, J = 9.1 Hz, 1H), 4.60 (d, J = 7.5 Hz,

1H), 4.20 (dd, J = 5.4, 1.7 Hz, 1H), 4.02 (tt, J = 8.8, 4.4 Hz, 1H), 3.80 (s, 3H), 3.64 (s, 1H), 3.60 (d, J = 6.8 Hz, 1H), 3.53 (dd, J = 9.7, 5.9 Hz, 1H), 3.35 (d, J = 6.6 Hz, 3H), 3.04 (t, J = 9.5 Hz, 1H), 2.73 (dd, J = 13.2, 6.3 Hz, 2H), 2.70–2.61 (m, 2H), 2.48 (d, J = 10.1 Hz, 1H), 2.32 (dd, J = 16.3, 10.8 Hz, 4H), 2.24 (s, 6H), 2.19 (d, J = 10.2 Hz, 1H), 1.87 (ddt, J = 12.8, 7.5, 7.0 Hz, 3H), 1.74 (dd, J = 12.9, 2.5 Hz, 1H), 1.67 (d, J = 14.7 Hz, 1H), 1.59 (dd, J = 15.1, 5.0 Hz, 1H), 1.51–1.40 (m, 1H), 1.36 (d, J = 12.5 Hz, 1H), 1.33–1.27 (m, 7H), 1.26 (s, 3H), 1.23 (d, J = 6.1 Hz, 4H), 1.19 (d, J = 7.4 Hz, 4H), 1.09 (d, J = 6.2 Hz, 3H), 1.03 (s, 4H), 0.91 (d, J = 6.7 Hz, 3H), 0.87 (t, J = 7.4 Hz, 4H), 0.79 (d, J = 7.5 Hz, 3H), ^{13}C NMR (101 MHz, $CDCl_3$) δ 178.41, 165.80, 164.02, 134.66, 132.92, 100.69, 95.24, 83.80, 78.69, 78.26, 77.69, 77.48, 74.52, 73.80, 73.24, 73.05, 70.20, 68.48, 65.87, 63.86, 62.47, 52.36, 49.54, 45.06, 42.35, 41.31, 40.83, 36.67, 35.15, 30.61, 27.37, 26.81, 22.10, 21.78, 21.33, 18.53, 16.36, 15.40, 11.33, 9.67, 7.86, 1.14, high resolution mass spectrometry (HRMS) m/z calculated (calcd) for $C_{43}H_{77}N_2O_{15}^+$ 861.53185, found: 861.53123, colorless solid, yield 7300 mg (71.3%), purity 95.1% via HPLC-evaporative light scattering detector (ELSD), Azithromycin (8.9 g, 11.9 mmol) was dissolved in dichloromethane (DCM) and triethylamine (665 µL) was added. As reactive species MMF was added as acid chloride. The acid chloride was prepared in which MMF (1885 mg, 14.3 mmol) and oxalyl chloride (1458 µL, 17.1 mmol) were dissolved in DCM and dimethylformamide (100 µL) was added as catalyst. The solution was stirred at room temperature until 1 h after the end of gas emission. All volatiles were removed in vacuo. The resulting acid chloride was distilled under vacuum (approx. 20 mbar) at 130 °C. The macrolide solution and acid chloride were then combined and stirred at room temperature. Progress was detected via TLC and mass spectrometry (MS). Work up was done after 6 days, when reaction was completed. Liquid–liquid extraction was performed to extract product from solution. First with citric acid solution (5%, 3x), in a second step the citric acid solution was washed twice with ethyl acetate. Acidic solution was then neutralized with sodium carbonate and macrolide transferred into organic phase (ethyl acetate) with liquid–liquid extraction three times. Organic phases were combined and washed with brine/water two times, dried with sodium sulphate and solvent evaporated.

Compound 2 (2S,3R,4S,6R)-4-(dimethylamino)-2-(((2R,3S,4R,5R,8R,10R,11R,12S,13S,14R)-2-ethyl-3,4,10-trihydroxy-13-(((2R,4R,5S,6S)-4-methoxy-5-(((E)-4-methoxy-4-oxobut-2-enoyl)oxy)-4,6-dimethyltetrahydro-2H-pyran-2-yl)oxy)-3,5,6,8,10,12,14-heptamethyl-15-oxo-1-oxa-6-azacyclopentadecan-11-yl)oxy)-6-methyltetrahydro-2H-pyran-3-yl methyl fumarate, ^{1}H NMR (400 MHz, $CDCl_3$) δ 6.87–6.83 (m, 2H), 6.82 (d, J = 2.2 Hz, 2H), 5.11 (d, J = 4.7 Hz, 1H), 4.86 (dd, J = 10.6, 7.6 Hz, 1H), 4.78–4.70 (m, J = 12.9, 5.5 Hz, 2H), 4.66 (d, J = 7.8 Hz, 1H), 4.40 (dq, J = 12.4, 6.1 Hz, 1H), 4.18 (dd, J = 5.0, 1.6 Hz, 1H), 3.80 (d, J = 4.0 Hz, 6H), 3.62 (s, 1H), 3.54 (d, J = 6.7 Hz, 1H), 3.35 (s, 3H), 2.80–2.60 (m, 4H), 2.50 (d, J = 10.0 Hz, 1H), 2.44–2.33 (m, 2H), 2.31 (s, 3H), 2.25 (s, 5H), 2.23 (s, 1H), 2.05 (dd, J = 16.3, 7.0 Hz, 1H), 1.92–1.82 (m, 2H), 1.82–1.76 (m, 1H), 1.69–1.59 (m, 2H), 1.51–1.37 (m, 2H), 1.36–1.27 (m, 2H), 1.26 (s, 3H), 1.19 (s, 2H), 1.18–1.14 (m, 8H), 1.11 (s, 3H), 1.08 (d, J = 6.9 Hz, 3H), 1.02 (s, 3H), 0.92–0.84 (m, 7H), 0.79 (d, J = 7.5 Hz, 3H), ^{13}C NMR (101 MHz, $CDCl_3$) δ 165.80, 16 5.29, 164.65, 164.04, 134.67, 133.98, 133.45, 132.92, 100.18, 95.02, 83.46, 80.00, 78.27, 77.61, 77.36, 74.42, 73.77, 73.17, 73.13, 70.21, 67.70, 63.66, 63.13, 62.72, 52.49, 52.35, 49.58, 45.13, 42.00, 40.80, 40.75, 36.55, 35.18, 30.65, 27.35, 26.74, 26.20, 22.06, 21.56, 21.43, 21.35, 21.19, 17.99, 16.30, 11.32, 9.39, 7.70, HRMS m/z calcd for $C_{48}H_{81}N_2O_{18}^+$ 973.54789 found: 973.54749, colorless solid, yield 900 mg (23.1%), purity 96.1% via HPLC-ELSD, for the synthesis of **2**, monomethyl fumarate and dicyclohexyl carbodiimide were dissolved in ethyl acetate and a spatula tip of 4-(dimethylamino)pyridine was added as catalyst. Subsequently, Azithromycin was added. The reaction was stirred at room temperature and frequent reaction controls via MS and TLC were performed. The reaction showed complete conversion after 2 days and was worked up. Liquid–liquid extraction was performed to extract product from solution and done as described in synthesis of compound **1**. Afterwards residue was purified by flash chromatography (stationary phase: silica gel, 2.5 µm, Ø = 3 cm, h = 14 cm, mobile phase: cyclohexane/ethyl acetate/acetone with triethylamine) to yield product.

Compound 3 (2S,3S,4R,6R)-6-(((2R,3S,4R,5R,8R,10R,11R,12S,13S,14R)-11-(((2S,3R,4S,6R)-4-(dimethylamino)-3-hydroxy-6-methyltetrahydro-2H-pyran-2-yl)oxy)-2-ethyl-3,4,10-trihydroxy-3,5,6,8,10,12,14-heptamethyl-15-oxo-1-oxa-6-azacyclopentadecan-13-yl)oxy)-4-methoxy-2,4-dimethyltetrahydro-2H-pyran-3-yl methyl fumarate, ^{1}H NMR (400 MHz, $CDCl_3$) δ 6.86 (s, 2H), 5.19 (d, J = 4.7 Hz, 1H), 4.76 (d, J = 9.8 Hz, 1H), 4.70 (dd, J = 9.8, 2.4 Hz, 1H), 4.57 (d, J = 7.3 Hz, 1H), 4.50–4.40 (m, 1H), 4.26 (dd, J = 4.2, 1.8 Hz, 1H), 3.81 (s, 2H), 3.81–3.73 (m, 2H), 3.67 (s, 1H), 3.60 (d, J = 7.1 Hz, 1H), 3.32 (s, 3H), 3.29–3.21 (m, 1H), 2.92 (s, 1H), 2.76 (dt, J = 11.8, 5.9 Hz, 1H), 2.69 (dd, J = 13.7, 6.6 Hz, 1H), 2.53 (d, J = 10.4 Hz, 1H), 2.41 (d, J = 15.2 Hz, 1H), 2.32 (d, J = 11.5 Hz, 9H), 2.10–1.94 (m, 3H), 1.89 (ddd, J = 14.3, 7.6, 2.5 Hz, 1H), 1.76 (d, J = 14.6 Hz, 2H), 1.64 (dd, J = 15.1, 5.0 Hz, 1H), 1.46 (ddd, J = 14.4, 9.8, 7.3 Hz, 1H), 1.33–1.23 (m, 8H), 1.21–1.17 (m, 4H), 1.16 (d, J = 6.1 Hz, 5H), 1.12–1.06 (m, 9H), 1.05 (d, J = 7.6 Hz, 3H), 0.88 (t, J = 7.4 Hz, 7H), ^{13}C NMR (101 MHz, $CDCl_3$) δ 178.87, 165.34, 164.69, 133.93, 133.53, 102.54, 94.95, 83.59, 80.11, 78.19, 77.65, 74.49,

74.13, 73.79, 73.11, 71.14, 70.24, 68.06, 65.87, 63.12, 62.58, 52.50, 49.62, 45.29, 42.43, 42.06, 40.52, 36.52, 35.17, 29.82, 29.19, 27.59, 26.93, 22.10, 21.76, 21.43, 17.97, 16.35, 14.91, 11.37, 9.30, 7.67, HRMS m/z calcd for $C_{43}H_{77}N_2O_{15}^+$ 861.53185, found: 861.53226, colorless solid, yield 145 mg (81.9%), purity 97.0% via HPLC-ELSD, **2** was dissolved in methanol and stirred at room temperature. Reaction was monitored via TLC and MS. After 2 days solvents were evaporated. In a next step the residue was purified by flash chromatography (stationary phase: silica gel, 2.5 µm, Ø = 3 cm, h = 14 cm, mobile phase: cyclohexane/acetone) to yield white solid powder.

Compound 4 (2S,3R,4S,6R)-4-(dimethylamino)-2-(((2R,3S,4R,5R,8R,10R,11R,12S,13S,14R)-2-ethyl-3,4,10-trihydroxy-13-(((2R,4R,5S,6S)-5-hydroxy-4-methoxy-4,6-dimethyltetrahydro-2H-pyran-2-yl) oxy)-3,5,6,8,10,12,14-heptamethyl-15-oxo-1-oxa-6-azacyclopentadecan-11-yl)oxy)-6-methyltetrahydro-2H-pyran-3-yl methyl succinate, ^{1}H NMR (400 MHz, $CDCl_3$) δ 5.10 (d, J = 4.6 Hz, 1H), 4.75 (dd, J = 10.5, 7.5 Hz, 1H), 4.67 (dd, J = 9.7, 2.2 Hz, 1H), 4.53 (d, J = 7.5 Hz, 1H), 4.21 (dd, J = 4.1, 1.8 Hz, 1H), 4.03 (dq, J = 12.4, 6.1 Hz, 1H), 3.70–3.63 (m, 4H), 3.56 (d, J = 7.1 Hz, 1H), 3.53–3.44 (m, 1H), 3.33 (d, J = 10.6 Hz, 3H), 3.03 (s, 1H), 2.75–2.65 (m, 3H), 2.62 (d, J = 1.9 Hz, 4H), 2.60–2.55 (m, 1H), 2.50 (d, J = 10.3 Hz, 1H), 2.34 (d, J = 14.9 Hz, 1H), 2.30 (s, 3H), 2.23 (s, 6H), 2.18–2.09 (m, 1H), 2.09–1.98 (m, 1H), 1.98–1.81 (m, 3H), 1.71 (dd, J = 12.3, 3.1 Hz, 1H), 1.65 (d, J = 14.8 Hz, 1H), 1.58 (dd, J = 15.2, 5.0 Hz, 1H), 1.51–1.38 (m, 1H), 1.32–1.28 (m, 4H), 1.25 (t, J = 8.1 Hz, 7H), 1.19 (dd, J = 12.6, 6.7 Hz, 7H), 1.08 (d, J = 6.7 Hz, 4H), 1.05 (s, 2H), 0.92–0.83 (m, 10H), ^{13}C NMR (101 MHz, $CDCl_3$) δ 178.66, 172.90, 171.11, 100.72, 94.86, 83.39, 78.29, 78.10, 77.64, 74.45, 73.86, 73.21, 72.28, 70.23, 68.40, 65.79, 64.04, 62.62, 51.84, 49.51, 45.28, 42.23, 41.90, 40.80, 36.47, 34.97, 30.63, 29.71, 29.25, 27.54, 26.82, 26.30, 24.85, 22.06, 21.75, 21.40, 21.31, 18.39, 16.35, 14.91, 11.34, 9.12, 7.62, HRMS m/z calcd for $C_{43}H_{79}N_2O_{15}^+$ 863.54750, found: 863.54790, colorless solid, yield 455 mg 13.2%), purity 95.0% via HPLC-ELSD, Azithromycin (3 g) was dissolved in ethyl acetate. To this solution 1.1 eq of monomethyl succinate (580 mg, 4.4 mmol) was added. Subsequently, 1.1 eq of dicyclohexyl carbodiimide (910 mg, 4.4 mmol) was dissolved in ethyl acetate and added to the Azithromycin solution. A spatula tip of 4-(dimethylamino)pyridine was further added to the solution. Reaction monitoring showed partial conversion, so another 1.1 eq of monomethyl succinate and dicyclohexyl carbodiimide were added. The reaction was stirred at room temperature and frequent reaction controls via MS and TLC were performed. The reaction showed conversion after 10 days and was worked up. Liquid–liquid extraction was performed to extract product from solution and done as described in synthesis of compound **1** (yield = 3.4 g). In a next step the residue was purified by flash chromatography (stationary phase: silica gel, 2.5 µm, Ø = 3 cm, h = 14 cm, mobile phase: cyclohexane/acetone) to yield white solid powder.

Formation of Azi-Fum-GSH derivatives

Formation of glutathione fumarate adducts in mechanistic experiments were tested in situ and ex vivo. For in situ tests, compounds **1**–**3** were dissolved (diluted from 10 mM dimethyl sulfoxide (DMSO) stock to 10 µM final concentration) in water with 0.5% triethylamine. Glutathione (diluted from 100 mM DMSO stock to 100 µM final concentration) was added to the solution and reaction was monitored via MS. Formed adducts (see table 2 supporting information (SI)) were used to tune HPLC–MS/MS for screening assays. For ex vivo experiments whole blood was taken from tail vein of healthy male wistar rat. Compound **1**–**3** were added to rat blood (diluted from 10 mM DMSO stock to 10 µM final concentration) and incubated for 1 h at 37 °C and analyzed via MS/MS. Additionally, three C57BL/6 female mice were euthanized, livers explanted, immersed in ice-cold phosphate buffered saline pH 7.4 (PBS), minced and washed with the same solution. The mince was homogenized with Fastprep (FastPrep-24 5G, MP Biomedicals) using double amount of PBS to the liver. The homogenate was centrifuged at 700 × *g* for 10 min at 4 °C. The pellet was discarded and the supernatant was used as liver homogenate. 20 µM of each compound was added separately from 10 mM DMSO Stock (1 µL in 500 µL homogenate), vortexed and incubated at 37 °C. Samples were after 4 h and analyzed via MS/MS.

Quantification and monitoring of analytes using HPLC–MS/MS & MS/MS

Quantification of analytes was performed with an Agilent 1290 Infinity system coupled to a triple quadrupole Sciex API 4000 MS/MS detector. An Agilent C_{18} Poroshell 120 column (4.6 × 50 mm, 2.7 µm) was used for separation. The mobile phase was composed of water containing 0.1% formic acid (eluent A) and acetonitrile containing 0.1% formic acid (eluent B). Gradient used was: 10% B for 1 min, to 100% B in 2 min, 100% B for 3 min, to 5% B in 1 min, 5% for 3 min. MS detection parameters can be found in SI table 2. Reaction monitoring and fragmentation of synthesis products and of possible adducts was performed via MS/MS.

In vitro assays

Human blood products used in the in vitro assays (used for cell stimulation, viability, stability and uptake assays) were obtained from the center for transfusion medicine in Tübingen, Germany (Zentrum für

Klinische Transfusionmedizin Tübingen GmbH, (ethical approval number ZKT-FoPro202106-2305-01 and ZKT-FoPro202012-2211)).

Cytokine studies

PBMCs were isolated from buffy coat by density gradient centrifugation using PBMC Spin medium (pluriSelect SKU 60-00092-10). PBMCs were seeded at a density of 2×10^5 cells/well in 96-well flat-bottom plates (Sarstedt 83.3924) and left untreated or stimulated with either: (a) 1 µg/mL LPS and 10 ng/mL interferon gamma (IFNγ), (b) 1 µg/mL LPS and 75 µM Imiquimod (IMQ) or (c) 10 ng/mL LPS and 1 µM Nigericin. Cells were then treated with compounds or DMSO at the indicated concentrations for 24 h at 37 °C. Supernatant was taken after centrifugation at 400 × *g* and directly used for ELISA. Supernatant was diluted 1:10 for human TNFα (bio-techne R&D system DY210) and human IL-1β (Biolegend 437016) readout and 1:2 to detect human IL-12 p70 (Biolegend 431701). OD was measured at 450 nm using VersaMax (Molecular Devices). ELISA was performed according to the respective manual. Cytokine concentrations were calculated using a linear standard curve (7 standard concentrations; 100–1000 pg/mL).

Viability assays

Human PBMCs were prepared as above. For MTT (3-(4,5-Dimethyl-2-thiazolyl)-2,5-diphenyltetrazolium) assay after treatment, cells were mixed with 1 mg/ml 3-(4,5-Dimethyl-2-thiazolyl)-2,5-diphenyltetrazolium bromide (MTT; Acros organics) and incubated for 1 h at 37 °C. Cells were centrifuged at 400 × *g* and supernatant was removed completely. DMSO was added to the wells. After 2 h incubation on a shaker in the dark at room temperature, OD was measured at 570 nm using a microplate spectrophotometer (VersaMax, Molecular Devices). For live/dead staining, cells (1 Mio cells per mL) were harvested by centrifugation at 400 × *g*, washed once in FACS-Buffer (1xPBS without Ca^{2+} Mg^{2+} 3% FBS (Biowest S1810-500) + 3 mM K_2EDTA) and resuspended in 50 nM Helix NIR® (Biolegend 425301) in FACS-Buffer. Samples were acquired on a Guava EasyCyte 8HT (Merck) and analyzed using FCS Express 7 Research Edition (De Novo Software).

Stability assay

1 mL of either, human whole blood or plasma was mixed with 1 µL of a 10 mM DMSO stock of tested compound and incubated at 37 °C. At indicated time points 50 µL of blood or plasma was transferred to 150 µL of acetonitrile. Mixture was vortexed, sonicated for 5 min and centrifuged for 7 min at 20.000 *g* at 4 °C. Supernatant was transferred to HPLC vials and analyzed as describe in the *Quantification of analytes using HPLC–MS/MS & MS/MS* section.

Uptake assay

Human buffy coat was prepared to contain 5×10^6 cells/mL. 1 mL was mixed with 1 µL of a 10 mM DMSO stock of tested compounds. At time points 0 and 30 min sample was centrifuged for 5 min at 400 × *g* at 4 °C. 50 µL of supernatant was added to 150 µL of acetonitrile, remaining supernatant was discarded. Pellet was resuspended in 50 µL of ice cooled PBS and centrifuged again (5 min, 400 × *g*, 4 °C). Supernatant was discarded and pellet resuspended in another 50 µL of PBS. Cell suspension was transferred to 150 µL of acetonitrile. Mixture was vortexed, sonicated for 5 min and centrifuged for 7 min at 20.000 *g* at 4 °C. Supernatant was transferred to HPLC vials and analyzed as describe in the *Quantification of analytes using HPLC–MS/MS & MS/MS* section.

Kinetic assay of the Michael addition to GSH

For kinetic measurements 100 mM stocks of compounds **1**–**4** were prepared in DMSO, and stocks of DMF, MMF and GSH in water. For each compound (**1**–**4**, DMF or MMF) 1 µL were mixed with 10 µL of GSH in 989 µL of buffered solution. Buffers were prepared at pH 5 (250 mM sodium acetate/acetic acid buffer), pH 7.3 (250 mM NaH_2PO_4/Na_2HPO_4) and pH 8 (250 mM NaH_2PO_4/Na_2HPO_4). Absorption was measured with NanoPhotometer NP80 Implen at 226 nm every 90 s for 15 min.

In vivo studies

All study protocols were approved by the local Animal Care and Ethics Committee (Federal government ethics committee, Tübingen, Germany under the licenses 35/9185.81-7/SYN 06/20; 35/9185.81-7/SYN 07/18; and 35/9185.81-7/SYN 11/19). Mice used in these studies (BALB/c and C57BL/6, all female and 8 weeks old) were purchased from Janvier Labs (Le Genest-Saint-Isle). Animals were acclimatized for at least 1 week with standard chow (Mouse Maintenance, V1534-000, Ssniff Spezialdiäten GmbH, Germany) and drinking water ad libitum before the start of the experiment. Animals were housed in type IV cages (4 animals per cage), with bedding and enrichment material and kept at 22 °C (± 1 °C), 45–65% humidity, with 12/12 h dark/light cycles period. Animals were monitored daily and at the end of the experiment, terminated painlessly with overflow of CO_2.

Pharmacokinetic studies

For this study, 18 female BALB/c mice were utilized and each experimental group consisted of 3 animals. Animals were treated orally once with the testing compounds dissolved in 0.1% citric acid (12 µmol/kg). Tail blood was collected after 5, 15, 30, 45, 60, 90 min. Animals were euthanized with CO_2. and organs collected 2 and 4 h after treatment. Collected samples stored at -25 °C until further processing, as published (Straß et al. 2021).

Cream-induced mouse model

In this study, 56 female BALB/c mice were examined and each experimental group consisted of 8 animals (4 animals per cage). On day 0, prior to psoriasis induction, dorsal skin was shaved using a clipper, followed by application of depilatory cream to complete fur removal. Psoriasis was induced by daily application of an induction cream. Briefly, the cream was formulated with IMQ (5%), DMSO (3.8%) and isostearic acid (25%; supplier TCI I0184), mixed with a spatula till homogenous, then hydroxypropyl methylcellulose (HPMC, 2%, dry) was added. At the end, base cream (Deutscher Arzneimittel Codex) DAC was added and homogenized. Cream was stored at 4 °C. From day 1 to day 6, 50 mg of induction cream was weighed and applied using a spreader to achieve homogeneity on 4 cm^2 of depilated skin. Treatments (compounds **1–3**, DMF and vehicles) were administered orally once daily. For oral administration the vehicle was a mixture of 0.5% citric acid and 0.5% hydroxypropyl methylcellulose (HPMC, dry). Parameters measured were: daily body weight (BW), skin thickness, skin redness and scaling (0 = no change, 1 = marginal effects, 2 = moderate effects, 3 = strong effects, 4 = maximum). Animals were euthanized on day 7, 27 h after last exposure to cream and 4 h after last treatment. At termination, pictures of back skin were taken (*ante mortem*) and skin samples (for histology and for gene expression) were collected and the weights of spleen and liver were recorded.

Acute peritonitis

Acute peritonitis was induced with the intraperitoneal injection of MSU crystals, which were prepared following protocols published earlier (Roberge et al. 1994). The in-house prepared crystals were characterized by examination under microscope and in in vitro assays versus commercially available MSU crystals (Invivogen, data not shown). C57BL/6 mice (male, 8 weeks) were treated per oral with either compound 3 (n = 15) or PBS (n = 5) and were injected with MSU crystals (200 µL of a 15 mg/mL suspension of MSU crystals in sterile PBS) intraperitoneal15 min later. Animals were euthanized after 4 h. At termination heart plasma and peritoneal lavage (sampled with 1–2 mL of ice-cold PBS) were collected and samples analyzed via ELISA for cytokine concentrations of IL-1β, IL-6 and IL-10 following protocols described in section *cytokine studies*.

Real-time polymerase chain reaction (qRT-PCR)

Flash frozen skin samples were homogenized in lysis buffer using a standard fast prep procedure. Subsequently, RNA was isolated using the Qiagen RNeasy® MiniKit. 3.6 µg of RNA was used for cDNA synthesis, using PerfeCTa DNase I (Quanta Bioscience) and 5 × PrimeScript RT Mastermix (Takara). Gene-specific primers used for qPCR are listed in Table 4 SI. The qPCR reaction was performed in duplicates with Blue S'Green qPCR Mix Sepa-rate ROX (Biozym) in 96-well plates. Amplification was carried out in the QuantStudio® 3 qPCR system (ThermoFisher Scientific/Quantstudio™ Design & Analysis Software v.1.4.3). Cycle conditions were set as 95 °C for 2 min followed by 40 cycles of 95 °C for 5 s and 60 °C for 17 s; a melt-curve analysis was performed for each qPCR reaction. Primer efficiency was determined for each primer pair to ensure linear standard curve and high amplification efficiency. Threshold cycle (Ct) values were used for the calculation of the relative gene expression levels. For this, all values were first normalized to respective Ct values of the (hypoxanthine–guanine phosphoribosyltransferase) HPRT housekeeping gene. Then, normalized ΔCt values of the different treatment groups were compared to the ΔCt levels of the vehicle treated control group which was set to 1. Normalized expression ratios ($2(-\Delta\Delta Ct)$) are given for all treatment groups relative to the vehicle group. Ct values of all samples were normalized to the respective Ct values obtained for HPRT housekeeping gene, resulting in the ΔCt value for each sample: ΔCt (gene x) = Ct (gene x)−Ct (HPRT). To calculate the ΔΔCt value, the ΔCt average of the control condition (vehicle) was used. This analysis was also performed for the individual control condition samples to determine variance within the control group. Subsequently, ΔΔCt values of each sample were transformed into normalized expression ratio which gives the fold increase (or decrease) of the target gene expression compared to the control condition (vehicle) and normalized to the reference gene (HPRT). Normalized expression ratio (fold change) = $2^{-\Delta\Delta Ct}$. Data were plotted as scatter plots using GraphPad Prism 9.1.0.

Statistics

All experimental results were first tested for normal distribution using Shapiro–Wilk for normality. Statistical analysis between multiple groups was done using two-way ANOVA followed by Bonferroni correction. Kruskal–Wallis test was used for non-parametric data. Non-marked bars are

considered as not significant by which statistical significance was considered at the level of p-value < 0.05. Calculations of e.g., half-life were made with GraphPad Prism 9.3.1.

Results

Design of targeted fumarates—from synthesis to mechanistic insights

Structures and substitution patterns were confirmed by NMR (Straß et al. 2021). Specific shifts in ^{1}H spectra of compounds **1** to **4** at proposed positions 2′ and/or 4″ were observed. NMR spectra of given compounds can be found in supplemental information (SI). Additional, MS/MS experiments showed distinct fragmentation patterns of synthesized compounds (Table 1 SI). Purity was tested via HPLC–UV/ELSD. A substance was declared pure at greater than 95%.

GSH conjugation

Based on previous studies from Schmidt et al. we incubated DMF, MMF and compounds **1**–**4** at different pH values (5, 7.3 and 8) with GSH (1/10 the fumarate concentration) and measured the absorbance at 226 nm (maximum of double bond) over time. At pH 8 (SI Fig. 1) compound **1** hydrolyzed and there was no change in absorbance. Compounds **2**, **3** and DMF show similar initial kinetics of GSH conjugation, but **3** stabilizes earlier, suggesting that the reaction stops before the available double bonds are depleted. LC–MS/MS confirmed the conversion to conjugates (data not shown). MMF and compound **4** do not show any reaction to GSH in the given time. MMF is believed to not react or only over a long period (Schmidt et al. 2007). Compound **4** does not carry the necessary double bond and is therefore used as a negative control. At pH 5 (SI Fig. 1) hydrolysis is slowed down for all fumarate diesters providing more diester for the GSH conjugation to occur. At pH 5, DMF conjugates to GSH more slowly, than the macrolide fumarate esters. At the physiological pH 7.3 (Fig. 2A), we observed an increased conjugation rate for the macrolide fumarate esters **1**–**3** compared to DMF. Compounds **1**–**3** react within seconds to minutes ($T_{1/2}$ of **1** 25 s; **2** 103 s and **3** 153 s), whilst DMF has the longest half-life ($T_{1/2}$ = 17 min). Although, conversion for **1** can be detected, absorption at 226 nm is higher compared to compounds **2** and **3**. This might be due to high hydrolysis rate and therefore conversion to MMF. Overall, these results lead to the conclusion that the new fumarate diesters have, compared to DMF, a faster conjugation rate at physiological pH towards possible Michael donors, like GSH.

Addition of GSH to our fumarate esters can be shown not only via change in absorbance of the double bond, but also as a stable Azithromycin-fumarate-GSH complex via MS (Fig. 2B). These peaks were not only found in situ, but also after incubation in rat whole blood and mouse liver homogenates (SI Fig. 2 to 7). Adducts of fumarates with hydrolysis of the macrolide core system were not identified. At higher pH values hydrolysis of the methyl ester at the fumarate side was observed by MS (SI Fig. 4). The GSH conjugates were relatively stable and could be detected over a longer time course.

Stability and uptake

Stability assays in human whole blood and plasma (SI Fig. 10) showed that the 2′ position hydrolyses almost immediately. Compounds carrying fumaric esters in this position (found in compounds **1** and **2**) form their more stable metabolites very rapidly. 4″ esters (found in compounds **2** and **3**) were slow to hydrolyze, with low levels of the free macrolide detected. However, the total amount of these substances decreases over time. This is due to the fact that stable GSH adducts form with this class. In general, it was observed that hydrolysis of the 2′ position is slower in whole blood compared to plasma. This is due to accumulation to acidic cell compartments and stabilizing effects of the lower pH value. The stabilization was already shown in previous publications by our group using SCFA esters of azithromycin (Straß et al. 2021).

In addition, we have performed cellular uptake experiments to show possible accumulation into immune cells. Human buffy coat was therefore incubated with compounds **1** to **3** at a concentration of 10 µM for a total of 30 min and compared to concentrations at t_0. We measured total macrolidic concentration and found an intra- vs. extracellular factor of 14× for compound **1**, 6× for compound **2** and 8× for compound **3** (SI table 5). All compounds partition to immune cells and accumulate over time. Factors would be even higher, but compounds bound to GSH or other cysteine carrying peptides were not quantified.

Effects on inflammatory cytokines in vitro

Cytokine concentrations were measured 24 h after stimulation of PBMCs with LPS/INFy and treatment with DMF or compounds **1**–**4** at different concentrations (Fig. 2D). Experiments were performed according to protocols published by Lehmann et al. (Lehmann et al. 2007). The results indicate that the mechanism of DMF and the set of new compounds is likely to be similar. The negative control **4** (2′-succinate) and compound **1** (2′-fumarate) don't exert a major influence on the measured cytokines. Compound **1** hydrolyses to the inactive MMF too quickly to influence cytokine levels (Straß et al. 2021). Compounds **2** and **3** carry a fumaric ester in the 4″ position. This position hydrolyzes more slowly than the 2′ and seems to have major influence on cytokine production.

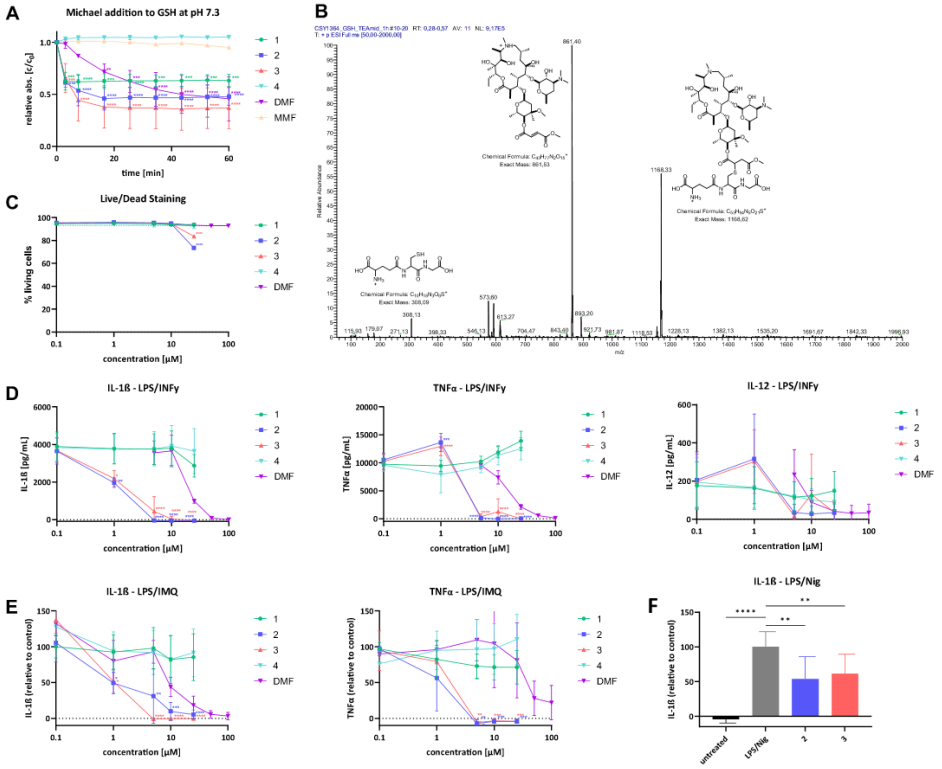

Fig. 2 **A** Relative absorption (c/c_0) at 226 nm of DMF, MMF and compounds **1**–**4** (100 µM) with GSH (1 mM) monitored over 60 min in PBS (n = 3). **B** Mass spectra of compound **3** (10 µM) 1 h after incubation at room temperature with GSH (100 µM) and 5% triethylamine as base. **C** Direct toxic effects were tested in human PBMCs (stimulated with 1 µg/mL LPS and 10 ng/mL INFγ) at different concentrations after 24 h (n = 2). **D** Human PBMCs were stimulated with LPS (1 µg/mL) and INFγ (10 ng/mL) and treated with either DMF or compounds **1**–**4** at different concentrations. Cytokine secretion (IL-1β, TNFα and IL-12) measured via ELISA from supernatant after 24 h (n = 3). (E) Human PBMCs were stimulated with LPS (1 µg/mL) and IMQ (75 µM) and treated with either DMF or compounds **1**–**4** at different concentrations. Cytokine secretion (IL-1β and TNFα) were measured via ELISA from supernatant after 24 h (n = 3). (F) Human PBMCs were stimulated with LPS (10 ng/mL) and Nigericin (1 µM) and treated with compounds **2** and **3** at 5 µM. Cytokine secretion (IL-1β) measured via ELISA from supernatant after 24 h (n = 3). P values ≤ 0.0001 are indicated with ****p ≤ 0.001 are indicated as ***p ≤ 0.01 are indicated as **p ≤ 0.05 are indicated as*

Results from PBMCs for **2**, **3** and DMF show significant reduction in released cytokines IL-1β and TNFα, but not for IL-12. This reduction can be seen for **2** and **3** from 1 µM for IL-1β and 5 µM for TNFα. DMF reduces IL-1β and TNFα from 25 µM suggesting that DMF is 5 to 25-fold less active in vitro. The results for the control **4** suggest that this cytokine effect is not due to the macrolide itself.

To further investigate the possible underlying mechanism and assess the effects of inflammatory cytokines in cream induced psoriasis we stimulated human PBMCs, according to Hoyle et al. (2022) first with LPS (and co-treatment with substances) and in a second stimulus with IMQ. This stimulus induced a fast increase of proinflammatory cytokines in these cells. DMF and the compounds **2** and **3** (Fig. 2E) were able to significantly reduce the levels of IL-1β and TNFα. The reduction of IL-1β and TNFα can be seen in the range between 1 and 5 µM for compound **3** and 10 to 25 µM for compound **2** and DMF. The negative control compound **4** and the 2′ fumaric ester compound **1** were inactive in this assay.

In a next step tested the compounds' possible effects in the inflammasome pathway. Our set of compounds is similar to DMF and expected act in a similar way. DMF is known to play a role in the inflammasome response via binding to cysteine residues on gasdermin D (Humphries et al. 2020). NLRP3 inhibition has been shown to be more potent for DMF than MMF (Miglio et al. 2015; Hoyle et al. 2022). Inflammasome activation was done by priming PBMCs with LPS (and co-treatment with substances) and nigericin as second stimulus. This was done for compound **2** and **3** at 5 µM. Both substances reduced IL-1β levels significantly, with compound **2** being slightly more effective (Fig. 2F).

Taken together, compounds **2** and **3** showed anti-inflammatory effects in different stimulation settings and that they are typically at least an order of magnitude more potent than DMF in vitro.

Viability assay

The Viability assays (live/dead staining and MTT) performed in peripheral blood mononuclear cells (PBMCs), (Fig. 2C) under the same conditions as the cytokine assays (macrolides are solubility limited) suggest, that the observed cytotoxicity is not related to the cytokine effects. For compounds **2** and **3**, the highest concentration (25 µM) induced apoptosis mainly in monocytes. These effects are known for DMF starting from 10 µM (Michell-Robinson et al. 2016). Our data (SI Fig. 8) shows similar effect for DMF, **2** and **3** at concentrations starting at 25 µM. However, due to high cell uptake, the effective concentration of the macrolides in these cells is much higher (see stability and uptake) (Bosnar et al. 2005; Straß et al. 2021; Burnet et al. 2018).

Given that fumaric esters (MMF as well as DMF) are capable of influencing cell metabolism via inhibition of glycolysis (modification of GAPDH) in the tricarboxylic acid (TCA) cycle (Kornberg et al. 2018; Angiari and O'Neill 2018; Park et al. 2019; Ocana et al. 2021) we assessed metabolism via the MTT assay. Compounds **2** and **3** (SI Fig. 9) reduced MTT more than DMF with a 20-fold difference in potency. At 5 µM, however, the difference was reduced to twofold difference in the observed effects. Compounds **1** and **4** did not show any influence on the metabolic activity.

New fumarates and their in vivo action

Psoriasis mouse model

Compounds **1**–**3** were tested in a dose response setting in a cream-induced psoriasis model, to find an optimal dose range for each compound. All studies consisted of cream application on the skin for seven consecutive days to induce psoriasis. Doses were based on pharmacokinetic results (Fig. 4), in vitro results (Fig. 2) and previous studies with similar compounds (e.g. (Straß et al. 2021; Burnet et al. 2018)). DMF was used in one study as positive control with a dose of 30 mg/kg based on reported activity in the literature (Lehmann et al. 2002; Chen et al. 2014; Liu et al. 2016b).

The 2′ monoester of MMF, compound **1**, reduced score at all doses (0.03, 0.06, 0.12 and 0.24 mg/kg) (Fig. 3A). This substance hydrolyses relatively quickly, showing the lowest interaction with GSH in vitro. However, since the macrolidic substances partition to acidic compartments in vivo, they tend to be more stable than in cell-based assays. The 0.12 mg/kg dose was ideal for most parameters for this substance, with most prominent effects on erythema (redness) (SI Fig. 12). At termination, the induction cream group (labelled as IMQ) had an average score (consisting of three parameters redness, scaling and thickness of the skin) of 6.5, while the 0.12 mg/kg group was score 3.3. At a dose of 0.12 mg/kg the compound **1** tended to from protect body weight change. Loss of BW is an effect of IMQ and was maximal at day 3. The area under the score-time curve is also optimal at 0.12 mg/kg. Skin thickness was most reduced at doses of 0.06 and 0.12 mg/kg compared to induction cream. Spleen and liver sizes showed no significant differences between all groups (SI Fig. 11).

The 2′, 4″ macrolide diester, compound **2,** showed beneficial effects vs. the induction cream in terms of skin score and area under the curve at 0.03 and 0.06 mg/kg (about half the dose of the monoester **1**) (Fig. 3B). This can be explained by the effectively two moles of fumarate per mole at the same dose in mg/kg for this compound. On the final day, the non-treated group had score 5 vs. score 4.3, 3.1, 2.9 and 4.4 for 0.015, 0.03, 0.06 and 0.12 mg/kg respectively. These data suggest, as seen in other substances, that effects on other immune functions (e.g. gut homeostasis) may develop as dose increases. Liver and spleen weights did not show significant differences (SI Fig. 11). Skin thickness on termination was improved in the 0.015 mg/kg and 0.03 mg/kg doses (SI Fig. 11). Compound **2** performed better than compound **1** in GSH conjugation in vitro. It shares the 2′ ester with compound **1** and the 4″ ester with compound **3**.

The 4″ monoester, compound **3** was given at the same doses as compound **1** (0.03, 0.06, 0.12 and 0.24 mg/kg) so that the molar dose of MMF was the same (Fig. 3C). DMF was included as a comparison at 30 mg/kg—being between 125 and 1000 times higher than the doses used for Compound **3**. DMF effects were slow in onset and first visible at day six, as were the effects of compound **3** at 0.24 mg/kg. At termination, total scores for induction cream (labelled as IMQ) were at 6.8, vehicle 5.8 and DMF was at 5.1. Compound **3** was 5.8, 5.1, 5.4 and 4.5 at 0.03, 0.06, 0.12 and 0.24 mg/kg respectively. Significantly lower area under the curve was only found for the positive control DMF at 30 mg/

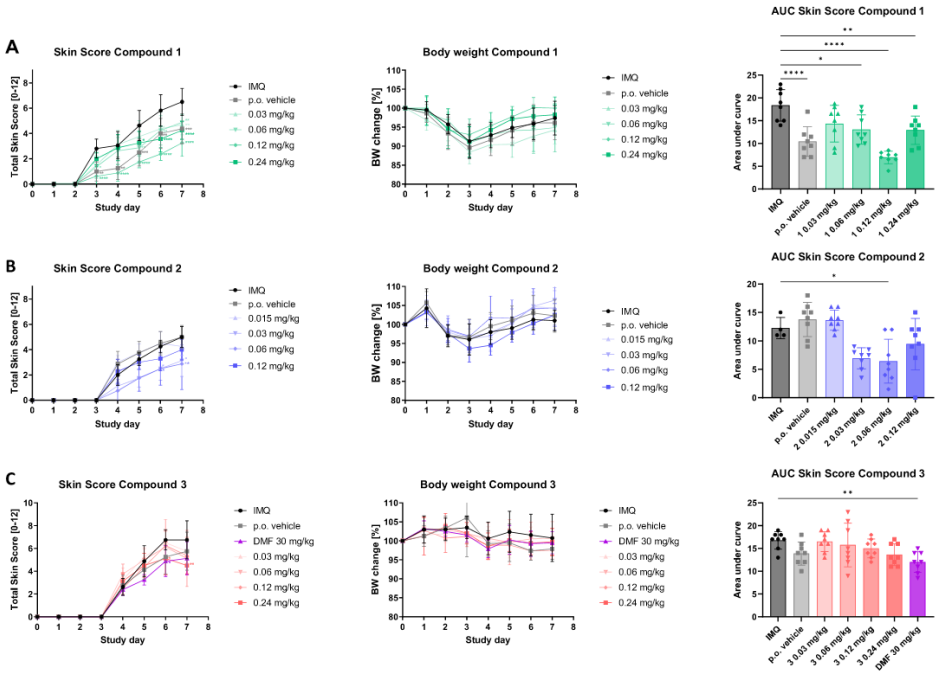

Fig. 3 All studies were conducted in 6–10 weeks old female BALB/c mice n = 8 (only exception is IMQ control group for compound **2** (C) where n = 4). Animals treated with induction cream (50 mg) for seven consecutive days. Back skin was scored daily for parameters redness, thickness and scaling (scores each between 0 and 4, with 4 being most severe). Body weight was recorded daily. Induction cream consisted of 5% IMQ solved in 3.6% DMSO and 25% isostearic acid in DAC base cream. 0.5% citric acid and 0.5% HPMC in water served as vehicle. First graph in each row shows accumulated skin score of compounds **1**–**3**, DMF, IMQ and p.o. vehicle scored over 7 days. Second graph in each row shows change of body weight of groups treated with compounds **1**–**3**, DMF, IMQ or p.o. vehicle. Daily measured, in comparison to day 0. Third graph in each row shows total area under the curve for skin score of each treatment. P values ≤ 0.0001 are indicated with ****p ≤ 0.001 are indicated as ***p ≤ 0.01 are indicated as **p ≤ 0.05 are indicated as*. Groups were statistically analyzed against IMQ treatment

kg (Fig. 3C). There was no difference in BW, skin thickness, liver or spleen weight.

Compound **3** differs from compounds **1** and **2** in that it is most GSH bound and that the 4″ site is the most stable of the esters. Thus, it is most likely to react with GSH and the least likely to release free MMF. To investigate distribution and fate, a subgroup of mice received 10 mg/kg compound **3** by oral gavage, 2 h before termination. Analysis of blood, skin, spleen, lung, liver, colon, thymus (via HPLC–MS/MS) showed no major amounts of **3** (m/z = 861), its GSH adduct (m/z = 1168), nor, its major metabolite detected in stability assays, Azithromycin (m/z = 749) (SI table 3). Since elimination of macrolides is known to be slower and accumulation and distribution of similar molecules has been published already (Straß et al. 2021) the most likely possibility is that the compounds bind to other cysteine carrying molecules or proteins as reported for DMF (McGuire et al. 2016) and this may be relevant to **3**.

Inflammatory processes in psoriatic skin lesions are initially driven by the proinflammatory cytokines IL-23 and IL-12. These cytokines stimulate Th17 cells to induce the release of IL-17, IL-22 and TNFα. Analysis of gene expression of induced back skin in our performed studies showed significant differences in most inflammatory markers (Fig. 4). Lowered TNFα levels compared to NTC animals were detected for treatment groups and one IMQ group. Overall, TNFα mRNA levels are low compared to NTC. Compound **1** even lowered TNFα significantly. The IL-17 subtypes IL-17A and F were upregulated (50-to-300-fold change) in skins of mice induced but not treated, whilst mice

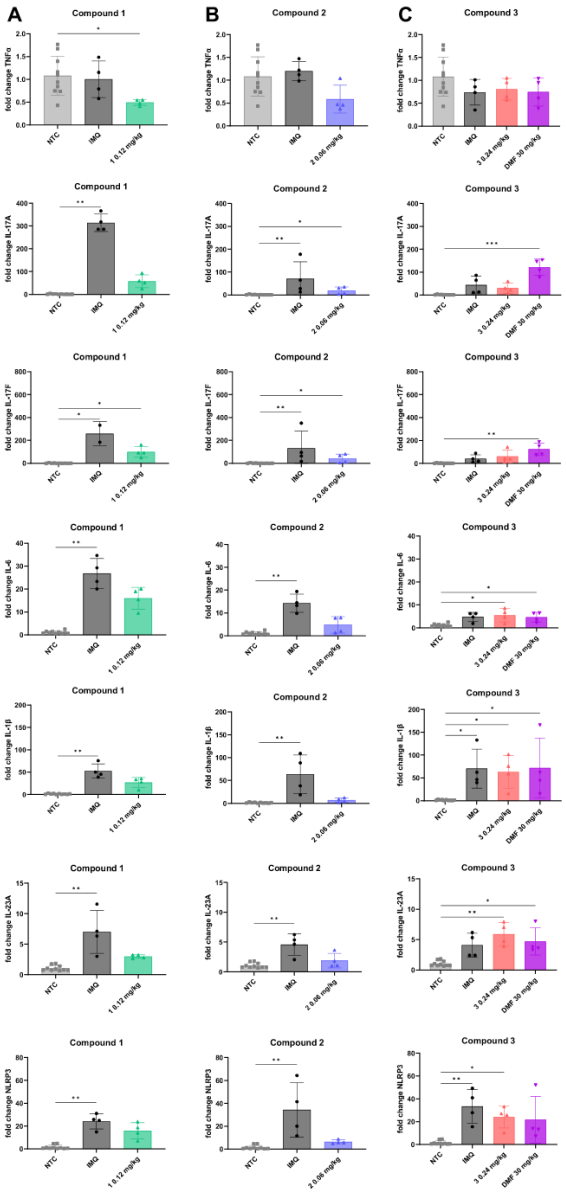

Fig. 4 Cytokine induction measured in skin samples collected from 6–10 weeks old female BALB/c mice. Samples were collected on final day of studies (day 7) and analyzed via qPCR. Analyzed were best performing (in regards of total skin score; see Fig. 3) treatment groups vs. induction cream receiving groups from this study (IMQ) vs. not induced and not treated animals (NTC). **A** NTC vs. IMQ vs. compound **1** at 0.12 mg/kg. **B** NTC vs. IMQ vs. compound **2** at 0.06 mg/kg. **C** NTC vs. IMQ vs. compound **3** at 0.24 mg/kg vs. DMF at 30 mg/kg. P values ≤ 0.0001 are indicated with ****$p \leq 0.001$ are indicated as ***$p \leq 0.01$ are indicated as **$p \leq 0.05$ are indicated as*. Groups were statistically analyzed against NTC. Kruskal–Wallis test with Dunn's comparison was used after Shapiro–Wilk test for normality. Data represented as means with error bars as SD (n = 8)

treated with compound **1** and **2** (Fig. 4A, B) showed only minor changes in comparison to NTC mice. For compound **3,** there were no major changes in cytokine expression level compared to IMQ induced reference group. DMF in contrast showed higher levels of IL-17A and F then IMQ and compound **3**. Gene expression levels of IL-23A, important for initial activation of Th17 cells, is significantly upregulated in IMQ groups and DMF and compound **3** receiving groups. Compound **1** and **2** showed to have beneficial effects for reduction of IL-23A (almost same levels as NTC). The same pattern is seen for IL-6 induction. Inflammasome activation is displayed by RNA levels of IL-1β and NLRP3. Both parameters are increased with induction cream in all studies. Reduction from these levels can be seen for compounds **1** and **2**.

Pharmacokinetics

Pharmacokinetic studies aimed to assess the compounds distribution and hydrolysis effects further. Initial pharmacokinetics for compound **1** (Fig. 5A and SI Fig. 13) suggested that the macrolide esters of MMF had a high volume of distribution and adequate exposure to circulating immune cells as well as immune organs like the spleen and to skin. These properties, combined with the much lower dose should result in a more selective exposure to compartments relevant immune-mediated diseases, as psoriasis. Conclusions on the distribution of compounds **2** and **3** (Fig. 5B, C) can only be made to a limited extent, since a large proportion of the substance quantities were not detected. This is a further indication of binding to thiol-bearing groups in proteins. However, compounds **2** and **3** show sufficient concentrations (> 100 nM) in skin tissue compared with liver for some activity to be expected. The more metabolically active liver may hydrolyze the fumaric esters faster than the skin.

Acute peritonitis mouse model (MSU crystal-induced)

The MSU crystal induced peritonitis model is a murine model for human acute gout. We treated C57BL/6 mice (male, 8 weeks, 15 animals per group and 5 animals PBS vehicle) orally with 0.1 mg/kg Compound **1** and injected MSU crystals into the peritoneum 15 min after treatment. Animals were terminated 4 h post-MSU induction to determine cytokine concentration in plasma and peritoneal lavage. Animals treated with compound **3** (0.1 mg/kg p.o.) (Fig. 6) showed a significant reduction of the proinflammatory cytokine IL-6 in both, peritoneal lavage and heart plasma. However, IL-1β and IL-10 were not significantly reduced in peritoneal lavage and plasma by the treatment (SI Fig. 14).

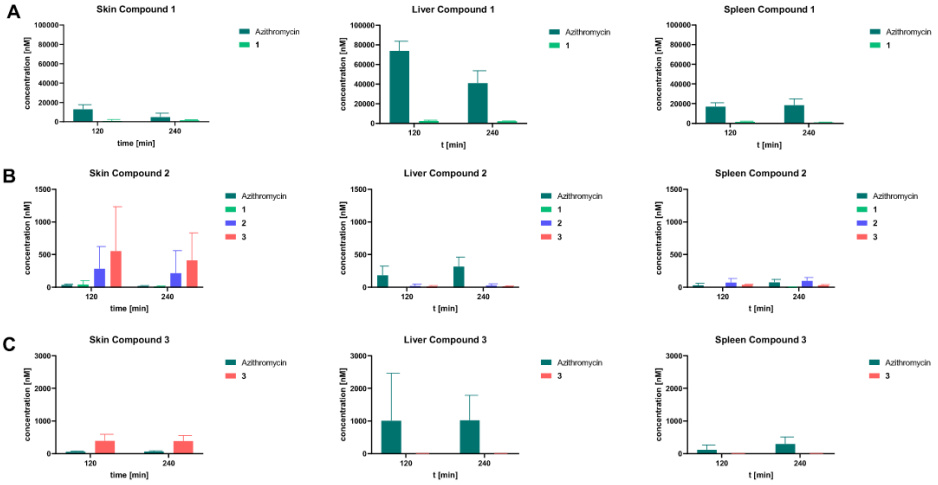

Fig. 5 Comparison of pharmacokinetic data (BALB/c mice, female, 8 weeks old, n = 3) of lead substances **1**–**3** in different organs via oral route (12 µmol/kg). **A** Compound **1** and metabolite Azithromycin in skin, liver and spleen after 120 and 240 min. **B** Compound **2** and metabolites Azithromycin, **1** and **3** in skin, liver and spleen after 120 and 240 min. **C** Compound **3** and metabolite Azithromycin in skin, liver and spleen after 120 and 240 min. Results are expressed as means with SD. Remaining organ data in SI Fig. 13. Data represented as means with error bars as SD (n = 3)

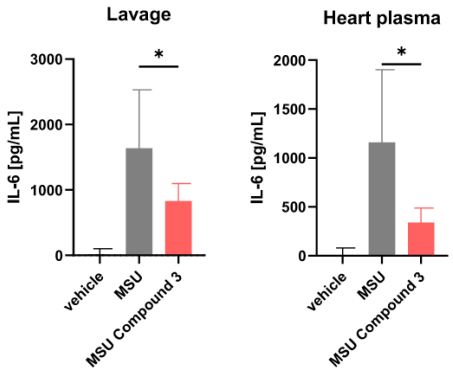

Fig. 6 Cytokine concentrations of IL-6 in peritoneal lavage and heart plasma sampled from mice treated with PBS (vehicle and MSU group) or Compound 3 (0.1 mg/kg) and terminated 4 h after administration of MSU crystals. P values ≤ 0.0001 are indicated with ****p ≤ 0.001 are indicated as ***p ≤ 0.01 are indicated as **p ≤ 0.05 are indicated as*. Groups were statistically analyzed against MSU treatment. Kruskal–Wallis test with Dunn's comparison (for heart plasma) or Brown-Forsythe and Welch test with Dunnett's comparison (for lavage) was used after Shapiro–Wilk test for normality. Data represented as means with error bars as SD (n = 15)

Discussion

Design of targeted fumarates—from synthesis to mode of action

Monomethyl fumarate (MMF) has risen to prominence as a treatment for MS where it is commercialized as Tecfidera, a DMF preparation in which DMF is considered the pro-drug of MMF. DMF was commercialized in the past as a treatment for psoriasis in a mixed ester salt formulation. The mode of action of DMF/MMF is not fully understood, however, recent reports of its use in MS suggest that it tends to drive immune cell subsets towards anti-inflammatory response, notably Th1 and Th17 cells (Mills et al. 2018). It is thought to be proapoptotic, and this may explain the reduction of specific lymphocyte sub-sets in treatment. At the molecular level, these effects are proposed to be related to: (i) interactions with NF-kB signaling, (ii) binding to GPR109A, (iii) conjugation to glutathione, (iv) binding to cysteines in GAPDH and (v) interactions with the Nrf2 pathway.

As a therapeutical use in human, the typical dose of DMF is about 500 mg daily, which approximates to 7–8 mg/kg or 75 µmol/kg. The majority of DMF is converted to MMF on uptake and circulates as MMF in plasma. MMF appears not to be thiol reactive, however, DMF entering the gut mucosa is thiol reactive prior to hydrolysis of the first ester. If thiol reactivity was important to the mode of action in the autoimmune setting, more stable esters, such as longer chain alcohol groups, would be favored, which appears not to be the case.

Here, we have developed novel fumarate diesters to differentiate effects on immune cell activation and thiol conjugation. Our hypothesis was that GPR109A is the primary target and that the most relevant form is in immune cells. To test this hypothesis, we synthesized substances that concentrate MMF into the endosomes of immune cells where it could maintain GPR109A in its activated or bound form in the endosome. These compounds are approximately 300–900-fold more potent than DMF in vivo on a molar basis in a murine psoriasis model. Given their high uptake into target cells, and their concentration in endosomes, a target located in the endosome could explain the potency gain exhibited by these substances.

However, the substances also exhibit much faster reaction with GSH than that of DMF (initial rates 10-200-fold faster) which implies that this mode of action should also be considered. GSH is required for oxidative burst reactions in myeloid cells (Brennan et al. 2015), and its depletion can limit activation reactions. Similarly, GSH is located in the endo- and lysosomes, where the conjugates concentrate (Xu et al. 2018). Nonetheless, the abundance of GSH, cysteines and protein thiols, is such that they can titrate low doses (e.g. 0.03 mg/kg) of substance. Furthermore, in both clinical and preclinical studies (Mrowietz et al. 2018; Dibbert et al. 2013; Linker and Haghikia 2016), MMF is the dominant product detected in plasma and MMF conjugates with GSH at much lower rate (see Fig. 1) (Schmidt et al. 2007). It is difficult to estimate to what extent DMF or the conjugate diesters may be bound to thiols in large molecules, however, comparing recovery of thiol binding and non-binding compounds, the difference suggests that 90% is reacting with thiols in large molecules. Thus, the balance of data suggests that the thiol binding aspect is most likely a secondary effect that is more relevant in vitro, where the total volume of medium relative to cells is higher (> 1000x) and where the total substance available can titrate a higher proportion of thiols. In areas where the substance is more abundant relative to cells, such as the gut, there may also be thiol binding effects and these may interfere with innate immune reactions. These in turn may impact innate control of gut bacteria in the epithelium and be the cause of tolerability issues in the gut.

The effects of DMF in vitro reported here reflect data reported by others. McGuire et al. (2016) showed reduction of cytokines in bone marrow-derived macrophages (BMDMs) after stimulation with LPS at DMF concentrations starting at 25 µM. Lehmann et al. (2007) reported reduction of pro-inflammatory cytokines (including TNFα in PBMCs stimulated with LPS/INF-y and IL-1β in PBMCs

stimulated with phytohemagglutinin (PHA) with different fumaric esters, with best effects using diesters at concentrations higher than 30 µM. Our assays confirm these values for DMF. In contrast, the endosomal directed compounds (**2** and **3**) show efficacy from 1 µM on TNFα and IL-1β, suggesting at least a 20-fold increase in potency in vitro, when using substances with strong cellular uptake.

Striking in these studies was the relatively low ratio in the concentrations between effective and potentially toxic effects of fumarate esters. We monitored cell viability using the MTT assay which reports on mitochondrial metabolic activity. McGuire et al. (2016) showed a loss in cell viability over time at 50 µM DMF in BMDMs. Michell-Robinson et al. (2016) showed specific toxicity on monocytes and Sebök et al. (1994) showed cytotoxic effects on keratinocytes. In all these previous studies and ours (see Fig. 2) a margin between the lowest effective dose and lowest toxic dose of DMF was observed in the range of 2–4.

Taken together, the results from MTT assay (hence reduction of metabolic activity) and GSH binding (hence Michael addition to cysteines) might suggest a covalent binding to GAPDH and thus reducing its enzymatic activity by blocking the binding of NAD^+ as a mechanism of action. This could lead to a lower concentration of cytokines simply through the inhibition of cell activity and energy supply. While potentially valid in vitro, it strikes one as unlikely in vivo except under conditions of very high substance to cell ratio. As noted above, these conditions may be found in segments of the gut after oral administration, but are unlikely in systemic circulation.

New fumarates and their in vivo action

Dose response studies in the psoriasis model were conducted to estimate the relative potency increase generated via the macrolide esters. The rationale was that most DMF provided by the oral route is preferentially delivered to the gut where it appears to be associated with occasional signs of discomfort. We hypothesized that by using a carrier, we could deliver MMF to the immune cell compartment and, potentially more importantly, the endosome where GPR109A may be most amenable to interactions with its ligand and the stabilization of signaling.

A further argument for extensive dose response studies was the observation that the high potency of short chain fatty acid analogs can impact bacterial processing and thus, a secondary goal of our studies was to identify doses at which we could analyze effects on innate immune function such as gut homeostasis and bacterial killing (Straß et al. 2021).

Differences between in vitro and in vivo data are especially prominent for the novel conjugates. In vitro, conjugation to the 4″ position was most effective in reducing inflammatory cytokines, whilst in vivo, in the psoriasis models, the 2′-esters appeared to be more effective. The 4″ conjugates react at least 10-times faster with glutathione while the 2′ esters readily hydrolyze to MMF. In vitro, MMF was essentially inactive, suggesting that either the free carboxy group impedes cellular uptake, or, that interaction with glutathione is the more important aspect of in vitro activity (see medium volume to cellular mass concept above). Given that compound **1** has significant uptake into cells, the issue of access to the cytoplasm appears less relevant for this compound. MMF released in cells from Compound **1** after uptake appears not to interact with GSH and may be subject to efflux. In vivo, Compound **1** had the more standard pharmacokinetics but exhibited steady loss of the MMF 2′ ester. It was also the most active in the psoriasis model. These data suggest that MMF is the more relevant agent in vivo.

If MMF is the effective agent in vivo, hydrolyzed MMF can then ligate to the target receptor GPR109A. The pharmacokinetics of Compound **1** show that it is preferentially taken up to immune cells and steadily hydrolyzed. From similar compounds, the site of uptake is the lysosomal compartment where GPR109A is located. The concentration at the site of action is consistent with the more potent effect of this substance in vivo and an interaction with GPR109A and not thiols.

In the murine model for human acute gout the MSU crystals act as putative ligands for CD14, TLR2, and TLR4 and can, within the peritoneum of mice, activate macrophages which release proinflammatory cytokines via the activation of NLRP3 inflammasome complex (Mariotte et al. 2020; Khameneh et al. 2017). Effects seen here on IL-6 may be useful given that it is one of the central cytokines involved in the acute phase of MSU induced gout (Guerne et al. 1989). This might be explained by the direct effect of fumaric diesters on inflammasome activity. That DMF is in this model more effective compared to MMF was published earlier (Miglio et al. 2015; Hoyle et al. 2022) and is consistent with our results in this model.

Conclusion

Here we investigated the mode of action of DMF/MMF using novel conjugates that differentiate thiol binding activities while targeting the immune cell compartment. Based on the observations of these conjugates, we propose a mode of action based on MMF binding to GPR109A in the lysosomal membrane. Effective doses in mice of 0.03–0.12 mg/kg correspond to human doses in the range of 1–2 mg (given the higher body weight, but lower metabolic rate). These very low amounts provide for both dramatic economies in terms of bulk ingredient and pill burden, but they also provide opportunities to avoid tolerance issues and adverse effects. More generally, the substances described here demonstrate

that delivery to the lysosome can dramatically increase or modulate efficacy for substances where the target is lysosomal. Given that lysosomes are probably less than 1% of overall cell volume, targeting the compartment provides for efficiency and dose reductions. Finally, these data provide insight into the role of GSH in immune functions. In vitro data from this study suggests that titrating GSH with a Michael acceptor dampens inflammatory reactions in cultured cells and primary immune cells.

Supplementary Information The online version contains supplementary material available at https://doi.org/10.1007/s10787-023-01186-0.

Acknowledgements We would like to thank colleagues from Synovo GmbH and the University of Tübingen who assisted in this research. Special thanks to the members of the in vivo facility and the team of the analytics/bioanalytics department at both institutions.

Author contributions All authors have read and agreed to the published version of the manuscript. Conceptualization, SS, TLS and MB; methodology, SS, NC, TLS and MB; validation, SS and TLS; formal analysis, SS and TLS; investigation, JG, SS, TLS, LDO, NS, SG and AS; resources, MB and SL; writing—original draft preparation, SS; writing—review and editing, TLS, MB and JHG; visualization, SS; supervision, MB, JHG and SL; project administration, MB; funding acquisition, MB.

Funding This research received no external funding.

Data availability Enquiries about data availability should be directed to the authors.

Declarations

Conflict of interest S.S., J.G., N.C., M.M., S.G., A.S., N.S., L.D.O., J.H.G., T.L.S. are employees of Synovo GmbH. M.B. is general manager of Synovo GmbH. Synovo GmbH holds patent rights to the published structures.

Institutional review board statement All study protocols were approved by the local Animal Care and Ethics Committee (Federal government ethics committee, Tübingen, Germany under the licenses 35/9185.81-7/SYN 06/20; 35/9185.81-7/SYN 07/18; and 35/9185.81-7/SYN 11/19). Human blood products used in the in vitro assays (used for cell stimulation, viability, stability and uptake assays) were obtained from the center for transfusion medicine in Tübingen, Germany (Zentrum für Klinische Transfusionmedizin Tübingen GmbH, (ethical approval number ZKT-FoPro202106-2305-01 and ZKT-FoPro202012-2211)).

References

Angiari S, O'Neill LA (2018) Dimethyl fumarate: targeting glycolysis to treat MS. Cell Res 28(6):613–615. https://doi.org/10.1038/s41422-018-0045-3

Balloy V et al (2014) Azithromycin analogue CSY0073 attenuates lung inflammation induced by LPS challenge. Br J Pharmacol 171(7):1783–1794. https://doi.org/10.1111/bph.12574

Bermudez Y, Benavente CA, Meyer RG, Coyle WR, Jacobson MK, Jacobson EL (2011) Nicotinic acid receptor abnormalities in human skin cancer: implications for a role in epidermal differentiation. PLoS One. https://doi.org/10.1371/journal.pone.0020487

Bosnar M, Kelnerić Ž, Munić V, Eraković V, Parnham MJ (2005) Cellular uptake and efflux of azithromycin, erythromycin, clarithromycin, telithromycin, and cethromycin. Antimicrob Agents Chemother. https://doi.org/10.1128/AAC.49.6.2372-2377.2005

Brennan MS et al (2015) Dimethyl fumarate and monoethyl fumarate exhibit differential effects on KEAP1, NRF2 activation, and glutathione depletion in vitro. PLoS One. https://doi.org/10.1371/journal.pone.0120254

Burnet M et al (2015) Anti-inflammatory macrolides to manage chronic neutrophilic inflammation. RSC Drug Discov Ser 201(40):206–234

Burnet MW et al. (2018) Novel anti-infective and anti-inflammatory compounds. US20200262857

Carryn S, Chanteux H, Seral C, Mingeot-Leclercq MP, Van Bambeke F, Tulkens PM (2003) Intracellular pharmacodynamics of antibiotics. Infect Dis Clin North Am. https://doi.org/10.1016/S0891-5520(03)00066-7

Chen H et al (2014) Hydroxycarboxylic acid receptor 2 mediates dimethyl fumarate's protective effect in EAE. J Clin Invest 124(5):2188–2192. https://doi.org/10.1172/JCI72151

Dibbert S, Clement B, Skak-Nielsen T, Mrowietz U, Rostami-Yazdi M (2013) Detection of fumarate-glutathione adducts in the portal vein blood of rats: evidence for rapid dimethylfumarate metabolism. Arch Dermatol Res 305(5):447–451. https://doi.org/10.1007/s00403-013-1332-y

Gambhir D et al (2012) GPR109A as an anti-inflammatory receptor in retinal pigment epithelial cells and its relevance to diabetic retinopathy. Invest Ophthalmol Vis Sci 53(4):2208–2217. https://doi.org/10.1167/iovs.11-8447

Ghoreschi K et al (2011) Fumarates improve psoriasis and multiple sclerosis by inducing type II dendritic cells. J Exp Med 208(11):2291–2303. https://doi.org/10.1084/jem.20100977

Gillard GO et al (2015) DMF, but not other fumarates, inhibits NF-κB activity in vitro in an Nrf2-independent manner. J Neuroimmunol 283:74–85. https://doi.org/10.1016/j.jneuroim.2015.04.006

Guerne P-A, Terkeltaub R, Zuraw B, Lotz M (1989) Inflammatory microcrystals stimulate interleukin-6 production and secretion by human monocytes and synoviocytes. Arthritis Rheum 32(11):1443–1452. https://doi.org/10.1002/anr.1780321114

Helwa I, Choudhary V, Chen X, Kaddour-Djebbar I, Bollag WB (2017) Anti-psoriatic drug monomethylfumarate increases nuclear factor erythroid 2-related factor 2 levels and induces aquaporin-3 mRNA and protein expression. J Pharmacol Exp Ther 362(2):243–253. https://doi.org/10.1124/jpet.116.239715

Hoyle C, Green JP, Allan SM, Brough D, Lemarchand E (2022) Itaconate and fumarate derivatives inhibit priming and activation of the canonical NLRP3 inflammasome in macrophages. Immunology 165(4):460–480. https://doi.org/10.1111/imm.13454

Huang S-W, Shieh J-J (2016) The antibiotic azithromycin improves the severity of imiquimod-induced psoriasis-like skin inflammation in mice. J Dermatol Sci 84(1):e68. https://doi.org/10.1016/j.jdermsci.2016.08.210

Humphries F et al (2020) Succination inactivates gasdermin D and blocks pyroptosis. Science (80-) 369(6511):1633–1637. https://doi.org/10.1126/science.abb9818

Kadam DP, Suryakar AN, Ankush RD, Kadam CY, Deshpande KH (2010) Role of oxidative stress in various stages of psoriasis. Indian J Clin Biochem 25(4):388–392. https://doi.org/10.1007/s12291-010-0043-9

Khameneh HJ et al (2017) C5a regulates IL-1β production and leukocyte recruitment in a murine model of monosodium urate crystal-induced peritonitis. Front Pharmacol 8(JAN):1–11. https://doi.org/10.3389/fphar.2017.00010

Kornberg MD et al (2018) Dimethyl fumarate targets GAPDH and aerobic glycolysis to modulate immunity. Science (80-) 360(6387):449–453. https://doi.org/10.1126/science.aan4665

Kostylina G, Simon D, Fey MF, Yousefi S, Simon HU (2008) Neutrophil apoptosis mediated by nicotinic acid receptors (GPR109A). Cell Death Differ 15(1):134–142. https://doi.org/10.1038/sj.cdd.4402238

Lehmann M et al (2002) Fumaric acid esters are potent immunosuppressants: inhibition of acute and chronic rejection in rat kidney transplantation models by methyl hydrogen fumarate. Arch Dermatol Res 294(9):399–404. https://doi.org/10.1007/s00403-002-0347-6

Lehmann JCU et al (2007) Dimethylfumarate induces immunosuppression via glutathione depletion and subsequent induction of heme oxygenase 1. J Invest Dermatol 127(4):835–845. https://doi.org/10.1038/sj.jid.5700686

Li G et al (2010) Internalization of the human nicotinic acid receptor GPR109A is regulated by Gi, GRK2, and arrestin3. J Biol Chem 285(29):22605–22618. https://doi.org/10.1074/jbc.M109.087213

Linker RA, Gold R (2013) Dimethyl fumarate for treatment of multiple sclerosis: Mechanism of action, effectiveness, and side effects. Curr Neurol Neurosci Rep. https://doi.org/10.1007/s11910-013-0394-8

Linker RA, Haghikia A (2016) Dimethyl fumarate in multiple sclerosis: latest developments, evidence and place in therapy. Ther Adv Chronic Dis 7(4):198–207. https://doi.org/10.1177/2040622316653307

Liu X et al (2016a) Dimethyl fumarate ameliorates dextran sulfate sodium-induced murine experimental colitis by activating Nrf2 and suppressing NLRP3 inflammasome activation. Biochem Pharmacol. https://doi.org/10.1016/j.bcp.2016.05.002

Liu X et al (2016b) Dimethyl fumarate ameliorates dextran sulfate sodium-induced murine experimental colitis by activating Nrf2 and suppressing NLRP3 inflammasome activation. Biochem Pharmacol 112:37–49. https://doi.org/10.1016/j.bcp.2016.05.002

Mariotte A et al (2020) A mouse model of MSU-induced acute inflammation in vivo suggests imiquimod-dependent targeting of Il-1β as relevant therapy for gout patients. Theranostics 10(5):2158–2171. https://doi.org/10.7150/thno.40650

McGuire VA et al (2016) Dimethyl fumarate blocks pro-inflammatory cytokine production via inhibition of TLR induced M1 and K63 ubiquitin chain formation. Sci Rep. https://doi.org/10.1038/srep31159

Michell-Robinson MA et al (2016) Effects of fumarates on circulating and CNS myeloid cells in multiple sclerosis. Ann Clin Transl Neurol 3(1):27–41. https://doi.org/10.1002/acn3.270

Miglio G, Veglia E, Fantozzi R (2015) Fumaric acid esters prevent the NLRP3 inflammasome-mediated and ATP-triggered pyroptosis of differentiated THP-1 cells. Int Immunopharmacol 28(1):215–219. https://doi.org/10.1016/j.intimp.2015.06.011

Mills EA, Ogrodnik MA, Plave A, Mao-Draayer Y (2018) Emerging understanding of the mechanism of action for dimethyl fumarate in the treatment of multiple sclerosis. Front Neurol. https://doi.org/10.3389/fneur.2018.00005

Mrowietz U, Morrison PJ, Suhrkamp I, Kumanova M, Clement B (2018) The pharmacokinetics of fumaric acid esters reveal their in vivo effects. Trends Pharmacol Sci 39(1):1–12. https://doi.org/10.1016/j.tips.2017.11.002

Ocana C, C Yang, M Bernal, AR Quesada, MÅ Medina (2021) The anti-angiogenic compound dimethyl fumarate inhibits the serine synthesis pathway and increases glycolysis in endothelial cells. pp. 1–78. https://doi.org/10.1101/2021.12.13.472337

Park JB, Park H, Son J, Ha SJ, Cho HS (2019) Structural study of monomethyl fumarate-bound human gapdh. Mol Cells 42(8):597–603. https://doi.org/10.14348/MOLCELLS.2019.0114

Pleńkowska J, Gabig-Cimińska M, Mozolewski P (2020) Oxidative stress as an important contributor to the pathogenesis of psoriasis. Int J Mol Sci 21(17):1–15. https://doi.org/10.3390/ijms21176206

Roberge CJ, R de Medicis, JM Dayer, M Rola-Pleszczynski, PH Naccache, PE Poubelle Crystal-induced neutrophil activation. V. Differential production of biologically active IL-1 and IL-1 receptor antagonist. J Immunol, vol. 152, no. 11, pp. 5485–5494, 1994, [Online]. Available: http://www.ncbi.nlm.nih.gov/pubmed/8189066

Saxena VN, Dogra J (2010) Long-term oral azithromycin in chronic plaque psoriasis: a controlled trial. Eur J Dermatology 20(3):329–333. https://doi.org/10.1684/ejd.2010.0930

Schmidt TJ, Ak M, Mrowietz U (2007) Reactivity of dimethyl fumarate and methylhydrogen fumarate towards glutathione and N-acetyl-l-cysteine-Preparation of S-substituted thiosuccinic acid esters. Bioorganic Med Chem 15(1):333–342. https://doi.org/10.1016/j.bmc.2006.09.053

Sebök B, Bonnekoh B, Geisel J, Mahrle G (1994) Antiproliferative and cytotoxic profiles of antipsoriatic fumaric acid derivatives in keratinocyte cultures. Eur J Pharmacol Environ Toxicol 270(1):79–87. https://doi.org/10.1016/0926-6917(94)90083-3

Straß S, Schwamborn A, Keppler M, Guse J, Burnet M (2021) Synthesis, characterization and in vivo distribution of intracellular delivered macrolide SCFA derivatives. ChemMedChem 16:1–16

Sullivan LB et al (2013) The proto-oncometabolite fumarate binds glutathione to amplify ROS-dependent signaling. Mol Cell 51(2):236–248. https://doi.org/10.1016/j.molcel.2013.05.003

Togami K, Chono S, Morimoto K (2013) Subcellular distribution of azithromycin and clarithromycin in rat alveolar macrophages (NR8383) in vitro. Biol Pharm Bull 36:1494. https://doi.org/10.1248/bpb.b13-00423

Wollina U (2011) Fumaric acid esters in dermatology. Indian Dermatol Online J 2(2):111. https://doi.org/10.4103/2229-5178.86007

Xu Z et al (2019) The visualization of lysosomal and mitochondrial glutathione via near-infrared fluorophore and in vivo imaging application. Sens Actuators B Chem 290(December 2018):676–683. https://doi.org/10.1016/j.snb.2019.03.114

Zheng L et al (2015) Fumarate induces redox-dependent senescence by modifying glutathione metabolism. Nat Commun. https://doi.org/10.1038/ncomms7001

9. „Isostearic acid is an active component of imiquimod formulations used to induce psoriaform disease models“

Straß, S., Geiger, J., Martorelli, M., Geiger, S., Cloos, N., Keppler, M., Fischer, T., Riexinger, L., Schwamborn, A., Guezguez, J., Späth, N., Cruces, S., Guse, J.-H., Sandri, T. L., Burnet, M., & Laufer, S. (2023). Isostearic acid is an active component of imiquimod formulations used to induce psoriaform disease models. *Inflammopharmacology*. https://doi.org/10.1007/s10787-023-01175-3

Eigenanteil an Publikation

Die Ausarbeitung, Planung und Konzeptualisierung des Projekts wurden von Dr. Lucas Sandri, Dr. Burnet, Herrn Keppler, Frau Späth und mir durchgeführt. *In vivo* Experimente wurden von Frau J. Geiger, Herr Cruces, Dr. Burnet, Frau Cloos, Dr. Lucas Sandri und mir geplant und durchgeführt. Die Aufarbeitung, Analyse und Messung der Proben aus den Studien und die Entwicklung der Methode für die HPLC-MS/MS wurde von Dr. Guezguez, Frau Schwamborn und mir getätigt. Die qPCR-Analyse wurde von Frau J. Geiger und Dr. Lucas Sandri geplant und durchgeführt. Frau Martorelli war verantwortlich für die Planung und Auswertung der histologischen Daten. Die histologischen Arbeiten wurden von Frau Riexinger und Frau Fischer durchgeführt. Die schriftliche Ausarbeitung und Visualisierung erfolgten durch mich und Dr. Lucas Sandri. Alle AutorInnen haben das Manuskript überprüft und korrigiert. Prof. Laufer und Dr. Guse wirkten bei der Arbeit unterstützend und betreuend.

Inflammopharmacology
https://doi.org/10.1007/s10787-023-01175-3

Inflammopharmacology

ORIGINAL ARTICLE

Isostearic acid is an active component of imiquimod formulations used to induce psoriaform disease models

Simon Straß[1,2] · Johanna Geiger[2] · Mariella Martorelli[1,2] · Sophia Geiger[2] · Natascha Cloos[2] · Manuel Keppler[2] · Tina Fischer[2] · Laura Riexinger[2] · Anna Schwamborn[2] · Jamil Guezguez[2] · Nadja Späth[2] · Santiago Cruces[2] · Jan-Hinrich Guse[2] · Thaisa Lucas Sandri[2,3] · Michael Burnet[2] · Stefan Laufer[1]

Received: 2 December 2022 / Accepted: 19 February 2023

Abstract
Topical imiquimod based creams are indicated as immune stimulants for papillomas and various skin neoplasms. Imiquimod is considered a TLR7 ligand. These creams are also used in research to induce skin inflammation in mice as a model for psoriasis. We observed that this inflammatory response was not strictly imiquimod dependent and we set out to establish which components drive the proinflammatory effects. To this end, we examined the induction response in a BALB/cJRj mouse model, in which 50 mg of cream is applied to 2 cm^2 of skin (125 mg/kg imiquimod—5% W/V, and/or 625 mg/kg isostearic acid—25% W/V). Comparing cream formulations containing isostearic acid, imiquimod and the combination, we observed that isostearic acid causes skin inflammation within 2 days, whereas imiquimod requires up to 5 days for initial signs. Isostearic acid activated an inflammasome response, stimulated release of proinflammatory cytokines and upregulated the IL-23/17 axis. Animals treated with isostearic acid had enlarged livers (+40% weight), which was not observed with imiquimod alone. Imiquimod was readily metabolized and cleared from plasma and liver, but was maintained at high levels in the skin throughout the body (200 mM at area of application; 200 µM in untreated skin). Imiquimod application was associated with splenomegaly, cytokine induction/release and initial body weight loss over 3 days. Despite high imiquimod skin levels throughout the animal, inflammation was only apparent in the treated areas and was less severe than in isostearic acid groups. As the concentrations in these areas are well above the 10 µM required for TLR7 responses in vitro, there is an implication that skin inflammation following imiquimod is due to effects other than TLR7 agonism (e.g., adenosine receptor agonism). In brain, isostearic caused no major changes in cytokine expression while imiquimod alone sightly stimulated expression of IL-1β and CCL9. However, the combination of both caused brain induction of CCL3, -9, CXCL10, -13, IL-1β and TNFα. The implication of these data is that isostearic acid facilitates the entry of imiquimod or peripherally secreted cytokines into the brain. Our data suggest that psoriaform skin responses in mice are more driven by isostearic acid, than generally reported and that the dose and route used in the model, leads to profound systemic effects, which may complicate the interpretation of drug effects in this model.

Keywords Psoriasis · Dermatitis · Isostearic acid · Imiquimod

Introduction

Psoriasis is a chronic skin disease, that causes visible and painful inflammation and hyperproliferation of skin. Its etiology is not fully understood but includes genetic, environmental, infectious and lifestyle factors (Global Report on Psoriasis 2023; Girolomoni et al. 2017). In Western countries around 1–2% of the population is affected by various degrees of psoriasis (Nakajima and Sano 2018). Treatment options include topical, systemic, and photo-therapy (Global Report on Psoriasis 2023). Systemic treatments include

✉ Michael Burnet
michael.burnet@synovo.com

[1] Pharmaceutical Chemistry, Institute for Pharmaceutical Sciences, Eberhard Karls University Tübingen, Tübingen, Germany

[2] Synovo GmbH, Tübingen, Germany

[3] Institute of Tropical Medicine, Eberhard Karls University Tübingen, Tübingen, Germany

Published online: 21 March 2023

antibodies (e.g. inhibitors of interleukin-23: ustekinumab, guselkumab, tildrakizumab, and Risankizumab; TNFα: etanercept, adalimumab; IL-17: secukinumab (AIN457), ixekizumab (LY2439821), and brodalumab (AMG827) (Yang et al. 2021; Zhang et al. 2022) as well as small molecules (e.g., glucocorticoids, methotrexate, cyclosporine and fumarates). The central goal of therapy, is to reduce psoriatic activity without generally suppressing the immune system. In this regard, the introduction of therapy directed to IL-17 and IL-23 has led to substantial improvements in quality of life.

Psoriatic inflammation is driven by *i.a.* dendritic cells (DCs), T cells and macrophages (Girolomoni et al. 2017; Nakajima and Sano 2018; Fits et al. 2009). The inflammation is supported mainly by the proinflammatory cytokines interleukin (IL)-23 and IL-12, released by myeloid DCs which stimulate Th17 cells to secrete proinflammatory IL-17, tumor necrosis factor α (TNFα) and IL-22. Activation of IL-22R mediates proliferation and migration of keratinocytes (Girolomoni et al. 2017; Nakajima and Sano 2018; Fits et al. 2009; Brück et al. 2018). Activation of toll-like receptors (TLRs) plays a distinct role in the pathogenesis of psoriasis. TLR9 activates plasmacytoid DCs (pDCs). Activation of TLR7/8 triggers autoinflammatory processes in psoriasis (Nakajima and Sano 2018; Chiricozzi et al. 2018; Flutter and Nestle 2013; Sun et al. 2018).

Finding improved therapies for psoriasis requires disease models, that recapitulate the disease mechanisms either in combination or alone. The involvement of TLR receptor, therefore, provides at least one means to easily mimic disease in WT animals. Van der Fits et al. first proposed in 2009 a murine model for psoriasis, based on repeated topical application of Imiquimod (IMQ) formulated as Aldara® (Fits et al. 2009), which activates murine TLR7, the proposed target of IMQ. This activation leads to a proinflammatory response similar to human acute phase psoriasis. IMQ containing cream (clinical formulation of Aldara®), is applied on the depilated dorsal skin of mice on consecutive days to induce the IL-17/23 axis (Fits et al. 2009; Brück et al. 2018; Flutter and Nestle 2013). Clinical signs include local thickening, scaling, redness and inflammation of the skin. This leads to psoriasis like lesions: thickening of the epidermis through hyperproliferation of keratinocytes, a reduced layer of granules (hypogranulosis), redness of skin because of dilation of blood vessels, accumulation of neutrophils in stratum corneum (Munro's microabscesses), and infiltration from clusters of $CD4^+$, $CD8^+$ and antigen presenting DCs in dermis and epidermis (Nakajima and Sano 2018; Brück et al. 2018). The Aldara® induced psoriasis model is widely used because of its rapid development, low cost and simple read out. However, although operationally straightforward, the molecular biology and immunology of the model is less simple (Walter et al. Mar. 2013; Horváth et al. 2019; Hawkes et al. 2017; Luo et al. 2016). IMQ also acts systemically causing splenomegaly, lymphadenopathy and possibly elevated systemic cytokines (Hawkes et al. 2017) and is likely to also be an adenosine receptor inhibitor (Fits et al. 2009; Schön and Schön 2007; Schön et al. 2006). Walter et al. (2013) showed that isostearic acid, (25% by weight of Aldara®), also has proinflammatory effects in vitro and in vivo (Walter et al. 2013). Although isostearic acid is thought to be included for its physical formulation properties (it is a weak acid while imiquimod is a weak base), it appears to be immunologically and systemically active. Thus, isostearic acid present in the formulation of Aldara® may have a functional role irrespective of the initial intentions behind its inclusion.

We have been employing the model to study the effects of anti-inflammatory drug candidates for pharmaceutical developers. In the course of such studies, we have observed that compounds that should influence the model, were sometimes more or less active than expected, depending on the mode of action. We also observed that in topical formulations of certain compounds, there were cases of significant effects of the vehicle on the performance of Aldara® as an inducer of disease. To better control the model, we then set out to create a "sham cream" that did not contain IMQ, that could be used as a better control vs. the IMQ induced disease. We used this preparation, in which IMQ could be added to a final concentration of 5% W/V which is the same as that in the original imiquimod containing Aldara®. Studies with this material showed that it produced a different disease pattern to that of Aldara®. Further studies demonstrated that isostearic acid was active alone in this formulation, and in some ways synergistic to the effects of IMQ, especially locally. The formulated in-house creams are based on DAC cream (40% H_2O, 25.5% Vaseline, 10% propylene glycol, 7.5% triglyceride, 7% Macrogol-20-glycerol-monostearate, 6% cetyl alcohol, 4% 60-glycerol-monosterate) (Höfel and "Basiscreme DAC" 2018).

Here we demonstrate that the isostearic acid is a major contributor to the local skin inflammatory reaction, whilst IMQ tends to act only in combination with isostearic acid. This gives a better understanding of the Aldara® induced psoriasis model and the modes of action that may be active in the model. We demonstrate a clear effect of isostearic acid and/or IMQ to inflammatory response, spleen and liver weight and scaling, redness and thickness of the skin of female BALB/cJRj mice. Finally, we quantified the effects of the combination on uptake to skin and distribution systemically. These observations may be useful to researchers in the field attempting to interpret results obtained with this in vivo model. In particular, the knowledge that the model is based on multiple disease inducers may explain cases where treatments with a very specific mode of action do not fully suppress disease signs.

Materials and methods

All chemicals, consumables and supply products were purchased from commercial sources and used as received. All study protocols were approved by the local Animal Care and Ethics Committee (Federal government ethics committee, Tübingen, Germany).

HPLC–MS/MS and MS/MS studies

Quantification of analytes (imiquimod and isostearic acid; MS tunes in Table 1) was performed with an Agilent 1260 Infinity system coupled to a triple quadrupole Sciex API 4000 MS/MS detector. An Agilent C_{18} Poroshell 120 column (4.6 × 50 mm, 2.7 µm) was used for separation. The mobile phase was composed of water containing 0.1% formic acid (eluent A) and acetonitrile containing 0.1% formic acid (eluent B). Gradient used was: 10% B for 1 min, to 100% B in 2 min, 100% B for 3 min, to 5% B in 1 min, 5% B for 3 min.

Real-time polymerase chain reaction (qPCR)

Analysis of gene expression was done by isolating RNA from flash frozen skin samples, using the Qiagen RNeasy® MiniKit (Qiagen). 3.6 µg of RNA was used for reverse transcription into complementary DNA (cDNA) using PerfeCTa DNase I (Quanta Bioscience) and 5× PrimeScript RT Mastermix (Takara). Gene-specific primers used for qPCR are listed in Table 2. The qPCR reaction was performed in duplicates with Blue S'Green qPCR Mix Separate ROX (Biozym) in 96-well plates. Amplification was carried out in the QuantStudio® 3 qPCR system (ThermoFisher Scientific/Quantstudio™ Design & Analysis Software v.1.4.3). Cycle conditions were set at 95 °C for 2 min followed by 40 cycles of 95 °C for 5 s and 60 °C for 17 s; a melt-curve analysis was performed for each qPCR reaction. Primer efficiency was determined for each primer pair to ensure linear standard curve and high amplification efficiency. Threshold cycle (C_t) values were used for the calculation of the relative gene expression levels. For this, all values were first normalized to respective C_t values of the HPRT (hypoxanthine phosphoribosyltransferase) housekeeping gene. Then, normalized ΔC_t values of the different treatment groups were compared to the ΔC_t levels of the vehicle treated control group which was set to 1. Normalized expression ratios ($2(-\Delta\Delta C_t)$) are given for all treatment groups relative to the vehicle group. C_t values of all samples were normalized to the respective C_t values obtained for HPRT housekeeping gene, resulting in the ΔC_t value for each sample: ΔC_t (gene x) = C_t (gene x) − C_t (HPRT). To calculate the $\Delta\Delta C_t$ value, the ΔC_t average of the control condition (vehicle) was used. This analysis was also performed for the individual control condition samples to determine variance within the control group. Subsequently, $\Delta\Delta C_t$ values of each sample were transformed into normalized expression ratio which gives the fold increase (or decrease) of the target gene expression compared to the control condition (vehicle) and normalized to the reference gene (HPRT). Normalized expression ratio (fold change) = $2-\Delta\Delta C_t$. Data are shown as scatter plots using GraphPad Prism 9.1.0.

Table 1 Specific tunes of substances in HPLC–MS/MS

Substance	Q1 mass	Q3 mass	DP (V)	CE (V)	CXP (V)
IMQ	241	185	96	33	36
Isostearic acid	329	283	15	20	11

Cream formulation

Compositions of the different tested creams can be found in Table 3 for the first study and Table 4 for the second study. As applicable, IMQ (Chempur), cetyl alcohol (TCI), DMSO (Carl Roth) and/or isostearic acid (TCI) were mixed with a spatula until homogenous, then hydroxypropyl methylcellulose (HPMC, Sigma Aldrich, 2.0%, dry) was added and mixed. To this mixture, base cream DAC (40% H_2O, 25.5% Vaseline, 10% propylene glycol, 7.5% triglyceride, 7% Macrogol-20-glycerol-monostearate, 6% cetyl alcohol,

Table 2 Primers used for qRT-PCR

Cytokine	Forward sequence (5′ → 3′)	Reverse sequence (5′ → 3′)
HPRT	AGTTCTTTGCTGACCTGCTG	CCACCAATAACTTTTATGTCCCC
TNFα	CCACCACGCTCTTCTGTCTA	CTGATGAGAGGGAGGCCATT
IL-17A	GAAGGCCCTCAGACTACCTC	CTTTCCCTCCGCATTGACAC
IL-17F	GAGGGAAGAAGCAGCCATTG	GGCAAGTCCCAACATCAACA
IL-6	ACTTCACAAGTCGGAGGCTTA	TCTGCAAGTGCATCATCGTT
IL-1β	TGACGGACCCCAAAAGATGA	TCTCCACAGCCACAATGAGT
IL-23A	TGAGCCCTTAGTGCCAACAG	CTTGCCCTTCACGCAAAACA
NLRP3	TCCCAGACACTCATGTTGCC	GTCCAGTTCAGTGAGGCTCC
IL-22	CTGCTTCTCATTGCCCTGTG	GAACAGTTTCTCCCCGATGAG

Table 3 Composition of creams used in optimization study

Group name	IMQ	Isostearic acid	Cetyl alcohol	DMSO	Amount applied
1—Aldara®	5%	25%	2.2%	–	50 mg
2—Cetyl alcohol + isostearic acid	–	25%	2.2%	–	50 mg
3—5% IMQ + cetyl alcohol	5%	–	2.2%	–	50 mg
4—7% IMQ + cetyl alcohol	7%	–	2.2%	–	50 mg
5—7% IMQ + cetyl alcohol + isostearic acid	7%	25%	2.2%	–	50 mg
6—5% IMQ + DMSO	5%	–	–	3.6%	50 mg
7—5% IMQ + DMSO + isostearic acid	5%	25%	–	3.6%	50 mg

Group 1 is commercial Aldara®. Groups 2–7 were prepared inhouse

Table 4 Composition of creams used in second optimization study

Group name	IMQ	Isostearic acid	Cetyl alcohol	DMSO	Amount applied
1—Vehicle DAC base cream	–	–	–	–	50 mg
2—5% IMQ + DMSO	5%	–	–	3.6%	50 mg
3—Isostearic acid	–	25%	–	–	50 mg
4—5% IMQ + DMSO + isostearic acid	5%	25%	–	3.6%	50 mg

Group 1 is vehicle cream, based on commercially available DAC. Groups 2–4 were prepared inhouse and are based on DAC

4% 60-glycerol-monosterate, Nordring Apotheke, Tübingen) was added, mixed and stored at 4 °C.

Cream-induced psoriatic murine model

All study protocols were approved by the local Animal Care and Ethics Committee (Federal government ethics committee, Tübingen, Germany under the license 35/9185.81-7/SYN 07/18). A total of 88 mice (BALB/cJRj, female, 8 weeks old) were used for the studies performed (divided into two separate studies. First study with 56 animals and second study with 32 animals) were purchased from Janvier Labs (Le Genest-Saint-Isle). Animals were acclimatized for at least one week with standard chow (Mouse Maintenance, V1534-000, Ssniff Spezialdiäten GmbH, Germany) and drinking water *ad libitum* before the start of the experiment. Animals were housed in type IV cages, with bedding and enrichment material and kept at 23 °C (± 1 °C), 50–60% humidity, with 12/12 h dark/light cycles period. Animals were monitored daily and at the end of the experiment, terminated painlessly with overflow of CO_2. For the first optimization study, mice were grouped in 8 animals per cage. Induction was performed with following creams: Aldara® (MEDA Pharma GmbH & Co. KG; Aldara® here referred as clinical cream or clinical formulation), Cetyl alcohol + isostearic acid, 5% IMQ + cetyl alcohol, 7% IMQ + cetyl alcohol, 7% IMQ + cetyl alcohol + isostearic acid, 5% IMQ + DMSO or 5% IMQ + DMSO + isostearic acid (see also Table 4). For the second optimization study, mice were grouped in 4 animals per cage and the following creams were used: vehicle DAC base cream, 5% IMQ + DMSO, Isostearic acid or 5% IMQ + DMSO + isostearic acid. On day 0, prior to psoriasis induction, dorsal skin was removed using a clipper, followed by application of depilatory cream for complete fur removal. From day 1 to day 6 (first study) or 7 (second study) 50 mg of each induction cream (see cream formulation section) was applied to 2 cm^2 of the depilated skin of the animals. The required amount of cream was weighed and applied using a spreader to achieve homogeneity. During the experiment, daily measured parameters were: body weight (BW), skin thickness, skin redness and scaling (0 = no change, 1 = marginal effects, 2 = moderate effects, 3 = strong effects, 4 = maximum). At termination, pictures of dorsal skin were taken (*ante mortem*), skin samples (for histology and gene expression) were collected and the weights of spleen and liver were recorded. Additional organ samples, including skin, were collected, washed to remove remnant cream, flash frozen, and kept at -20 °C until processing to determine tissue distribution of imiquimod and isostearic acid. Skin samples were kept in 4% paraformaldehyde solution until processing.

Sample preparation for pharmacokinetic assessment

Frozen organ samples were thawed and treated as described earlier (Straß et al. 2021). Briefly, samples were digested with Proteinase K in a buffer volume in µL corresponding to sample weight in mg (Proteinase K, VWR, diluted 1:40 in phosphate buffer 20 mM) for 1 h

at 50 °C and homogenized at 6 m/s for 40 s (FastPrep-24 5G, MP Biomedicals). Six volumes of acetonitrile were added, the mixture again homogenized, centrifuged (10 min at 14000*g*, Eppendorf Centrifuge 5417R) and the supernatant taken for HPLC–MS/MS analysis.

Histology

Paraffin-embedded skin sections were stained using the hematoxylin and eosin (H&E) method. Briefly, skin samples were fixed for 24 h in 4% PFA and then transferred to 70% ethanol until tissue preparation took place. Skin samples were placed into cassettes for the subsequent embedding process. Dehydration and clearance were by sequential incubation steps: 90% ethanol for 45 min, 100% ethanol for 45 min (2×), 100% ethanol for 60 min, 100% isopropanol for 60 min (2×), 100% isopropanol, overnight. Next day, organs were transferred into liquid paraffin for 30 min (55–65 °C) and cooled overnight at room temperature, to complete the embedding in paraffin. After deparaffinizing and hydration steps from xylol to several ethanol dilutions and H_2O, 8 µm sections of the tissue samples were stained with Mayer's hematoxylin to stain nuclei and Eosin Y 1% aqueous solution to stain cytoplasm (H&E staining). H&E-stained tissue was used to perform histopathological evaluation and quantitative analysis (derma and submucosa depth) using QuPath 3.0 software. Ki67 immunofluorescent staining was performed on formalin-fixed and paraffin-embedded skin samples previously cut on a microtome into 5 µm thick sections. The sections were deparaffinized in xylol and hydrated in decreasing concentrations of ethanol. Antigen retrieval was performed in heated citrate buffer (pH 6.0) and, after cooling to room temperature, Sudan Black buffer (Sigma-Aldrich 199664-25G; 0.1% in 10% ethanol; pH 7.4) was used to inhibit erythrocytes autofluorescence and goat serum (Vector Laboratories) was used as blocking solution. After sections were washed in 1× PBS (pH 7.4) 3 times, 5 min each, they were incubated with specific primary unconjugated antibody (BioLegend, rat anti-mouse, 652402), 2h, 37 °C. After sections were washed in 1× PBS (pH 7.4) 3 times, 5 min each, the specific secondary antibody (NovusBio, TX-RED, NBP1-731 49) was used in the reaction and, after nuclear counterstaining with DAPI glue mounting step, skins samples were scanned with KEYENCE BZ-X810 fluorescence microscope and investigated for further analysis. The positive stained cells were counted (per μm^2) for total epidermal immunostaining in the same 20× magnification field area and the% of the intensity was calculated vs the DAPI counter staining.

Statistics

All experimental results were first tested for normal distribution using Shapiro-Wilk for normality. Statistical analysis between multiple groups was done using two-way ANOVA followed by Bonferroni correction. Kruskal-Wallis test was used for non-parametric data. Non-marked bars are considered as not significant by which statistical significance was considered at the level of p value < 0.05. Calculations of e.g., half-life were made with GraphPad Prism 9.3.1.

Results

Differences to clinical products in induction of skin inflammation

The widely used Aldara® induced psoriatic skin model is not fully defined or understood (Horváth et al. 2019; Hawkes et al. 2017; Luo et al. 2016; Walter et al. 2013). We focused on the influence of components of imiquimod cream formulations. To study this, we induced skin inflammation in BALB/cJRj mice with different induction creams (Tables 3, 4). Isostearic acid may promote inflammasome activation, IL-1 release and apoptosis (Walter et al. 2013). Although DMSO is known to increase skin permeation, making substances more systemically available, this effect is not seen with IMQ (Telò et al. 2016). DMSO is used here to facilitate the incorporation of the substance into the cream and to overcome the poor solubility of IMQ (DMSO is permitted in human use up to 10% in creams).

In a first study, we tested different formulations for their ability to induce a psoriatic-like skin disease in mice. All of the creams used were mixed with inducing substances (either IMQ, isostearic acid or a mixture of the two) and none of the creams are considered to be vehicle creams. The usual concentration of IMQ in Aldara® or similar products is 5% W/V, however, we also tested higher concentrations (7% IMQ) to assess the effect on rate of onset of skin signs. Creams were applied 25 mg/cm^2 (50 mg total) corresponding to a total of 125 mg/kg IMQ (5%) or 175 mg/kg IMQ (7%) daily over seven consecutive days. In this initial experiment with different cream formulations (Table 3) the first changes in skin score were observed from day three on (Fig. 1A). Groups receiving isostearic acid were the first to show clinical signs in skin. Animals induced with Aldara® had a score plateau starting at day 5 (day 5–7 score of 5.9), while other groups induced with isostearic acid containing creams did not reach a plateau, but showed a reduced rate in score development (cetyl alcohol + isostearic acid: 5.5, 6.6 and 7.0; 7% IMQ + cetyl alcohol + isostearic acid: 5.6, 6.9 and 7.1; 5% IMQ + DMSO + isostearic acid: 5.3, 6.8 and 7.3 at days 5–7).

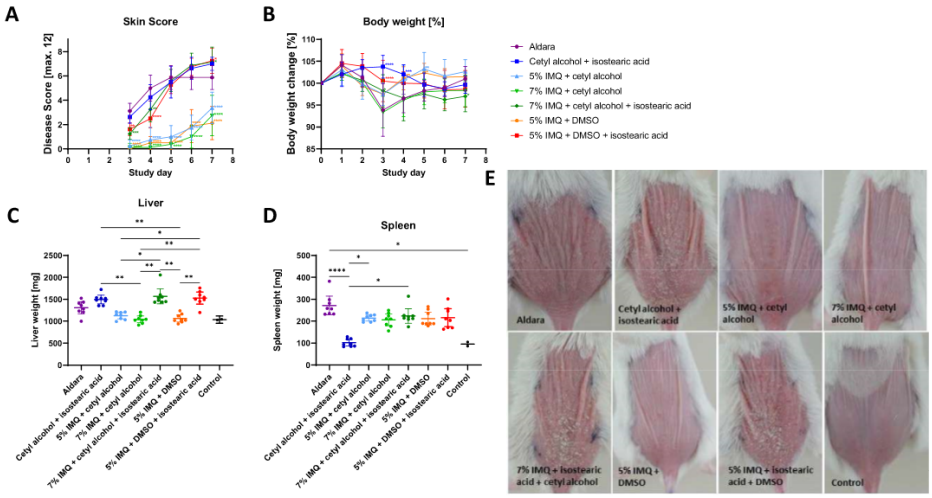

Fig. 1 **A** Accumulated skin score based on the parameters of redness, thickness and scaling (scores each between 0 and 4, with 4 being most severe). BALB/cJRj females (8 weeks old, n = 8 per group) were treated with different formulations of induction cream (50 mg) for seven consecutive days. Scores were based on dorsal skin and the first changes were observed on day 3. **B** Change of body weight during study vs day 0. **C** Weights of livers at day of termination (n = 8). **D** Weights of spleens at day of termination (n = 8). **E** Pictures of dorsal skin of one representative animal of each group at day 7 *ante mortem*. In graphs **A** and **B** groups were compared against Aldara® and tested with ordinary two-way ANOVA with Bonferroni's comparison. In graphs **C** and **D** Kruskal–Wallis test with Dunn's comparison was used after Shapiro–Wilk test for normality. Data represented as means with error bars as SD. p values ≤ 0.0001 are indicated with ****p ≤ 0.001 are indicated as ***p ≤ 0.01 are indicated as **p ≤ 0.05 are indicated as *

The cream containing isostearic acid and cetyl alcohol, but not IMQ showed a similar increase in score (2.6, 4.3, 5.5, 6.6, 7.0 from days 3–7), whilst the other groups treated with creams containing IMQ, but not isostearic acid, showed only minor signs in the first five to six days and a minor increase in skin score by day 7 (5% IMQ + cetyl alcohol: 3.4; 7% IMQ + cetyl alcohol: 2.8; 5% IMQ + DMSO + isostearic acid: 2.1 at day 7). Variation of cetyl alcohol or DMSO and the amount of IMQ did not change the scores to a significant extent. Consistent with literature reports, IMQ treatment in our studies also leads to a loss in body weight (Fig. 1B) (Horváth et al. 2019) peaking around day 3 (clinical cream 94%; 5% IMQ + cetyl alcohol: 98%; 7% IMQ + cetyl alcohol: 93%; 7% IMQ + cetyl alcohol + isostearic acid: 98%; 5% IMQ + DMSO: 98%; 5% IMQ + DMSO + isostearic acid: 101%) and suggesting that there was no difference in the availability of IMQ from the various formulations (see Fig. 1E, for lesions). Isostearic acid caused a severe reaction in terms of redness, scaling and thickness, however, without major loss in BW (tendency of loss in BW from day 4 on). IMQ also caused splenomegaly (Fig. 1D) with Aldara® induced animals, having the largest spleens (avg. spleen weights: cetyl alcohol + isostearic acid 102 mg; 7% IMQ + cetyl alcohol 206 mg; 5% IMQ + DMSO 212 mg; 5% IMQ + cetyl alcohol 214 mg; 5% IMQ + DMSO + isostearic acid 216 mg; 7% IMQ + cetyl alcohol + isostearic acid 224 mg; Aldara® 272 mg). Increased spleen size is linked to IMQ containing cream and is probably due to systemic inflammatory reactions (Fits et al. 2009; Horváth et al. 2019). Larger liver size (hepatomegaly) was observed for animals receiving creams containing isostearic acid (Fig. 1C). Creams without isostearic acid had liver weights similar to those in control animals. Mean liver weight of the Aldara®-treated group was between the two clusters (avg. liver weights: 7% IMQ + cetyl alcohol 1044 mg; 5% IMQ + DMSO 1065 mg; 5% IMQ + cetyl alcohol 1126 mg; Aldara® 1307 mg; cetyl alcohol + isostearic acid 1494 mg; 5% IMQ + DMSO + isostearic acid 1528 mg; 7% IMQ + cetyl alcohol + isostearic acid 1568 mg). Isostearic acid in the induction cream showed a direct effect on the weight of the liver independent of BW suggesting that it has a systemic effect, either via absorption by the topical route or via ingestion during grooming. The effects of IMQ on body weight were lost by day 7, consistent with a continuous attenuation of cytokine response after repeated application of IMQ or Resiquimod (data not shown) we observed in other studies. We assume that the observed

body weight pattern is an effect of the cytokine attenuation and the well-known reduction in TLR stimulation responses with time (Horváth et al. 2019).

The data from this study suggests that isostearic acid is playing a major role in the induction of skin inflammation in mice. To clarify aspects of the induction of psoriasis-like inflammation further, we investigated the key parameters in more detail in a second study.

Direct influence of isostearic acid on development of psoriasis in mice

We then directly compared IMQ (5%) containing cream with isostearic acid (25%) containing cream and a cream containing both substances versus a vehicle cream based on DAC (Table 4). Female BALB/cJRj mice were again treated with induction creams on seven consecutive days. Each animal (n = 8 per group) received 50 mg of cream dorsally on depilated skin (2 cm^2). Consistent with the results of the first study we observed changes in the skin areas treated with isostearic acid containing creams. Isostearic acid alone was sufficient to induce visible signs of skin inflammation (Fig. 2A, F). The onset of the disease in the isostearic acid containing creams was again at the third day and reached a plateau at day five until end of study (isostearic acid 4.4, 4.4, 3.8; 5% IMQ + DMSO + isostearic acid 4.3, 4.6, 4.8 at days 5–7). Scores for scaling in group 3 (isostearic acid alone) were reduced on day seven, when compared to day six (from 4.4 to 3.8) This was not observed for the IMQ/isostearic combination, which had a slightly higher total score on the final study day. Both isostearic acid containing creams showed a very similar course of induction. In animals treated with vehicle cream no changes were observed. Group 2 (IMQ containing cream) showed almost no changes over the course of the study. Individual animals of this group showed very slight thickening and redness of the skin, but significantly less than in the isostearic acid groups. As observed in our first study it appears that isostearic acid is the main stimulant of changes in skin and the development of lesions. This can be observed for all three parameters (thickness, redness and scaling). However, in contrast to the first study, no additive induction with IMQ was found here. In general, this study showed a milder course of the disease. A maximum score of 4.8 was observed for the IMQ/isostearic acid combination (isostearic acid alone 3.8 at final day). In the first study isostearic acid reached 7.0, Aldara 5.9, and 7.2 (combination of 5% IMQ + DMSO + isostearic acid) and 7.1 (7% IMQ + cetyl alcohol + isostearic acid) for the IMQ/isostearic acid combinations, respectively. Photographs taken on the final day of the studies (Figs. 1E, 2E) provide further qualitative impressions of the signs at termination.

Increased liver weights in groups that received isostearic acid and increased spleen weights in groups that were treated with IMQ containing creams (Fig. 2C, D), confirmed observations from the first study. Body weight distribution (Fig. 2B) did not follow a clear trend. Initially, the animals induced with IMQ tend to lose body weight (95% at day 3), but a slight loss is also seen in the vehicle animals (96% BW at day 4). After four to five days, animals from IMQ induced group recover BW (97% at day 4 and 103% at day 5), while the animals induced with isostearic acid start to lose weight continuously displaying the lowest body weight values at the end of the study (95% at final day for isostearic acid group and 90% for IMQ and isostearic acid group). The same trend in weight loss (from day 4) was observed for animals induced with isostearic acid in the first study.

Differences in the development of skin parameters are apparent by histology (Fig. 2H). Skin treated with isostearic acid showed significant thickening in several layers. These trends are most notable in the thickness of the dermis, but not in the submucosa (Fig. 2G). Immunohistochemical staining of Ki67, a marker of cellular proliferation, was performed with skin samples from the final day of the study (Fig. 2H). Ki67 staining suggested lower proliferation for groups receiving isostearic acid.

These data suggest that visible skin lesions and hepatomegaly in BALB/cJRj mice are mostly driven by isostearic acid. This is surprising given that it is generally considered to be safe in most reports (CIR 2013) (up to 37.4% in rinse-off products and 21% in leave-on products) and may suggest a specific effect in mice or a consequence of the high concentration and/or overall dose—625 mg/kg or 6.25 mg/cm^2—in a small animal study in proportion to the skin area affected. Splenomegaly and proinflammatory cytokines appear to be due to TLR7 activation through IMQ (Horváth et al. 2020; Jabeen et al. 2020; Butchi et al. 2008). While IMQ and isostearic acid contribute to the disease model, the effects on the conventional signs of keratinocyte proliferation may be more related to isostearic acid in mice.

Upregulation of cytokine markers in course of disease

To investigate how the components of the induction creams influence the cytokine response we collected samples of brain and skin from animals at day 7 of both studies. Figure 3 displays results from skin samples collected in the first study (other results of this study are displayed in Fig. 1). Figure 4 displays results from skin samples collected at final day of second study (other results of this study are displayed in Fig. 2). Brain samples were collected to check systemic inflammation response of chemokines (Fig. 5) (McColl et al. 2016; Nerurkar et al. 2017). Samples gathered in first study were collected on day seven, 27 h after last application of creams when induction effects may have been reduced (Fig. 3).

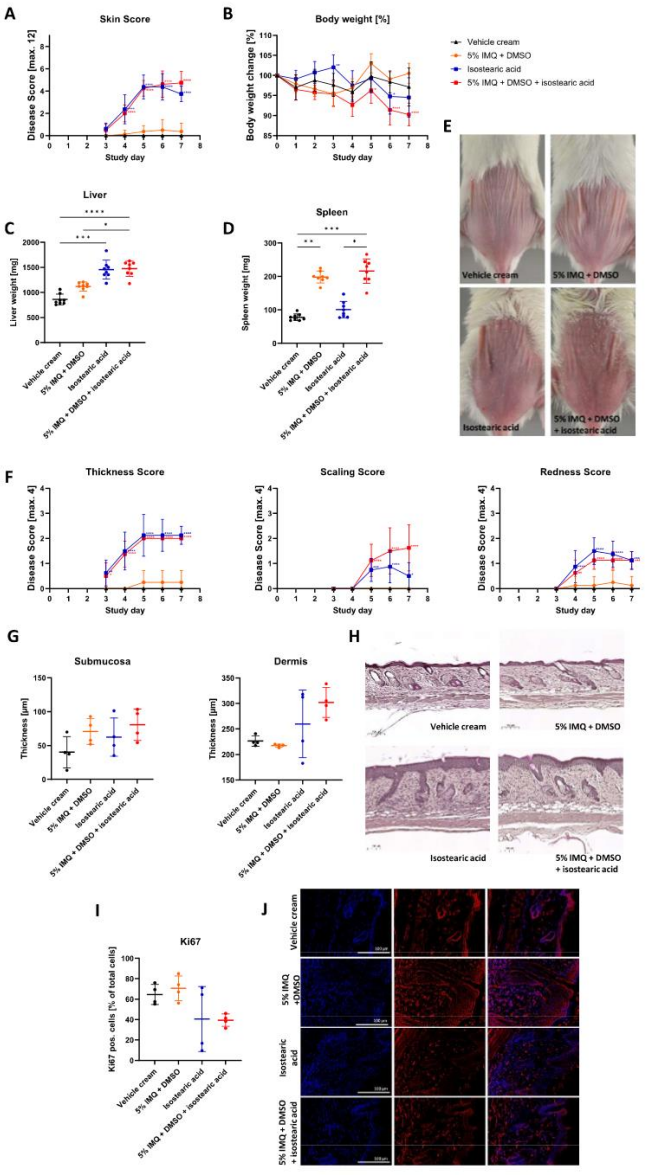

Fig. 2 **A** Accumulated skin score based on the parameters: redness, thickness and scaling (scores each between 0 and 4, with 4 being most severe). BALB/cJRj females (8 weeks old, n = 8 per group) were treated with different formulations of induction cream (50 mg) for seven consecutive days. Scored was dorsal skin and first changes were observed on day 3. **B** Change of body weight during study vs day 0 (n = 8). **C** Weights of livers at day of termination (n = 8). **D** Weights of spleens at day of termination (n = 8). **E** Pictures of dorsal skin of one representative animal of each group at day 7 ante mortem (scale bar represents 100 µm). **F** Skin score of parameters redness, thickness and scaling (scores each between 0 and 4, with 4 being most severe) (n = 4). **G** Analyzed histological parameters from dorsal skin collected at final day of study (n = 4). **H** H&E staining of skins collected at final day of study. **I** Analyzed Ki67 positive cells in dorsal skin collected at final day of study (n = 4). **J** Ki67 staining (TxRed) on DAPI nuclear counterstaining captured at ×40 (scale bar represents 100 µm). In graphs **A**, **B** and **F** groups were compared against vehicle cream and tested with ordinary two-way ANOVA with Bonferroni's comparison. In graphs **C** and **D** Kruskal–Wallis test with Dunn's comparison was used after Shapiro–Wilk test for normality. Data represented as means with error bars as SD. p values ≤ 0.0001 are indicated with ****p ≤ 0.001 are indicated as ***p ≤ 0.01 are indicated as **p ≤ 0.05 are indicated as *Groups were compared with vehicle cream

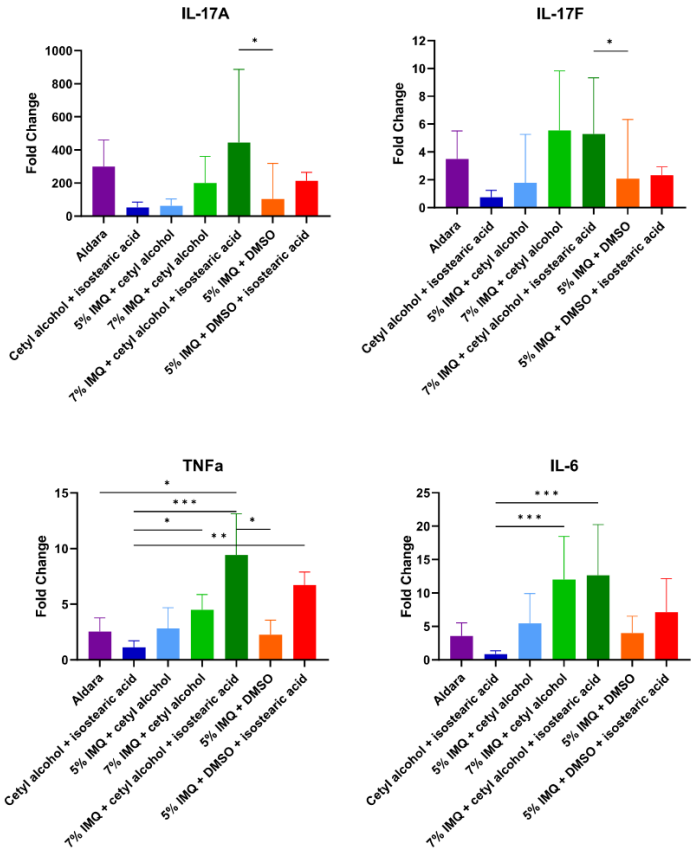

Fig. 3 Levels of IL-17A, IL-17F, TNFa and IL-6 mRNA in dorsal skin samples collected 27 h after the last application of cream. Fold change compared to untreated control. Fold changes were compared to Aldara®. Kruskal–Wallis test with Dunn's comparison was used after Shapiro–Wilk test for normality. Data represented as means with error bars as SD ($n=8$). p values ≤ 0.0001 are indicated with ****$p \leq 0.001$ are indicated as ***$p \leq 0.01$ are indicated as **$p \leq 0.05$ are indicated as *

Although isostearic acid caused the highest skin score a higher inflammatory reaction at a gene expression level was observed in IMQ induced dorsal skin samples in this experiment, and was highest in 7% IMQ induced samples where a dose dependence between cytokines and IMQ concentration can be observed. Addition of DMSO had no effect on cytokine expression. Clinical cream was more effective on IL-17A and IL-17F cytokine expression than other 5% IMQ formulations without increasing TNFα or IL-6 signal (Fits et al. 2009). These results show a tendency to induce psoriasis relevant proinflammatory cytokines, which indicates a role of IMQ in this model. However, effects may depend on the time between substance application and measurement. In this study, we chose a period of 27 h after the last application (overnight) which reflects conditions in published models and potentially a means to observe the "chronic" or "trough" expression levels following repeated stimulus.

In the second study, we sampled 2 h after the last application of cream and we assessed a wider range of relevant targets, (Fig. 4) including inflammasome related markers, IL-1β and NLRP3 which are influenced in the model (Walter et al. 2013). TNFα and IL-6 were slightly upregulated while other markers (IL-17A, IL-17F, IL-23A and IL-22) were significantly upregulated. The IL-17 family cytokines and IL-22 are known to play a central role in clinical psoriasis (Yang et al. 2021). The relative effects of IMQ and isostearic acid were differed as in previous reports (see Fig. 3 and Fits et al. 2009), however, these samples were taken 2 h after the final application of the cream which may increase effects of isostearic acid and explain the variations in the results. The implication is that responses to isostearic acid are shorter

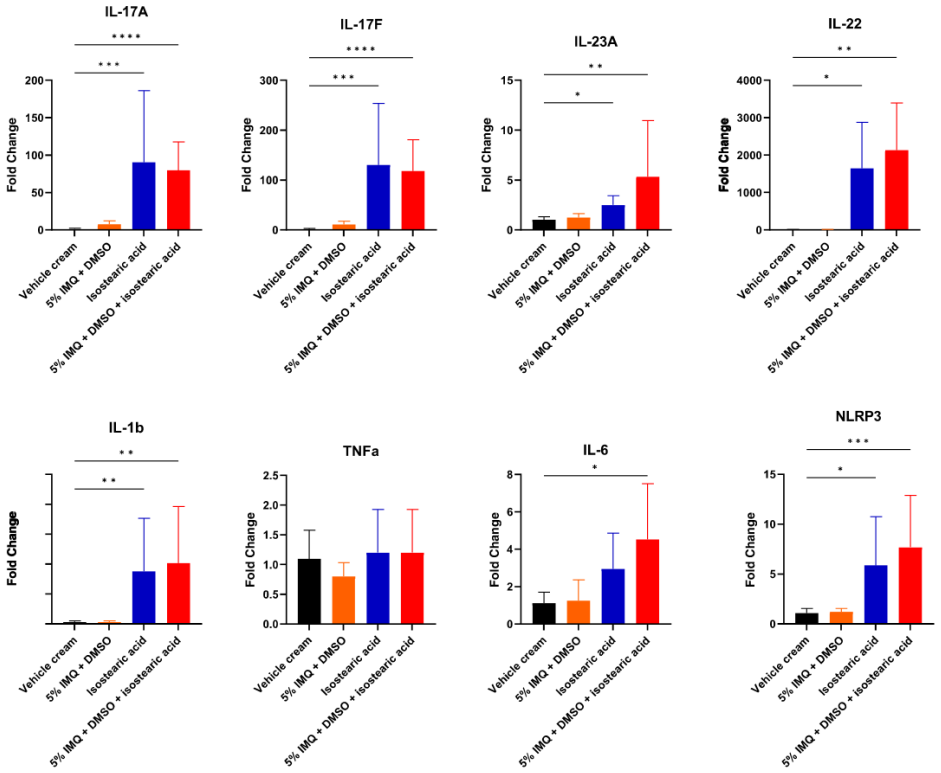

Fig. 4 Levels of IL-17A, IL-17F, IL-23A, IL-22, IL-1b, TNFa, IL-6 and NLRP3 mRNA in dorsal skin samples from study 2 by qPCR. Fold change compared to untreated (sham) control. Kruskal–Wallis test with Dunn's comparison was used after Shapiro–Wilk test for normality. Data represented as means with error bars as SD (n = 8). p values ≤ 0.0001 are indicated with ****p ≤ 0.001 are indicated as ***p ≤ 0.01 are indicated as **p ≤ 0.05 are indicated as *. Groups were compared with a clinical imiquimod cream

in duration than those to IMQ and possibly indicate a more local proinflammatory reaction.

In addition to skin samples, we analyzed samples from brain (Fig. 5) collected at the same time as skin samples (Fig. 4). However, unlike skin, changes in gene expression in the brain can only be seen in animals receiving the combination cream. Systemic IMQ has been shown to influence chemokines in brain tissue (Nerurkar et al. 2017), but here we show that only the combination is able to induce these chemokines via the topical route. Disruption of the blood-brain-barrier by one of the compounds could play a role (Nerurkar et al. 2017; Bourgognon et al. 2019), however, substance concentrations in brain tissue are neither elevated for IMQ nor isostearic acid in groups receiving the combination (Fig. 6) suggesting that disruption is unlikely. The main markers that we found to upregulated in brain (chemokines, IL-1β, TNFα) were not those that were upregulated in skin (IL-22, IL-23). The chemokines are closely connected with virus-induced neuroinflammation (Butchi et al. 2008). Nerurkar et al. (2017) were able to measure elevated levels of chemokine markers after topical treatment with Aldara®. They explained their results by a priming phenomenon due to peripheral immune stimulation with IMQ. The concentration of IMQ in the brain tissue that we report here was low, compared with a study published by Butchi et al. (2008), where IMQ was directly injected into the brain. These data suggest the hypothesis, that the combination of IMQ elevates chemokine levels without overcoming the blood-brain-barrier (see Fig. 6 for IMQ brain concentration).

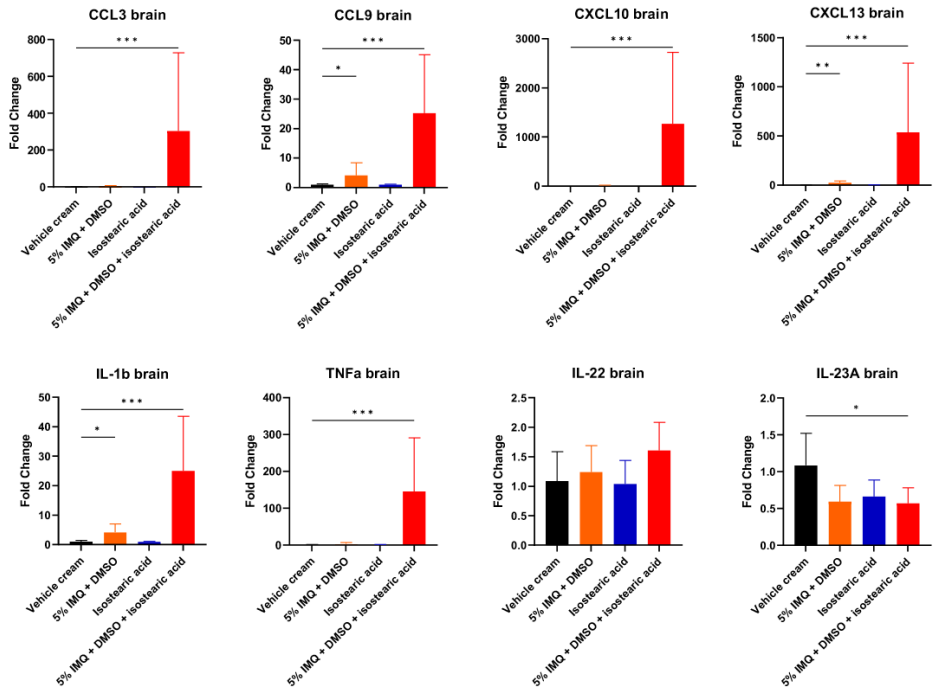

Fig. 5 RNA levels of CCL3, CCL9, CXCL10, CXCL13, IL-1b, TNFa, IL-22 and IL23A in collected brain samples from second study were measured via qPCR. Fold change compared to untreated (sham) control. Kruskal–Wallis test with Dunn's comparison was used after Shapiro–Wilk test for normality. Data represented as means with error bars as SD (n = 8). p values ≤ 0.0001 are indicated with ****p ≤ 0.001 are indicated as ***p ≤ 0.01 are indicated as **p ≤ 0.05 are indicated as *

Retention of substances in skin

We assessed animals for distribution of IMQ and isostearic acid 2 or 27 h after last application of creams (both after 7 days of consecutive application of cream) on dorsal skin using HPLC-MS/MS. Previous studies showed that IMQ is rapidly distributed to tissue with a particular affinity to skin (oral and dermal application) (Jabeen et al. 2020; Pharmaceuticals 2009; Paula et al. 2008). Although, IMQ is quickly metabolized by a first-pass effect, topical application prolongs systemic exposure (Pharmaceuticals 2009). IMQ is able to penetrate into skin and it is retained in the stratum corneum (Jabeen et al. 2020; Paula et al. 2008). The local concentration can increase over six days with continued application (Jabeen et al. 2020).

In dorsal inflamed skin we observed high concentrations of IMQ (20 mM in the IMQ group and 13 mM in IMQ/isostearic acid group) 2 h after cream application (Fig. 6). Lower concentrations were also detected in healthy (non-inflamed) ventral skin (0.4 mM in the IMQ group and 1 mM in IMQ/isostearic acid group). For IMQ/isostearic acid cream, concentrations were also measured 27 h after application. IMQ concentrations were significantly lower in both, dorsal (0.2 mM) and ventral skin (0.15 mM). Concentrations in the two areas almost equalized over this period. Other organs showed IMQ concentrations in lower µM ranges. Ranges, nonetheless, high enough to stimulate proinflammatory responses based on known TLR7 affinity. No major changes were observed in IMQ levels in organs other than skin over the course of time. The skin might act as a IMQ depot and release it over time and thus generates a prolonged systemic stimulation. The fact that levels in ventral skin were as high as in dorsal skin (site of application) after 27 h, suggest that either it was re-distributing within skin or via grooming, or that it was accumulating from the systemic circulation. The levels in the ventral skin were not associated

with any form of obvious “psoriatic” transformation and this is, in turn, consistent with the observation that IMQ itself is less effective in causing psoriaform lesions.

Quantification of isostearic acid (Fig. 6, lower panel) showed ca. 70 mM in dorsal skin where the combination cream was applied. Local concentrations in dorsal skin are elevated 2 h after application. The contribution of remnant cream on the skin is difficult to assess because overly vigorously washing could also leach material from the skin itself, nonetheless, rinsing steps ensure that detected levels are from skin associated material. Absorbed cream is distributed to organs, like spleen and liver, where concentrations reflect the treatment type. Naturally occurring “stearic acid isomers” were detected in nontreated animals (parent masses and retention times being similar). Brain levels of isostearic acid were not elevated in combination with IMQ. The high levels of Isostearic acid in dorsal skin could act as a local proinflammatory stimulus as concentrations are substantially elevated for hours.

Discussion

There is often a degree of time sensitivity in pharmacology studies with short duration models favored over longer versions for reasons of efficiency, ethics or simplicity. Often, shorter duration is obtained with higher dosed challenges or, indeed, more complex challenges. In developing a model based only on IMQ we faced questions about not only the degree of severity (50–60% of clinical formulations) but also duration (9–10 days instead of 5–7). These data suggest that a “pure” IMQ “psoriasis” model can be conducted, it requires only more time. While it is unlikely that simply inhibiting TLR7 signaling would be sufficient for a therapeutic effect in human patients, we suspect that the transition to skin pathology with IMQ is not strictly driven by TLR7 agonism alone. Rather, we propose that the effects in skin may be related to inhibition of the adenosine receptors A(1) and A(2A) in addition to or in concert with cytokine increases related to TLR7 agonism (Schön et al. 2006; Wolff et al. 2013). Indeed, in such a mixed challenge model (IMQ/isostearic acid), a number of pathways are activated locally and systemically. Some effects are caused by multiple pathways, and others are specifically related to one challenge agent. Thus, it should not be assumed that compounds with a “single specific mode of action” should influence all aspects of pathology unless they impact an extremely central regulator. Action on a very central regulator is not always desirable in terms of safety (see glucocorticoids). Rather, assessing a range of signals will help deconvolute which aspects a given therapy can influence. It may also lead to assessment in a more focused model where there is less complex activation of different pathways.

Finally, mouse strain selection may play a greater role than is often appreciated and while many models are conducted in the C57BL/6 background, others like this one

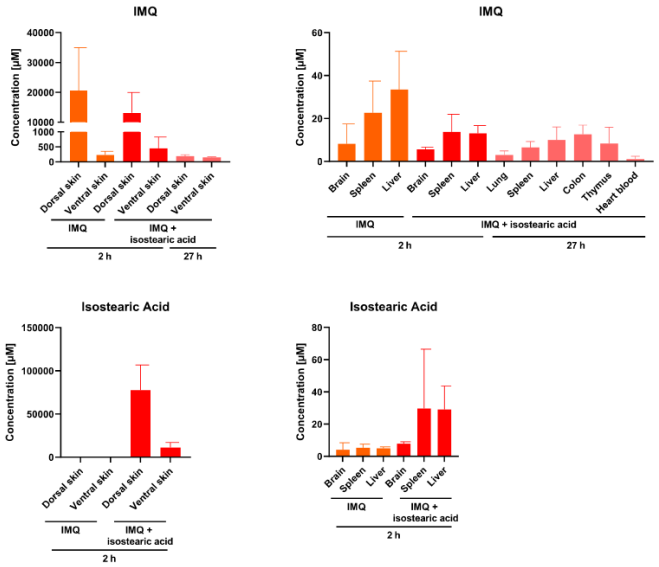

Fig. 6 Organ samples collected at end of IMQ-induced psoriasis study (n = 8), 2 or 27 h after last cream application. Samples were analyzed with HLPC-MS/MS. Top row shows measured concentrations of IMQ in organs. Bottom row shows results for concentration of isostearic acid in organs

use BALB/cJRj for the simple convenience of more easily observing the skin score and reddening. However, contrasting results have been obtained in C57BL/6 mice, including the suggestion that high doses of IMQ (156 mg/kg) cause systemic vs. local signs which are reported to be just as apparent at 50 mg/kg IMQ with the lower dose actually associated with more significant local score (Horváth et al. 2019). These data may suggest a form of "spillover" to the systemic circulation at high doses that may be in excess of that required for local effect, especially when skin appears to accumulate or retain the substance. In this context, we will continue to examine effects of the two most eliciting components of clinical imiquimod formulations in both mouse strains, taking account of the effects of melanin and other C57BL/6 immune attributes in follow-up studies.

While clinical imiquimod formulations provide a convenient means to induce psoriasiform like lesions in mice with IL-17 involvement, the composition in relation to the mode of action is potentially more complex than is widely appreciated. It is important to recall that the original proposed use was to stimulate rejection of warts, and more recently, clinical imiquimod formulations have demonstrated efficacy in rejection of early skin cancers (Rosso 2005). Biochemical investigations suggest a range of effects of IMQ, which was widely considered to be the active principle in the induction of psoriaform like lesions in mice (TLR7 agonism, adenosine receptor inhibition and interactions with the hedgehog pathway) (Schön et al. 2006; Wolff et al. 2013). However, in human use, while redness/erythema is noted, effects are rarely "psoriasiform" and isostearic acid is considered an uncontroversial ingredient in human cosmetics (CIR 2013; Bergfeld et al. 2018). The difference between human use and murine uses is almost certainly first the dose. Human use would rarely exceed one sachet or 250 mg of cream—12.5 mg of imiquimod (assuming use of the full sachet), or 0.5 mg/cm^2 or 0.18 mg/kg. In contrast, the dose commonly used to induce the model in mice is between 62.5 and 156 mg/kg—350–870-fold higher. The dose for isostearic acid would be 62.5 mg or 2.5 mg/cm^2, or 0.9 mg/kg in human patients. In mice, it is of the order of 625 mg/kg (ca. 700-fold higher) or 6.25 mg/cm^2. These differences in overall dose probably explain both systemic spillover in mice and more profound local effects. Accounting for metabolic rate, the exposure in mouse is still at least 100-fold over that which is common in human use. On the other hand, a lower sensitivity to TLR-agonist induced inflammation can be observed in mice with doses used in murine models showing intolerable adverse effects in clinical studies (see Resiquimod) (Pockros et al. 2007). This further points to the possibility that the contributions individual components of clinical IMQ formulations have on inflammation differ significantly between a murine and human setting.

Data reported here demonstrate that isostearic acid appears to have an important role in stimulating initial skin signs in the psoriasiform model. In contrast, IMQ appears to take longer to induce skin effects and is instead rather potent in cytokine induction. Our observations suggest that the clinical formulation is, in many ways, optimal in terms of cytokine induction, and compositions with the same amount of IMQ and isostearic acid differ in subtle ways from the formulation sold as Aldara® in disease induction. Nonetheless, should workers wish to use a defined, non-commercial, preparation, the cream formulations we describe can at least be reproduced in their functional properties with and without the key ingredients. This should make it more straightforward to deconvolute drug effects.

Conclusion

The induction of psoriaform skin inflammation in mice is not solely due to a stimulus by IMQ. Isostearic acid, one of the main components of clinical formulations is a key trigger in the disease model. Studies using clinical creams for induction need to take this into account. Further analysis, especially regarding cellular mechanisms, should elucidate the exact role of isostearic acid in vivo in mice.

Acknowledgements We would like to thank colleagues from Synovo GmbH and the University of Tübingen who assisted in this research. Special thanks to the members of the in vivo facility and the team of the analytics/bioanalytics department at both institutions.

Author contributions All authors have read and agreed to the published version of the manuscript. Conceptualization, SS, TLS and MB; methodology, SS, TLS, MM and MB; validation, SS, TLS and MB; formal analysis, SS, MM and TLS; investigation, JG, SS, SC, MM, MK, TLS, NS, TF and AS; resources, MB and SL; writing—original draft preparation, SS; writing—review and editing, TLS, MB and JHG; visualization, SS; supervision, MB, JHG and SL; project administration, MB; funding acquisition, MB.

Funding This research received no external funding.

Data availability Enquiries about data availability should be directed to the authors.

Declarations

Conflict of interest SS, JG, MM, TF, NC, MK, LR, AS, NS, SC, JHG, TLS are employees of Synovo GmbH. MB is general manager of Synovo GmbH. Synovo provides models of inflammation to the pharmaceutical industry as a service and the investigation of disease model mechanisms is part of this commercial offering.

Institutional review board statement All study protocols were approved by the local Animal Care and Ethics Committee (Federal government ethics committee, Tübingen, Germany under the license 35/9185.81-7/SYN 07/18).

References

Bergfeld et al (2018) Safety assessment of fatty acids and soaps as used in cosmetics. In: The 2018 Cosmetic Ingredient Review Expert Panel members are: Chair, Wilma F. [Online]. Available: http://www.cir-safety.org/supplementaldoc/preliminary-search-engines-and

Bourgognon J, Suessmilch M, McColl A, Cavanagh J (2019) Abstract #4297 blood brain barrier breakdown following topical aldara treatment. Brain Behav Immun 81:24–25. https://doi.org/10.1016/j.bbi.2019.08.086

Brück J, Dringen R, Amasuno A, Pau-Charles I, Ghoreschi K (2018) A review of the mechanisms of action of dimethylfumarate in the treatment of psoriasis. Exp Dermatol 27(6):611–624. https://doi.org/10.1111/exd.13548

Butchi NB, Pourciau S, Du M, Morgan TW, Peterson KE (2008) Analysis of the neuroinflammatory response to TLR7 stimulation in the brain: comparison of multiple TLR7 and/or TLR8 agonists. J Immunol 180(11):7604–7612. https://doi.org/10.4049/jimmunol.180.11.7604

Chiricozzi A, Romanelli P, Volpe E, Borsellino G, Romanelli M (2018) Scanning the immunopathogenesis of psoriasis. 19(1)

CIR (2013) Safety assessment of fatty acids and fatty acid salts as used in cosmetics

De Paula D, Martins CA, Bentley MVLB (2008) Development and validation of HPLC method for imiquimod determination in skin penetration studies. Biomed Chromatogr 22(12):1416–1423. https://doi.org/10.1002/bmc.1075

Del Rosso JQ (2005) The use of topical imiquimod for the treatment of actinic keratosis: a status report. Cutis 76(4):241–248

Flutter B, Nestle FO (2013) TLRs to cytokines: mechanistic insights from the imiquimod mouse model of psoriasis. Eur J Immunol 43(12):3138–3146. https://doi.org/10.1002/eji.201343801

Girolomoni G et al (2017) The role of IL-23 and the IL-23/TH17 immune axis in the pathogenesis and treatment of psoriasis. J Eur Acad Dermatol Venereol 31(10):1616–1626. https://doi.org/10.1111/jdv.14433

Global Report on Psoriasis (2023)

Graceway Pharmaceuticals (2009) Center for drug evaluation and pharmacology review: 201153Orig1s000

Hawkes JE, Gudjonsson JE, Ward NL (2017) The snowballing literature on imiquimod-induced skin inflammation in mice: a critical appraisal. J Invest Dermatol 137(3):546–549. https://doi.org/10.1016/j.jid.2016.10.024

Horváth S, Komlódi R, Perkecz A, Pintér E, Gyulai R, Kemény Á (2019) Methodological refinement of Aldara-induced psoriasiform dermatitis model in mice. Sci Rep 9(1):1–8. https://doi.org/10.1038/s41598-019-39903-x

Horváth S, Kemény Á, Pintér E, Gyulai R (2020) A localized aldara (5% imiquimod)–induced psoriasiform dermatitis model in mice using Finn chambers. Curr Protoc Pharmacol 90(1):1–12. https://doi.org/10.1002/cpph.78

Jabeen M et al (2020) Advanced characterization of imiquimod-induced psoriasis-like mouse model. Pharmaceutics 12(9):1–18. https://doi.org/10.3390/pharmaceutics12090789

Luo D, Wu H, Zhao Y, Liu J, Wang F (2016) Different imiquimod creams resulting in differential effects for imiquimod-induced psoriatic mouse models. 1733–1738. https://doi.org/10.1177/1535370216647183

McColl A, Thomson CA, Nerurkar L, Graham GJ, Cavanagh J (2016) TLR7-mediated skin inflammation remotely triggers chemokine expression and leukocyte accumulation in the brain. J Neuroinflammation 13(1):1–16. https://doi.org/10.1186/s12974-016-0562-2

Nakajima K, Sano S (2018) Mouse models of psoriasis and their relevance. J Dermatol 45(3):252–263. https://doi.org/10.1111/1346-8138.14112

Nerurkar L, Mccoll A, Graham G, Cavanagh J (2017) The systemic response to topical aldara treatment is mediated through direct TLR7 stimulation as imiquimod enters the circulation. Sci Rep. https://doi.org/10.1038/s41598-017-16707-5

Pockros PJ et al (2007) Oral resiquimod in chronic HCV infection: Safety and efficacy in 2 placebo-controlled, double-blind phase IIa studies. J Hepatol 47(2):174–182. https://doi.org/10.1016/j.jhep.2007.02.025

Schön MP, Schön M (2007) Imiquimod: mode of action. Br J Dermatol 157(SUPPL. 2):8–13. https://doi.org/10.1111/j.1365-2133.2007.08265.x

Schön MP, Schön M, Klotz KN (2006) The small antitumoral immune response modifier imiquimod interacts with adenosine receptor signaling in a TLR7- and TLR8-independent fashion. J Invest Dermatol 126(6):1338–1347. https://doi.org/10.1038/sj.jid.5700286

Straß S, Schwamborn A, Keppler M, Guse J, Burnet M (2021) Synthesis, characterization and in vivo distribution of intracellular delivered macrolide SCFA derivatives. 1–16. https://doi.org/10.1002/cmdc.202100139

Sun L et al (2018) Comparison of normal versus imiquimod-induced psoriatic skin in mice for penetration of drugs and nanoparticles. Int J Nanomed 13:5625–5635. https://doi.org/10.2147/IJN.S170832

Telò I, Pescina S, Padula C, Santi P, Nicoli S (2016) Mechanisms of imiquimod skin penetration. Int J Pharm 511(1):516–523. https://doi.org/10.1016/j.ijpharm.2016.07.043

van den Höfel N (2018) Basiscreme DAC. https://flexikon.doccheck.com/de/Basiscreme_DAC#

van der Fits L et al (2009) Imiquimod-induced psoriasis-like skin inflammation in mice is mediated via the IL-23/IL-17 axis. J Immunol 182(9):5836–5845. https://doi.org/10.4049/jimmunol.0802999

Walter A et al (2013) Aldara activates TLR7-independent immune defence. Nat Commun 4(1):1–13. https://doi.org/10.1038/ncomms2566

Wolff F, Loipetzberger A, Gruber W, Esterbauer H, Aberger F, Frischauf AM (2013) Imiquimod directly inhibits Hedgehog signalling by stimulating adenosine receptor/protein kinase A-mediated GLI phosphorylation. Oncogene 32(50):5574–5581. https://doi.org/10.1038/onc.2013.343

Yang K, Oak ASW, Elewski BE (2021) Use of IL-23 inhibitors for the treatment of plaque psoriasis and psoriatic arthritis: a comprehensive review. Am J Clin Dermatol 22(2):173–192. https://doi.org/10.1007/s40257-020-00578-0

Zhang D et al (2022) Comparison of efficacy of anti-interleukin-17 in the treatment of psoriasis between caucasians and asians: a systematic review and meta-analysis. Front Med 8(January):1–9. https://doi.org/10.3389/fmed.2021.814938

10. „Imidazoquinolines with improved pharmacokinetic properties induce a high IFNα to TNFα ratio *in vitro* and *in vivo*“

Keppler, M., **Straß, S.** (geteilte Erstautorenschaft), Sophia Geiger, Tina Fischer, Nadja Späth, Thilo Weinstein, Anna Schwamborn, Jamil Guezguez, Jan Hinrich Guse, Stefan Laufer, Michael Burnet (2023). Imidazoquinolines with improved pharmacokinetic properties induce a high IFNα to TNFα ratio in vitro and in vivo. Eingereicht am 17.02.2023 in Frontiers in Immunology (für *Supporting Information* siehe Anhang).

Eigenanteil an Publikation

Die Idee zur Synthese der gelisteten Stoffe wurde von Herr Keppler, Dr. Burnet, Dr. Guse und mir ausgearbeitet. Alle aufgeführten Synthesen wurden von mir durchgeführt. Die Aufnahme der NMR-Spektren erfolgte durch die Uni Tübingen über die Arbeitsgruppe Laufer. Die Auswertung der Spektren, die Charakterisierung und die Strukturaufklärung wurde von mir, unter Anleitung von Dr. Guse, durchgeführt. Frau S. Geiger, Frau Späth, Frau Fischer, Herr Keppler und ich waren verantwortlich für die Struktur und Ausführung der *in vitro* Experimente und die Aufarbeitung von anfallenden Proben für die Analyse. *In vivo* Experimente wurden von Herrn Weinstein, Dr. Burnet, Frau S. Geiger und Herrn Keppler geplant und durchgeführt. Die Aufarbeitung, Analyse und Messung der Proben aus den Studien, sowie der Proben aus den Stabilitäten und die Entwicklung der Methode für die HPLC-MS/MS wurde von Frau Schwamborn, Herrn Keppler, Dr. Guezguez und mir getätigt. Die schriftliche Ausarbeitung und Visualisierung erfolgten durch Herrn Keppler, Frau S. Geiger, mich und Dr. Burnet. Alle AutorInnen haben das Manuskript überprüft und korrigiert. Prof. Laufer wirkte bei der Arbeit unterstützend und betreuend.

frontiers

Imidazoquinolines with improved pharmacokinetic properties induce a high INFα to TNFα ratio *in vitro* and *in vivo*

Manuel Keppler[1+], Simon Straß[2+], Sophia Geiger[1], Tina Fischer[1], Nadja Späth [1], Thilo Weinstein[1], Anna Schwamborn[1], Jamil Guezguez[1], Jan Hinrich Guse[1], Stefan Laufer[2], Michael Burnet[1*]

[1] Synovo GmbH, Tübingen

[2] Eberhard Karls Universität Tübingen

[+] Shared first authors

*** Correspondence:**
Michael Burnet
michael.burnet@synovo.com

Keywords: TLR7, TLR8, Resiquimod, Imidazoquinoline, Macrolide, Interferon α, Cytokine Spectrum, Pharmacokinetics

1 Abstract

TLR Agonists have promising activity in preclinical models of viral infection and cancer. However, clinical use is only in topical application. Systemic uses of TLR-ligands such as Resiquimod, have failed due to adverse effects that limited dose and thus, efficacy. This issue could be related to pharmacokinetic properties that include fast elimination leading to low AUC with simultaneously high c_{max} at relevant doses. The high c_{max} is associated with a sharp, poorly tolerated cytokine pulse, suggesting that a compound with a higher AUC/c_{max}-ratio could provide a more sustained and tolerable immune activation.

Our approach was to design TLR7/8-agonist Imidazoquinolines with endosomal tropism *via* acid trapping using a macrolide-carrier. This can potentially extend pharmacokinetics and simultaneously direct the compounds to the target compartment. The compounds have hTLR7/8-agonist activity (EC50 of the most active compound in cellular assays: 75-120 nM hTLR7, 2.8-3.1 µM hTLR8) and maximal hTLR7 activation between 40 and 80% of Resiquimod. The lead candidates induce secretion of IFNα from human Leukocytes in the same range as Resiquimod but induce at least 10-fold less TNFα in this system., consistent with a higher specificity for human TLR7. This pattern was reproduced *in vivo* in a murine system, where small molecules are thought not to activate TLR8. We found that Imidazoquinolines conjugated to a macrolide or, substances carrying an unlinked terminal secondary amine, had longer exposure compared with Resiquimod. The kinetics of pro-inflammatory cytokine release for these substances *in vivo* were slower and more extended (for comparable AUCs, approximately half-maximal plasma concentrations). Maximal IFNα plasma levels were reached 4 h post application. Resiquimod-treated groups had by then returned to baseline from a peak at 1 h. We propose that the characteristic cytokine profile is likely a consequence of altered pharmacokinetics and, putative endosomal tropism of the novel substances. In particular, our substances are intended to partition to cellular compartments where the target receptor and a distinct combination of signaling molecules relevant IFNα-release are located. These properties could address the tolerability issues of

TLR7/8 ligands and provide insight into approaches to fine-tune the outcomes of TLR7/8 activation by small molecules.

2 Introduction

The term immunotherapy is mostly associated with the treatment of cancer by checkpoint inhibitors, cell-based approaches or vaccinations.(1). In a broader sense, immunotherapy describes therapeutic concepts aimed at modulating the host immune system to treat conditions related to neoplasia and infection as well as autoimmune conditions (2)(3)(4). The possibility of harnessing the diverse defense mechanisms of the immune system itself circumvents some of the limitations of pathogen- or neoplasm-directed pharmaceuticals, particularly the development of resistance to those drugs by mutations in their molecular targets. Correspondingly, immune activating therapies could be useful for infectious diseases for which a drug specifically targeting the pathogen itself is not yet available (4)(5)(6). One of the first treatments relying on immune activation to interfere with an ongoing infection or neoplasm was the use of recombinant Interferon alpha (IFNα) in the treatment of Hairy Cell Leukemia, Hepatitis B and Hepatitis C (before HBV/HCV were identified) (7)(8)(9). Indeed, recombinant IFNα was the first approved immunotherapeutic agent and the most thoroughly clinically characterized immune stimulant. It has been used for decades as a treatment of various viral diseases and cancers (8). While there has been a considerable focus on checkpoint blockade *via* antibodies targeting the PD1/PD-L1-axis (10), stimulation of the immune system through activation of pattern recognition receptors (PRRs) and particularly Toll-like-receptors (TLRs) is another promising concept that has been widely investigated, especially in dermatological cancers (11)(12)(13). In contrast to immunotherapies focused on blocking of inhibitory receptors and thus overcoming immunosuppression, agonists to PRRs activate immune response through increasing the expression of surface-bound and secreted mediators of inflammation making this stimulatory approach more similar to the direct use of recombinant cytokines such as IFNα as therapeutic agents (13)(14)(15)(16)(17).

Toll-like receptors are membrane-integral PRRs with varied representation in different species – 10 subtypes have been identified in humans and 12 in mice. Regardless of species, TLRs can generally be subdivided based on the orientation of their ectodomains either towards the extracellular space or the luminal space of endosomal vesicles. In humans, TLR1/2/4/5/6/10 are localized in the plasma membrane while TLR3/7/8/9 are restricted to vesicular membranes. TLR10 is not present in mice but TLR11/12/13 are and all localize to membranes of intracellular compartments (18). Ligand binding results in the formation of receptor dimers and recruitment of adapter proteins containing a TIR domain which vary with receptor type. The signaling cascade of all TLRs except for TLR3 uses the common adapter MyD88 to subsequently activate NfκB and IRF1/3/5/7/8 depending on receptor and cell type, with activation of NfκB and IRF5 being linked to the induction of pro-inflammatory cytokines and IRF1/3/5/7/8 having a role in regulating expression of type I interferons (19)(20)(21).

The endosomal nucleic acid-sensing TLRs 7/8/9 are similar in terms of their natural ligands, localization and direct engagement of MyD88. This is in contrast to plasma membrane-localized TLRs which employ additional adapters such as TIRAP and TRAM or TLR3 which uses TRIF as its downstream adapter. TLR7/8/9 can therefore be classified as a sub-family of TLRs (14)(19). TLR7 and 9 are highly expressed in plasmacytoid dendritic cells (pDCs), which play a central role at the interface between the innate and adaptive immune response to viral infections (22). However, their impact on cancer and immune evasion is ambiguous (23)(24). TLR8 is highly expressed in monocytes, macrophages and myeloid dendritic cells (mDCs) (25).

Novel TLR7/8 agonists with improved pharmacokinetic properties

The outcome of intracellular TLR activation can vary considerably as a consequence of receptor expression being limited to specific cell types with characteristic signaling cascades and downstream mediators of inflammation (26). For example, TLR7-mediates release of large amounts of Type I IFN from pDCs. This is in contrast to its role in monocytes, where TLR7 activation by Imiquimod induces secretion of the classical inflammatory cytokines Interleukin-6 (IL6) and -1β (IL1β) but IFNα/β release is instead mediated by TLR8(22)(27).

Ligand-dependent cytokine expression patterns in a single cell type have been demonstrated for TLR9, for which several classes of synthetic oligodeoxynucleotides (ODNs) with different signaling outcomes have been identified. A distinct induction of either IRF- or NfκB-relayed signaling was originally reported to be dependent on ODN sequence and has later been demonstrated to vary based on the subcellular location of receptor engagement (28)(29)(30)(31). In this context TRAF3 and IKKα act as the central mediator of IRF7 phosphorylation and induction of type I IFNs following the activation of TLR9 and 7 (32)(33)(34)(35).

Given the similarities in the respective signaling cascades, a similar spatial factor to the outcome of TLR7 activation is plausible, although not yet demonstrated (35). Clear differentiation of the signaling by TLR7 and 8 in native cells will, however, be complicated because there is some overlap also in their ligand preferences. TLR9 signaling, however, can be distinguished because it recognizes unmethylated CpG motifs in DNA (36).

In addition to their ability to bind specific nucleic acid sequences, TLR7/8/9 possess dedicated binding sites for either guanosine (TLR7), uridine (TLR8) or cytosine (TLR9) and simultaneous engagement of both binding sites enhances receptor activation (11). While signaling through TLR9- appears to require a longer oligonucleotide ligand, several synthetic small molecules (mononucleotide analogs) sufficient to activate TLR7/8 are available. The most widely used class of small-molecule TLR7/8-activators are Imidazoquinolines, particularly the most prominent members of this class, Resiquimod (TLR7/8) and Imiquimod (TLR7). Imiquimod is the only FDA-approved agonist to an intracellular TLR to date. Its applications include the topical treatment of basal cell carcinoma or genital warts. Imiquimod probably interacts with other receptors in addition to TLR7 but its efficacy appears to depend on induction of IFNα, tumor necrosis factor α (TNFα), interleukin 12 (IL12) and other pro-inflammatory mediators (15).

The more potent Imidazoquinoline, Resiquimod originally showed promise in various pre-clinical models of neoplastic or infectious disease (37)(38)(39), however, these results have not translated in wider clinical trials. Topical treatment of genital herpes with Resiquimod had encouraging effects in Phase II but not in Phase III (40). In the treatment of chronic Hepatitis C, oral Resiquimod could transiently reduce viral titers but effective doses caused systemic adverse effects consistent with an excess induction of inflammatory cytokines, particularly IFNα (41). Similar adverse events were observed for daily Imiquimod use (42). These adverse effects, often in the form of “flu like” symptoms, limit the systemic use of TLR7 and 8 activators and likewise IFNα. In the latter case, efforts have been made to increase the therapeutic window by PEGylation of recombinant IFNα to improve the pharmacokinetic profile (9), lengthen circulating half-life and allow longer intervals between treatments. Efficacy and adverse event benefits compared with the un-PEGylated cytokine were variable (43)(44).

Following a similar rationale, we hypothesized that the therapeutic index of small molecule TLR agonists like Resiquimod is limited by a range of factors: very steep dose response characteristics (all or nothing), the short half-life and poor tissue distribution necessitating the use of relatively high

doses to achieve sufficient activation, the transient stimulation and, correspondingly, the high maximal concentrations relative to the AUC of pro-inflammatory cytokines that are induced.

The transient effects are due to the fact that Resiquimod is unstable and rapidly metabolized. After oral application major metabolites are 6-OH-Resiquimod and 7-OH-Resiquimod *via* CYP1A2; desethyl or N-oxide Resiquimod *via* CYP3A4; or 8-OH-Resiquimod *via* one of both enzymes. Unchanged Resiquimod is only detectable in minor amounts in either urine (< 5%) or feces (< 1%) (45)(46). Imiquimod metabolism is associated with the formation of at least five different monohydroxylated metabolites through CYP1A isoforms (47).

The binding sites of known small-molecule agonists of TLR7 and 8 are each located in the same motif. The aminoquinolyl moiety mediates agonistic receptor binding through stacking effects and through hydrogen bonds (48)(49)(50)(51). The butyl side chain interacts hydrophobically with the binding pocket of the receptors. The length of 4 atoms appears optimal for interaction with hTLR7 while heteroatoms in this side group, such as an oxygen in Resiquimod, moderately increase the affinity (52,53). A smaller contribution to the binding affinity is made by van der Waals interactions of the 2-methylpropan-2-ol side chain (49)(54).

Due to the slightly lower importance of that interaction, the 2-methylpropan-2-ol side chain was chosen as the starting point for modification and linking *via* side groups listed in reaction scheme 1 in Figure S1 (A1 to A4), which could be further extended by a macrolide (A1-mac and A2-mac; see Figure S2). The linking molecules functioned as a spacing between TLR agonistic imidazoquinolinone and macrolide but can also contribute hydrogen bonds as in the 2-methyl-propan-2-ol of Resiquimod. The macrolide site consists of Azithromycin coupled to the TLR binding site at the desosamine *via* an N-methyl iminodiacetyl. Azithromycin provides a high volume of distribution, concentration in immune cell endo/lysosomes, high exposure to liver, lung and spleen and sub-cellular separation from cytochrome p450 containing organelles (55)(56). Compared with other common macrolides, it exhibits increased stability to acids, low hERG affinity, and a greater ability to concentrate in cells due to its dual amines (57)(58). Many of these effects are related to its properties as an amphiphilic di-basic compound for which the pk_as of the amines correspond well to those required to be neutral during membrane traverse but charged in acidic intracellular compartments.

Building on our previous experience with lysosome-directed compounds(55,59), we set out to prepare TLR7/8 ligands with high exposure to the endo/lysosomal lumen by exploiting the properties of acid trapping in the assumption that amphiphiles would be ideal ligands for endosomal TLRs. We designed these ligands in a way that would make them suitable for linkage to carrier molecules, such as Azithromycin, peptides or proteins, i.e. retain activity, when conjugated. The ligands described here were directed to their target organelles, either by manipulating the properties of the ligand substituents themselves, or *via* conjugation to Azithromycin, which would dominate the properties of the resulting compound. In parallel we optimized for high *in vivo* stability as well as favorable pharmacokinetic properties following parenteral application. Based on the expected pharmacokinetic properties of our ligands, we expected differences in release kinetics of inflammatory mediators, when compared to other Imidazoquinolines and, correspondingly, changes in maximal and cumulative plasma concentrations of those mediators. What we did not expect were changes in the cytokine spectrum induced by our ligands that may improve tolerability. Here we report the initial characterization of the compounds as small molecules, that may be useful as immune stimulants in cancer and infection.

3 Methods

3.1 Synthesis and Characterization

All chemicals were purchased from commercial sources and used as received. Reaction monitoring was performed *via* mass spectrometry (Finnigan LCQ Deca XP MAX, Software Xcalibur 2.0.7 SP1) and TLC (Merck TLC Silica gel 60 F254). TLC spots were detected with Hanessian's stain, based on a Cerium Molybdate solution and heat. NMR spectra were recorded with a Bruker Avance 400 (400 MHz) or Bruker Avance III (300 MHz). Substances were dissolved in $CDCl_3$ and chemical shifts (ppm) were referenced to $CHCl_3$/tetramethyl silane. Coupling constants (*J*) are given in Hz. After reaction steps solvents were evaporated with rotary evaporator (RV8 IKA, KNF SC 920) under vacuum. To purify substances, flash chromatography was performed (Interchim puriFlash 5.020 with Interchim PF-15SIHP-F0040 or PF-50SIHP-F0040 columns). Purity of reaction products was determined *via* HPLC (Varian ProStar) and ELS detection (Sedere Sedex 80). Mobile phases contained water (0.05 % formic acid) and methanol (0.05 % formic acid) as gradients. Stationary phase was ReproSil-Pur 120 C_{18}-AQ, 5 µm, 75x3 mm (Dr. Maisch). High resolution mass spectra were recorded with a Bruker maXis 4G ESI-TOF from Daltonik [JL1], using ESI^+ mode with following settings: Capillary voltage 4.5 kV, source temperature 200 °C, gas flow 6 L/min, nebulizer gas pressure 1.2 bar, end plate offset – 0.5 kV and an m/z range of 100 to 1350. Detailed synthesis and reaction procedure can be found in SI.

3.2 Stability in whole blood, U937 and RPMI

Human blood products used in the *in vitro* assays (for cell stimulation and stability) were obtained from the center for transfusion medicine in Tübingen, Germany (Zentrum für Klinische Transfusionmedizin Tübingen GmbH, (ethical approval number ZKT-FoPro202106-2305-01). Test compounds (1 µM) in either culture medium (RPMI-1640 medium containing 10% fetal bovine serum, 60 mg/l Penicillin G sodium salt and 100 mg/l Streptomycin sulfate (all Biowest)), human blood (diluted 1:1 with culture medium) or a suspension of $5x10^6$ cells/ml U937 in culture medium were incubated at 37 °C, 450 rpm on a shaking incubator. At the indicated time points 50 µL of blood, cell suspension or medium were collected and prepared for HPLC-MS/MS-Analysis as detailed below.

3.3 HPLC-MS/MS

All samples were extracted with 3 or 6 volumes acetonitrile containing terbuthylazine as an internal standard (ACN) relative to either sample weight or volume. Liquid samples (plasma, culture medium, cell suspensions in stability experiments) were diluted in either 3 (culture medium, cell suspensions) or 6 (plasma) volumes ACN, pellet and blood samples were extracted by addition of ACN followed by sonication for 5 min. Organ samples were digested with 0.5 µg/mg Proteinase K (Genaxxon) for 1 h at 50 °C before being homogenized using a Fastprep FP-24 5G instrument (MP-Biomedicals). Homogenates were diluted with 6 volumes ACN and homogenized again. All extracts were cleared by centrifugation at ~20.000xg for 10 min at 4°C.

Quantification of analytes was performed on an Agilent 1260/1290 Infinity system fitted with an Agilent C18 Poroshell 120 column (4.6 x 50 mm, 2.7 µm) coupled to a triple quadrupole Sciex API 4000 MS/MS detector. The mobile phase was composed of water containing 0.1 % formic acid (eluent A) and acetonitrile containing 0.1 % formic acid (eluent B). Gradient used was: 5 % B for 0.5

min, to 100 % B in 4.5 min, 100 % B for 2 min, to 5 % B in 0.5 min, 5 % for 2.5 min. MS detection parameters are listed in SI Table S1.

3.4 TLR7/8 SEAP reporter Assay (HEK blue)

HEK blue hTLR7 or hTLR8 reporter cells (Invivogen) were cultivated in DMEM High Glucose (Biowest) according to the manufacturer's instructions. Cells were treated with test compounds and controls at various concentrations in serum-free DMEM and incubated at 37°C, 5% CO_2 for 24 h before supernatants were collected.

Relative secreted embryonic alkaline phosphatase (SEAP) activity in the supernatants was determined by quantification of para-Nitrophenyl Phosphate (pNPP)-turnover. Supernatants were diluted 10-fold in a solution containing 1 mM $MgCl_2$, 1 M diethanolamine and 1 mg/mL pNPP and incubated at RT for 15 min before the reaction was stopped by the addition of 0.25 volumes of 1 M NaOH. Absorbance was measured at 405 nm on a Versamax microplate reader (Molecular Devices) and normalized to the mean of >5 solvent controls.

3.5 Viability assay and live-dead staining (MTT and Dye Exclusion)

3-(4,5-dimethylthiazol-2-yl)-2,5-diphenyltetrazolium bromide (MTT) turnover was used to identify potential compound effects on cell metabolism and indirectly assay changes in cell number or viability. HEK Blue reporter cells were cultured and exposed to compounds as described above and 20 µl supernatant were collected for SEAP activity assays. U937 monocyte-like cells were cultured in RPMI-1640 containing 10 % FBS, differentiated by addition of 100 nM PMA for 2 days and exposed to compounds at varying concentrations or solvent for 2 days. MTT dissolved in PBS was added to the cells to a final concentration of 1 mg/ml. Cells were then incubated at culture conditions for 1 h. Supernatants were removed after centrifugation at 400xg for 5 min and the formed formazan dye was dissolved in DMSO. Absorbance was measured at 570 nm and readings were normalized to solvent treated controls.

Exclusion of Helix NIR (BioLegend) was used to assay membrane integrity following compound treatment. Culture conditions for U937 were as described above, undifferentiated cells were incubated with varying concentrations of compound or with solvent. Helix NIR was added to the cells to a final concentration of 10 nM, cells were incubated at RT for 10 min and acquired on a ZE5 Cell Analyzer (Bio-Rad). The cutoff for positive staining was set to approximately the 99^{th} percentile of unstained cells.

3.6 Full blood stimulation Assay

Human peripheral blood of healthy donors was diluted in an equal volume of culture medium as described in 3.2, blood was treated with test compounds or controls at various concentrations and incubated at 37°C, 5% CO_2 for 6 h. Cells were pelleted by centrifugation at 400xg for 5 min and supernatants were collected.

3.7 Quantification of cytokines by ELISA or cytometric bead array

Cytokine concentrations in samples were quantified either by ELISA (hTNFα, R&D Systems; hIFNα, Mabtech) or cytometric bead arrays (CBA, LegendPlex mouse anti-virus response panel, BioLegend) according to the manufacturer's instructions. CBAs were acquired on a ZE5 Cell Analyzer (Bio-Rad) and analyzed using the LegendPlex Software Suite (Qognit/BioLegend).

Absorbance of ELISA-samples was quantified using a Versamax microplate reader (Molecular Devices).

3.8 Experimental animals, sampling and compound formulation

Experimental Animals. All animal experiments were carried out in accordance with German law (application 35/9185.81-7). Mice, 8-18 weeks old, were purchased from Janvier Laboratories and maintained in a specific-pathogen-free animal facility with chow and water *ad libitum*. After arrival mice acclimated for a minimum of 7 days.
Formulation. Test compounds were prepared for application in either 1 % Tween 80, 9 % PEG400 in ultrapure water (Biowest) (Figure 3) or 5 mM citric acid in 0.9 % saline (Braun) (Figure 4, 5 and 6). If compounds were administered subcutaneously, injections were carried out into the neck crease.
Collection of Samples. Mice were bled from the tail vein at various timepoints. Heparin (Sigma) or K_2-EDTA (Sigma) was added to blood samples to a final coagulant concentration of 10-15 Unit or 5 mM. Plasma was generated by centrifugation at 6800xg for 8 min at 4 °C and stored at -80 °C until analyzed by ELISA or CBA. Animals were sacrificed after the indicated time points by CO_2 inhalation. Heart blood and organs for compound quantification by HPLC-MS/MS were collected post mortem and stored at –20 °C until extracted as described above.

4 Results

Activity of the new compounds (Figure 1) on TLR7/8 was confirmed using the commercially available HEK Blue reporter system. Corresponding to the dual specificity of structurally similar compounds described by others (1)(2), HEK-Blue hTLR-7 and hTLR-8 were used to assess relative potency on each receptor relative to Resiquimod (RSQ) as a reference compound. Results of the initial screening are in Table 1 and Figure 2A. While all structural variants retained TLR-7-agonism, activation of hTLR-8 was reduced for compounds linked to a macrolide, carrying a protective group or a longer spacer between the aromatic polycycle and the piperidine as in A1. Maximal induction of SEAP varied between compounds and was generally highest for RSQ in repeated experiments, while other compounds either reached a lower maximum and subsequent decrease in signal at lower concentrations or became insoluble under the conditions used for the assay before reaching a plateau. Average maximal activity in HEK-Blue hTLR-7 relative to RSQ was 58% for A1, 55% for A1-boc and 41 % for A1-mac. The methyl-piperidine variants reached a higher maximal induction (A2-boc 86%, A2 81%, A2-mac 63%). SEAP secretion from HEK Blue hTLR-8 was close to baseline for A1 as well as the protected or macrolide-bound variants A1-boc, A1-mac, A2-boc and A2-mac, with the former two showing low induction at very high concentrations without reaching a plateau at sub-toxic concentrations. A2 (57%), A3 (36%) and A4 (18%) retained activity, although at a lower maximal induction than that of RSQ.

The compound specific EC50 for the HEK Blue system is listed in Table 1. To obtain reliable estimates, replicate measurements of a minimum of 2 experiments were normalized to the maximal SEAP activity of a compound in a given experiment and pooled before fitting a non-linear function to the data. For all compounds, we observed a reduction in SEAP activity in the supernatants above certain compound concentrations. Data points above those concentrations were excluded before curve fitting (Figures 2B, S3, S4).

The decrease in signal was assumed to be caused by toxic effects above certain concentrations, as indicated by a change in cell morphology and reduced attachment to the plate surface. Sensitivity of the reporter cells to toxic effects seemed to be closely related to serum concentrations during the assay and was less apparent if higher serum concentrations were used (Figure S5A). To confirm this,

we performed an MTT assay on the HEK cells after collection of the supernatants for SEAP quantification (Figure 1 C upper two panels). While there was some reduction in MTT conversion at concentrations similar to those for which we observed a decrease in SEAP secretion, obvious toxicity could only be observed at 20 μM and is likely to be related to poor solubility and crystalizing of the compounds at those concentrations. Further, a reduction in MTT conversion could be observed in U937 cells and was again most apparent for the poorly soluble A1-boc, with 50% dye formation relative to solvent controls at the highest concentration of 25 μM. Imiquimod and A1 reduced signal to <90% at concentrations ≥6.25 μM. In contrast, a dye exclusion assay in U937 cells could only confirm negative effects on membrane integrity for cells treated with 25 μM A1-boc, pointing to additional compound effects on metabolism and proliferation of the cells as opposed to cell death.

A1 and A1-mac were selected for further studies based on their similar specificity and activity. Blood from 8 human donors was stimulated at varying concentrations of either test compounds or reference for 6 hours. Secretion of key cytokines was quantified by ELISA. IFNα and TNFα were selected as indicators for either NfκB- or IRF3/7-mediated signaling following stimulation. Maximal supernatant concentrations of both cytokines varied considerably between donors (Figure 2E, Figure S5B). When normalized to the maximal observed concentration for a given donor, relative IFNα induction was robust and similar for both A1 and A1-mac as well as the reference, while the highest TNFα concentrations were almost exclusively measured in supernatants of RSQ-treated samples (Figure 2D). This is consistent with the reduced affinity to TLR8 apparent in the reporter assay (Figure 2A). IFNα response for a given concentration was comparable for all compounds, in contrast to the lower activity of A1/A1-mac in the HEK-blue system. However, overexpression of a given TLR and signal transduction exclusively *via* NfκB instead of IRF3/7 make the HEK system useful to estimate affinity to a given receptor but might not reflect a more complex system with multiple adapter molecules involved in a primary immune cell.

One of the issues we addressed by coupling a TLR-activating structure to a macrolide was poor bioavailability of available TLR-agonists and the resulting limitations in possible routes for systemic treatment. We confirmed the stability of our macrolide conjugates in biological systems *in vitro*. In whole blood and cell based (U937) assays, compounds A1-mac and A2-mac were stable (Figure 3A) over 24 h. We next sought to investigate whether stable coupling to a carrier known for good tissue penetration and -distribution would translate to more favorable pharmacokinetics *in vivo*. To this end we compared bioavailability following intravenous (i.v.), oral (p.o.) or intraperitoneal (i.p.) application with cassettes containing A1-mac, A2-mac and RSQ. Blood samples taken from the tail vein at various times and organ samples collected terminally were then analyzed for compound concentrations by HPLC-MS/MS. Doses of compounds were selected based on known tolerance of TLR agonists per route and restricted by detection limits of analytical methods (i.v. 0.5 mg/kg; i.p. 2 mg/kg; p.o. 2 mg/kg). As expected, i.v. application (i.v. 0.5 mg/kg) showed highest blood concentrations for all substances (c_{max}: RSQ 854 nM; A1-mac 392 nM; A2-mac 352 nM 15 min after application) but also showed fast elimination (baseline level after 120 min) (Figure 3B) and low tissue distribution (Figure 3C). Surprisingly, the oral availability of macrolide bound TLR agonists was lower than expected and on the same level as RSQ (c_{max} RSQ 41 nM; A1-mac 28 nM, A2-mac 22 nM 15 min after application). This observation was unexpected, as macrolide-based substances usually possess good oral availability. This is generally accompanied by good systemic distribution and accumulation in tissues (55)(56)(60) and the relatively low plasma concentrations in this case may also reflect retention in the gut epithelium, which has been observed for other similar conjugates. In contrast, i.p. administration showed a distribution more similar to other macrolide-conjugates described previously by us (55). Like i.v. treatment, i.p. (2 mg/kg), had rapid partition to blood (c_{max} RSQ 123 nM; A1-mac 299 nM; A2-mac 138 nM 15 min after application) and high

concentrations of compounds A1-mac and A2-mac in tissue with high levels in the liver (RSQ < LOD; A1-mac 3390 nM; A2-mac 2522 nM) and kidney (RSQ < LOD; A1-mac 586 nM; A2-mac 449 nM). Given the low levels following oral application and the risk that it may stimulate the gut excessively, the oral route was not used in subsequent *in vivo* studies.

We then compared the activity of A1 and A1-mac *in vivo*. Since receptor engagement and activities *in vitro* were very similar for A1 and A1-mac, we hoped to be able to identify changes in activity directly related to the macrolide carrier. Compounds were applied subcutaneously at 3, 6 or 12 µmol/kg. Plasma samples taken at various times before and after treatment were analyzed for cytokine concentrations. Organs, terminal heart blood and peripheral blood 1 h post-treatment were analyzed by HPLC-MS/MS. As in the last study (Figure 3B+C), high concentrations of A1-mac were found in liver (5099 nM for 12 µmol/kg) and kidney (5481 nM for 12 µmol/kg) 8 h after treatment (Figure 4A). This was not found for RSQ (33 nM in liver and 51 nM in kidney for 12 µmol/kg) and A1 (173 nM in liver and 636 nM in kidney for 12 µmol/kg). Levels of A1 were dose dependent for all organs, with lung (868 nM for 12 µmol/kg) and tail blood high after 1 h (1557 nM for 12 µmol/kg). Concentrations measured for RSQ were generally lower with spleen being (202 nM for 6 µmol/kg and 158 nM for 12 µmol/kg) the highest of the organs analyzed.

These pharmacokinetic data confirm the known effects of macrolides on half-life and volume of distribution, are in line with our previous study (Figure 3) and show that s.c. is a suitable application route. For A1, the higher concentrations across all tissues point to better overall penetration and stability when compared to RSQ, further supported by higher concentrations of A1 in peripheral blood 1 h post application (A1: 1557 nM, A1-mac: 696 nM, RSQ: 175 nM, for 12 µmol/kg). Whole blood was analyzed in these studies to take account of material portioned to cells.

Similar to the blood stimulation assays described earlier (Figure 2D), the induction of pro-inflammatory cytokines and IFNα was clearly different between groups receiving RSQ and either A1 or A1-mac (Figure 4B). While RSQ treatment resulted in a sharp increase in TNFα and IFNα plasma levels, peaking 90 min post treatment and falling close to baseline after 240 min, release kinetics were generally slower in the groups receiving A1 or A1-mac. Mice treated with A1-mac had a lower TNFα peak at 90 min while in A1-treated mice it was at 120 min. IFNα levels stayed elevated over the 8 h period of the study in A1 and A1-mac treated groups.

Most striking was that in RSQ-treated groups, the peak TNFα concentrations were over 10 times higher than in A1 or A1-mac groups. The area under the curve calculated from the TNFα plasma values of mice receiving the lowest dose of 3 µmol/kg RSQ was about 4 times larger than the area calculated for any A1 or A1-mac treated group. In contrast to this, the AUCs for IFNα were similar between groups (Table 2 top section).

While we anticipated different release kinetics based on the differences in pharmacokinetics described earlier, the different cytokine release patterns were unexpected. Preference for TLR7 over TLR8 should not have an impact in murine systems (in which activity of RSQ is thought to be dependent on TLR7 under normal circumstances (61)(62)) and the release of TNFα as well as IFNα and other cytokines (Figure S6) were highest in the RSQ group receiving the lowest dose. We suspected this to be due to a saturation effect and possibly overshooting feedback mechanisms. The idea of negative feedback potentially decreasing the secretion of Type I IFN in RSQ treated animals after a short burst is supported by the higher IL10 levels observed only in those animals (Figure S6 bottom panels). In this case, differences in cytokine secretion could be explained simply by the higher potency of RSQ compared to A1/A1-mac. To rule out differences in potency as the reason for

the varying cytokine profiles, we reduced RSQ doses to 0.1, 0.3, 1 and 3 µmol/kg and added 1 µmol/kg as an additional dose for A1 and A1-mac in a follow-up study. The doses were chosen so the lowest dose for a given compound would be at the threshold of detectable activity while reflecting the differences in maximal TLR7-activation we originally observed in the HEK reporter assay. When comparing the AUC in this study, we found a dose ratio of roughly 6-10 times the molar dose of RSQ leading to comparable amounts of IFNα in A1 and A1-mac treated groups, while 30-40 times the molar dose were necessary to induce similar levels of TNFα. More specifically, we could not find a dose for which RSQ would induce similarly high levels of type I Interferon without also leading to much higher release of TNFα than A1 and A1-mac (Figure 5C, Table 2 bottom section).

We conclude from this that the specific induction of high levels of Type I IFN is a characteristic feature of A1 and A1-mac and cannot be reproduced by any dose of RSQ. These characteristics might be related to the different stability and pharmacokinetic profile when compared to RSQ, to varying receptor specificity or to differences in subcellular partitioning of the compounds.

Distribution of compounds to different organs was similar in pattern but varied in concentration when compared to the previous study (Figures 5B and 4A). Taking the different dose ranges into account, A1 and A1-mac reach higher concentrations in tissues than RSQ 8 h post compound application (in kidney at 3 µmol/kg RSQ: 10 nM A1: 469 nM A1-mac 2176 nM and in liver RSQ: <LLOQ A1: 45 nM A1-mac 6030 nM). Compound levels in peripheral plasma over time were analyzed in this study. We found that not only the macrolide conjugate but also the free agonist A1 was detectable in plasma over a longer period of time when compared to RSQ. This may, in part, be due to higher stability as well as retention at and slower release from the injection site for A1 and A1-mac (Figure 5B, narrow panels).

Since we could not attribute our observations to dose alone and there are specific cases in which murine TLR8 is reported to be activated (63), we added Imiquimod as the prototypical TLR7-agonist to act as an additional reference in our next study. Imiquimod itself is not solely reliant on TLR7 signaling to trigger its pro-inflammatory effects, being also an inhibitor of adenosine receptors (64). However, it is inactive on TLR8 and more similar to A1 and A1-mac in that regard. To account for the lower potency of Imiquimod when compared to the other compounds, we used a dose corresponding to the ~10-fold difference in potency relative to A1-mac indicated by the reporter assay detailed earlier. We further chose doses for A1, A1-mac and RSQ based on those which resulted in similar IFNα-AUC in the previous study and modified the protocol to include three consecutive daily treatments to assess the effect of repeated applications on pharmacokinetics (induced metabolism, accumulation) and cytokine induction.

Organ concentrations (Figure S7; collected after 4, 28 and 52 h) were similar to previous studies, with highest concentrations in liver (RSQ: <LLOQ IMQ: 630 nM A1: 63 nM A1-mac: 2617 nM after 4 h; RSQ: <LLOQ IMQ: 824 nM A1: 82 nM A1-mac: 4461 nM after 28 h; RSQ: <LLOQ IMQ: 645 nM A1: 94 nM A1-mac: 6352 nM after 52 h). Interestingly, measured brain tissues showed baseline or close to baseline levels for RSQ (most likely at least partly due to the comparatively low dose), A1 and A1-mac, whilst IMQ was detected with increasing concentrations over the course of the study (32 nM after 4 h; 135 nM after 28 h, 177 nM after 52 h), in line with earlier publications and our observations connecting IMQ brain concentrations with systemic inflammatory responses (65)(66). While there were some minor deviations in compound plasma levels between the first and consecutive treatments (all peaked 60 min after each application; day 1: RSQ <LLOQ IMQ 796 nM, A1 171 nM, A1-mac 755 nM; day 2: RSQ <LLOQ, IMQ 606 nM, A1 85 nM, A1-mac 585 nM; day 3: RSQ <LLOQ, IMQ 608 nM, A1 66 nM, A1-mac 639 nM), the most prominent effect of repeated doses is a decline in Interferon-secretion after the first treatment. Secretion of TNFα was fairly

similar after each of the repeated treatments and remained low for all treatments with A1 and A1-mac in comparison with IMQ and RSQ (Figure 6C shows days 1 and 2). IFNα induction was reduced after the second treatment for all compounds and plasma levels on the third day generally remained below the limit of detection. The decrease in INFα levels on the second day was more pronounced for A1 and A1-mac, both being at the limit of detection for type I Interferon concentrations in plasma after the second treatment.

The induction of IFNα and TNFα after treatment with RSQ or IMQ were very similar in their kinetics as well as the ratio of both cytokines. A1- and A1-mac-treated animals showed a delayed and more sustained induction of IFNα and little TNFα in peripheral plasma after the first treatment, as in previous studies.

5. Conclusion

The similarities between IMQ and RSQ in cytokine induction make differences in receptor specificity an unlikely explanation for the divergent cytokine profile induced by A1/A1-mac. We hypothesize that these observations are due to either PK and specifically release kinetics from the injection site or possibly partitioning to specific cellular compartments. The differences in PK are clear from the data reported here.

Additionally, we consider the option that subcellular location may be relevant in "polarizing" TLR7-mediated signaling based on: firstly, the observations made by others demonstrating the outcome of TLR9 activation is dependent on the cellular compartment in which activation occurs (28)(29)(30)(31); and, secondly, the considerable overlap between adapter molecules employed by TLR7 and 9 to either activate NfκB or cause phosphorylation of IRF7, particularly TRAF6 or TRAF3. Thirdly, our own observations that a structurally similar fluorescent tool compound consisting of a macrolide core conjugated to a coumarin dye accumulated in endosomal compartments (Laux *et al.*, in review) which could be organelles relevant to IRF7 activation. In conclusion, we consider the possibility that preferential uptake of our compounds in those organelles causes their characteristic cytokine induction, although preferential partitioning to specific endosomes needs to be explicitly demonstrated.

Irrespective of the exact mechanism causing them, these data suggest that the compounds have profound and distinct properties and biological activities relative to well-known compounds like RSQ and IMQ. The new class differs from previous compounds in stability, distribution, spectrum and duration of action. The conserved activity of the macrolide conjugate A1-mac indicates that the compounds tolerate large bulky substituents at the linkage position and are also suitable for linkage to other macromolecules This makes them potentially useful reagents for addition of immune stimulatory properties to other compounds and agents such as polymers, proteins and antibodies.

The absence of a strong TNFα signal could increase the tolerability of the compounds in clinical use. It remains to be seen whether this is advantageous for applications in oncology. However, a variety of tumors appear to benefit from high TNFα levels and this aspect may require more nuanced investigation.

This cytokine profile with its emphasis on IFNα may potentially suit applications in treatment of viral infections. The potency and specificity of the compounds as well as their induction of patient-specific quantities of type I IFN could make them suitable as an alternative to treatment with a fixed dose of

recombinant IFNα. Nevertheless, the loss of the IFNα response on successive application may indicate a risk of receptor saturation and immune exhaustion. The impact of time between treatments on this effect has been demonstrated for RSQ in the past (67) and careful attention is required to define a suitable dosing interval before application in a clinical setting.

Table 1: EC_{50} values for compounds in HEK-blue human TLR7 and human TLR8 receptor assay (expressed as 95% CI, ND noted for no calculation of curve fit possible (adj. $r^2 < 0.8$)) and average maximal SEAP secretion observed for a given compound relative to the maximum secretion observed in the assay.

Compound	TLR7 EC_{50} [µM]	TLR7 activity rel. to assay max	TLR8 EC_{50} [µM]	TLR8 activity rel. to assay max
RSQ	0.47 to 0.77	95%	2.9 to 3.6	96%
IMQ	5.2 to 8.3	35%	ND	3%
A1-boc	0.39 to 0.69	55%	ND	4%
A1	0.096 to 0.22	58%	ND	11%
A1-mac	0.40 to 0.74	41%	ND	5%
A2-boc	0.23 to 0.47	86%	ND	4%
A2	0.075 to 0.12	81%	2.8 to 3.1	57%
A2-mac	1.5 to 2.0	63%	ND	4%
A3	1.0 to 1.5	62%	8.2 to 8.5	36%
A4	1.5 to 2.1	84%	11 to 13	18%

Table 2: AUC of TNFα and IFNα measured in peripheral plasma over an 8 h period after application of equimolar doses (top section) or doses adjusted to the activity of the compounds (bottom section) in female C57BL/6. Plasma of 3 individual animals per group was pooled and analyzed *via* CBA.

	TNFα AUC [pg/ml*min]						IFNα AUC [pg/ml*min]					
	0.1	0.3	1	3	6	12	0.1	0.3	1	3	6	12

A1				6,50E +03	1,66E +04	3,49E +04				6,61E +05	1,27E +06	2,51E +06
A1 - mac				6,92E +03	2,38E +04	7,56E +04				4,15E +05	9,24E +05	3,11E +06
RSQ				3,29E +05	2,82E +05	2,63E +05				2,15E +06	7,83E +05	7,95E +05
A1			9,68E +03	1,12E +04	1,95E +04	4,38E +04			6,98E +04	4,92E +05	1,14E +06	1,93E +06
A1 - mac			7,17E +03	1,36E +04	3,79E +04	6,54E +04			3,25E +04	3,02E +05	1,59E +06	1,94E +06
RSQ	1,71E +04	5,02E +04	1,18E +05	1,52E +05			1,08E +05	5,56E +05	1,10E +06	9,72E +05		

5 Conflict of Interest

All authors except SL are employees of Synovo GmbH, the company developing the compounds described here. MK, SS, JHG, MB are named as inventors in the corresponding patent.

6 Author Contributions

SS, JHG were involved in compound synthesis and characterization. SG, NS, TF, SS, MK designed and carried out *in vitro* experiments and processed samples from *in vivo* studies. SG, TW, MB, MK designed and carried out *in vivo* experiments. AS, JG, SS, MK processed samples for and data from HPLC-MS/MS measurements. MK, SS, SG, MB wrote the manuscript. All authors proof-read the manuscript. MB, SL supervised the project and provided funding.

7 Funding

This research received no external funding.

8 Acknowledgments

We would like to thank colleagues from Synovo GmbH and the University of Tübingen who assisted in this research. Special thanks to the members of the *in vivo* facility and the team of the analytics/bioanalytics department at both institutions.

9 Supplementary Material

Supplementary Material will be uploaded separately.

10 Figure Captions

FIGURE 1 | Compound structures.

FIGURE 2 | *In vitro* characterization of candidate molecules **(A)** SEAP activity in supernatants of HEK Blue reporter cells after 24 h stimulation with varying concentrations of test compounds relative to solvent controls. **(B)** Dose response of A1 and A1-mac in HEK Blue hTLR7. Circles represent normalized replicate measurements pooled from 3 experiments. Lines represent non-linear functions fit to the data to calculate compound-specific EC50; values in grey have been excluded before fitting. **(C)** Percent MTT conversion of compound-treated HEK-Blue reporter cells (top panels) or PMA-differentiated U937 relative to solvent controls OR percent of undifferentiated U937 excluding Helix NIR dye. **(D)** TNFα/IFNα in supernatants of human blood stimulated with A1, A1-mac or RSQ for 6 h, n=8, concentrations normalized to the maximum concentration of each cytokine for a given donor, data presented as mean ± 95% CI. **(E)** TNFα/IFNα in supernatant for two individual donors.

FIGURE 3 | Stability and bioavailability of macrolide conjugates**. (A)** Stability of A1-mac and A2-mac was measured in human blood, U937 monocytes and RPMI medium over 24 h. **(B, C)** Concentration of RSQ, A1-mac and A2-mac in peripheral blood and organs was assessed *via* HLPC-MS after i.v., i.p. and p.o. compound administration in 10-week-old, female C57BL/6 mice (n=3 mice per group). Compounds were administered in cassettes (i.v. application: 1.6 µmol/kg RSQ, 0.4 µmol/kg A1-mac, 0.4 µmol/kg A2-mac; i.p. application: 3.2 µmol/kg RSQ, 1.7 µmol/kg A1-mac, 1.7 µmol/kg A2-mac, p.o. application: 3.2 µmol/kg RSQ, 3.3 µmol/kg A1-mac, 3.3 µmol/kg A2-mac). **(B)** Peripheral blood was collected 15, 30 60, 120, 180, 240, 360 and 1440 min after compound administration. **(C)** Organs were sampled 1440 min after compound administration. **(A, B, C)** Data are presented as mean ±SD.

FIGURE 4 | Concentration of RSQ, A1 and A1-mac in organs and cytokine profile in peripheral plasma over time after 3, 6 and 12 µmol/kg s.c. compound administration in 8-week-old, female C57BL/6 mice (n=3 mice per group). **(A)** Organs were sampled 8 h after treatment and compound concentration was determined *via* HPLC-MS/MS. Data are presented as mean ± SD. **(B)** Cytokine levels in tail plasma over time were determined *via* cytometric bead array. At each sampling timepoint the plasma of mice in one treatment group was pooled.

FIGURE 5 | Pharmacokinetics and induction of TNFα, IFNα by A1 and A1-mac and RSQ. **(A, B, C)** Female, 18-week-old, C57BL/6 mice were treated s.c. with 1, 3 6 or 12 µmol/kg RSQ, A1 or A1-mac (n=3 mice per group). Compound concentration in **(A)** peripheral blood collected *via* tail bleeding before, 15, 30 60, 120, 240, 360 and 480 min after s.c. compound application and **(B)** organs collected after 8 h was assessed *via* HPLC-MS/MS. **(A, B)** Data are presented as mean ± SD. **(C)** Levels of TNFα and IFNα in tail plasma over time was determined *via* cytometric bead array. Area under the curve (AUC) of each cytokine was plotted against compound concentration. Data are represented as mean ± 95 % confidence interval.

FIGURE 6 | Effect of repeated applications of A1, A1-mac, RSQ and IMQ. Dotted lines indicate the time of repeated compound applications. **(A)** Cytokine levels in pooled tail plasma of mice from individual treatment groups (n=3 per pool and time point), error bars represent range of two replicate measurements. **(B)** Peripheral blood was collected from the tail vein before, 15, 30 60, 120, 240, 360 and 480 min after s.c. treatment. Compound concentration in peripheral plasma was analyzed by HPLC-MS/MS, data presented as mean ± SD. **(C)** AUC of TNFα/IFNα in peripheral plasma calculated from the data in (A) for days 1 and 2 of treatment, data represent calculated AUC ± 95% CI.

11 References

1. Waldman AD, Fritz JM, Lenardo MJ. A guide to cancer immunotherapy: from T cell basic science to clinical practice. Nat Rev Immunol 2020 2011 [Internet]. 2020 May 20 [cited 2022 Dec 17];20(11):651–68. Available from: https://www.nature.com/articles/s41577-020-0306-5

2. Immunotherapies for autoimmune diseases. Nat Biomed Eng 2019 34 [Internet]. 2019 Apr 5 [cited 2022 Dec 3];3(4):247–247. Available from: https://www.nature.com/articles/s41551-019-0394-3

3. Kaufmann SHE, Dorhoi A, Hotchkiss RS, Bartenschlager R. Host-directed therapies for bacterial and viral infections. Nat Rev Drug Discov 2017 171 [Internet]. 2017 Sep 22 [cited 2022 Dec 17];17(1):35–56. Available from: https://www.nature.com/articles/nrd.2017.162

4. Wallis RS, O'Garra A, Sher A, Wack A. Host-directed immunotherapy of viral and bacterial infections: past, present and future. Nat Rev Immunol 2022 [Internet]. 2022 Jun 7 [cited 2022 Dec 17];1–13. Available from: https://www.nature.com/articles/s41577-022-00734-z

5. Wykes MN, Lewin SR. Immune checkpoint blockade in infectious diseases. Nat Rev Immunol 2017 182 [Internet]. 2017 Oct 9 [cited 2022 Dec 17];18(2):91–104. Available from: https://www.nature.com/articles/nri.2017.112

6. McCulloch TR, Wells TJ, Souza-Fonseca-Guimaraes F. Towards efficient immunotherapy for bacterial infection. Trends Microbiol. 2022 Feb 1;30(2):158–69.

7. Aricò E, Castiello L, Capone I, Gabriele L, Belardelli F. Type I Interferons and Cancer: An Evolving Story Demanding Novel Clinical Applications. Cancers (Basel) [Internet]. 2019 Dec 1 [cited 2022 Dec 17];11(12). Available from: /pmc/articles/PMC6966569/

8. Borden EC. Interferons α and β in cancer: therapeutic opportunities from new insights. Nat Rev Drug Discov [Internet]. 2019 Mar 1 [cited 2022 Dec 17];18(3):219–34. Available from: https://pubmed.ncbi.nlm.nih.gov/30679806/

9. Heim MH. 25 years of interferon-based treatment of chronic hepatitis C: an epoch coming to an end. Nat Rev Immunol 2013 137 [Internet]. 2013 Jun 7 [cited 2022 Dec 5];13(7):535–42. Available from: https://www.nature.com/articles/nri3463

10. Twomey JD, Zhang B. Cancer Immunotherapy Update: FDA-Approved Checkpoint Inhibitors and Companion Diagnostics. AAPS J [Internet]. 2021 Mar 1 [cited 2022 Dec 17];23(2):1–11. Available from: https://link.springer.com/article/10.1208/s12248-021-00574-0

11. Fitzgerald KA, Kagan JC. Toll-like Receptors and the Control of Immunity. Cell. 2020 Mar 19;180(6):1044–66.

12. Chi H, Li C, Zhao FS, Zhang L, Ng TB, Jin G, et al. Anti-tumor Activity of Toll-Like Receptor 7 Agonists. 2017;8(May):1–10.

13. Pradere JP, Dapito DH, Schwabe RF. The Yin and Yang of Toll-like receptors in cancer. Vol. 33, Oncogene. Nature Publishing Group; 2014. p. 3485–95.

14. Kawai T, Akira S. TLR signaling. Semin Immunol. 2007 Feb 1;19(1):24–32.

15. Stanley MA. Imiquimod and the imidazoquinolones: Mechanism of action and therapeutic potential. Clin Exp Dermatol. 2002;27(7):571–7.

16. Chen X, Zhang Y, Fu Y. The critical role of Toll-like receptor-mediated signaling in cancer immunotherapy. Med Drug Discov. 2022 Jun 1;14:100122.

17. Kaczanowska S, Joseph AM, Davila E. TLR agonists: our best frenemy in cancer immunotherapy. J Leukoc Biol [Internet]. 2013 Jun 1 [cited 2022 Dec 17];93(6):847–63. Available from: https://onlinelibrary.wiley.com/doi/full/10.1189/jlb.1012501

18. Botos I, Segal DM, Davies DR. The Structural Biology of Toll-like Receptors. Structure. 2011 Apr 13;19(4):447–59.

19. Kawasaki T, Kawai T. Toll-like receptor signaling pathways. Front Immunol. 2014 Sep 25;5(SEP):461.

20. Schoenemeyer A, Barnes BJ, Mancl ME, Latz E, Goutagny N, Pitha PM, et al. The interferon regulatory factor, IRF5, is a central mediator of toll-like receptor 7 signaling. J Biol Chem [Internet]. 2005 Apr 29 [cited 2022 Nov 14];280(17):17005–12. Available from: https://www.researchgate.net/publication/8036509_The_Interferon_Regulatory_Factor_IRF5_Is_a_Central_Mediator_of_Toll-like_Receptor_7_Signaling

21. Jefferies CA. Regulating IRFs in IFN driven disease. Front Immunol. 2019 Mar 29;10(MAR):325.

22. Gilliet M, Cao W, Liu YJ. Plasmacytoid dendritic cells: sensing nucleic acids in viral infection and autoimmune diseases. Nat Rev Immunol 2008 88 [Internet]. 2008 Aug [cited 2022 Dec 6];8(8):594–606. Available from: https://www.nature.com/articles/nri2358

23. Poropatich K, Dominguez D, Chan WC, Andrade J, Zha Y, Wray B, et al. OX40+ plasmacytoid dendritic cells in the tumor microenvironment promote antitumor immunity. J Clin Invest [Internet]. 2020 Jul 1 [cited 2022 Dec 17];130(7):3528–42. Available from: https://doi.org/10.1172/JCI131992DS1

24. Zhou B, Lawrence T, Liang Y. The Role of Plasmacytoid Dendritic Cells in Cancers. Front Immunol. 2021 Oct 19;12:4414.

25. Cervantes JL, Weinerman B, Basole C, Salazar JC. TLR8: the forgotten relative revindicated. Cell Mol Immunol 2012 96 [Internet]. 2012 Oct 22 [cited 2022 Dec 17];9(6):434–8. Available

from: https://www.nature.com/articles/cmi201238

26. Gorden KB, Gorski KS, Gibson SJ, Kedl RM, Kieper WC, Qiu X, et al. Synthetic TLR agonists reveal functional differences between human TLR7 and TLR8. J Immunol [Internet]. 2005;174(3):1259–68. Available from: http://www.ncbi.nlm.nih.gov/pubmed/15661881

27. Marcken M de, Dhaliwal K, Danielsen AC, Gautron AS, Dominguez-Villar M. TLR7 and TLR8 activate distinct pathways in monocytes during RNA virus infection. Sci Signal. 2019;12(605):1–19.

28. Guiducci C, Ott G, Chan JH, Damon E, Calacsan C, Matray T, et al. Properties regulating the nature of the plasmacytoid dendritic cell response to Toll-like receptor 9 activation. J Exp Med [Internet]. 2006 Aug 7 [cited 2019 Dec 5];203(8):1999–2008. Available from: http://www.jem.org/lookup/doi/10.1084/jem.20060401

29. Haas T, Schmitz F, Heit A, Wagner H. Sequence independent interferon-α induction by multimerized phosphodiester DNA depends on spatial regulation of Toll-like receptor-9 activation in plasmacytoid dendritic cells. Immunology [Internet]. 2009 Feb [cited 2022 Feb 1];126(2):290. Available from: /pmc/articles/PMC2632690/

30. Honda K, Ohba Y, Yanai H, Hegishi H, Mizutani T, Takaoka A, et al. Spatiotemporal regulation of MyD88-IRF-7 signalling for robust type-I interferon induction. Nature. 2005;434(7036):1035–40.

31. Sasai M, Linehan MM, Iwasaki A. Bifurcation of toll-like receptor 9 signaling by adaptor protein 3. Science (80-) [Internet]. 2010 Sep 17 [cited 2021 Apr 19];329(5998):1530–4. Available from: /pmc/articles/PMC3063333/

32. Oganesyan G, Saha SK, Guo B, He JQ, Shahangian A, Zarnegar B, et al. Critical role of TRAF3 in the Toll-like receptor-dependent and -independent antiviral response. Nat 2005 4397073 [Internet]. 2005 Nov 23 [cited 2022 Dec 17];439(7073):208–11. Available from: https://www.nature.com/articles/nature04374

33. Häcker H, Redecke V, Blagoev B, Kratchmarova I, Hsu LC, Wang GG, et al. Specificity in Toll-like receptor signalling through distinct effector functions of TRAF3 and TRAF6. Nat 2005 4397073 [Internet]. 2005 Nov 23 [cited 2022 Dec 17];439(7073):204–7. Available from: https://www.nature.com/articles/nature04369

34. Hoshino K, Sugiyama T, Matsumoto M, Tanaka T, Saito M, Hemmi H, et al. IκB kinase-α is critical for interferon-α production induced by Toll-like receptors 7 and 9. Nat 2006 4407086 [Internet]. 2006 Apr 13 [cited 2022 Dec 17];440(7086):949–53. Available from: https://www.nature.com/articles/nature04641

35. Coroadinha S, Brown RJP, Weber L, Vieyres G. The Railmap of Type I Interferon Induction: Subcellular Network Plan and How Viruses Can Change Tracks. Cells 2022, Vol 11, Page 3149 [Internet]. 2022 Oct 6 [cited 2022 Dec 6];11(19):3149. Available from: https://www.mdpi.com/2073-4409/11/19/3149/htm

36. Blasius AL, Beutler B. Intracellular toll-like receptors. Immunity [Internet]. 2010 Mar 26 [cited 2019 Jul 2];32(3):305–15. Available from:

655 http://www.ncbi.nlm.nih.gov/pubmed/20346772

656 37. Jurk M, Heil F, Vollmer J, Schetter C, Krieg AM, Wagner H, et al. Human TLR7 or TLR8
657 independently confer responsiveness to the antiviral compound R-848. Nat Immunol 2002 36
658 [Internet]. 2002 [cited 2022 Dec 17];3(6):499–499. Available from:
659 https://www.nature.com/articles/ni0602-499

660 38. Michaelis KA, Norgard MA, Zhu X, Levasseur PR, Sivagnanam S, Liudahl SM, et al. The
661 TLR7/8 agonist R848 remodels tumor and host responses to promote survival in pancreatic
662 cancer. Nat Commun 2019 101 [Internet]. 2019 Oct 15 [cited 2022 Dec 17];10(1):1–15.
663 Available from: https://www.nature.com/articles/s41467-019-12657-w

664 39. Meyer T, Surber C, French LE, Stockfleth E. Resiquimod, a topical drug for viral skin lesions
665 and skin cancer. Expert Opin Investig Drugs. 2013 Jan;22(1):149–59.

666 40. Fife KH, Meng TC, Ferris DG, Liu P. Effect of Resiquimod 0.01% Gel on Lesion Healing and
667 Viral Shedding When Applied to Genital Herpes Lesions. Antimicrob Agents Chemother
668 [Internet]. 2008 Feb [cited 2022 Dec 17];52(2):477. Available from:
669 /pmc/articles/PMC2224757/

670 41. Pockros PJ, Guyader D, Patton H, Tong MJ, Wright T, McHutchison JG, et al. Oral
671 resiquimod in chronic HCV infection: Safety and efficacy in 2 placebo-controlled, double-
672 blind phase IIa studies. J Hepatol [Internet]. 2007 Aug 1 [cited 2022 Nov 29];47(2):174–82.
673 Available from: https://linkinghub.elsevier.com/retrieve/pii/S0168827807002565

674 42. Savage P, Horton V, Moore J, Owens M, Witt P, Gore ME. A phase I clinical trial of
675 imiquimod, an oral interferon inducer, administered daily. Br J Cancer [Internet]. 1996 [cited
676 2022 Dec 5];74(9):1482. Available from: /pmc/articles/PMC2074776/?report=abstract

677 43. Eigentler TK, Gutzmer R, Hauschild A, Heinzerling L, Schadendorf D, Nashan D, et al.
678 Adjuvant treatment with pegylated interferon α-2a versus low-dose interferon α-2a in patients
679 with high-risk melanoma: a randomized phase III DeCOG trial. Ann Oncol. 2016 Aug
680 1;27(8):1625–32.

681 44. Ichael M, Ried WF, Hiffman ILS, Ajender KR, Eddy R, Oleman C, et al. Peginterferon Alfa-
682 2a plus Ribavirin for Chronic Hepatitis C Virus Infection.
683 https://doi.org/101056/NEJMoa020047 [Internet]. 2002 Sep 26 [cited 2022 Dec
684 17];347(13):975–82. Available from: https://www.nejm.org/doi/10.1056/NEJMoa020047

685 45. Galderma. Clinical Trial Protocol RD.03.SPR.104003. Lausanne; 2019.

686 46. Abstracts from the 10th North American ISSX Meeting. 2532(2000).

687 47. Mescher M, Tigges J, Rolfes KM, Shen AL, Yee JS, Vogeley C, et al. The Toll-like receptor
688 agonist imiquimod is metabolized by aryl hydrocarbon receptor-regulated cytochrome P450
689 enzymes in human keratinocytes and mouse liver. Arch Toxicol [Internet]. 2019;93(7):1917–
690 26. Available from: https://doi.org/10.1007/s00204-019-02488-5

691 48. Tanji H, Ohto U, Shibata T, Miyake K, Shimizu T. Structural Reorganization of the Toll-Like
692 Receptor 8 Dimer Induced by Agonistic Ligands. Science (80-) [Internet]. 2013 Mar

693 22;339(6126):1426–9. Available from: https://www.science.org/doi/10.1126/science.1229159

694 49. Zhang Z, Ohto U, Shibata T, Krayukhina E, Taoka M, Yamauchi Y, et al. Structural Analysis
695 Reveals that Toll-like Receptor 7 Is a Dual Receptor for Guanosine and Single-Stranded RNA.
696 Immunity [Internet]. 2016;45(4):737–48. Available from:
697 http://dx.doi.org/10.1016/j.immuni.2016.09.011

698 50. Zhang Z, Ohto U, Shibata T, Taoka M, Yamauchi Y, Sato R, et al. Structural Analyses of Toll-
699 like Receptor 7 Reveal Detailed RNA Sequence Specificity and Recognition Mechanism of
700 Agonistic Ligands. Cell Rep [Internet]. 2018 Dec 18 [cited 2019 Jul 2];25(12):3371-3381.e5.
701 Available from: https://www.sciencedirect.com/science/article/pii/S2211124718318722

702 51. Yang Y, Csakai A, Jiang S, Smith C, Tanji H, Huang J, et al. Tetrasubstituted imidazoles as
703 incognito Toll-like receptor 8 a(nta)gonists. Nat Commun [Internet]. 2021;12(1):1–9.
704 Available from: http://dx.doi.org/10.1038/s41467-021-24536-4

705 52. Tanji H, Ohto U, Shibata T, Miyake K, Shimizu T. Structural reorganization of the toll-like
706 receptor 8 dimer induced by agonistic ligands. Science (80-) [Internet]. 2013 Mar 22 [cited
707 2023 Jan 30];339(6126):1426–9. Available from:
708 https://www.science.org/doi/10.1126/science.1229159

709 53. Zhang Z, Ohto U, Shibata T, Krayukhina E, Taoka M, Yamauchi Y, et al. Structural Analysis
710 Reveals that Toll-like Receptor 7 Is a Dual Receptor for Guanosine and Single-Stranded RNA.
711 Immunity [Internet]. 2016 Oct 18 [cited 2019 Jul 2];45(4):737–48. Available from:
712 https://www.cell.com/immunity/fulltext/S1074-7613(16)30380-
713 6?_returnURL=https%3A%2F%2Flinkinghub.elsevier.com%2Fretrieve%2Fpii%2FS1074761
714 316303806%3Fshowall%3Dtrue

715 54. Shukla NM, Malladi SS, Mutz CA, Balakrishna R, David SA. Structure-activity relationships
716 in human toll-like receptor 7-active imidazoquinoline analogues. J Med Chem. 2010;

717 55. Straß S, Schwamborn A, Keppler M, Cloos N, Guezguez J, Guse JH, et al. Synthesis,
718 Characterization, and in vivo Distribution of Intracellular Delivered Macrolide Short-Chain
719 Fatty Acid Derivatives. ChemMedChem. 2021;16(14):2254–69.

720 56. Garver E, Hugger ED, Shearn SP, Rao A, Dawson PA, Davis CB, et al. Involvement of
721 intestinal uptake transporters in the absorption of azithromycin and clarithromycin in the rat.
722 Drug Metab Dispos. 2008;36(12):2492–8.

723 57. Bosnar M, Kelnerić Ž, Munić V, Eraković V, Parnham MJ. Cellular uptake and efflux of
724 azithromycin, erythromycin, clarithromycin, telithromycin, and cethromycin. Antimicrob
725 Agents Chemother. 2005;

726 58. Togami K, Chono S, Morimoto K. Subcellular Distribution of Azithromycin and
727 Clarithromycin in Rat Alveolar Macrophages (NR8383) in Vitro. Vol. 36, Biol. Pharm. Bull.
728 2013.

729 59. Strass S, Heinzel C, Cloos N, Keppler M, Guse J, Burnet M, et al. P139 EFFECT OF
730 LYSOSOMAL SHORT CHAIN FATTY ACID DELIVERY ON IMMUNE RESPONSE.
731 Gastroenterology. 2020 Feb 1;158(3):S20.

60. Togami K, Chono S, Morimoto K. Distribution characteristics of clarithromycin and azithromycin, macrolide antimicrobial agents used for treatment of respiratory infections, in lung epithelial lining fluid and alveolar macrophages. Biopharm Drug Dispos. 2011 Oct;32(7):389–97.

61. Hemmi H, Kaisho T, Takeuchi O, Sato S, Sanjo H, Hoshino K, et al. Small-antiviral compounds activate immune cells via the TLR7 MyD88-dependent signaling pathway. Nat Immunol. 2002;3(2):196–200.

62. Forsbach A, Nemorin J-G, Montino C, Müller C, Samulowitz U, Vicari AP, et al. Identification of RNA sequence motifs stimulating sequence-specific TLR8-dependent immune responses. J Immunol [Internet]. 2008 Mar 15 [cited 2019 Jul 2];180(6):3729–38. Available from: http://www.ncbi.nlm.nih.gov/pubmed/18322178

63. Gorden KKB, Qiu XX, Binsfeld CCA, Vasilakos JP, Alkan SS. Cutting Edge: Activation of Murine TLR8 by a Combination of Imidazoquinoline Immune Response Modifiers and PolyT Oligodeoxynucleotides. J Immunol [Internet]. 2006 Nov 15 [cited 2022 Dec 17];177(10):6584–7. Available from: https://journals.aai.org/jimmunol/article/177/10/6584/74611/Cutting-Edge-Activation-of-Murine-TLR8-by-a

64. Schön MP, Schön M, Klotz KN. The small antitumoral immune response modifier imiquimod interacts with adenosine receptor signaling in a TLR7- and TLR8-independent fashion. J Invest Dermatol. 2006;126(6):1338–47.

65. McColl A, Thomson CA, Nerurkar L, Graham GJ, Cavanagh J. TLR7-mediated skin inflammation remotely triggers chemokine expression and leukocyte accumulation in the brain. J Neuroinflammation [Internet]. 2016;13(1):1–16. Available from: http://dx.doi.org/10.1186/s12974-016-0562-2

66. Nerurkar L, Mccoll A, Graham G, Cavanagh J. The Systemic Response to Topical Aldara Treatment is Mediated Through Direct TLR7 Stimulation as Imiquimod Enters the Circulation. Sci Rep [Internet]. 2017;(July):1–11. Available from: http://dx.doi.org/10.1038/s41598-017-16707-5

67. Bourquin C, Hotz C, Noerenberg D, Voelkl A, Heidegger S, Roetzer LC, et al. Systemic cancer therapy with a small molecule agonist of toll-like receptor 7 can be improved by circumventing TLR tolerance. Cancer Res [Internet]. 2011 Aug 1 [cited 2022 Dec 7];71(15):5123–33. Available from: https://aacrjournals.org/cancerres/article/71/15/5123/567671/Systemic-Cancer-Therapy-with-a-Small-Molecule

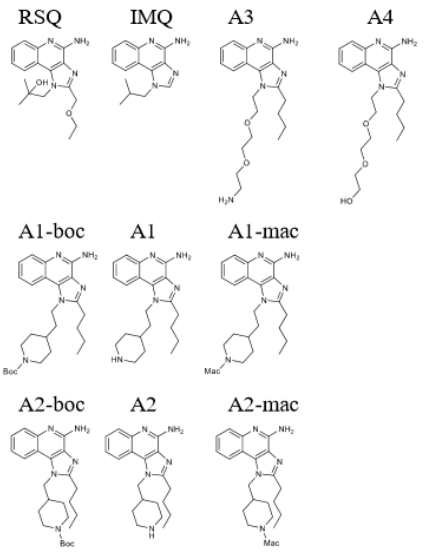

FIGURE 1 | Compound structures

TABLE 1 | EC_{50} values for compounds in HEK-blue human TLR7 and human TLR8 receptor assay (expressed as 95% CI, ND noted for no calculation of curve fit possible (adj. $r^2 < 0.8$)) and average maximal SEAP secretion observed for a given compound relative to the maximum secretion observed in the assay.

Compound	TLR7 EC_{50} [µM]	TLR7 activity rel. to assay max	TLR8 EC_{50} [µM]	TLR8 activity rel. to assay max
RSQ	0.47 to 0.77	95%	2.9 to 3.6	96%
IMQ	5.2 to 8.3	35%	ND	3%
A1-boc	0.39 to 0.69	55%	ND	4%
A1	0.096 to 0.22	58%	ND	11%
A1-mac	0.40 to 0.74	41%	ND	5%
A2-boc	0.23 to 0.47	86%	ND	4%
A2	0.075 to 0.12	81%	2.8 to 3.1	57%
A2-mac	1.5 to 2.0	63%	ND	4%
A3	1.0 to 1.5	62%	8.2 to 8.5	36%
A4	1.5 to 2.1	84%	11 to 13	18%

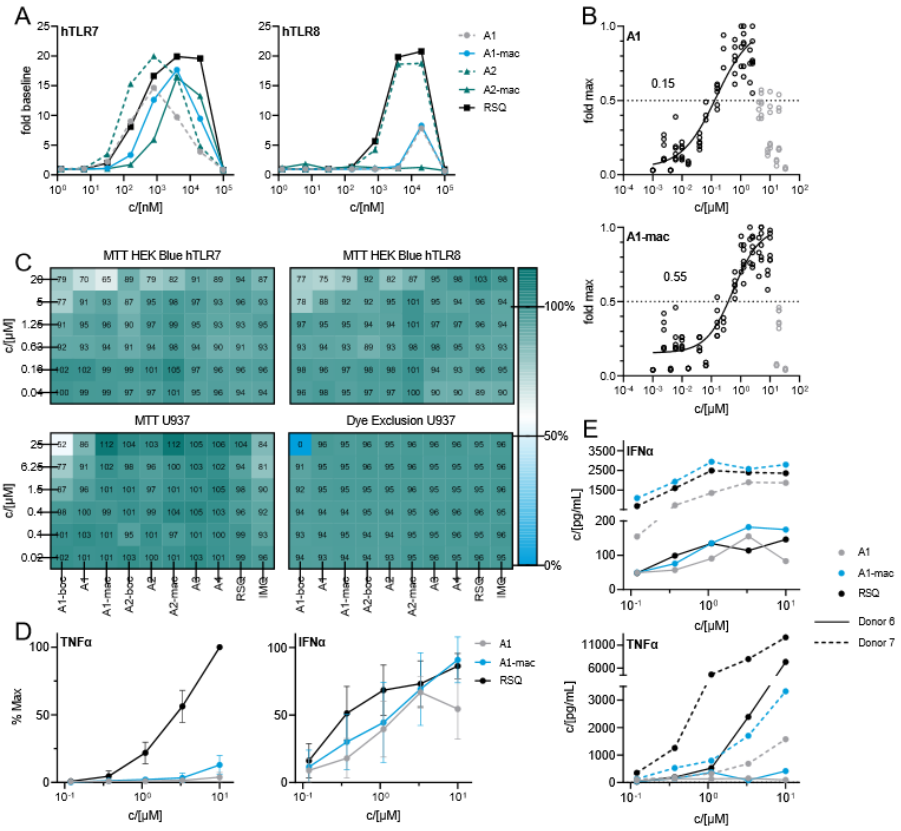

FIGURE 2 | In vitro characterization of candidate molecules **(A)** SEAP activity in supernatants of HEK Blue reporter cells after 24 h stimulation with varying concentrations of test compounds relative to solvent controls **(B)** Dose response of A1 and A1-mac in HEK Blue hTLR7. Circles represent normalized replicate measurements pooled from 3 experiments. Lines represent non-linear functions fit to the data to calculate compound-specific EC50, values in grey have been excluded before fitting. **(C)** Percent MTT conversion of compound-treated HEK-Blue reporter cells (top panels) or PMA-differentiated U937 relative to solvent controls OR percent of undifferentiated U937 excluding Helix NIR dye **(D)** TNFα/IFNα in supernatants of human blood stimulated with A1, A1-mac or RSQ for 6 h, n=8, concentrations normalized to the maximum concentration of each cytokine for a given donor **(E)** TNFα/IFNα in supernatant of blood for two individual donors

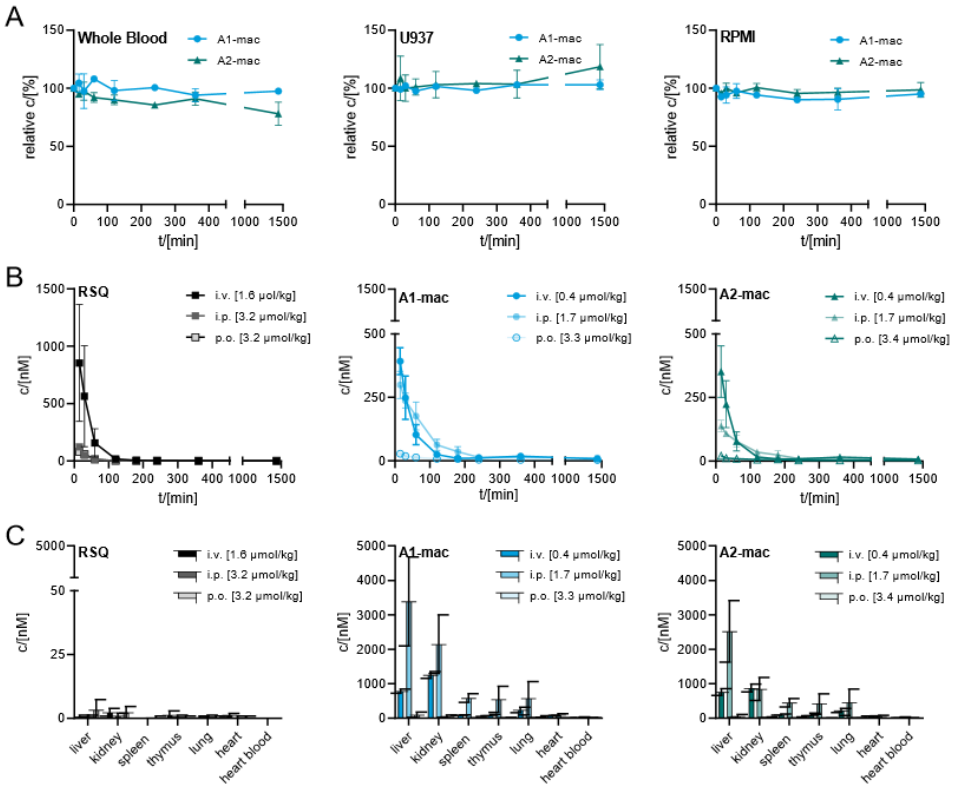

FIGURE 3 | Stability and bioavailability of lead compounds. **(A)** Stability of A1-mac and A2-mac was measured in human blood, U937 monocytes and RPMI medium over 24 h. **(B, C)** Concentration of RSQ, A1-mac and A2-mac in peripheral blood and organs was assessed via HLPC-MS after i.v., i.p. and p.o. compound administration in 10-weeks old, female C57BL/6 mice (n=3 mice per group). Compounds were administered in cassettes (i.v. application: 1.6 µmol/kg RSQ, 0.4 µmol/kg A1-mac, 0.4 µmol/kg A2-mac; i.p. application: 3.2 µmol/kg RSQ, 1.7 µmol/kg A1-mac, 1.7 µmol/kg A2-mac, p.o. application: 3.2 µmol/kg RSQ, 3.3 µmol/kg A1-mac, 3.3 µmol/kg A2-mac). **(B)** Peripheral blood was collected 15, 30 60, 120, 180, 240, 360 and 1440 min after compound treatment. **(C)** Organs were sampled 1440 min after compound treatment. **(A, B, C)** Data are presented as mean with SD.

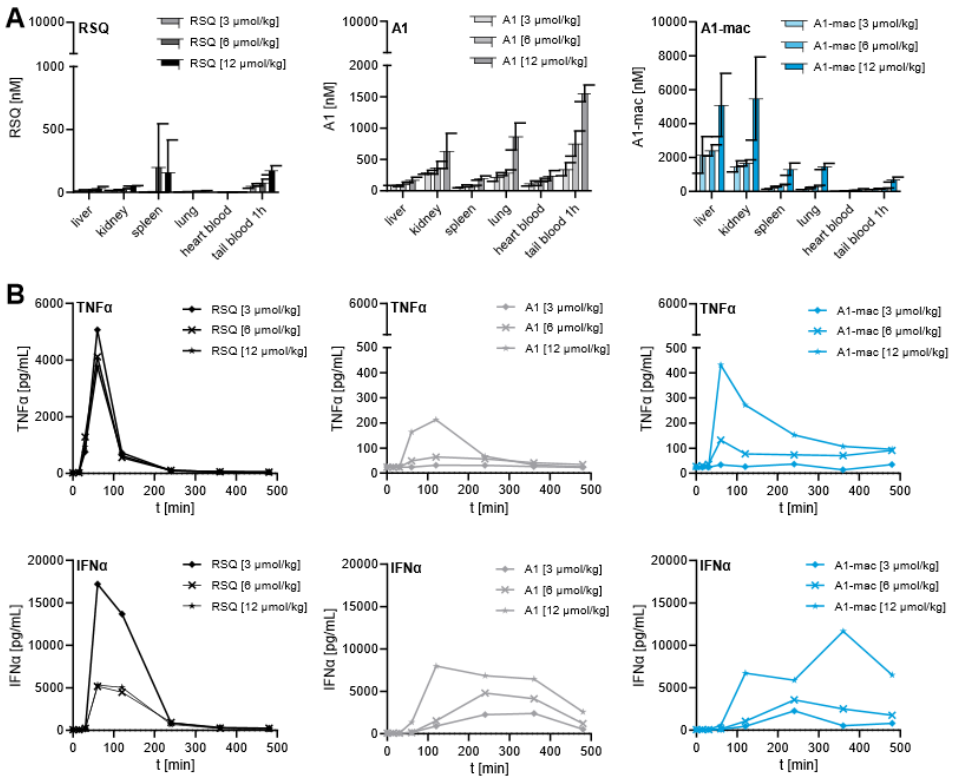

FIGURE 4 | Concentration of RSQ, A1 and A1-mac in organs and cytokine profile in peripheral blood over time after 3, 6 and 12 µmol/kg s.c. compound administration in 8 old, female C57BL/6 mice (n=3 mice per group). **(A)** Organs were sampled 8 h after treatment and compound concentration was determined via HPLC-MS. Data are presented as mean with SD. **(B)** Cytokine levels in tail plasma over time were determined via cytometric bead array. At each sampling timepoint the plasma of mice in one treatment group was pooled.

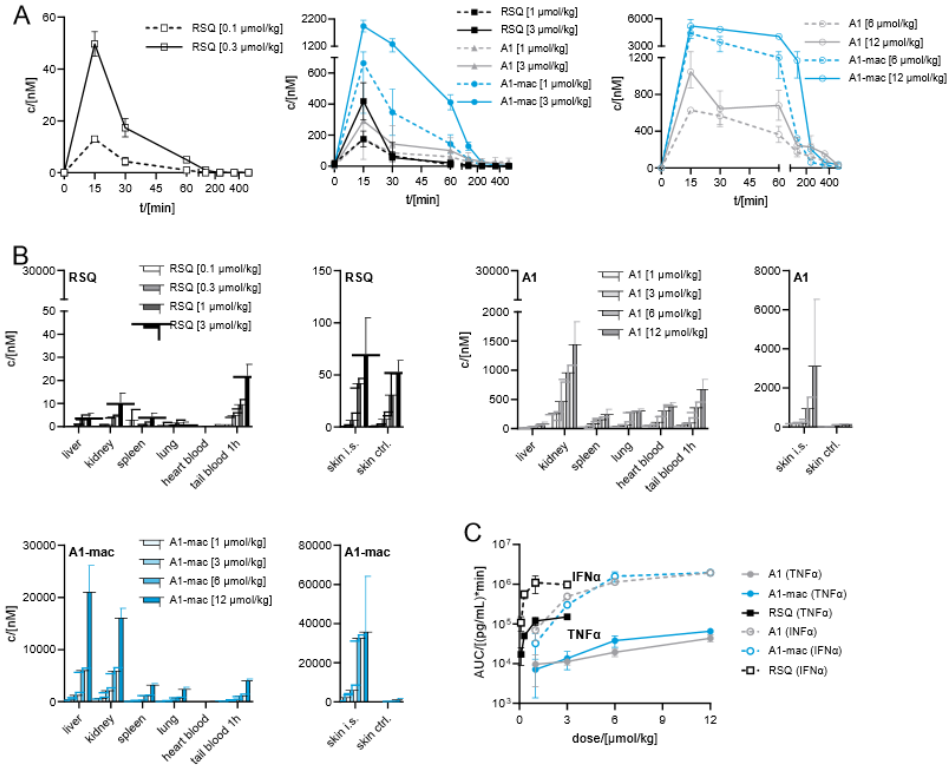

FIGURE 5 | Pharmacokinetic and TNFα, IFNα characterization of A1 and A1-mac compared to RSQ. **(A, B, C)** Female, 18-week old, C57BL/6 mice were treated s.c. with 1, 3 6 or 12 µmol/kg RSQ, A-1 or A1-mac (n=3 mice per group). **(A)** Peripheral blood was collected via tail bleeding before, 15, 30 60, 120, 240, 360 and 480 min after s.c. treatment. Compounds concentration in peripheral blood and **(B)** organs collected after 8 h was assessed via HPLC-MS. **(A,B)** Data are presented as mean with SD. **(C)** Level of TNFα and IFNα in tail plasma over time was determined with a cytometric bead array. Area under the curve (AUC) of each cytokine was plotted against compound concentration. Data are presented as mean with 95 % confidence interval.

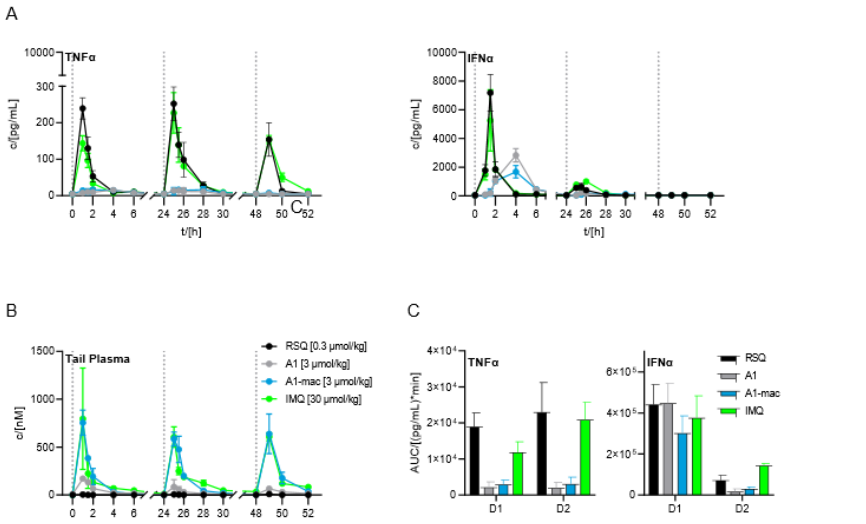

FIGURE 6 | effects of repeated applications of A1, A1-mac compared to RSQ and IMQ, dotted lines mark the time of repeated compound applications **(A)** Cytokine levels in pooled tail plasma of mice in one treatment group (n=3 per time point), error bars represent range of two replicate measurements **(B)** Peripheral blood was collected from the tail vein before, 15, 30 60, 120, 240, 360 and 480 min after s.c. treatment. Compound concentration in peripheral plasma were analyzed by HPLC-MS/MS, data presented as mean ± SD **(C)** AUC of TNFα/IFNα in peripheral plasma calculated from the data in (A) for days 1 and 2 of treatment, data represent calculated AUC ± 95% CI

11. Ausblick

Die entwickelten Substanzen haben Potential und sollen in weiteren Studien getestet werden. Dabei zeigte sich in bisher nicht publizierten Daten, dass die Derivate der kurzkettigen Fettsäuren einen Einfluss auf das Inflammasom haben. Des Weiteren wird diese Substanzklasse im Kontext von Infektionen getestet (vgl. hierzu auch A. Saris *et al.* (2022)) [94]. Einen Ansatz zur Behandlung von entzündlichen Darmerkrankungen konnte auch schon gezeigt werden (vgl. hierzu auch S. Straß *et al.* (2020)) und soll auch weiter untersucht werden [95].

Die Derivate der Fumarate konnten im direkten Vergleich zu DMF in einer deutlich geringeren Dosis angewandt werden. Dies kann in Bezug auf bekannte Nebenwirkungen (vor allem im Magen-Darm-Bereich) zu einer Verbesserung führen. Nach der Zulassung von DMF als Medikament für die von MS wurden vor kurzem Vumerity (Diroximelfumarat) und Bafiertam (Monomethylfumarat) zugelassen. Dies gibt einen Hinweis darauf, dass Bedarf für neue Fumarsäurederivate besteht.

Die TLR-Agonisten werden von uns in verschiedenen Krebsmodellen getestet und sollen auch in möglichen Vakzinierungsversuchen zum Einsatz kommen, außerdem sollen weitere Derivate mit anderen Seitenketten synthetisiert werden. Dies soll das vorhandene Portfolio erweitern und bessere Rückschlüsse auf die Struktur-Aktivitäts-Beziehung geben. Als Möglichkeit wird auch die Kopplung an Peptide und Proteine in Betracht gezogen.

Durch ein verbessertes Verständnis in der Induktion von Psoriasis-ähnlichen Hautveränderungen und der systemischen Entzündungsreaktion beim murinen Creme-induzierten Modell können Wirkstoffkandidaten besser getestet werden. Es entsteht ein besseres Verständnis der Wirkweise und durch die Verfeinerung und das bessere Verständnis des Tiermodells kann eine bessere Versuchsplanung durchgeführt werden und eine höhere Reproduzierbarkeit der Daten erreicht werden, was zu einer verringerten Tierzahl führen kann.

12. Danksagung

Zunächst einmal möchte ich mich bei Prof. Dr. Stefan Laufer bedanken, der mir die Möglichkeit gegeben hat in Zusammenarbeit mit der Synovo GmbH dieses spannende und abwechslungsreiche Thema zu bearbeiten und darüber hinaus bei Fragen immer zur Seite stand.

Dr. Michael Burnet danke ich für die Möglichkeit in der Synovo GmbH zu promovieren, das entgegengebrachte Vertrauen in meine Leistungen, die immer spannenden Ideen und das zur Verfügung stellen aller Ressourcen zur Vervollständigung dieser Arbeit.

Ein großer Dank geht an Dr. Jan Guse, welcher meine praktische Arbeit betreut hat, mit Ideen geholfen hat und sich die Zeit genommen hat mir die organische Chemie näher zu bringen.

Weiter geht mein Dank an die gesamte Synovo Gruppe, welche mich super aufgenommen hat und in der ich viele Freundschaften gefunden habe. Danke auch für die Unterstützung der internen Forschung, das Einbringen von guten Ideen und die Möglichkeit sehr viel zu lernen. Die weitestgehende harmonische TeamScience-Arbeitsatmosphäre und darüber hinaus die spaßigen Unternehmungen haben die Doktorarbeit deutlich angenehmer gestaltet und für die nötige Ablenkung gesorgt. Ich bedanke mich bei allen für den dreifachen Gewinn der Firmenrudermeisterschaften und hoffe den Pokal auch 2023 wieder bei uns ausstellen zu können.

Ein großer Dank geht an meine Familie, die es geschafft hat mich, wo sie konnte, zu unterstützen und immer an meine Ziele und meinen Ehrgeiz, die Arbeit zu einem Ende zu bringen, geglaubt hat.

Außerdem müssen Leonhart und Raimund erwähnt werden, welche mir die Feierabende versüßt und mich immerzu erheitert haben.

Und zu guter Letzt, mein Dank an Benedikte, welche mir immer den nötigen Beistand und den Rückhalt gegeben hat. Vielen Dank, dass du für mich da bist und ich auf deine Unterstützung zählen kann.

Diese Arbeit war meine bisher größte Herausforderung und ich freue mich sehr dieses Kapitel nun abzuschließen, freue mich jedoch auch auf weitere kommende und spannende Herausforderungen.

13. Literaturverzeichnis

1. Bosnar, M. *et al.* Immunomodulatory effects of azithromycin on the establishment of lipopolysaccharide tolerance in mice. *Int. Immunopharmacol.* **15**, 498–504 (2013).
2. Djokić, S. *et al.* Erythromycin series. Part 11. Ring expansion of erythromycin A oxime by the Beckmann rearrangement. *J. Chem. Soc., Perkin Trans. 1* 1881–1890 (1986) doi:10.1039/P19860001881.
3. Togami, K., Chono, S. & Morimoto, K. Distribution characteristics of clarithromycin and azithromycin, macrolide antimicrobial agents used for treatment of respiratory infections, in lung epithelial lining fluid and alveolar macrophages. *Biopharm. Drug Dispos.* (2011) doi:10.1002/bdd.767.
4. Lode, H. The pharmacokinetics of azithromycin and their clinical significance. *Eur. J. Clin. Microbiol. Infect. Dis.* **10**, 807–812 (1991).
5. LeBel, M. Pharmacokinetic Properties of Clarithromycin: A Comparison with Erythromycin and Azithromycin. *Can. J. Infect. Dis.* **4**, 148–152 (1993).
6. Trouet, A. Lysosomotropic agents. *Arch. Biol. (Liege).* **86**, 492–493 (1975).
7. Carlier, M. B., Garcia-Luque, I., Montenez, J. P., Tulkens, P. M. & Piret, J. Accumulation, release and subcellular localization of azithromycin in phagocytic and non-phagocytic cells in culture. *Int. J. Tissue React.* **16**, 211—220 (1994).
8. Bosnar, M., Kelnerić, Ž., Munić, V., Eraković, V. & Parnham, M. J. Cellular uptake and efflux of azithromycin, erythromycin, clarithromycin, telithromycin, and cethromycin. *Antimicrob. Agents Chemother.* (2005) doi:10.1128/AAC.49.6.2372-2377.2005.
9. Caengprasath, N. *et al.* Internalization-Dependent Free Fatty Acid Receptor 2 Signaling Is Essential for Propionate-Induced Anorectic Gut Hormone Release. *iScience* **23**, 101449 (2020).
10. Li, G. *et al.* Internalization of the human nicotinic acid receptor GPR109A is regulated by Gi, GRK2, and arrestin3. *J. Biol. Chem.* **285**, 22605–22618 (2010).
11. Chen, H. *et al.* Hydroxycarboxylic acid receptor 2 mediates dimethyl fumarate's protective effect in EAE. *J. Clin. Invest.* **124**, 2188–2192 (2014).
12. von Glehn, F. *et al.* Dimethyl fumarate downregulates the immune response through the HCA2/GPR109A pathway: Implications for the treatment of multiple sclerosis. *Mult. Scler. Relat. Disord.* **23**, 46–50 (2018).
13. Layden, B. T., Angueira, A. R., Brodsky, M., Durai, V. & Lowe, W. L. Short chain fatty acids and their receptors: New metabolic targets. *Transl. Res.* **161**, 131–140 (2013).
14. Li, M., van Esch, B. & Henricks, P. Pro- and anti-inflammatory effects of short chain fatty acids on immune and endothelial cells. *Eur. J. Pharmacol.* **831**, 52–59 (2018).
15. Ulven, T. Short-chain free fatty acid receptors FFA2/GPR43 and FFA3/GPR41 as new potential therapeutic targets. *Front. Endocrinol. (Lausanne).* **3**, 111 (2012).
16. Hamer, H. M. *et al.* Review article: The role of butyrate on colonic function. *Aliment. Pharmacol. Ther.* **27**, 104–119 (2008).
17. Ang, Z. *et al.* Human and mouse monocytes display distinct signalling and cytokine profiles upon stimulation with FFAR2/FFAR3 short-chain fatty acid receptor agonists. *Sci. Rep.* **6**, 34145 (2016).
18. Nüsslein-Volhard, C. The Toll gene in Drosophila pattern formation. *Trends Genet.* **38**, 231–245 (2022).
19. Takeda, K. & Akira, S. Toll-Like Receptors. *Curr. Protoc. Immunol.* **77**, (2007).
20. Botos, I., Segal, D. M. & Davies, D. R. The Structural Biology of Toll-like Receptors. *Structure* **19**, 447–459 (2011).

21. Mancuso, G. *et al.* Bacterial recognition by TLR7 in the lysosomes of conventional dendritic cells. *Nat. Immunol.* **10**, 587–594 (2009).
22. Vasilakos, J. P. & Tomai, M. A. The use of Toll-like receptor 7/8 agonists as vaccine adjuvants. *Expert Rev. Vaccines* **12**, 809–819 (2013).
23. Kawasaki, T. & Kawai, T. Toll-like receptor signaling pathways. *Front. Immunol.* **5**, 461 (2014).
24. Cervantes, J. L., Weinerman, B., Basole, C. & Salazar, J. C. TLR8: the forgotten relative revindicated. *Cell. Mol. Immunol. 2012 96* **9**, 434–438 (2012).
25. Gilliet, M., Cao, W. & Liu, Y. J. Plasmacytoid dendritic cells: sensing nucleic acids in viral infection and autoimmune diseases. *Nat. Rev. Immunol. 2008 88* **8**, 594–606 (2008).
26. Kusiak, A. & Brady, G. Bifurcation of signalling in human innate immune pathways to NF-kB and IRF family activation. *Biochem. Pharmacol.* **205**, 115246 (2022).
27. Iwanaszko, M. & Kimmel, M. NF-KB and IRF pathways: Cross-regulation on target genes promoter level. *BMC Genomics* **16**, 1–8 (2015).
28. Liu, T., Zhang, L., Joo, D. & Sun, S. C. NF-κB signaling in inflammation. *Signal Transduct. Target. Ther.* **2**, (2017).
29. Tian, B. *et al.* Identification of NF-κB-Dependent Gene Networks in Respiratory Syncytial Virus-Infected Cells. *J. Virol.* **76**, 6800–6814 (2002).
30. O'Neill, L. A. J. & Bowie, A. G. The family of five: TIR-domain-containing adaptors in Toll-like receptor signalling. *Nat. Rev. Immunol.* **7**, 353–364 (2007).
31. Odoardi, N. TLR Signaling Cascade.
32. Bosnar, M. *et al.* Azithromycin and Clarithromycin Inhibit Lipopolysaccharide-Induced Murine Pulmonary Neutrophilia Mainly through Effects on Macrophage-Derived Granulocyte-Macrophage Colony-Stimulating Factor and Interleukin-1β. *J. Pharmacol. Exp. Ther.* **331**, 104 LP – 113 (2009).
33. Meyer, M. *et al.* Azithromycin reduces exaggerated cytokine production by M1 alveolar macrophages in cystic fibrosis. *Am. J. Respir. Cell Mol. Biol.* **41**, 590–602 (2009).
34. Murphy, B. S. *et al.* Azithromycin alters macrophage phenotype. *J. Antimicrob. Chemother.* **61**, 554–560 (2008).
35. Hodge, S. *et al.* Azithromycin increases phagocytosis of apoptotic bronchial epithelial cells by alveolar macrophages. *Eur. Respir. J.* **28**, 486–95 (2006).
36. Hodge, S. *et al.* Nonantibiotic macrolides restore airway macrophage phagocytic function with potential anti-inflammatory effects in chronic lung diseases. *Am. J. Physiol. - Lung Cell. Mol. Physiol.* (2017) doi:10.1152/ajplung.00518.2016.
37. Mencarelli, A. *et al.* Development of non-antibiotic macrolide that corrects inflammation-driven immune dysfunction in models of inflammatory bowel diseases and arthritis. *Eur. J. Pharmacol.* **665**, 29–39 (2011).
38. Balloy, V. *et al.* Azithromycin analogue CSY0073 attenuates lung inflammation induced by LPS challenge. *Br. J. Pharmacol.* **171**, 1783–1794 (2014).
39. BRIGHT, G. M. *et al.* Synthesis, in vitro and in vivo activity of novel 9-deoxo-9a-aza-9a-homoerythromycin A derivatives; A new class of macrolide antibiotics, the azalides. *J. Antibiot. (Tokyo).* **41**, 1029–1047 (1988).
40. Yan, M. *et al.* Synthesis and Antibacterial Activity of Novel 11-O-Phenethylcarbamoylazithromycin Derivatives with 4"-elongated Side Chains. *Lett. Drug Des. Discov.* **9**, 833–839 (2012).
41. Vinolo, M. A. R., Rodrigues, H. G., Nachbar, R. T. & Curi, R. Regulation of inflammation by short chain fatty acids. *Nutrients* **3**, 858–876 (2011).
42. Corrêa-Oliveira, R., Fachi, J. L., Vieira, A., Sato, F. T. & Vinolo, M. A. R. Regulation of

immune cell function by short-chain fatty acids. *Clin. Transl. Immunol.* (2016) doi:10.1038/cti.2016.17.

43. Milligan, G., Stoddart, L. A. & Smith, N. J. Agonism and allosterism: The pharmacology of the free fatty acid receptors FFA2 and FFA3. *Br. J. Pharmacol.* **158**, 146–153 (2009).
44. View, P., Mishra, S. P., Karunakar, P. & Taraphder, S. Free Fatty Acid Receptors 2 and 3 as Microbial Metabolite Sensors to Shape Host Health : *Biomedicines* **8**, 154 (2017).
45. Singh, N. *et al.* Activation of Gpr109a, Receptor for Niacin and the Commensal Metabolite Butyrate, Suppresses Colonic Inflammation and Carcinogenesis. *Immunity* **40**, 128–139 (2014).
46. Schulthess, J. *et al.* The short chain fatty acid butyrate imprints an antimicrobial program in macrophages. *Immunity* 1–14 (2019) doi:10.1016/J.IMMUNI.2018.12.018.
47. Macia, L. *et al.* Metabolite-sensing receptors GPR43 and GPR109A facilitate dietary fibre-induced gut homeostasis through regulation of the inflammasome. *Nat. Commun.* **6**, (2015).
48. Thorburn, A. N., Macia, L. & Mackay, C. R. Diet, Metabolites, and 'Western-Lifestyle' Inflammatory Diseases. *Immunity* (2014) doi:10.1016/j.immuni.2014.05.014.
49. D'Souza, W. N. *et al.* Differing roles for short chain fatty acids and GPR43 agonism in the regulation of intestinal barrier function and immune responses. *PLoS One* **12**, 1–15 (2017).
50. Sun, M., Wu, W., Liu, Z. & Cong, Y. Microbiota metabolite short chain fatty acids, GPCR, and inflammatory bowel diseases. *J. Gastroenterol.* **52**, 1–8 (2017).
51. Machiels, K. *et al.* A decrease of the butyrate-producing species roseburia hominis and faecalibacterium prausnitzii defines dysbiosis in patients with ulcerative colitis. *Gut* **63**, 1275–1283 (2014).
52. Eichele, D. D. & Kharbanda, K. K. Dextran sodium sulfate colitis murine model: An indispensable tool for advancing our understanding of inflammatory bowel diseases pathogenesis. *World J. Gastroenterol.* **23**, 6016–6029 (2017).
53. Taghipour, N. *et al.* An experimental model of colitis induced by dextran sulfate sodium from acute progresses to chronicity in C57BL/6: Correlation between conditions of mice and the environment. *Gastroenterol. Hepatol. from Bed to Bench* **9**, 45–52 (2016).
54. Zisman, T. L. & Kane, S. V. Current and future therapies for inflammatory bowel disease. *Expert Rev. Gastroenterol. Hepatol.* **1**, 89–100 (2007).
55. Antoni, L., Nuding, S., Wehkamp, J. & Stange, E. F. Intestinal barrier in inflammatory bowel disease. *World J. Gastroenterol.* **20**, 1165–1179 (2014).
56. Roda, A. *et al.* A new oral formulation for the release of sodium butyrate in the ileo-cecal region and colon. *World J. Gastroenterol.* **13**, 1079–1084 (2007).
57. Geirnaert, A. *et al.* Butyrate-producing bacteria supplemented in vitro to Crohn's disease patient microbiota increased butyrate production and enhanced intestinal epithelial barrier integrity. *Sci. Rep.* **7**, 1–14 (2017).
58. Strass, S. *et al.* P139 EFFECT OF LYSOSOMAL SHORT CHAIN FATTY ACID DELIVERY ON IMMUNE RESPONSE. *Gastroenterology* **158**, S20 (2020).
59. McGuire, V. A. *et al.* Dimethyl fumarate blocks pro-inflammatory cytokine production via inhibition of TLR induced M1 and K63 ubiquitin chain formation. *Sci. Rep.* (2016) doi:10.1038/srep31159.
60. Naismith, R. T. *et al.* Diroximel Fumarate Demonstrates an Improved Gastrointestinal Tolerability Profile Compared with Dimethyl Fumarate in Patients with Relapsing–Remitting Multiple Sclerosis: Results from the Randomized, Double-Blind, Phase III EVOLVE-MS-2 Study. *CNS Drugs* **34**, 185–196 (2020).

61. Blair, H. A. Dimethyl Fumarate: A Review in Relapsing-Remitting MS. *Drugs* **79**, 1965–1976 (2019).
62. Lategan, T. W., Wang, L., Sprague, T. N. & Rousseau, F. S. Pharmacokinetics and Bioavailability of Monomethyl Fumarate Following a Single Oral Dose of Bafiertam™ (Monomethyl Fumarate) or Tecfidera® (Dimethyl Fumarate). *CNS Drugs* **35**, 567–574 (2021).
63. Tang, H., Lu, J. Y. L., Zheng, X., Yang, Y. & Reagan, J. D. The psoriasis drug monomethylfumarate is a potent nicotinic acid receptor agonist. *Biochem. Biophys. Res. Commun.* **375**, 562–565 (2008).
64. Schulze-Topphoff, U. *et al.* Dimethyl fumarate treatment induces adaptive and innate immune modulation independent of Nrf2. *Proc. Natl. Acad. Sci.* **113**, 4777–4782 (2016).
65. Gillard, G. O. *et al.* DMF, but not other fumarates, inhibits NF-κB activity in vitro in an Nrf2-independent manner. *J. Neuroimmunol.* **283**, 74–85 (2015).
66. Mrowietz, U., Morrison, P. J., Suhrkamp, I., Kumanova, M. & Clement, B. The Pharmacokinetics of Fumaric Acid Esters Reveal Their In Vivo Effects. *Trends Pharmacol. Sci.* **39**, 1–12 (2018).
67. Gambhir, D. *et al.* GPR109A as an anti-inflammatory receptor in retinal pigment epithelial cells and its relevance to diabetic retinopathy. *Invest. Ophthalmol. Vis. Sci.* **53**, 2208–2217 (2012).
68. Brennan, M. S. *et al.* Dimethyl fumarate and monoethyl fumarate exhibit differential effects on KEAP1, NRF2 activation, and glutathione depletion in vitro. *PLoS One* **10**, (2015).
69. Schmidt, T. J., Ak, M. & Mrowietz, U. Reactivity of dimethyl fumarate and methylhydrogen fumarate towards glutathione and N-acetyl-l-cysteine-Preparation of S-substituted thiosuccinic acid esters. *Bioorganic Med. Chem.* **15**, 333–342 (2007).
70. Sullivan, L. B. *et al.* The Proto-oncometabolite Fumarate Binds Glutathione to Amplify ROS-dependent signaling. *Mol. Cell* **51**, 236–248 (2013).
71. Zheng, L. *et al.* Fumarate induces redox-dependent senescence by modifying glutathione metabolism. *Nat. Commun.* **6**, (2015).
72. Onderdijk, A. J. *et al.* Regulated genes in psoriatic skin during treatment with fumaric acid esters. *Br. J. Dermatol.* **171**, 732–741 (2014).
73. Blair, H. A. Dimethyl Fumarate: A Review in Moderate to Severe Plaque Psoriasis. *Drugs* **78**, 123–130 (2018).
74. Nakajima, K. & Sano, S. Mouse models of psoriasis and their relevance. *J. Dermatol.* **45**, 252–263 (2018).
75. van der Fits, L. *et al.* Imiquimod-Induced Psoriasis-Like Skin Inflammation in Mice Is Mediated via the IL-23/IL-17 Axis. *J. Immunol.* **182**, 5836–5845 (2009).
76. Hawkes, J. E., Gudjonsson, J. E. & Ward, N. L. The Snowballing Literature on Imiquimod-Induced Skin Inflammation in Mice: A Critical Appraisal. *J. Invest. Dermatol.* **137**, 546–549 (2017).
77. Schön, M. P. & Schön, M. Imiquimod: Mode of action. *Br. J. Dermatol.* **157**, 8–13 (2007).
78. Schön, M. P., Schön, M. & Klotz, K. N. The small antitumoral immune response modifier imiquimod interacts with adenosine receptor signaling in a TLR7- and TLR8-independent fashion. *J. Invest. Dermatol.* **126**, 1338–1347 (2006).
79. Walter, A. *et al.* Aldara activates TLR7-independent immune defence. *Nat. Commun.* **4**, 1–13 (2013).
80. Mencarelli, A. *et al.* Development of non-antibiotic macrolide that corrects inflammation-driven immune dysfunction in models of inflammatory bowel diseases

and arthritis. *Eur. J. Pharmacol.* **665**, 29–39 (2011).
81. Laux, J. *et al.* Pharmacokinetic Optimization of Small Molecule Janus Kinase 3 Inhibitors to Target Immune Cells. *ACS Pharmacol. Transl. Sci.* **5**, 573–602 (2022).
82. Casili, G. *et al.* Dimethyl fumarate reduces inflammatory responses in experimental colitis. *J. Crohn's Colitis* **10**, 472–483 (2016).
83. Liu, X. *et al.* Dimethyl fumarate ameliorates dextran sulfate sodium-induced murine experimental colitis by activating Nrf2 and suppressing NLRP3 inflammasome activation. *Biochem. Pharmacol.* (2016) doi:10.1016/j.bcp.2016.05.002.
84. Kuriyama, T., Karasawa, T. & Williams, D. W. Antimicrobial Chemotherapy. in *Biofilms in Infection Prevention and Control* 209–244 (Elsevier, 2014). doi:10.1016/B978-0-12-397043-5.00013-X.
85. Stanley, M. A. Imiquimod and the imidazoquinolones: Mechanism of action and therapeutic potential. *Clin. Exp. Dermatol.* **27**, 571–577 (2002).
86. Yang, Y. *et al.* Tetrasubstituted imidazoles as incognito Toll-like receptor 8 a(nta)gonists. *Nat. Commun.* **12**, 1–9 (2021).
87. Tanji, H., Ohto, U., Shibata, T., Miyake, K. & Shimizu, T. Structural Reorganization of the Toll-Like Receptor 8 Dimer Induced by Agonistic Ligands. **482**, 1426–1430 (2013).
88. Zhang, Z. *et al.* Structural Analysis Reveals that Toll-like Receptor 7 Is a Dual Receptor for Guanosine and Single-Stranded RNA. *Immunity* **45**, 737–748 (2016).
89. Fife, K. H., Meng, T. C., Ferris, D. G. & Liu, P. Effect of Resiquimod 0.01% Gel on Lesion Healing and Viral Shedding When Applied to Genital Herpes Lesions. *Antimicrob. Agents Chemother.* **52**, 477 (2008).
90. Pockros, P. J. *et al.* Oral resiquimod in chronic HCV infection: Safety and efficacy in 2 placebo-controlled, double-blind phase IIa studies. *J. Hepatol.* **47**, 174–182 (2007).
91. Savage, P. *et al.* A phase I clinical trial of imiquimod, an oral interferon inducer, administered daily. *Br. J. Cancer* **74**, 1482 (1996).
92. Shukla, N. M., Malladi, S. S., Mutz, C. A., Balakrishna, R. & David, S. A. Structure-activity relationships in human toll-like receptor 7-active imidazoquinoline analogues. *J. Med. Chem.* **53**, 4450–4465 (2010).
93. Kayarmar, R. *et al.* Synthesis and characterization of novel imidazoquinoline based 2-azetidinones as potent antimicrobial and anticancer agents. *J. Saudi Chem. Soc.* **21**, S434–S444 (2017).
94. Saris, A. *et al.* The Azithromycin Pro-Drug CSY5669 Boosts Bacterial Killing While Attenuating Lung Inflammation Associated with Pneumonia Caused by Methicillin-Resistant Staphylococcus aureus. *Antimicrob. Agents Chemother.* **66**, e0229821 (2022).
95. Straß, S. *et al.* Effect of Lysosomal SCFA Delivery on Immune Response. (2020).

14. Anhang

14.1. *Supporting Information* für "*Synthesis, Characterization, and in vivo Distribution of Intracellular Delivered Macrolide Short-Chain Fatty Acid Derivatives*"

ChemMedChem

Supporting Information

Synthesis, Characterization, and in vivo Distribution of Intracellular Delivered Macrolide Short-Chain Fatty Acid Derivatives

Simon Straß, Anna Schwamborn, Manuel Keppler, Natascha Cloos, Jamil Guezguez, Jan-Hinrich Guse, Michael Burnet,* and Stefan Laufer

Supporting Information

Table 1. Tunes of butyrate and propionate derivatives in HPLC-MS/MS

Compound	MS-1 [m/z]	MS-2 [m/z]	Declustering potential [V]	Collision energy [V]	Collision cell exit potential [V]
Azithromycin	749.4	591.3	61	41	16
1a	959.7	731.5	86	39	22
1b	819.6	661.3	126	37	42
1c	819.7	228.2	126	47	42
1d	819.7	591.5	106	37	30
1e	889.8	731.7	111	37	22
1f	889.7	732.5	161	37	18
1g	889.8	661.4	156	41	18
2a	917.6	214.3	126	51	12
2b	403.4	324.2	51	19	18
2c	403.3	214.2	71	25	38
2d	403.3	215.1	61	19	14
2e	861.7	703.6	121	37	40
2f	861.7	454.4	131	51	28
2g	431.4	214.2	56	27	12

Table 2. Results of solubility testing of **1a** and **2a**

concentration [µM]	solubility 1a	solubility 2a
25	yes	yes
33.3	yes	yes
50	no	yes
100	no	yes
125	no	yes
150	no	yes
200	no	no
250	no	no
500	no	no

Table 3. Calculated LogP values of **1a** – **1g** and **2a** – **2g**. Calculations done with ChemDraw 20.0 PerkinElmer Informatics.

Compound	cLogP
1a	8.3681
1b	4.54915
1c	4.5463
1d	4.54915
1e	6.4572
1f	6.46005
1g	6.4572
2a	6.7811
2b	4.02015
2c	4.0173
2d	4.02015
2e	5.3992
2f	5.40205
2g	5.3992

^{1}H und ^{13}C NMRs

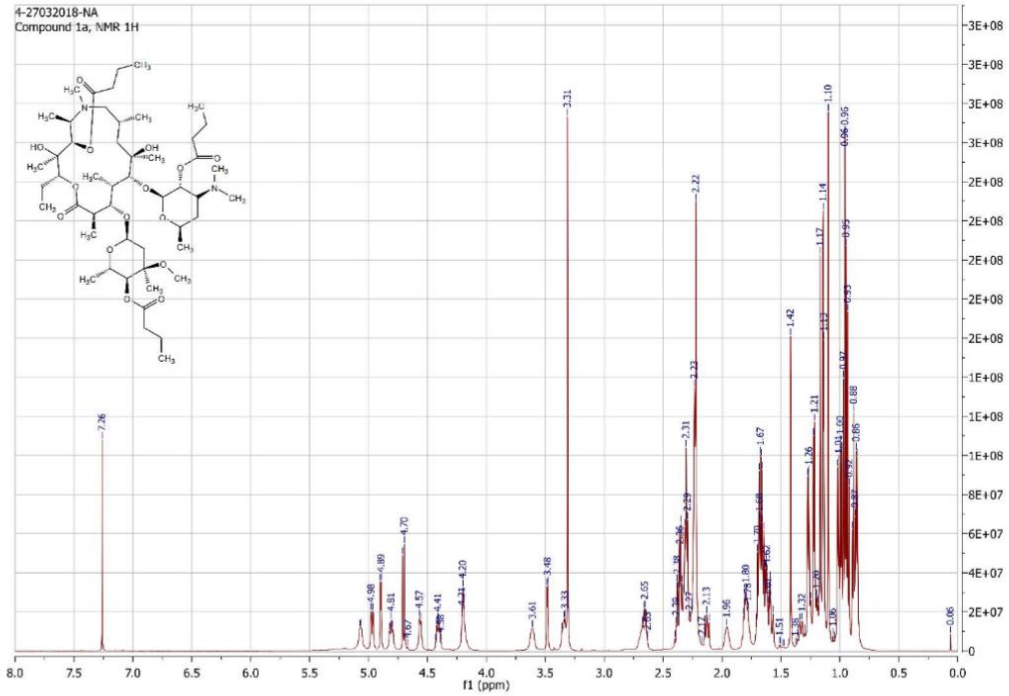

Figure 1. ^{1}H NMR of compound **1a**

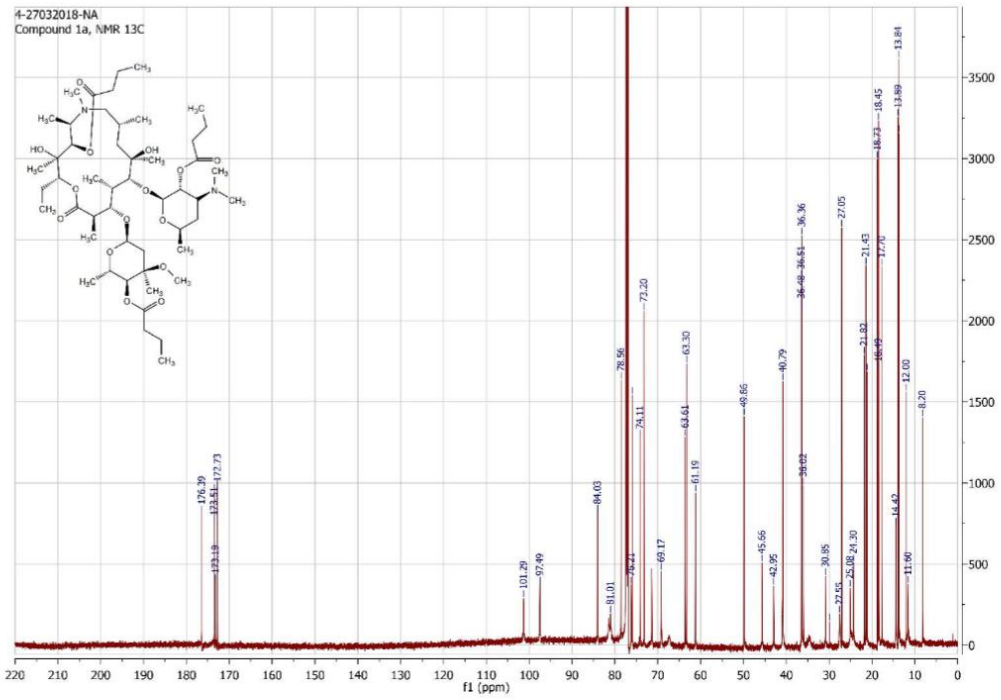

Figure 2. ^{13}C NMR of compound **1g**

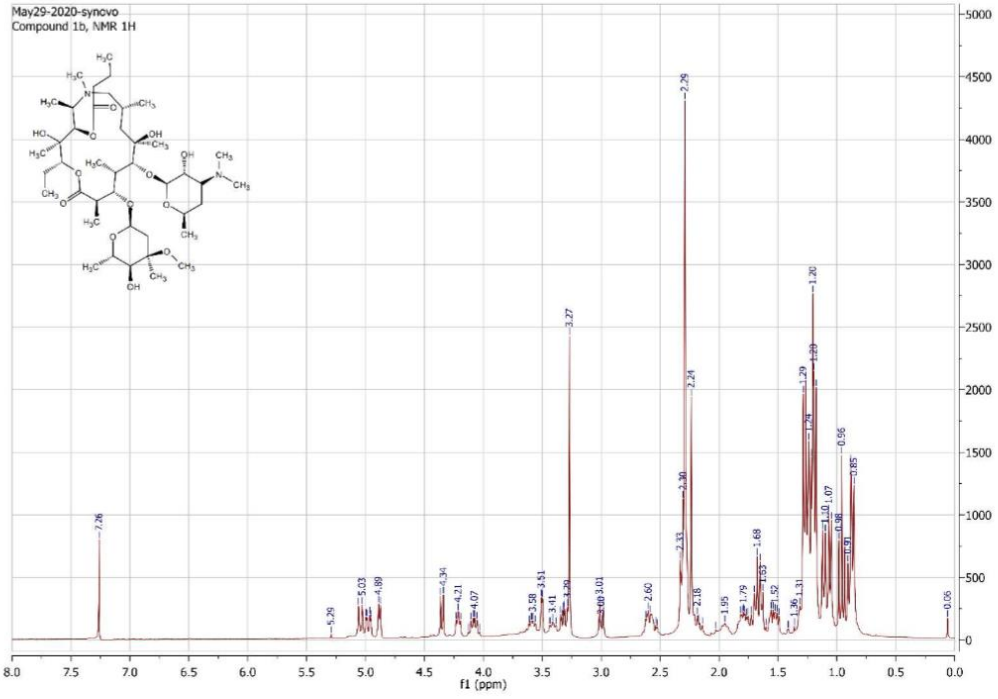

Figure 3. ^{1}H NMR of compound **1b**

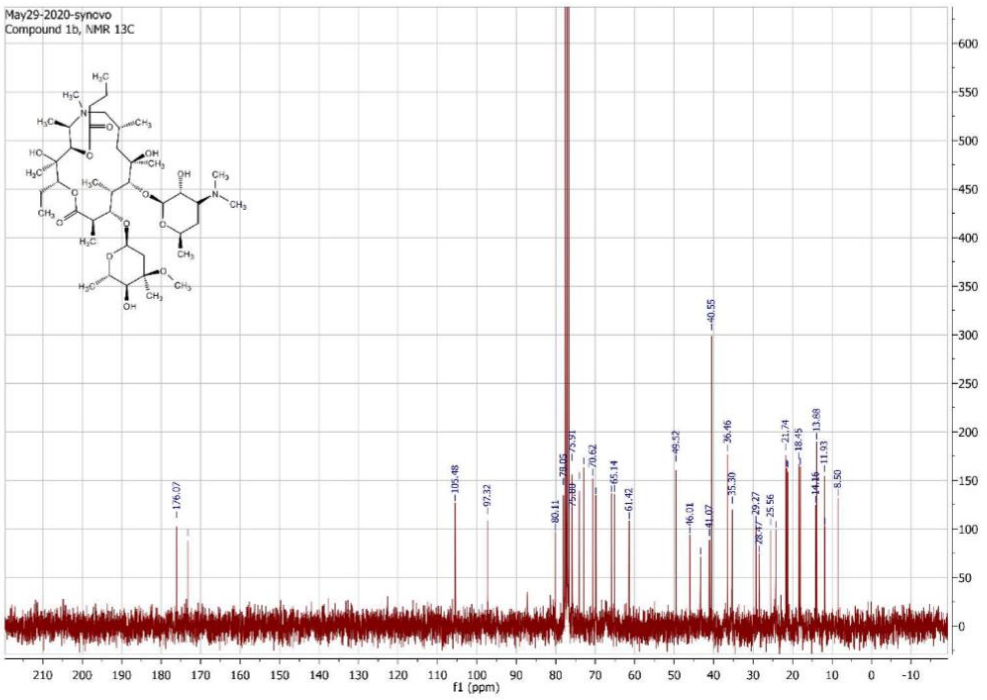

Figure 4. ^{13}C NMR of compound **1b**

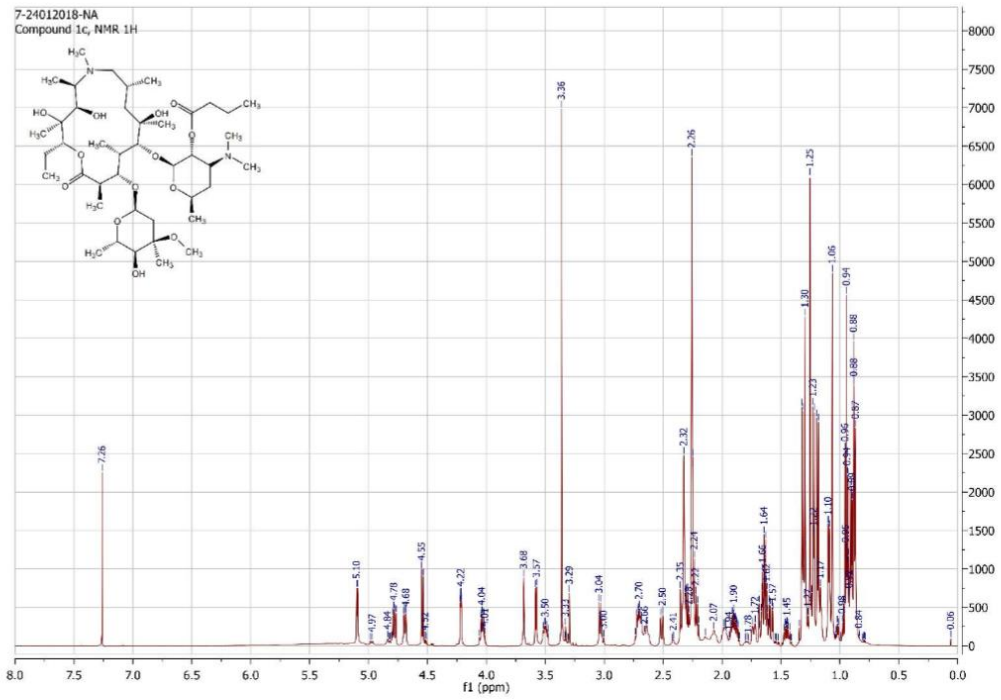

Figure 5. ^{1}H NMR of compound **1c**

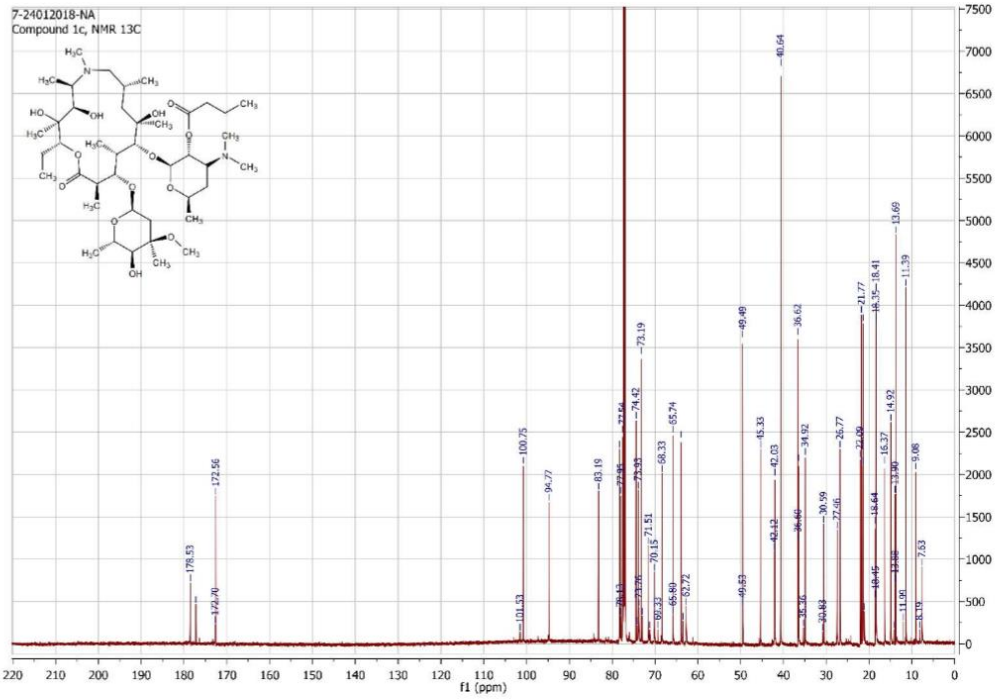

Figure 6. ^{13}C NMR of compound **1c**

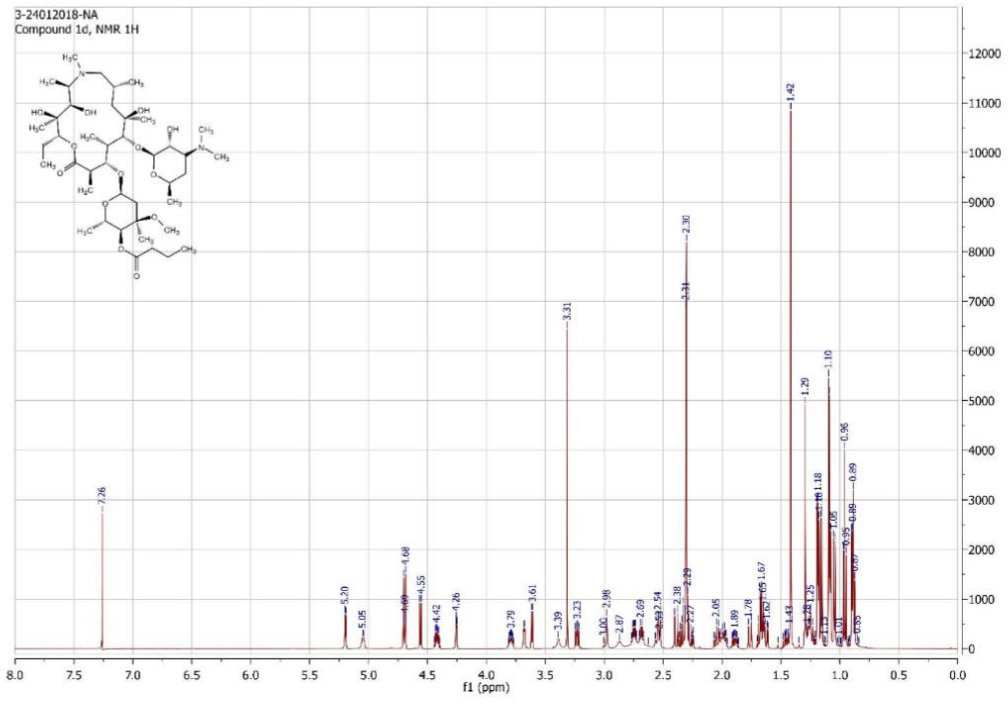

Figure 7. ^{1}H NMR of compound **1d**

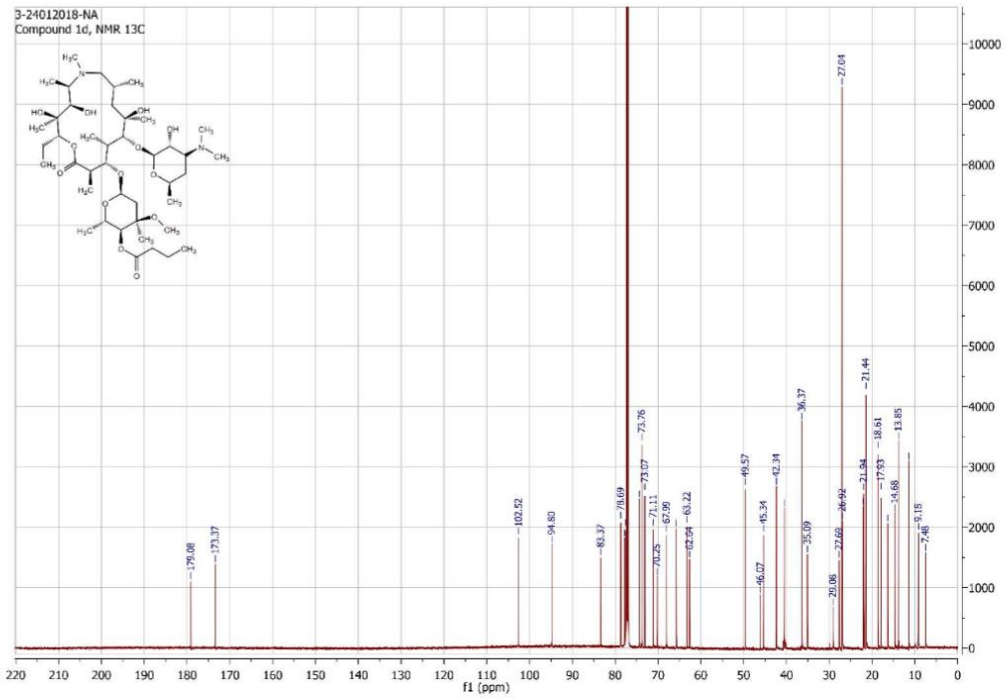

Figure 8. ^{13}C NMR of compound **1d**

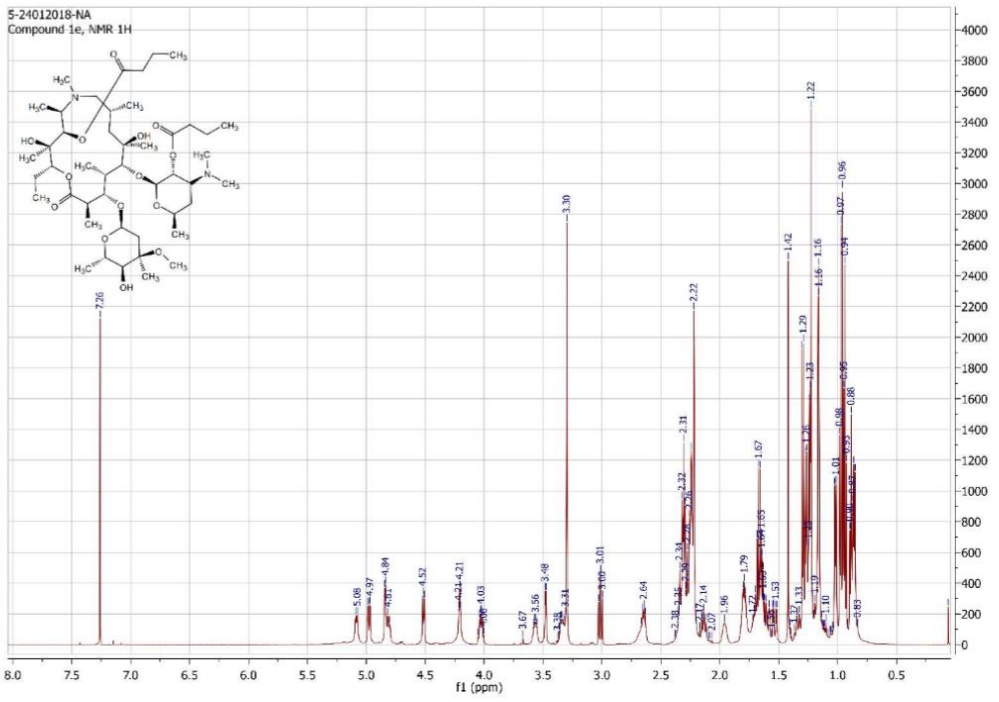

Figure 9. ^{1}H NMR of compound **1e**

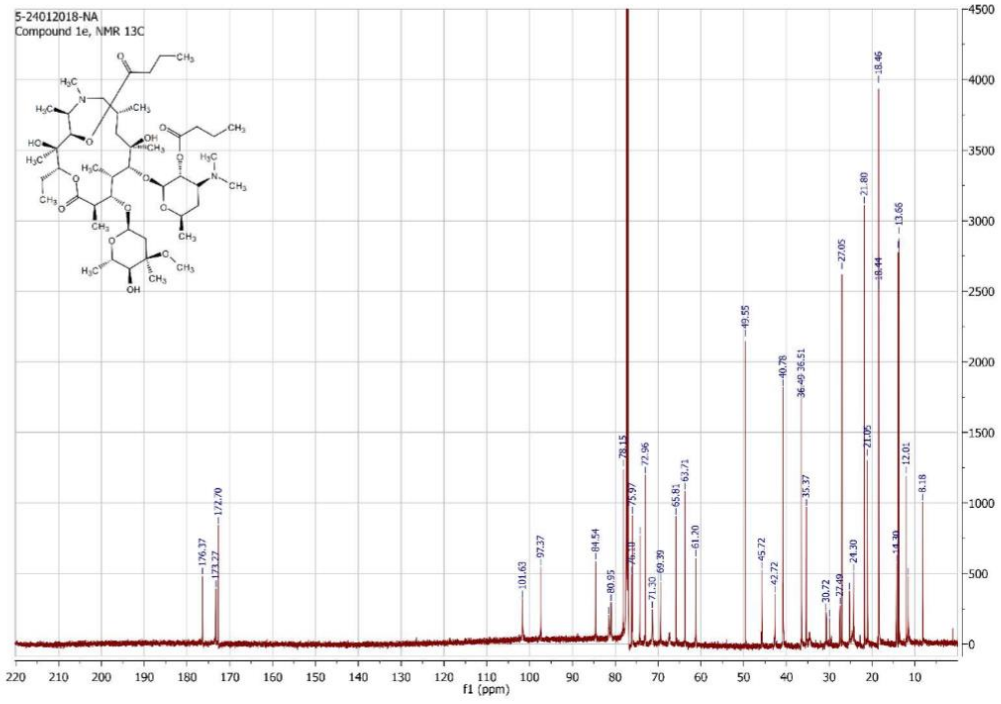

Figure 10. ^{13}C NMR of compound **1e**

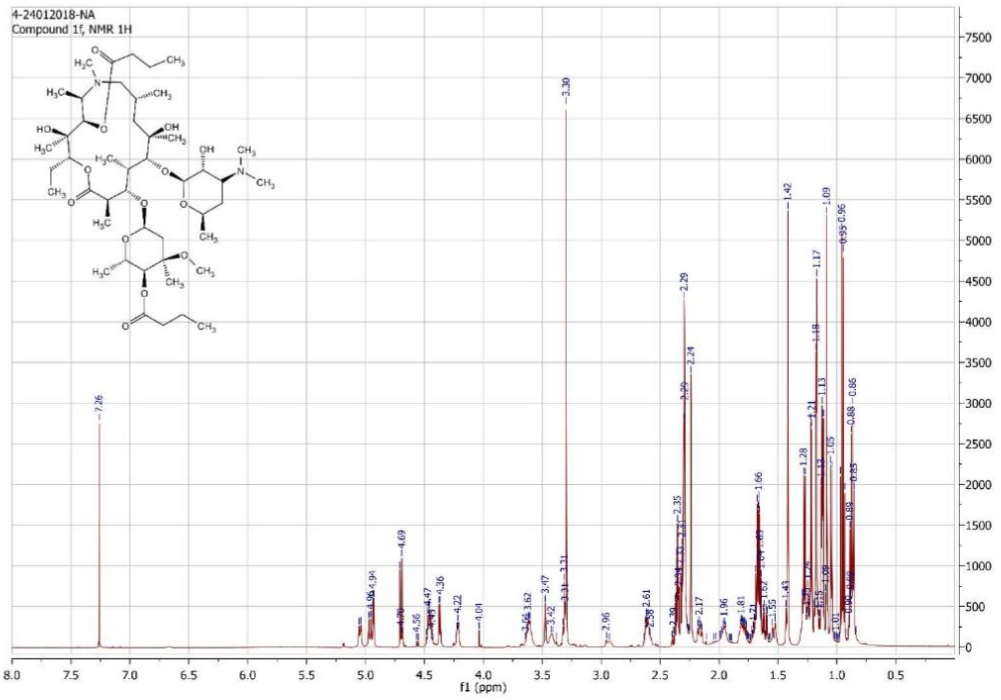

Figure 11. ^{1}H NMR of compound **1f**

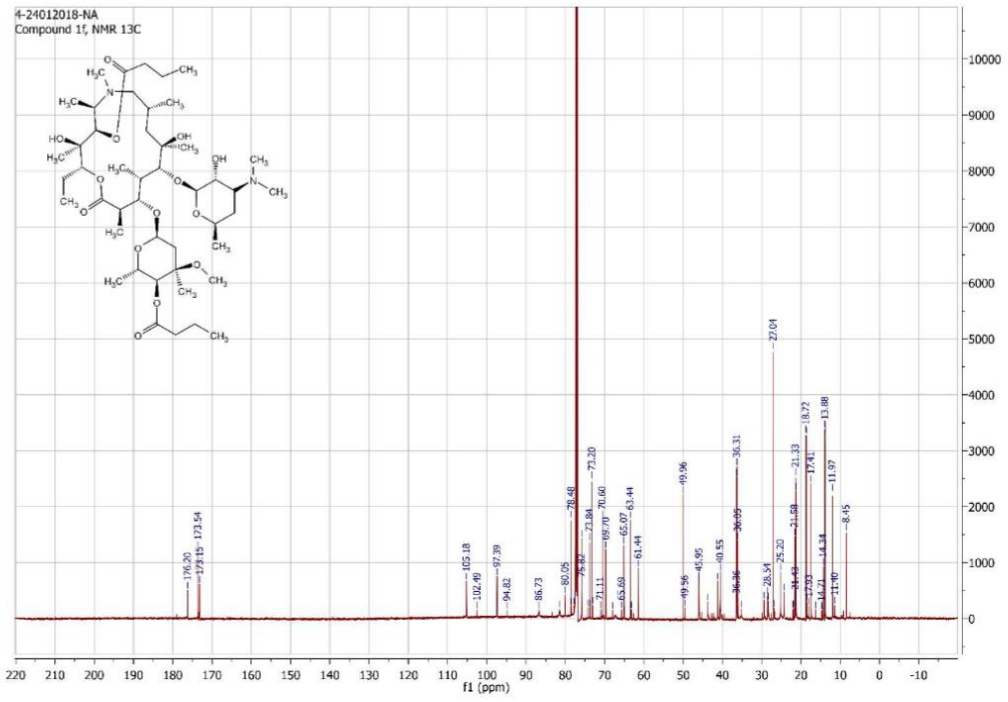

Figure 12. ^{13}C NMR of compound **1f**

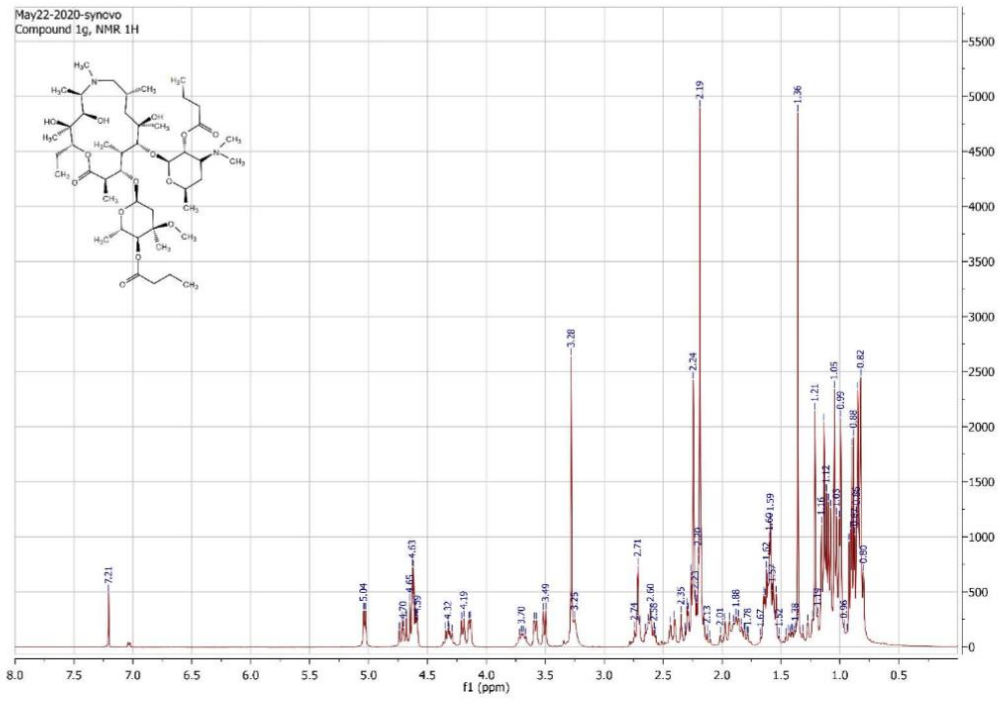

Figure 13. ^{1}H NMR of compound **1g**

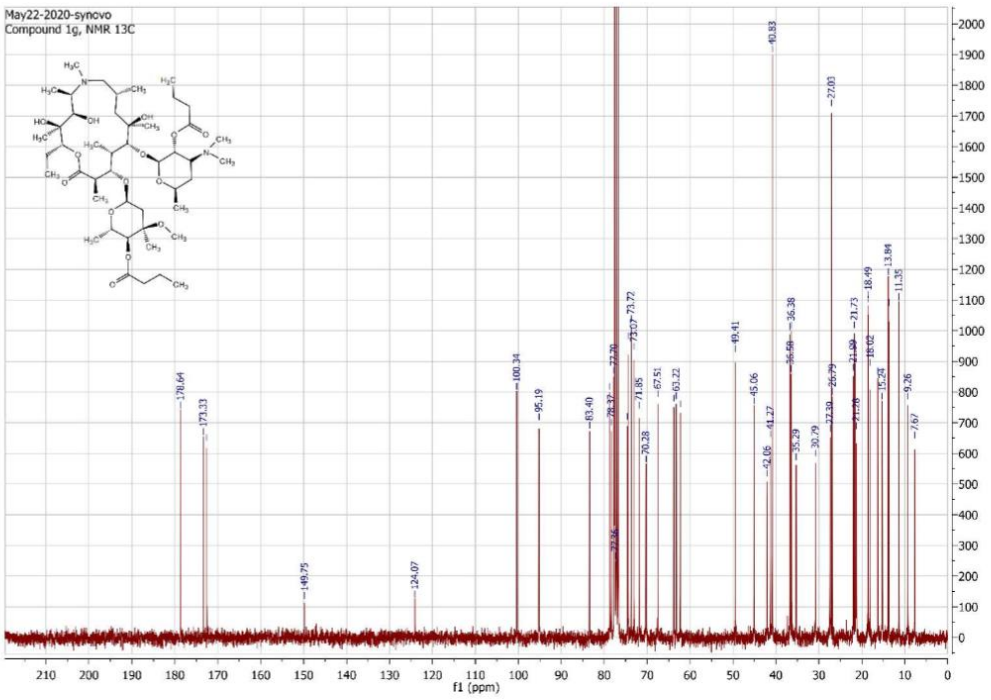

Figure 14. ^{13}C NMR of compound **1g**

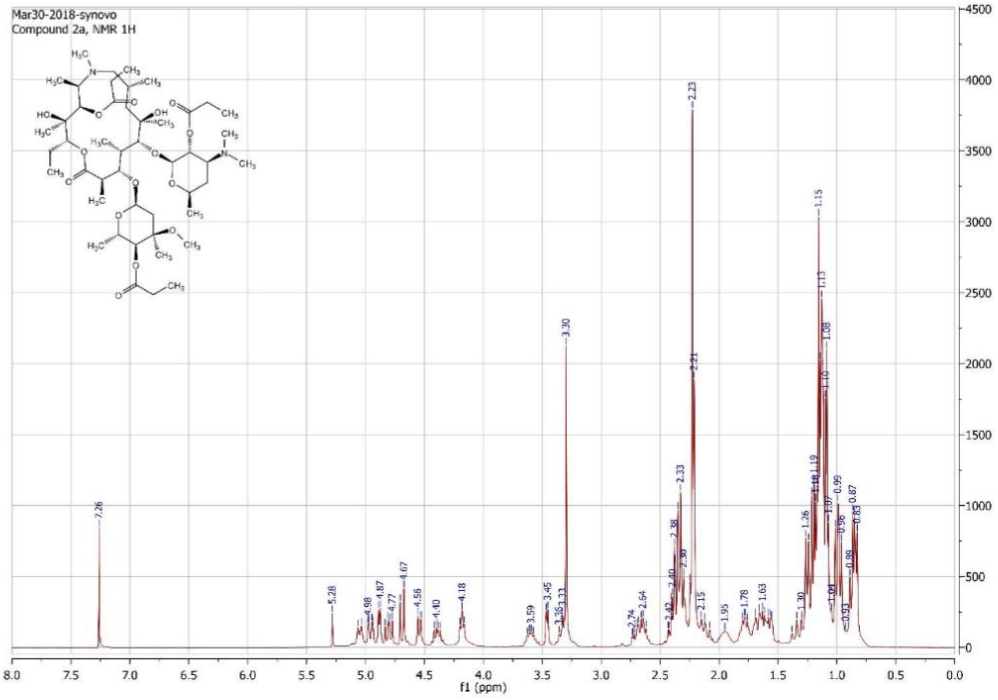

Figure 15. ^{1}H NMR of compound **2a**

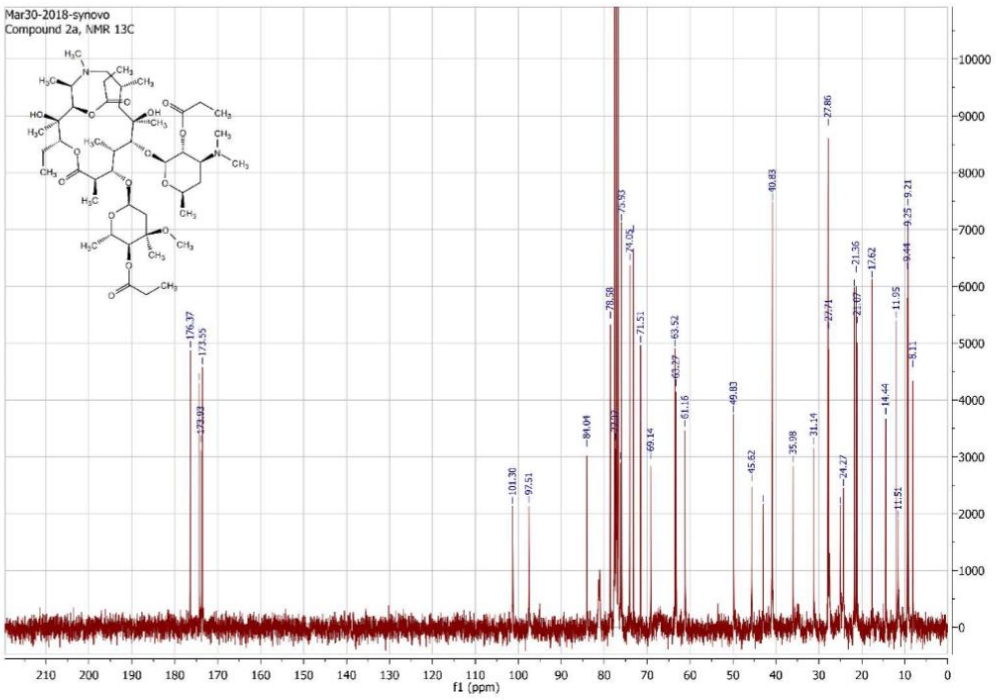

Figure 16. ^{13}C NMR of compound **2a**

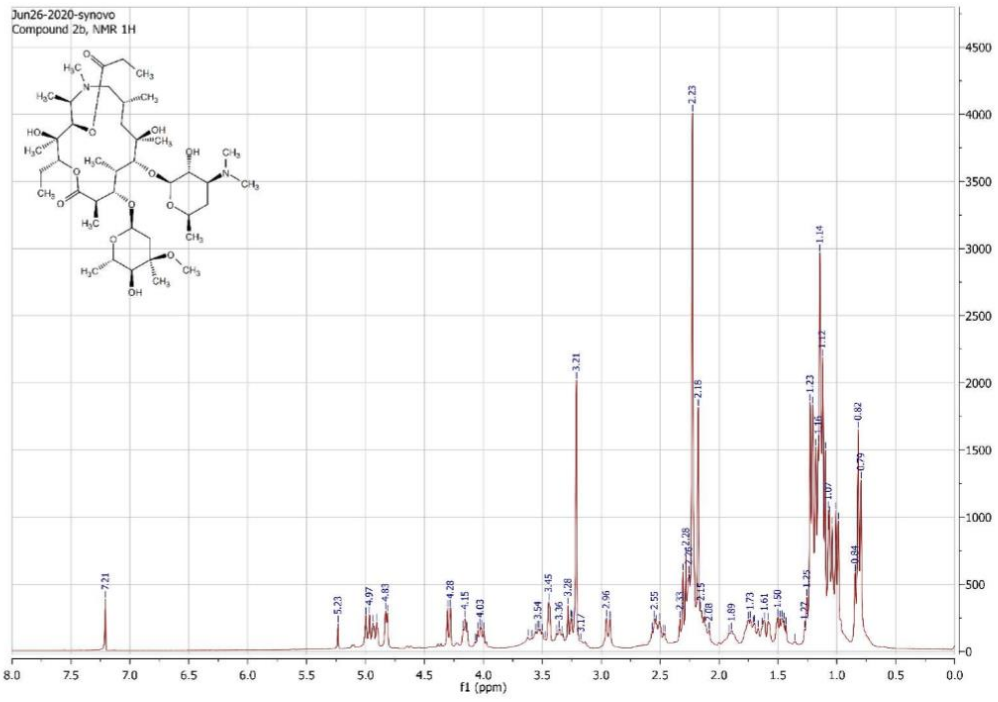

Figure 17. ^{1}H NMR of compound **2b**

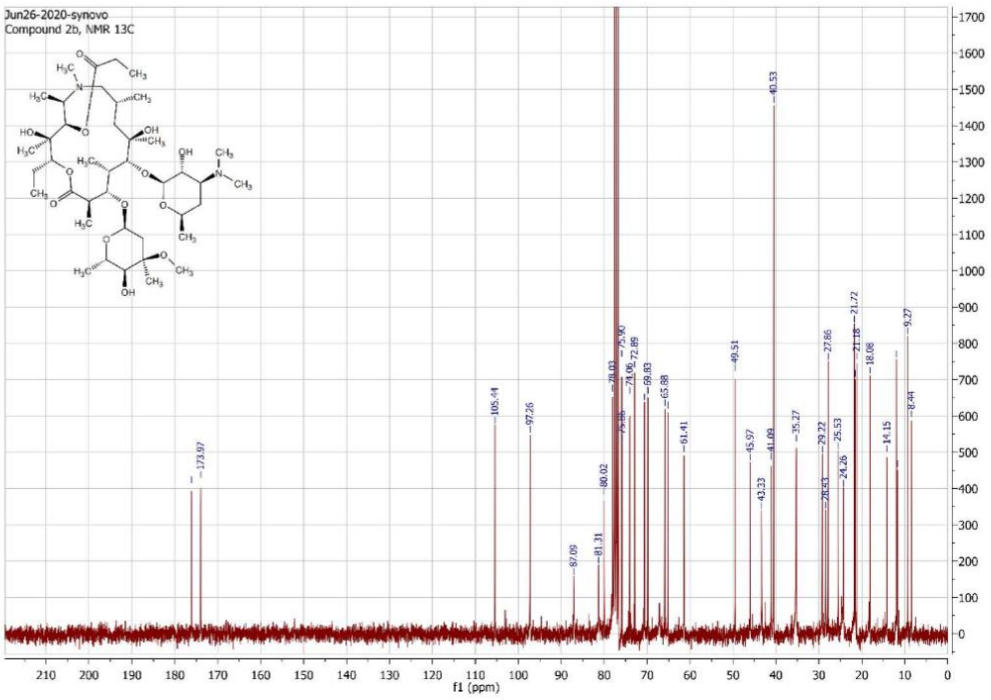

Figure 18. ^{13}C NMR of compound **2b**

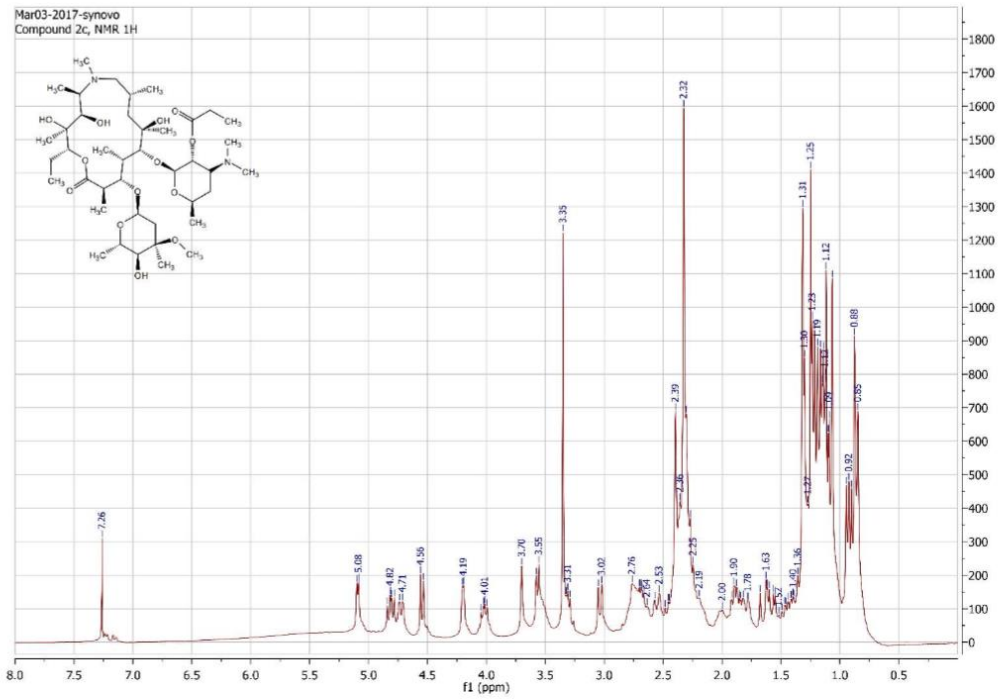

Figure 19. ^{1}H NMR of compound **2c**

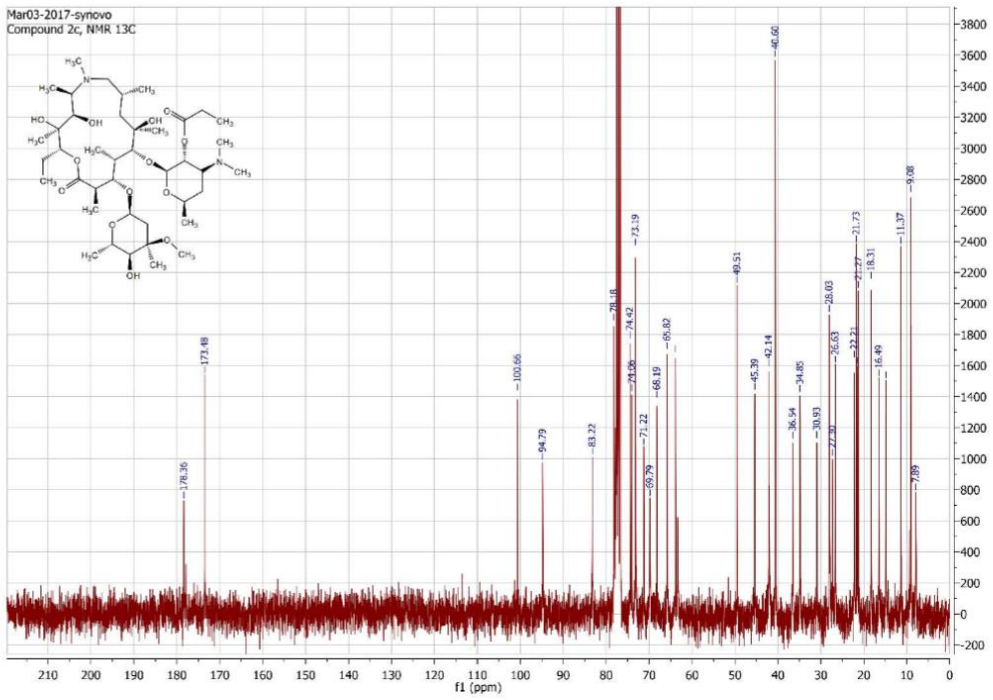

Figure 20. ^{13}C NMR of compound **2c**

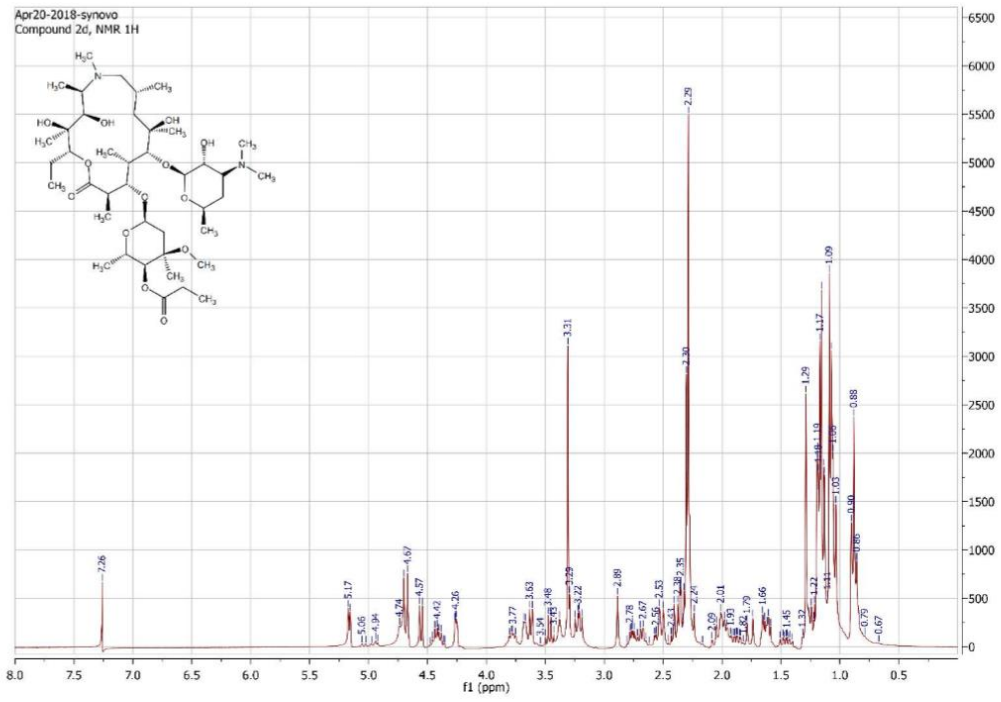

Figure 21. ^{1}H NMR of compound **2d**

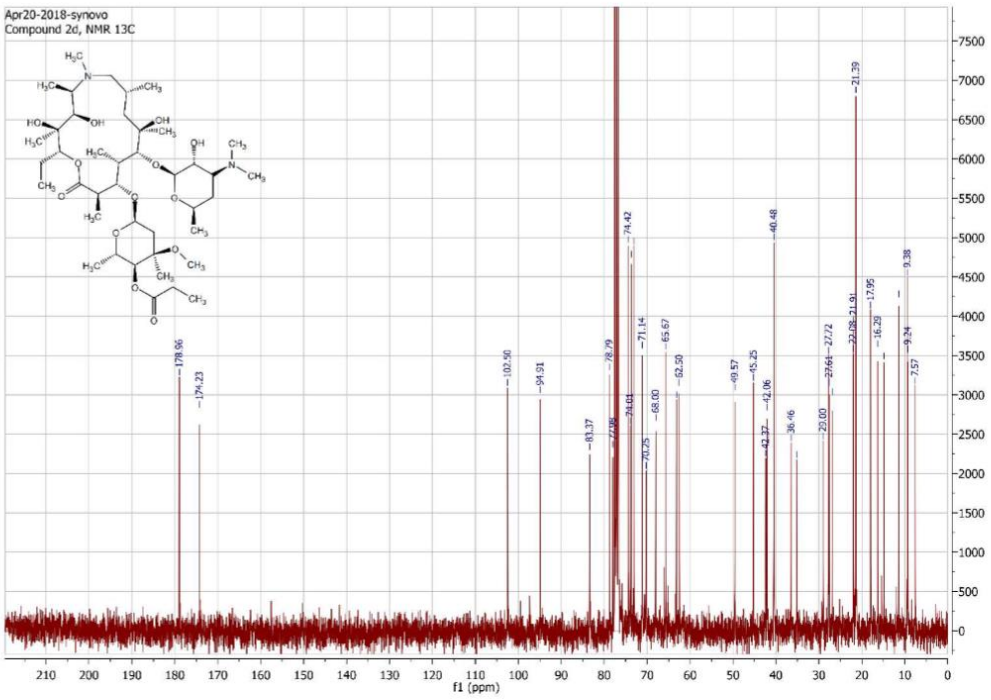

Figure 22. ^{13}C NMR of compound **2d**

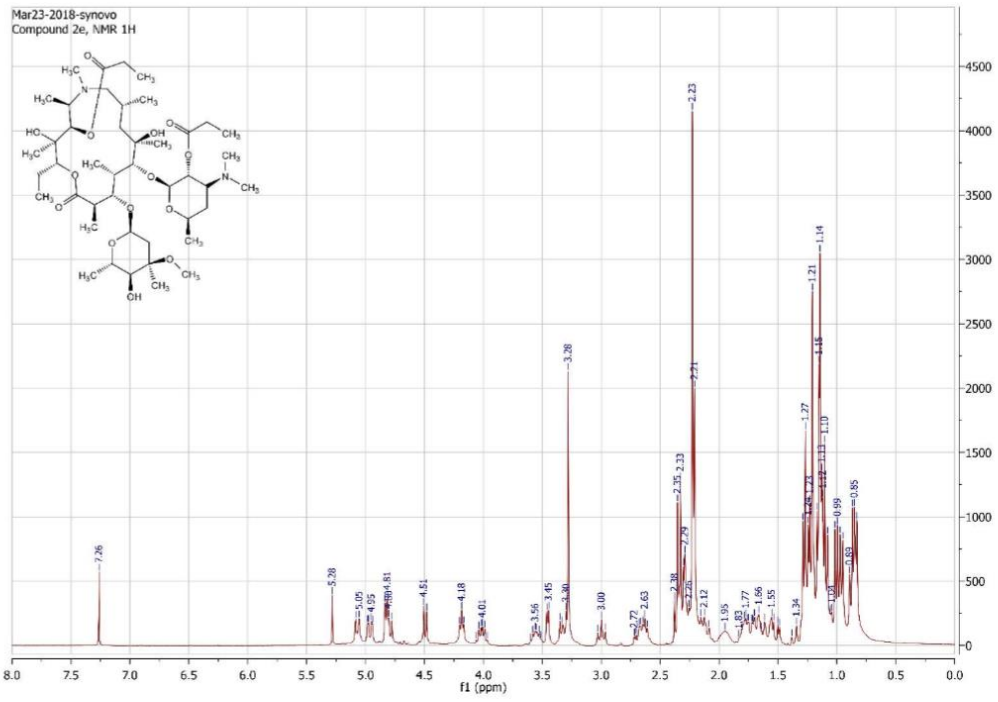

Figure 23. ^{1}H NMR of compound **2e**

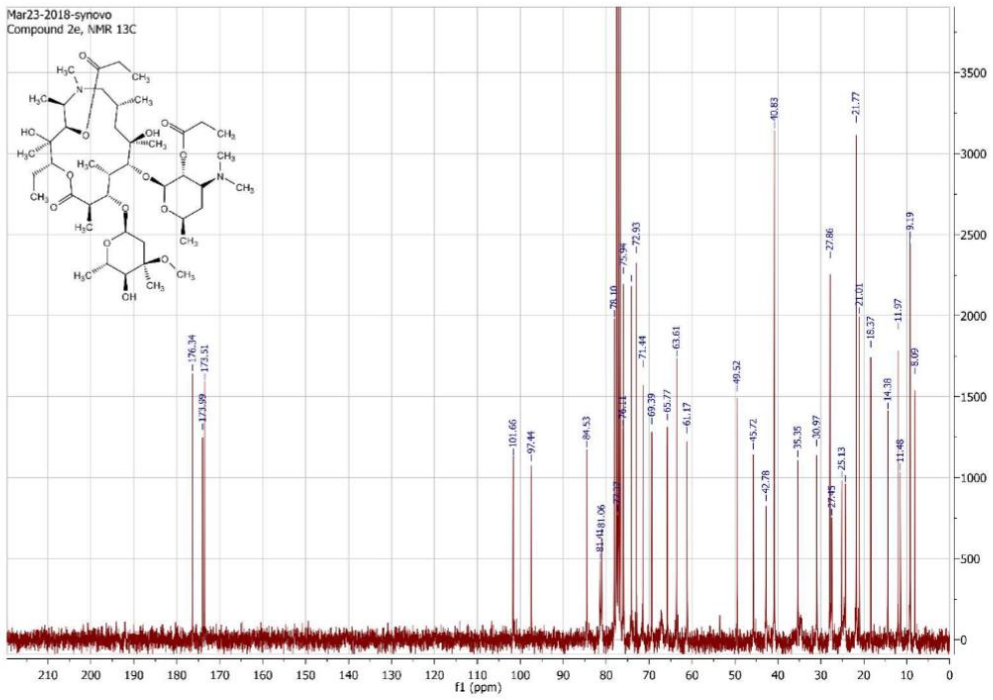

Figure 24. ^{13}C NMR of compound **2e**

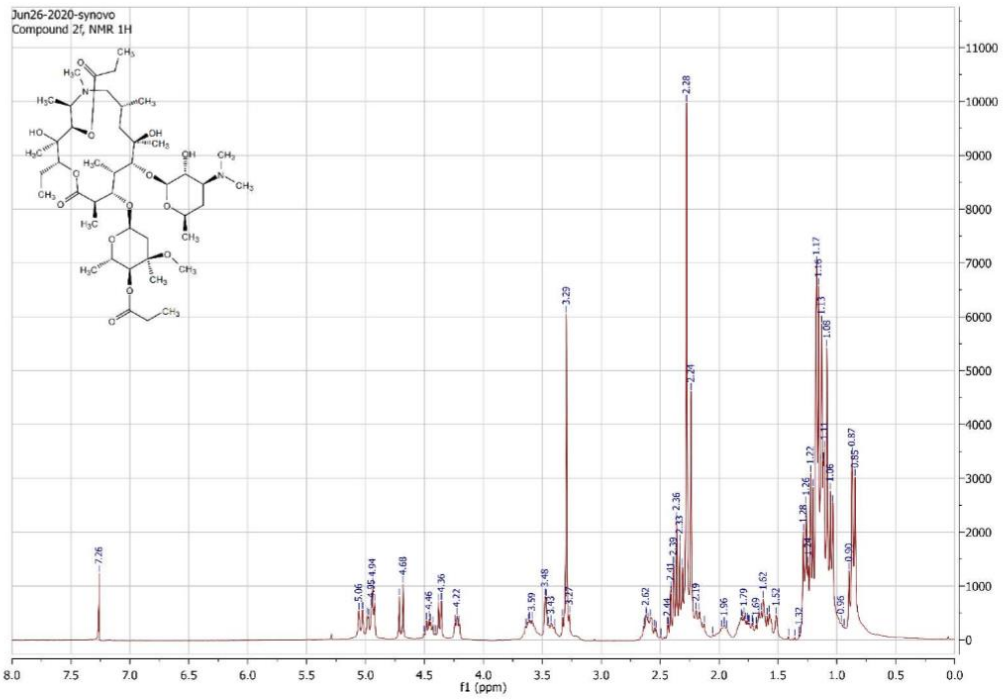

Figure 25. ^{1}H NMR of compound **2f**

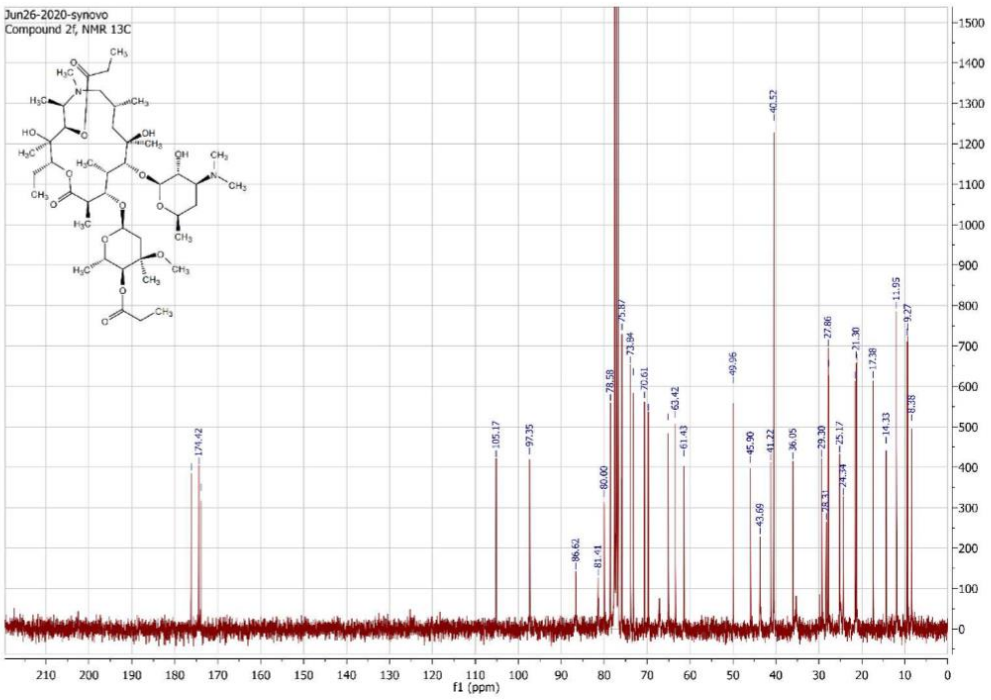

Figure 26. ^{13}C NMR of compound **2f**

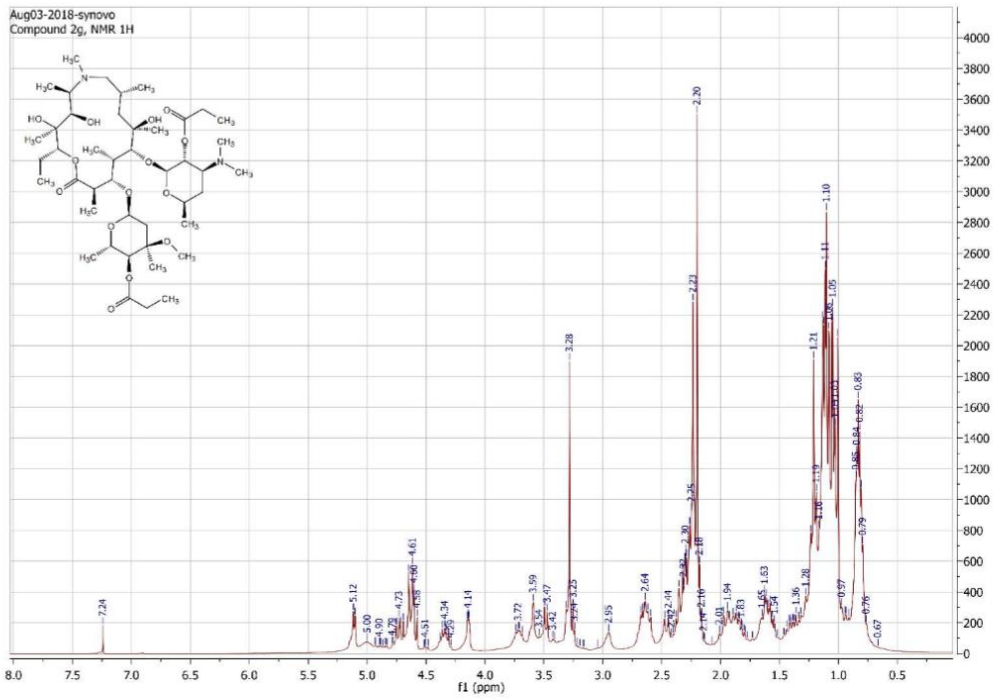

Figure 27. ^{1}H NMR of compound **2g**

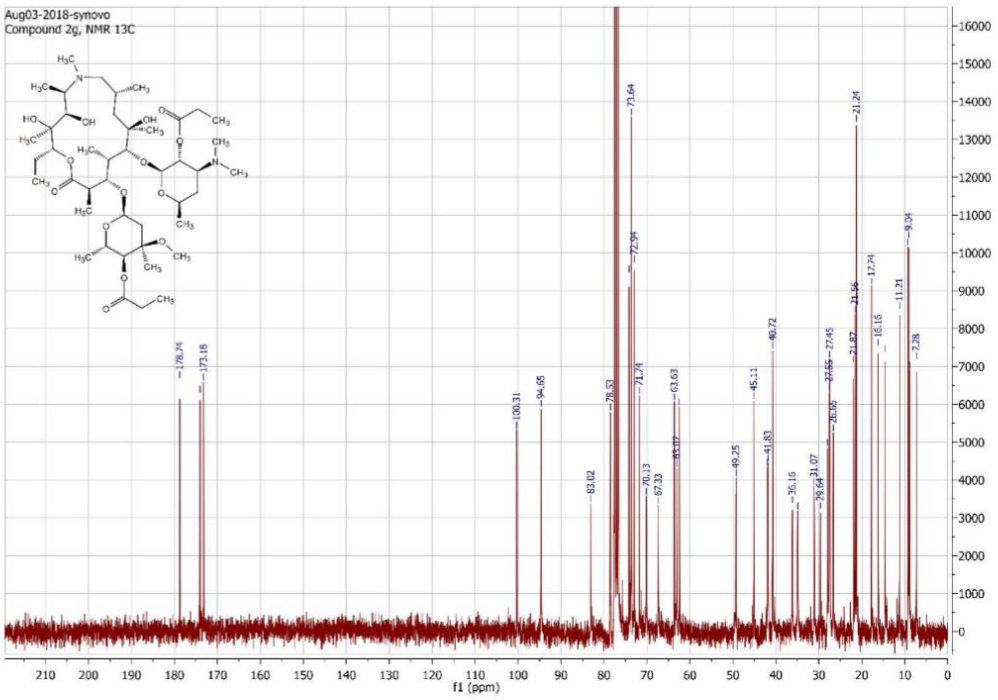

Figure 28. ^{13}C NMR of compound **2g**

HSQC data

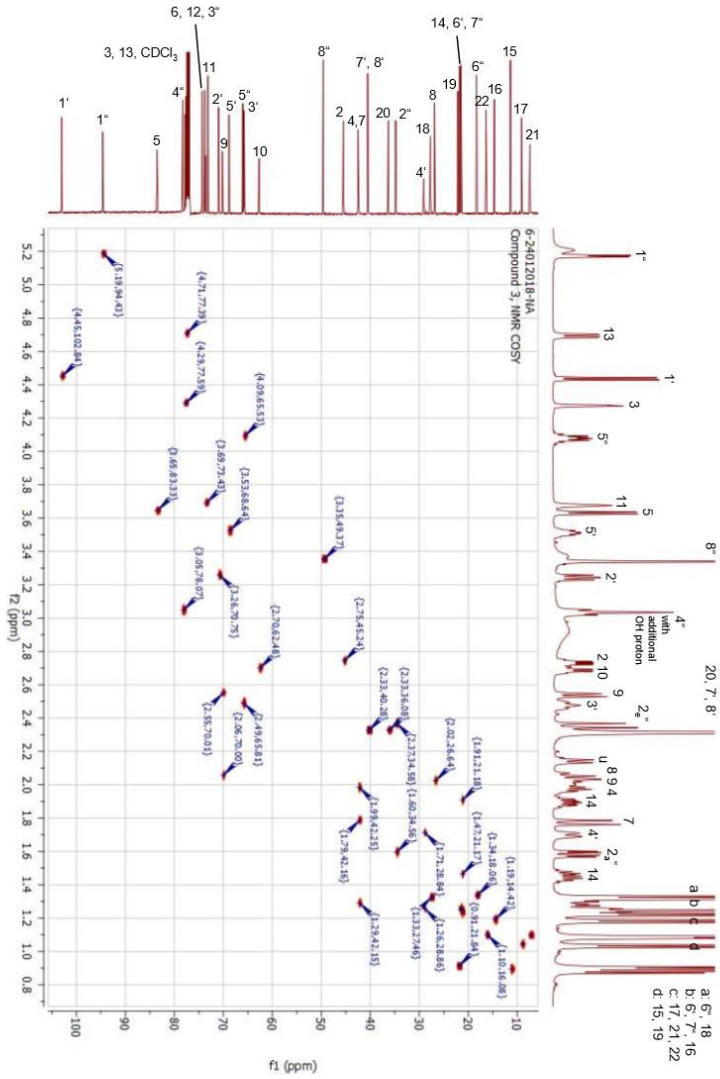

Figure 29. HSQC NMR of compound **3**

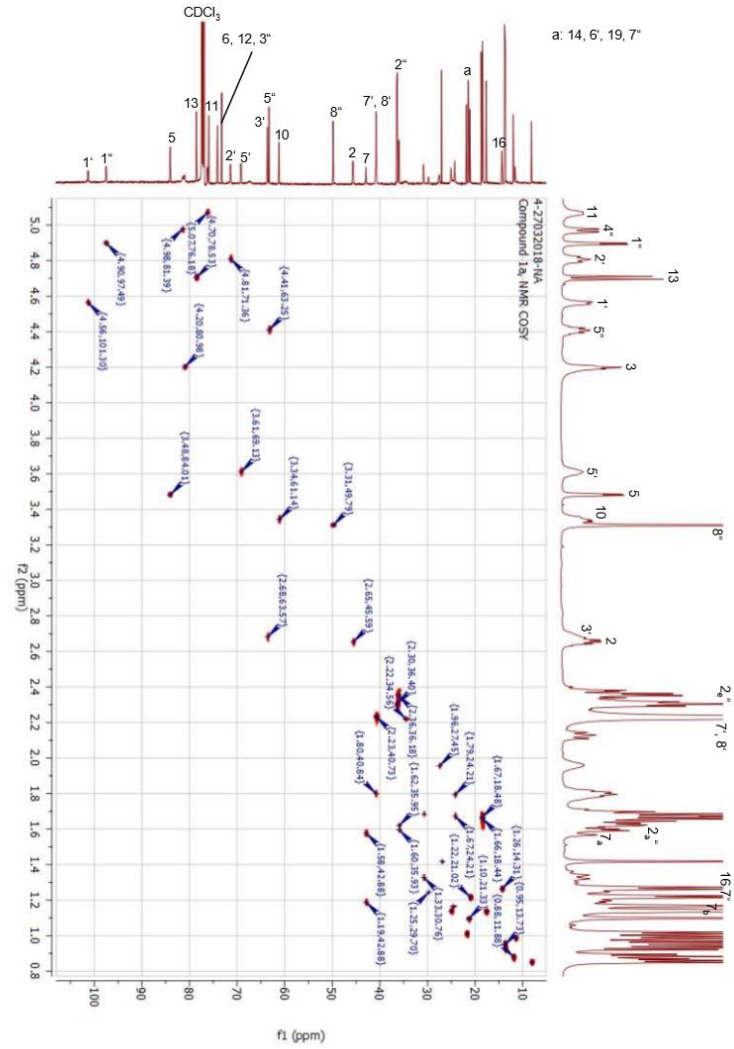

Figure 30. HSQC NMR of compound **1a**

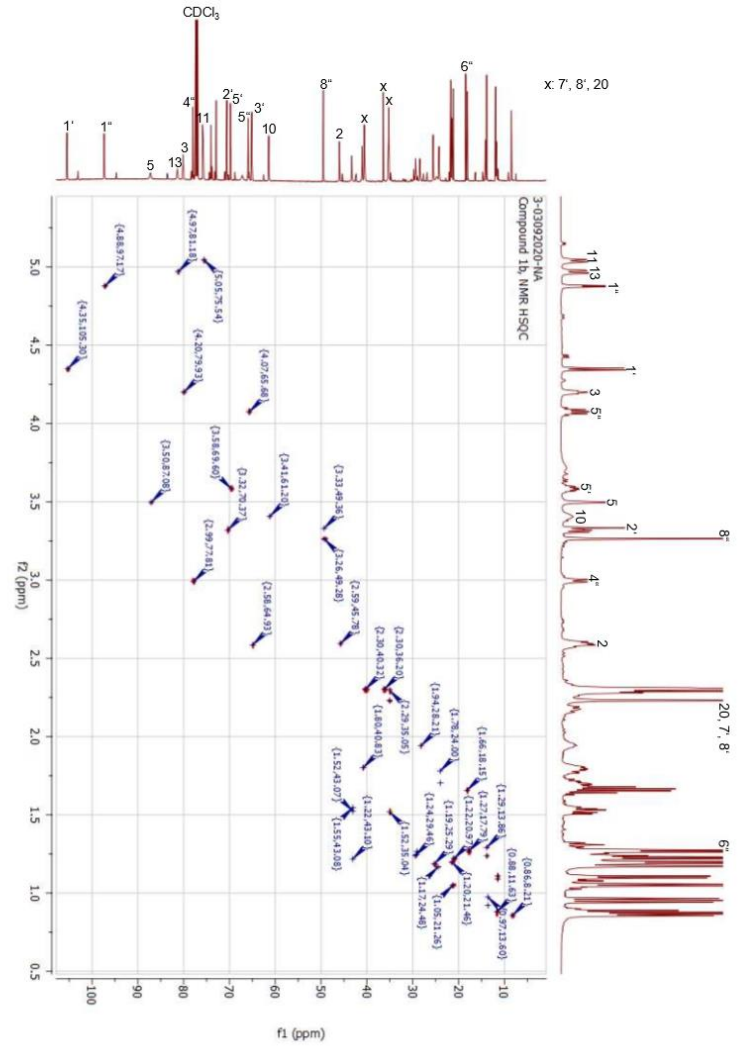

Figure 31. HSQC NMR of compound **1b**

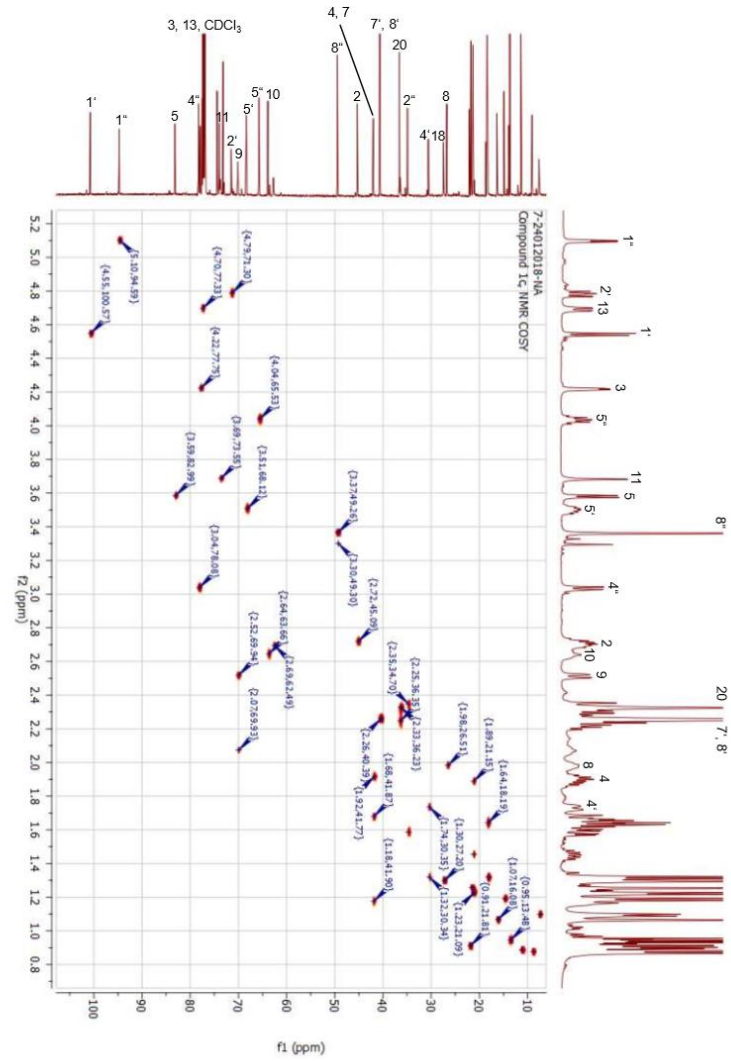

Figure 32. HSQC NMR of compound **1c**

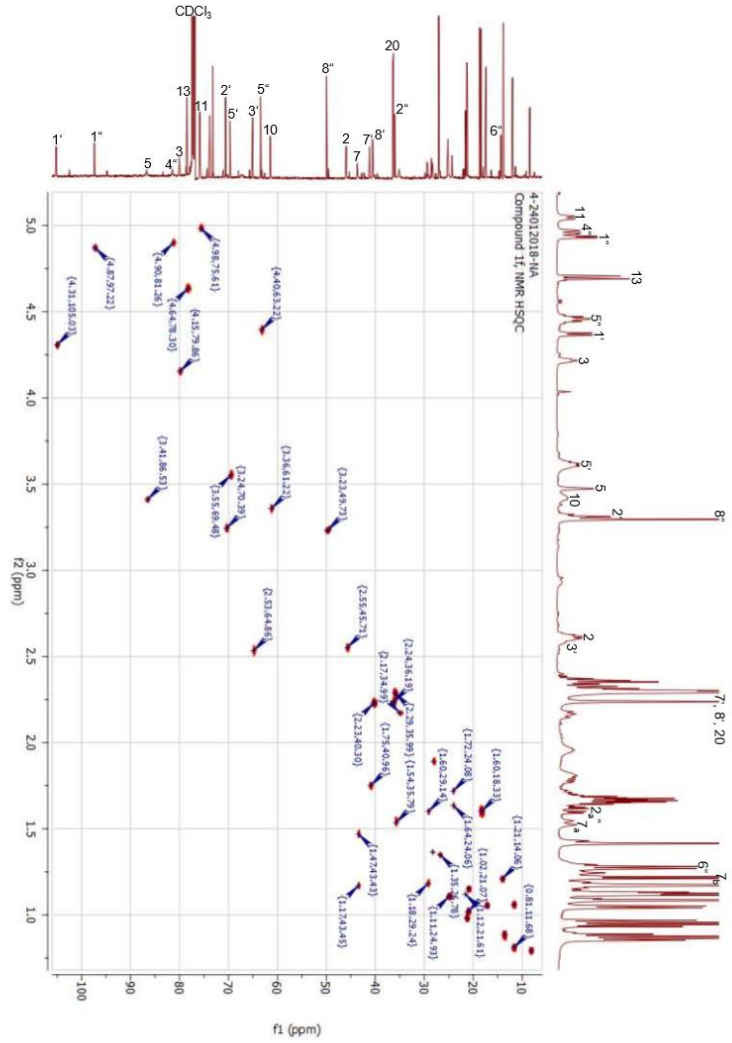

Figure 33. HSQC NMR of compound **1f**

H H COSY data

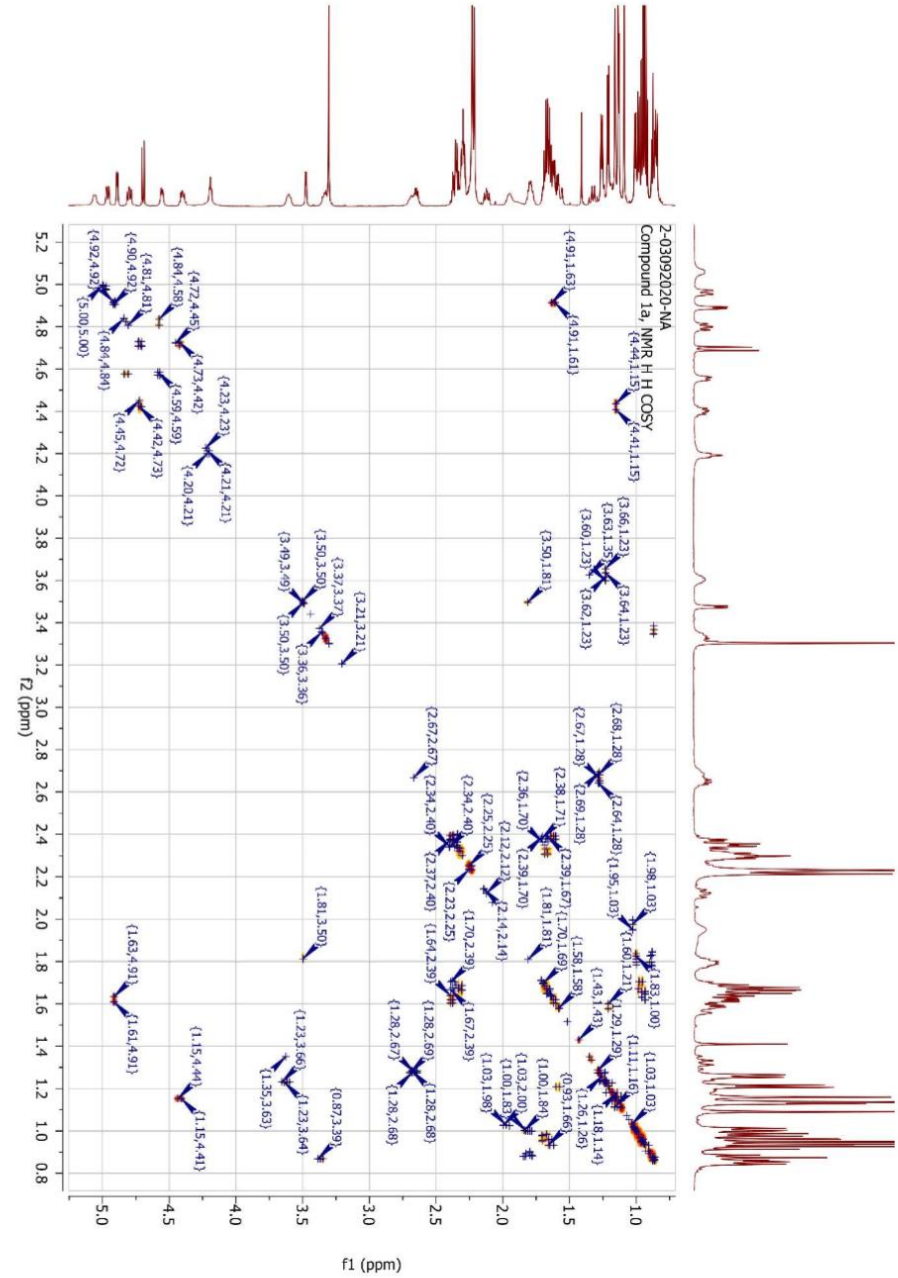

Figure 34. H H COSY NMR of compound **1a**

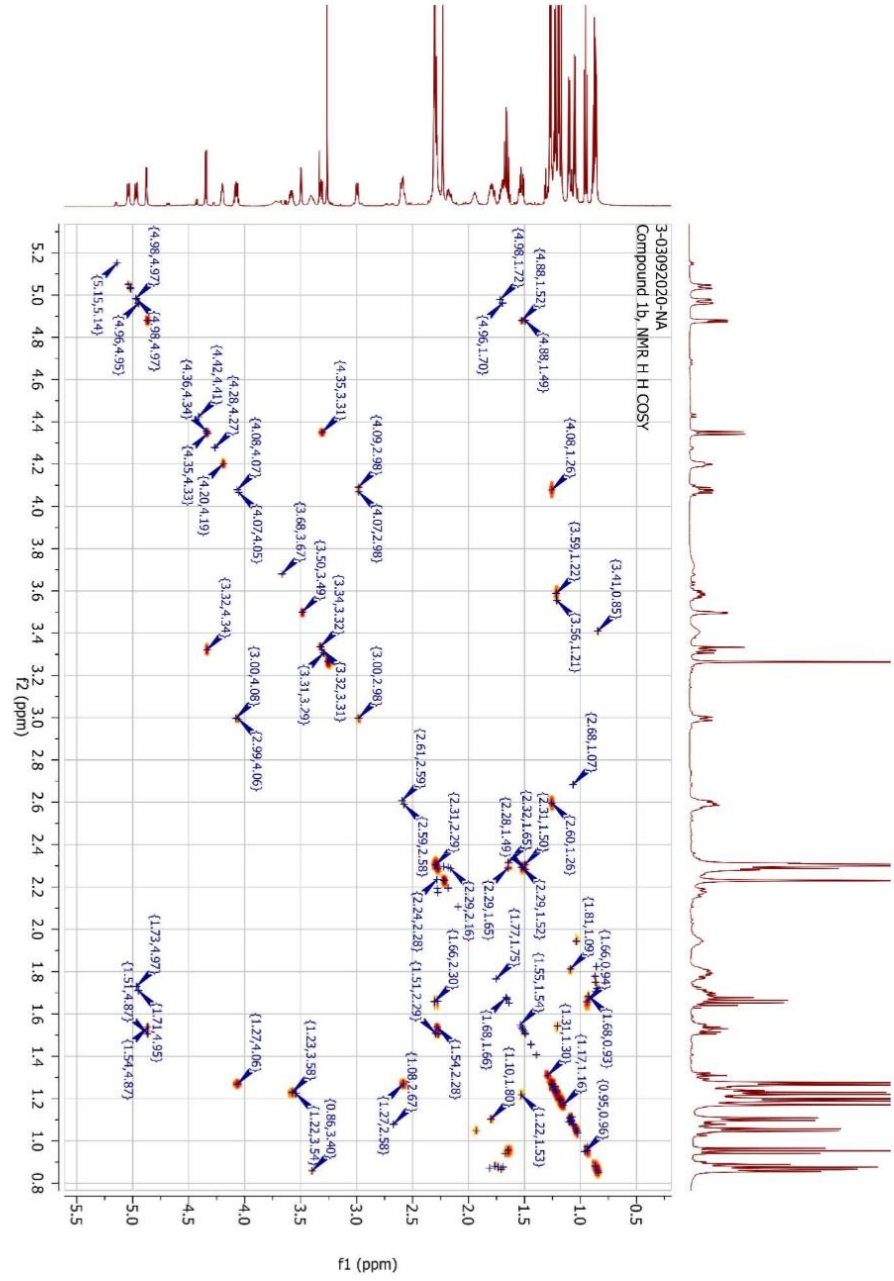

Figure 35. H H COSY NMR of compound **1b**

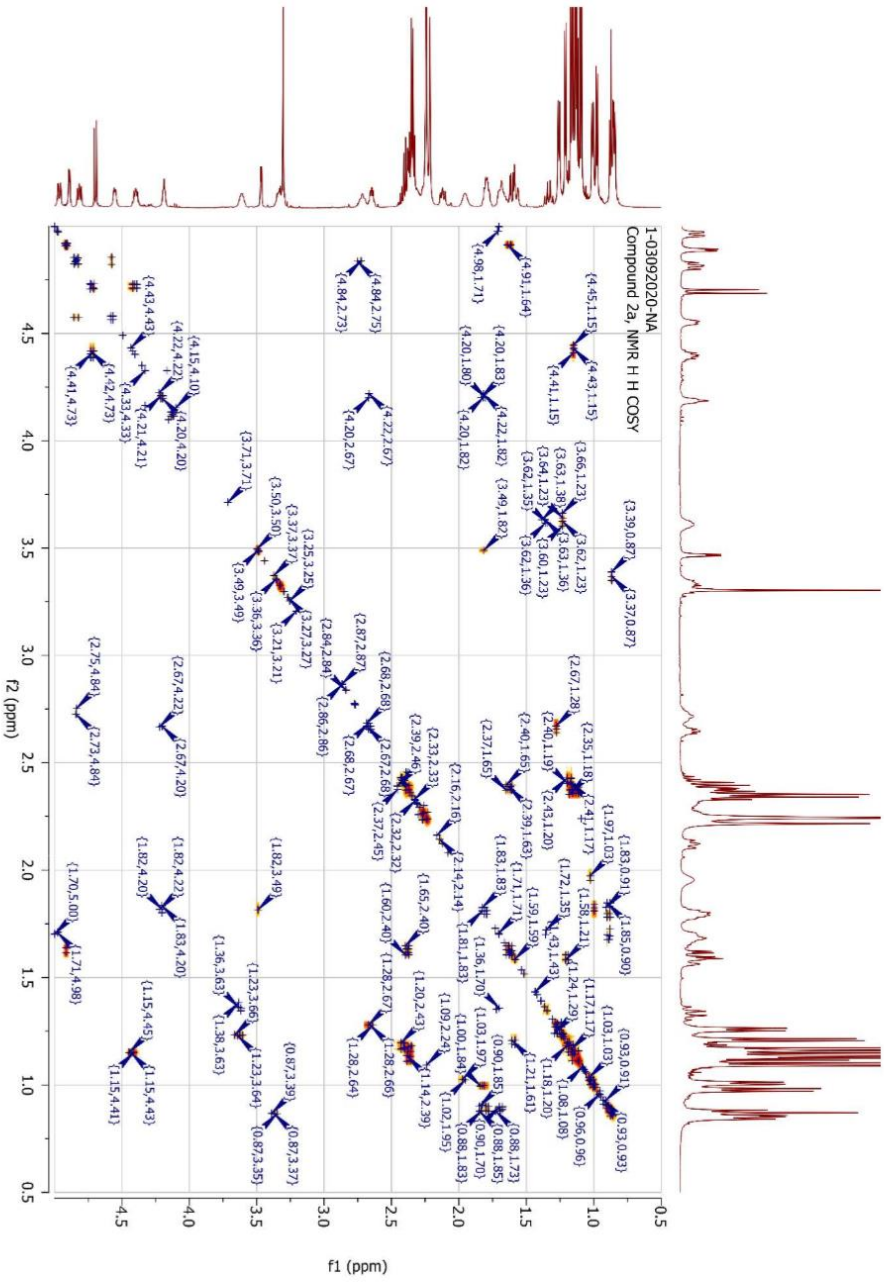

Figure 36. H H COSY NMR of compound **2a**

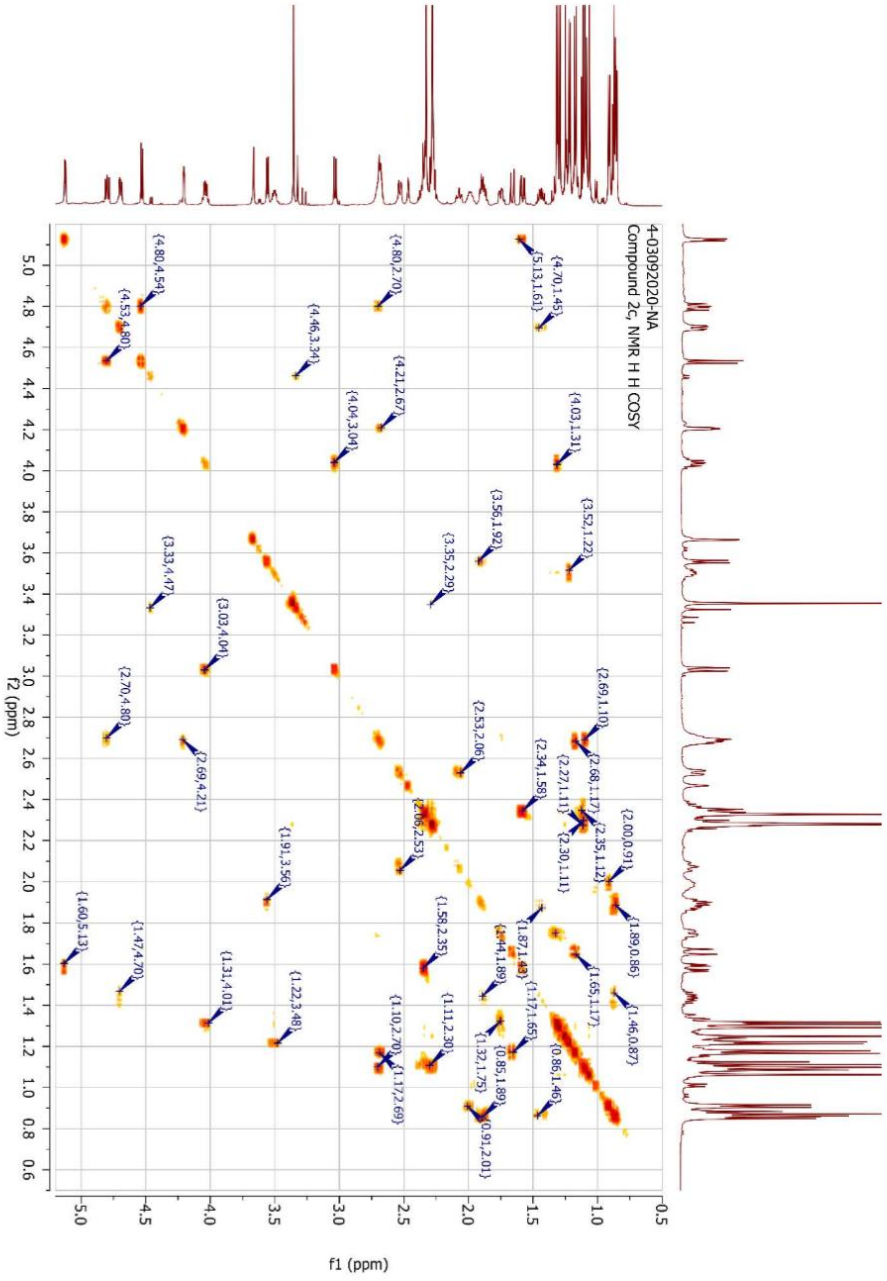

Figure 37. H H COSY NMR of compound **2c**

Metabolism schemes

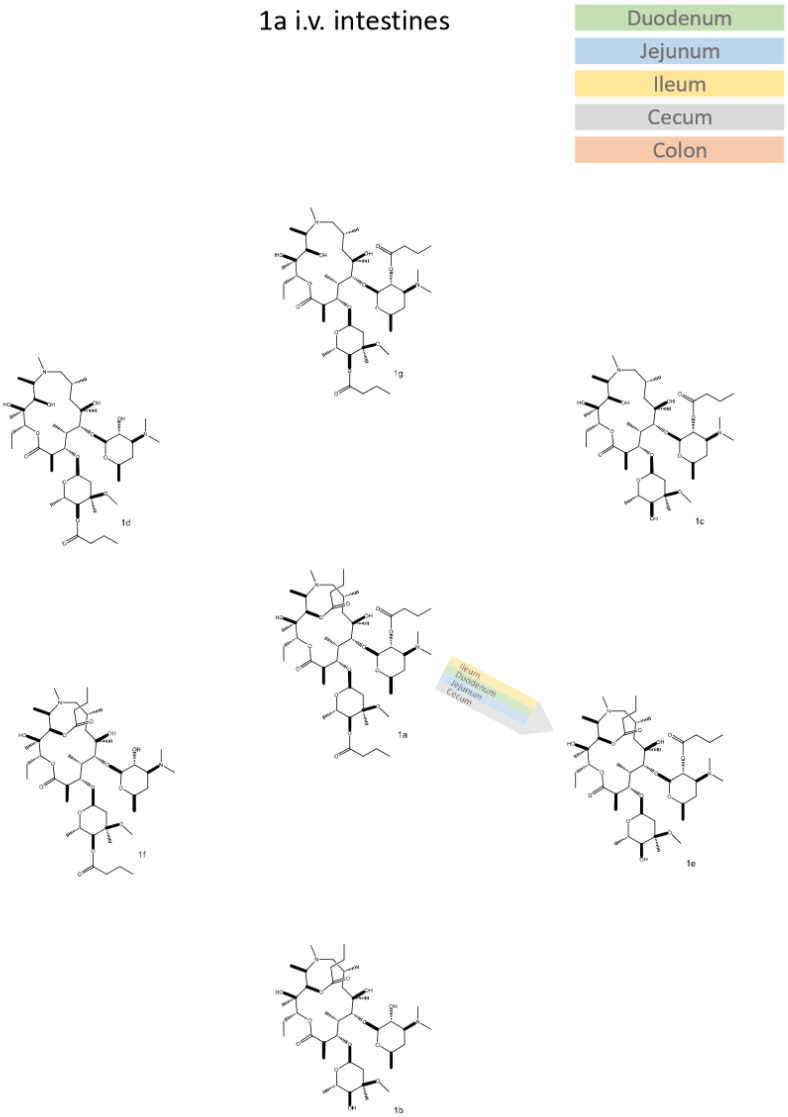

Figure 38. Schematic representations of pharmacokinetic data of **1a** in intestine organs and via intravenous route

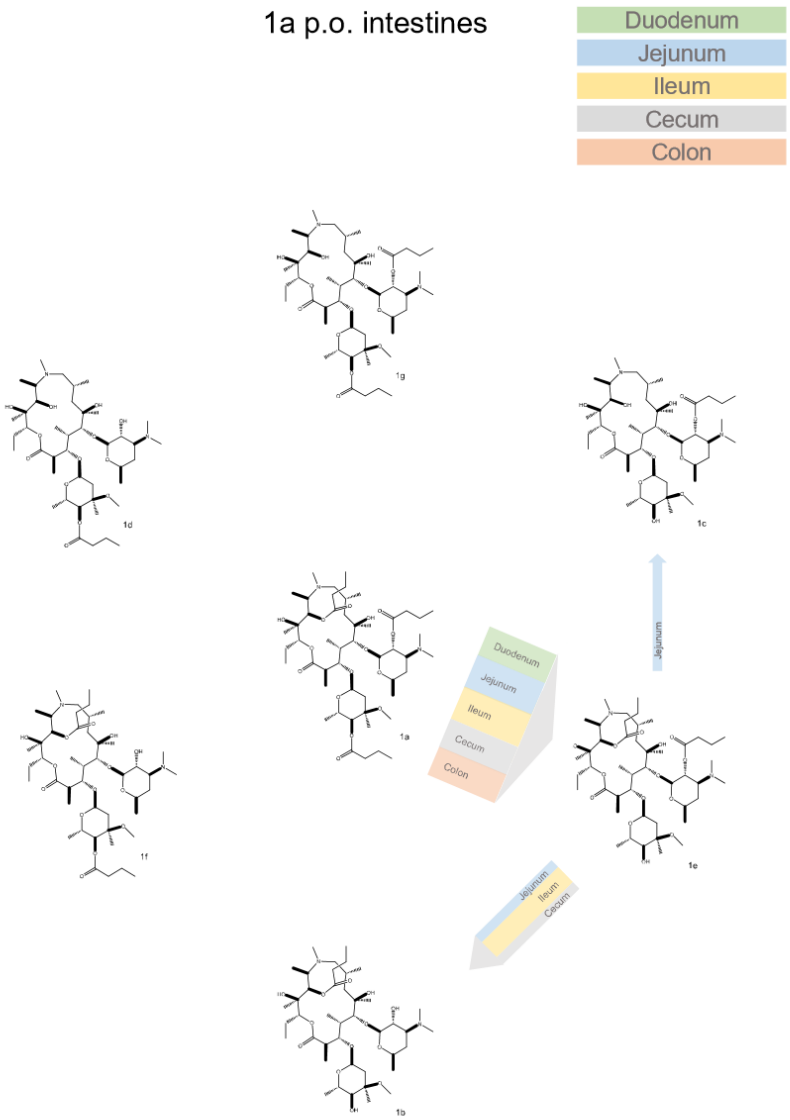

Figure 39. Schematic representations of pharmacokinetic data of **1a** in intestine organs and via oral route

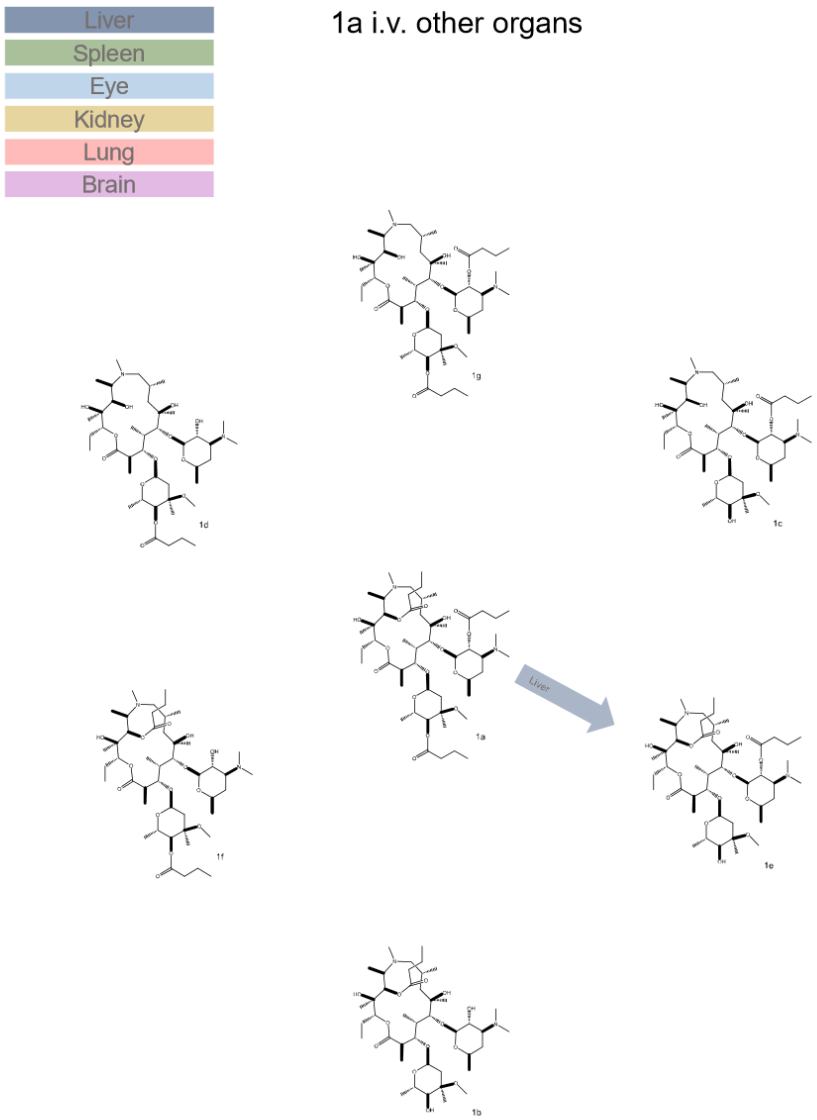

Figure 40. Schematic representations of pharmacokinetic data of **1a** in different organs and via intravenous route

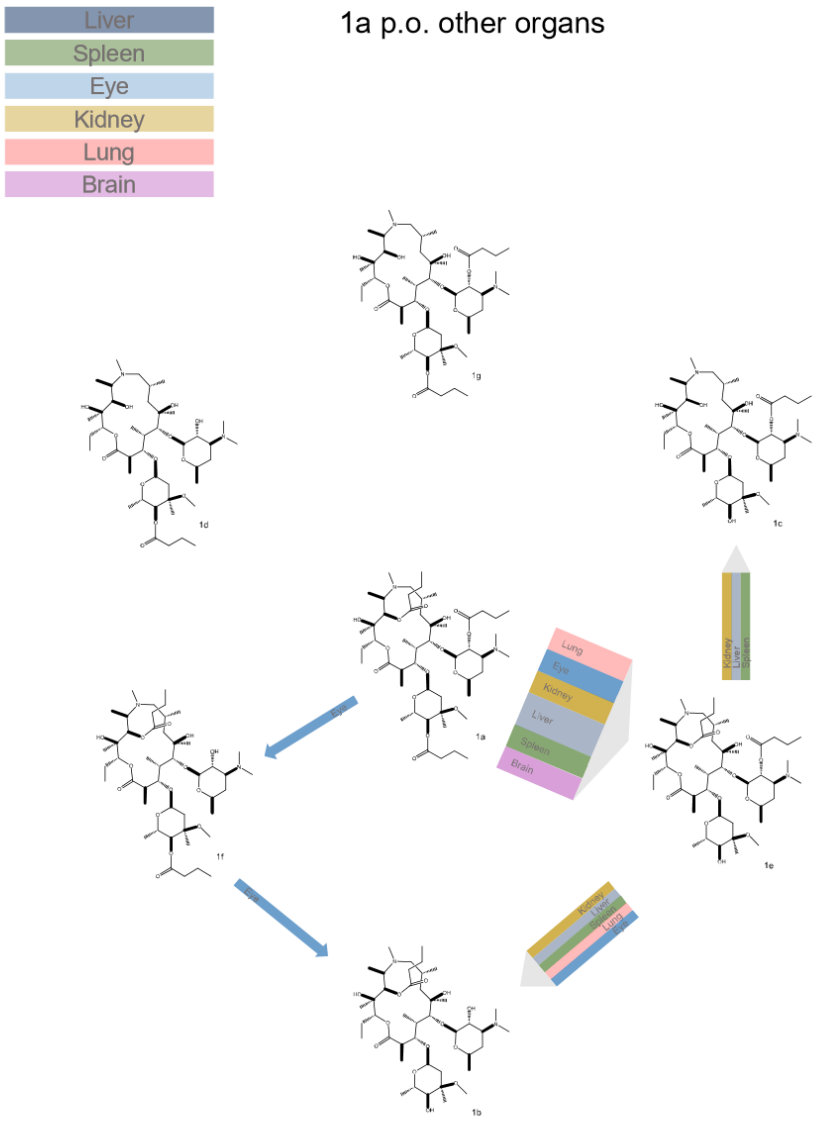

Figure 41. Schematic representations of pharmacokinetic data of **1a** in different organs and via oral route

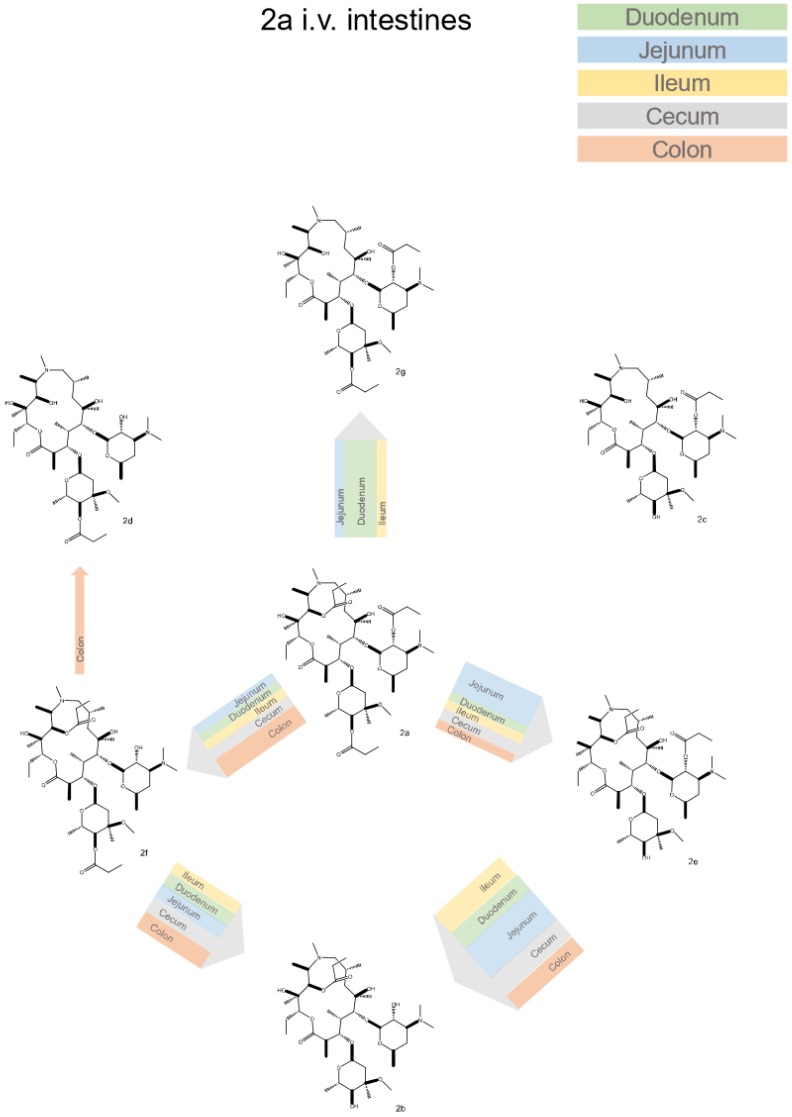

Figure 42. Schematic representations of pharmacokinetic data of **2a** in intestine organs and via intravenous route

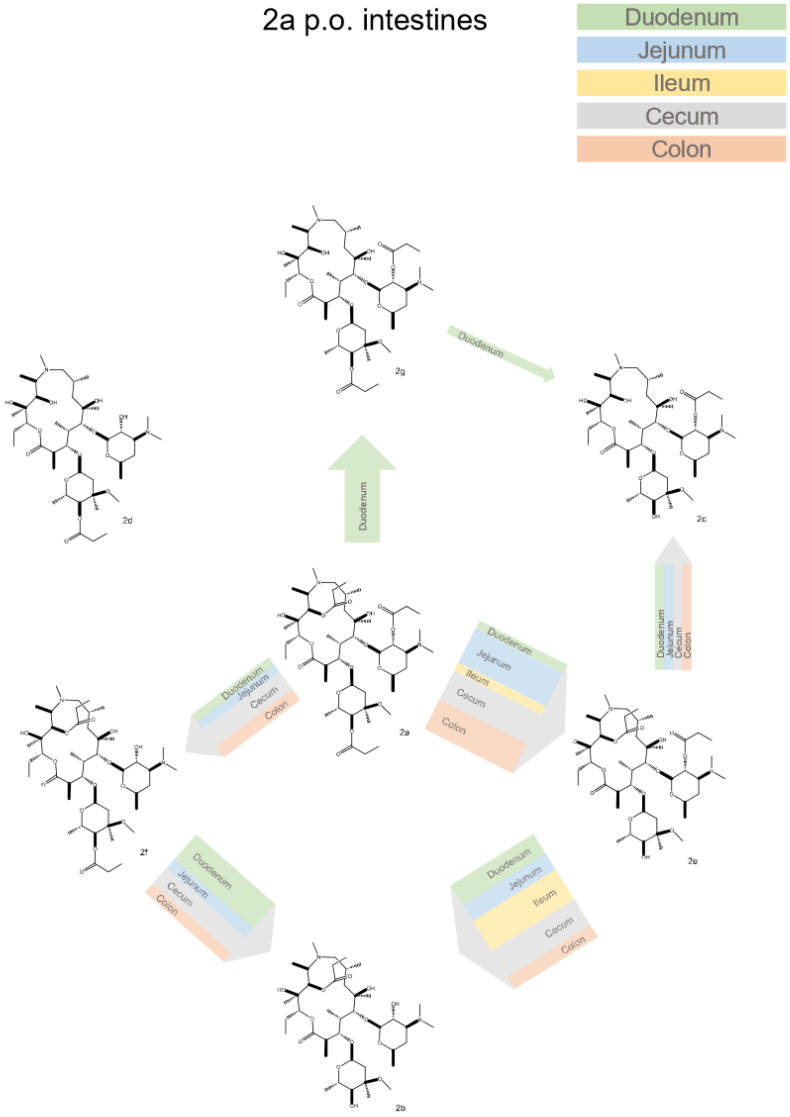

Figure 43. Schematic representations of pharmacokinetic data of **2a** in intestine organs and via oral route

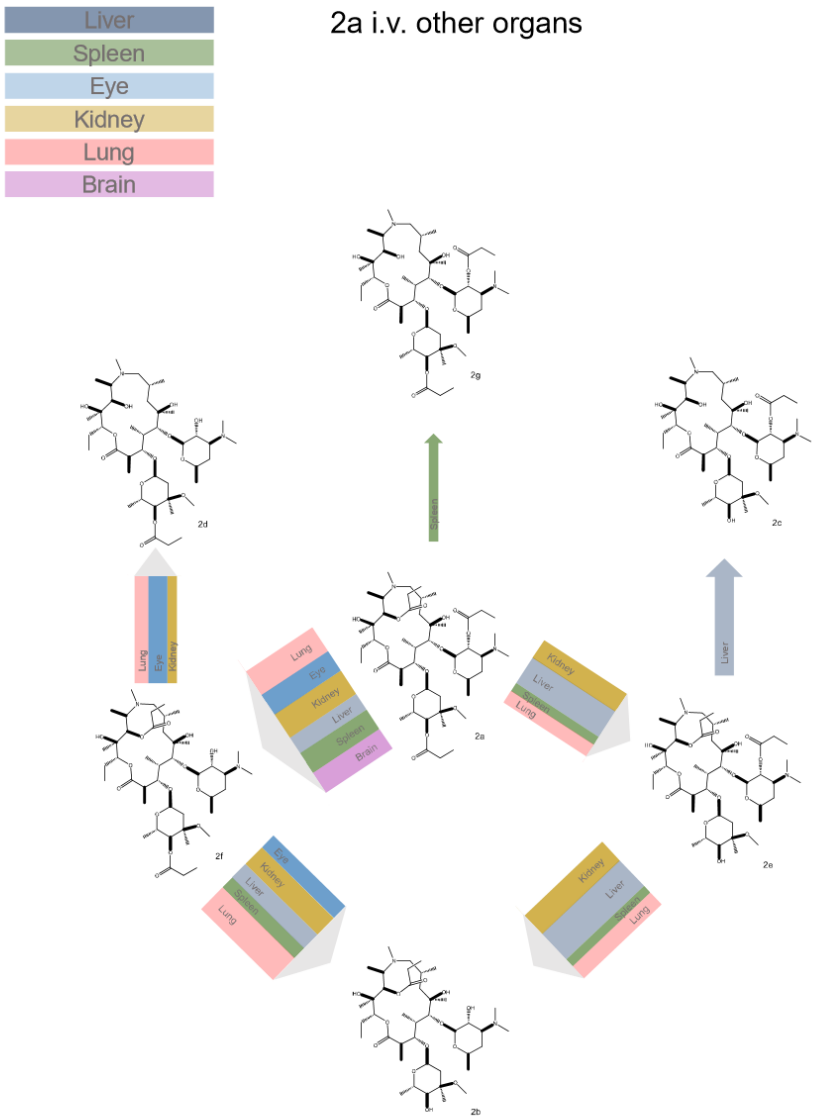

Figure 44. Schematic representations of pharmacokinetic data of **2a** in different organs and via intravenous route

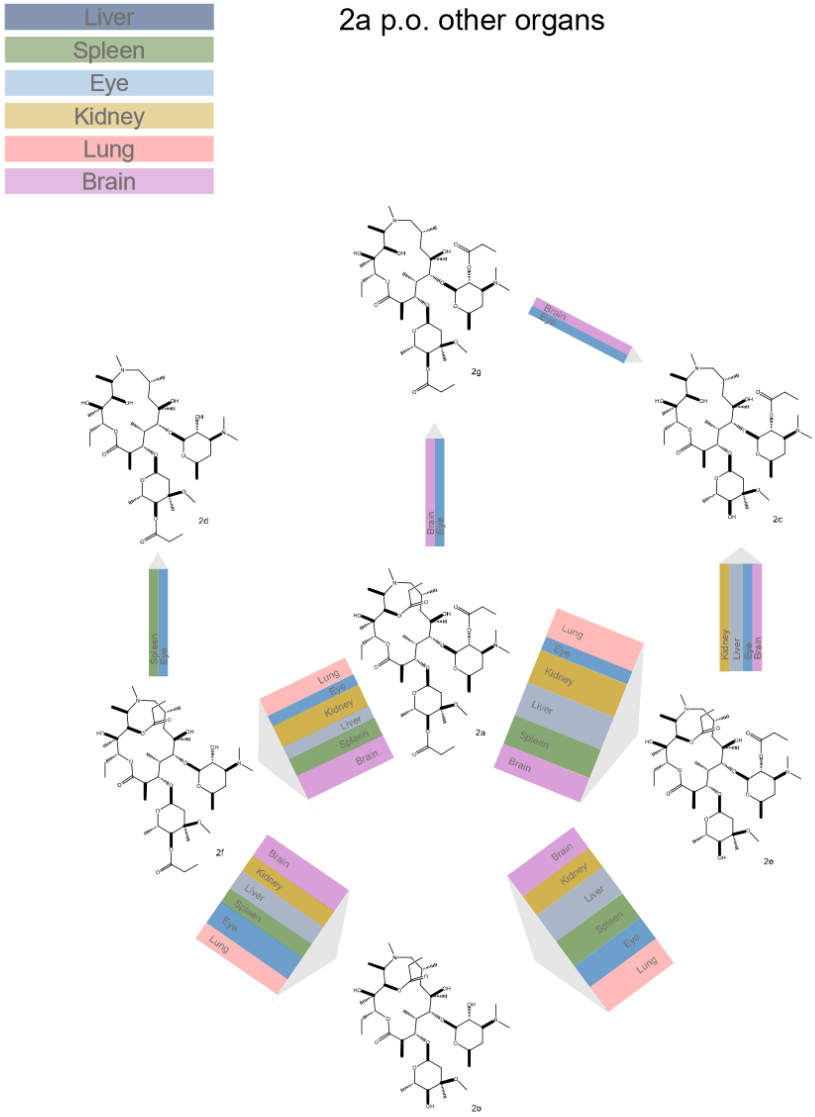

Figure 45. Schematic representations of pharmacokinetic data of **2a** in different organs and via oral route

Pharmacokinetic data

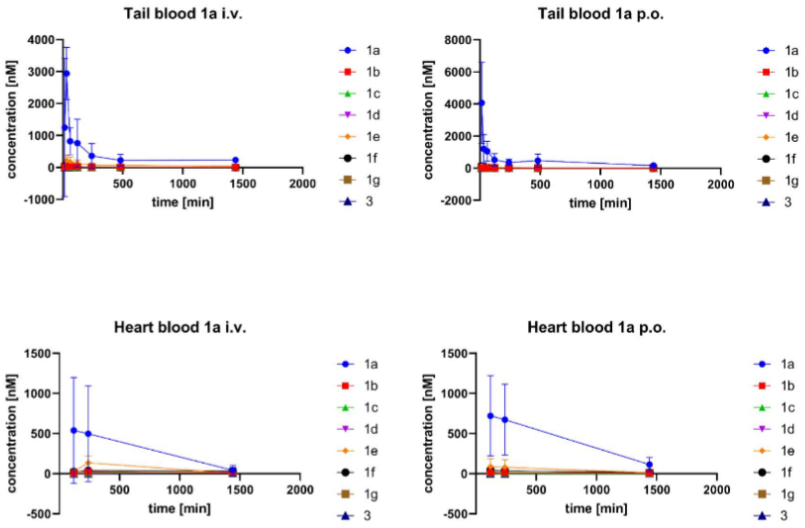

Figure 46. Graphs of pharmacokinetic data of **1a** and its metabolites in tail blood and heart blood (i.v. and p.o.)

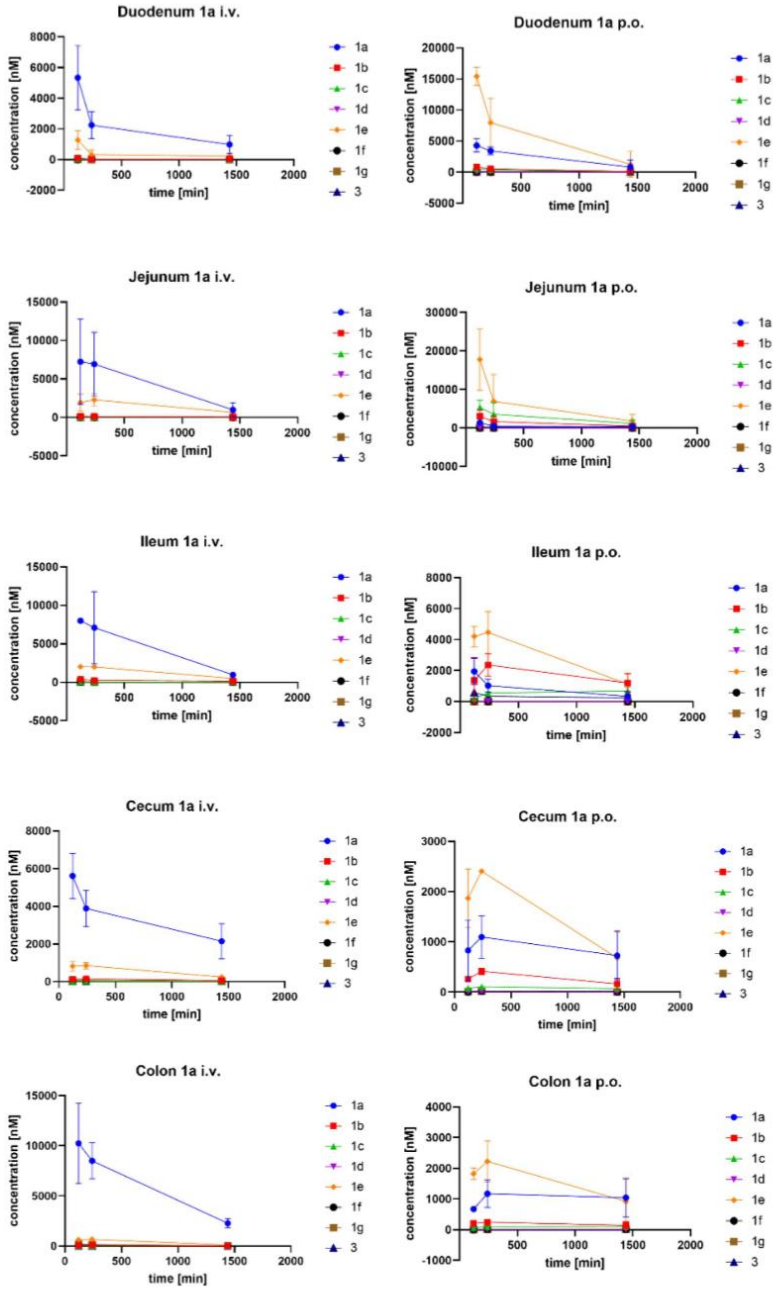

Figure 47. Graphs of pharmacokinetic data of **1a** and its metabolites in duodenum, jejunum, ileum, cecum and colon (i.v. and p.o.)

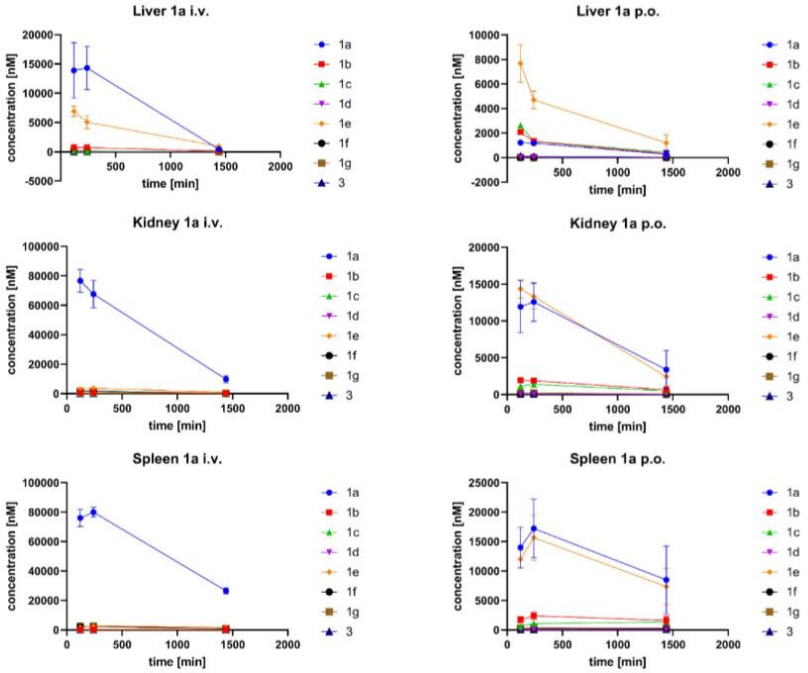

Figure 48. Graphs of pharmacokinetic data of **1a** and its metabolites in liver, kidney and spleen (i.v. and p.o.)

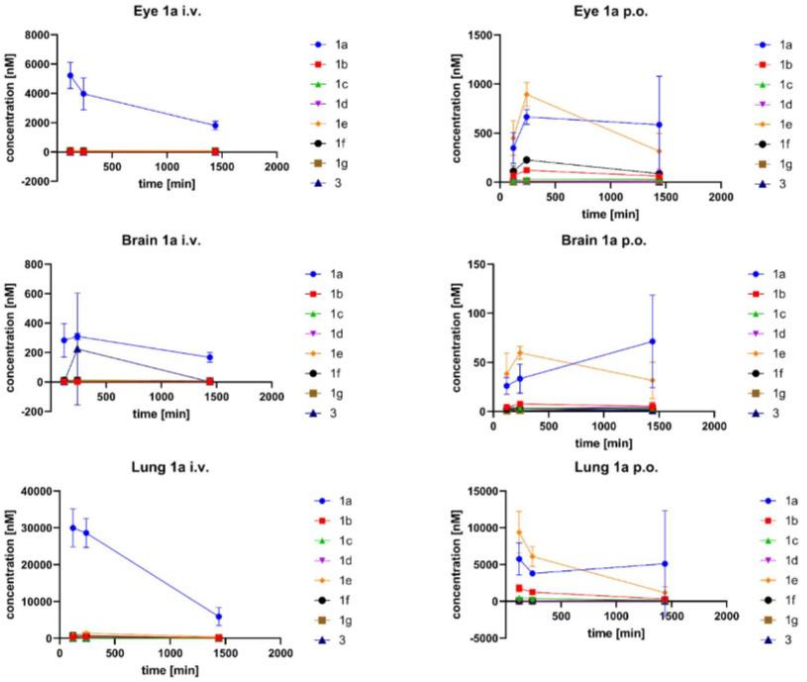

Figure 49. Graphs of pharmacokinetic data of **1a** and its metabolites in eye, brain and lung (i.v. and p.o.)

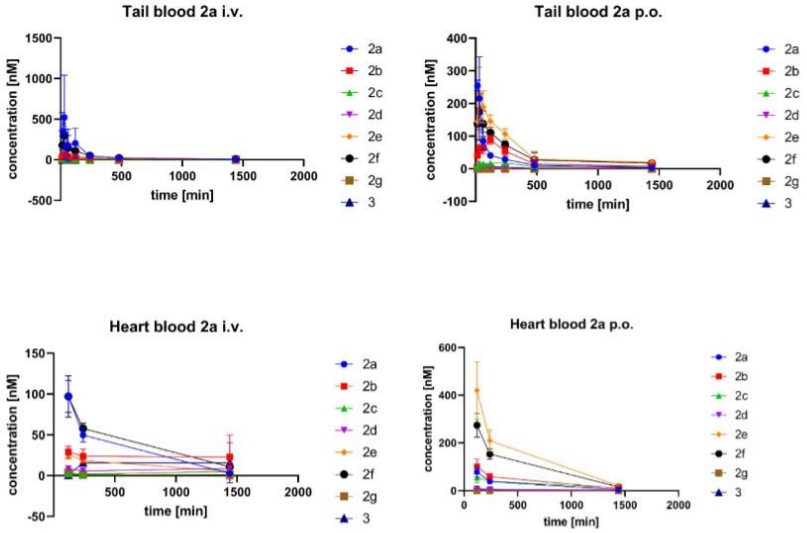

Figure 50. Graphs of pharmacokinetic data of **2a** and its metabolites in tail blood and heart blood (i.v. and p.o.)

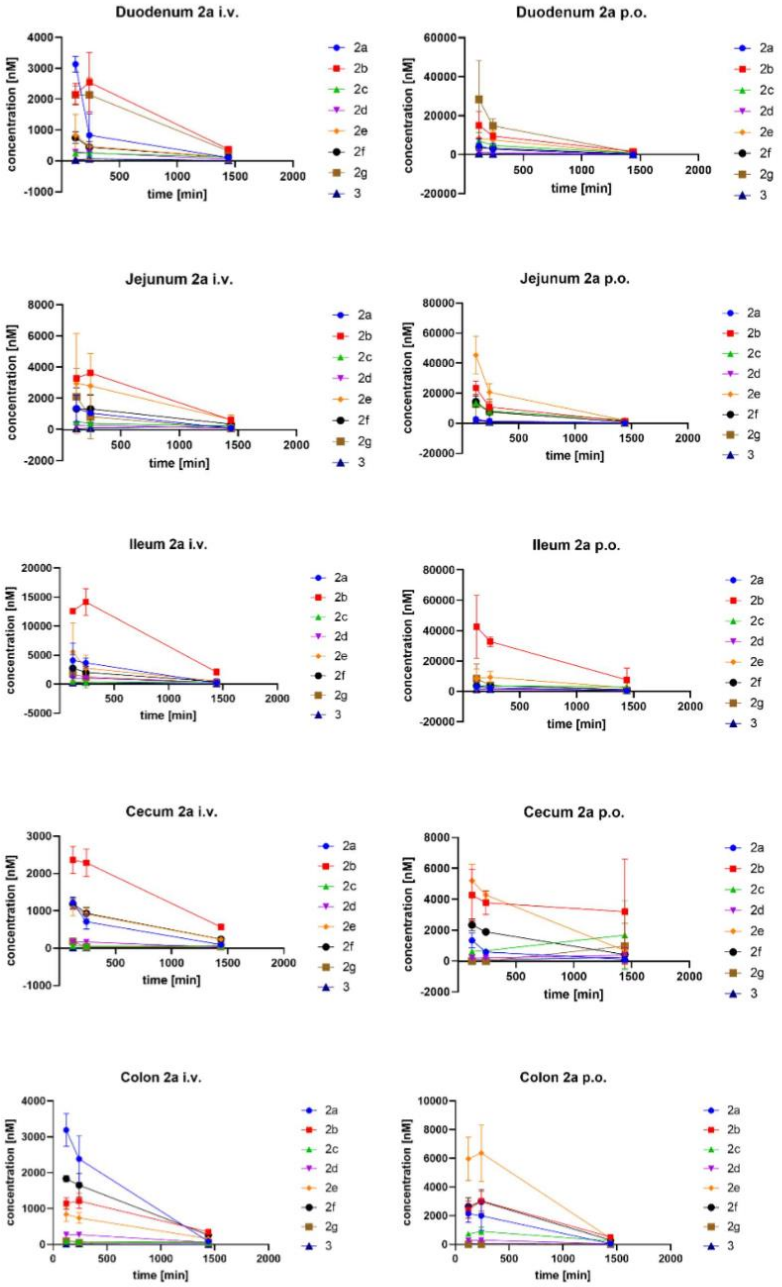

Figure 51. Graphs of pharmacokinetic data of **2a** and its metabolites in duodenum, jejunum, ileum, cecum and colon (i.v. and p.o.)

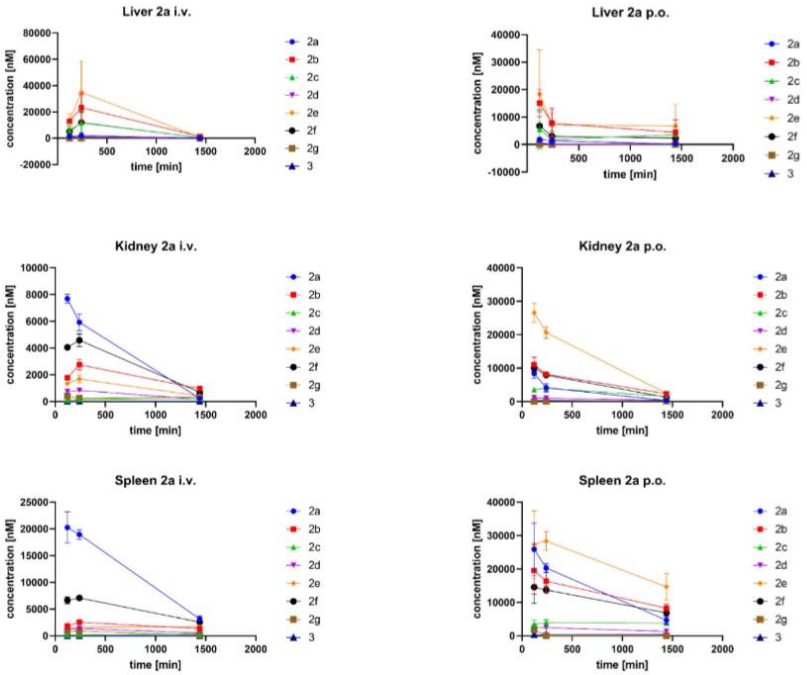

Figure 52. Graphs of pharmacokinetic data of **2a** and its metabolites in liver, kidney and spleen (i.v. and p.o.)

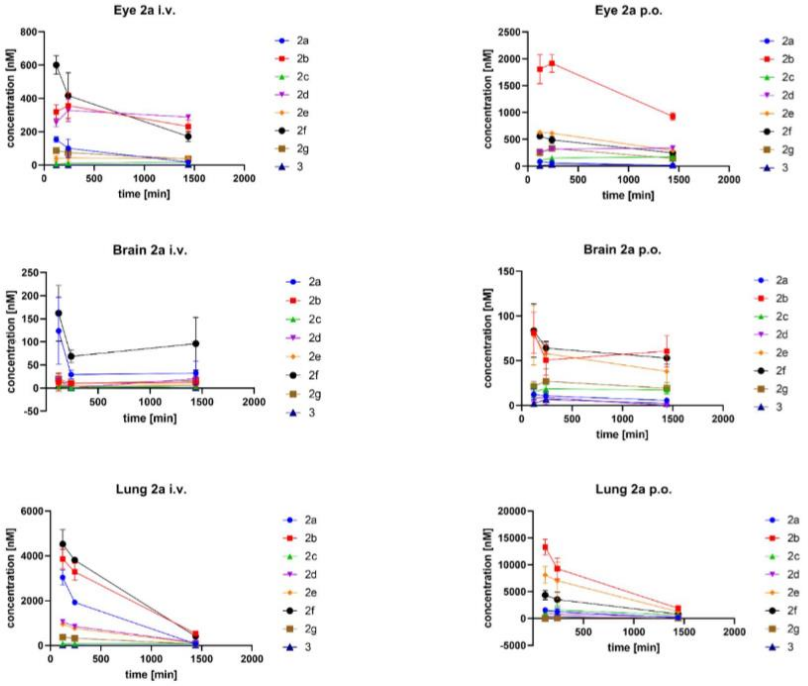

Figure 53. Graphs of pharmacokinetic data of **2a** and its metabolites in eye, brain and lung (i.v. and p.o.)

In vitro stability graphs

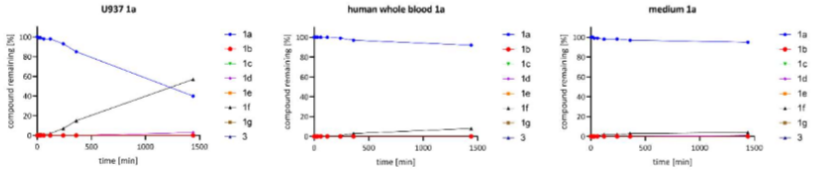

Figure 54. In vitro stability data of **1a** in U937 cells, human whole blood, and RPMI medium.

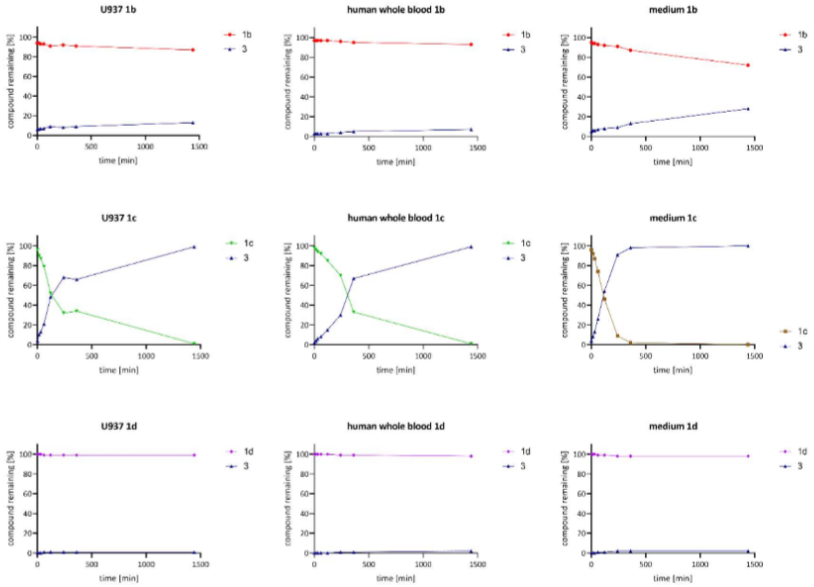

Figure 55. In vitro stability data of **1b**, **1c** and **1d** in U937 cells, human whole blood, and RPMI medium

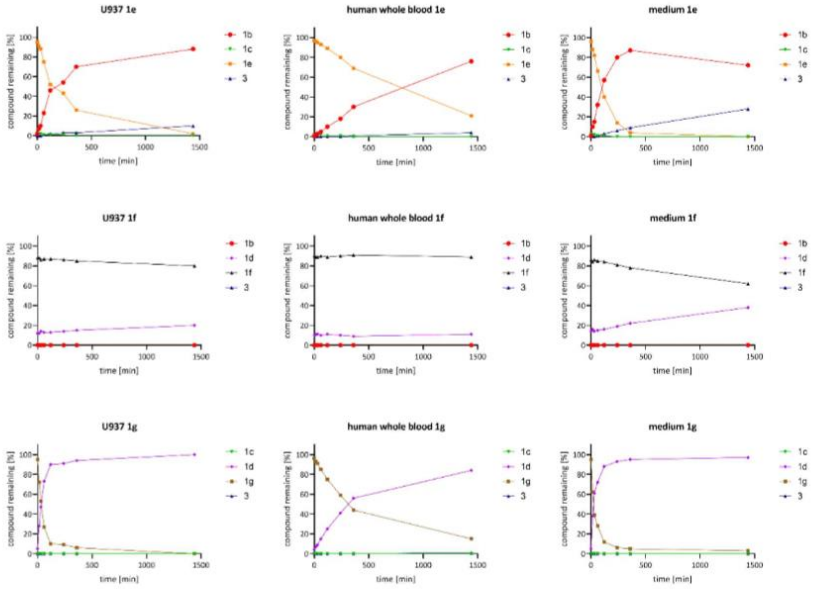

Figure 56. In vitro stability data of **1e**, **1f** and **1g** in U937 cells, human whole blood, and RPMI medium

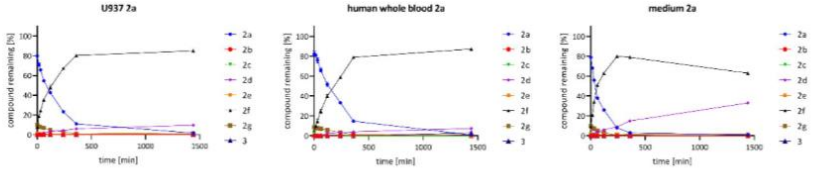

Figure 57. In vitro stability data of **2a** in U937 cells, human whole blood, and RPMI medium

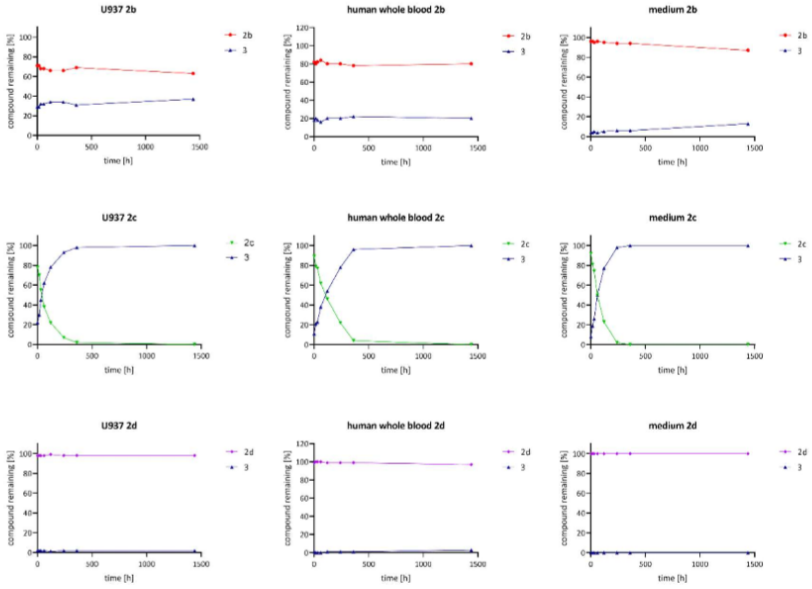

Figure 58. In vitro stability data of **2b**, **2c** and **2d** in U937 cells, human whole blood, and RPMI medium

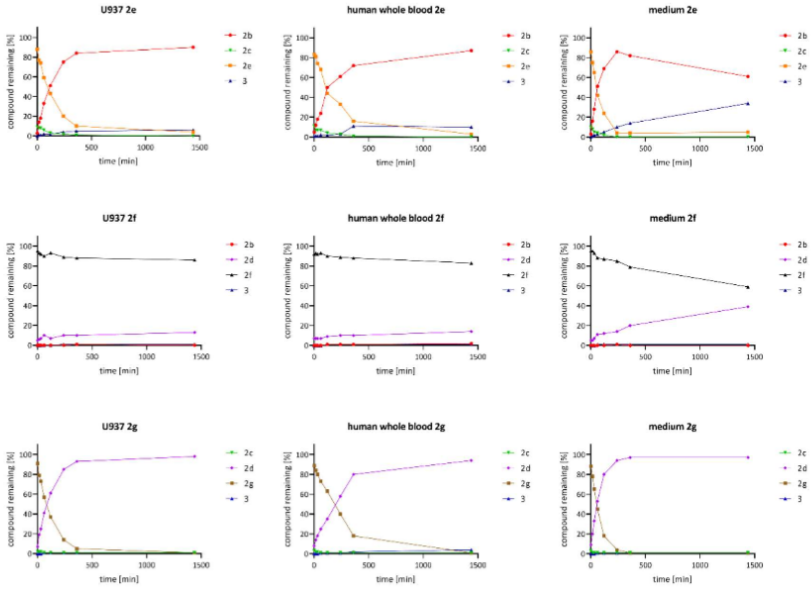

Figure 59. In vitro stability data of **2e**, **2f** and **2g** in U937 cells, human whole blood, and RPMI medium

14.2. *Supporting Information* für "*Immune cell targeted Fumaric Esters support a role of GPR109A as a primary target of Monomethyl Fumarate in vivo*"

Table 1 Specific MS/MS fragmentation patterns of synthesized compounds **1-4**

Substance	$[M+H]^+_{theo}$	$[M+H]^+_{measured}$	Frag 1	Frag 2
1	861.53	861.60	703.33	685.33
2	973.55	973.60	703.29	685.12
3	861.53	861.80	591.45	573.16
4	863.55	863.68	705.28	272.12

Table 2 Specific tunes of substances in HPLC-MS/MS

Substance	Q1 mass	Q3 mass	DP (V)	CE (V)	CXP (V)
1	861.547	703.5	156	10	41
2	973.685	703.4	171	10	45
3	861.599	591.300	151	43	38
Azithromycin	749.406	591.300	61	41	16
3 as GSH adduct	1168.542	591.400	281	59	34

Table 3 Quantitative analysis of pharmacokinetic study of compound **3** HPLC-MS/MS. Compond was given Balb/C (N=8) via oral route with 10 mg/kg. Azithromycin was analyzed as possible metabolite

Organ	Avg. conc. 3 (nM)	SD 3 (nM)	Avg. conc. Azi (nM)	SD Azi (nM)
Heart blood	3	1	13	2
Lung	1	1	49	22
Spleen	3	2	58	18
Healthy skin Belly	3	2	25	15
Back skin	2	2	17	6
Liver	7	5	332	62
Colon	9	4	128	57
Thymus	5	2	28	6

Table 4 Primer sequences for qPCR analysis

Cytokine	Forward sequence	Reverse sequence
HPRT	AGTTCTTTGCTGACCTGCTG	CCACCAATAACTTTTATGTCCCC
TNFa	CCACCACGCTCTTCTGTCTA	CTGATGAGAGGGAGGCCATT
IL-17A	GAAGGCCCTCAGACTACCTC	CTTTCCCTCCGCATTGACAC
IL-17F	GAGGGAAGAAGCAGCCATTG	GGCAAGTCCCAACATCAACA
IL-6	ACTTCACAAGTCGGAGGCTTA	TCTGCAAGTGCATCATCGTT
IL-1ß	TGACGGACCCCAAAAGATGA	TCTCCACAGCCACAATGAGT
IL-23A	TGAGCCCTTAGTGCCAACAG	CTTGCCCTTCACGCAAAACA
NLRP3	TCCCAGACACTCATGTTGCC	GTCCAGTTCAGTGAGGCTCC
IL-22	CTGCTTCTCATTGCCCTGTG	GAACAGTTTCTCCCCGATGAG

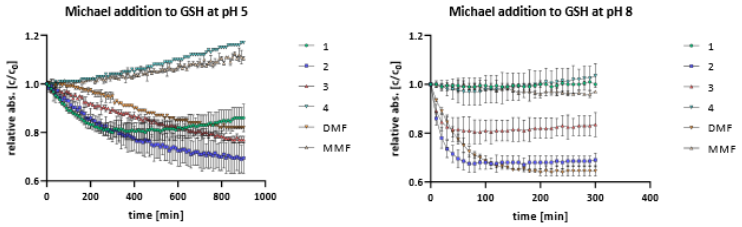

Figure 1 Relative absorption (c/c_0) at 226 nm of DMF, MMF and compounds **1-4** (100 µM) with GSH (1 mM) monitored over 900 or 300 min iat pH 5 or 8 (n=3)

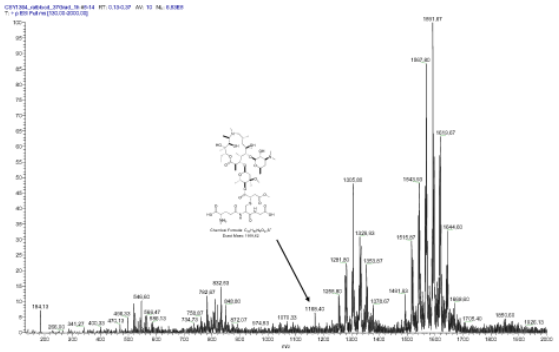

Figure 2 Mass spectra of compound **3** (10 µM) 1 h after incubation at 37 °C in rat blood

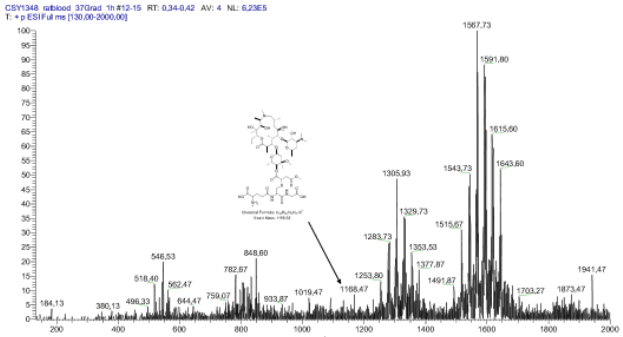

Figure 3 Mass spectra of compound **2** (10 µM) 1 h after incubation at 37 °C in rat blood

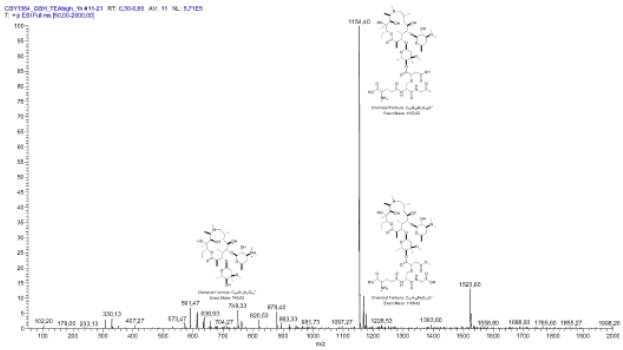

Figure 4 Mass spectra of compound **3** (10 µM) 1 h after incubation at room temperature with GSH (100 µM) and 10 % triethylamine as base

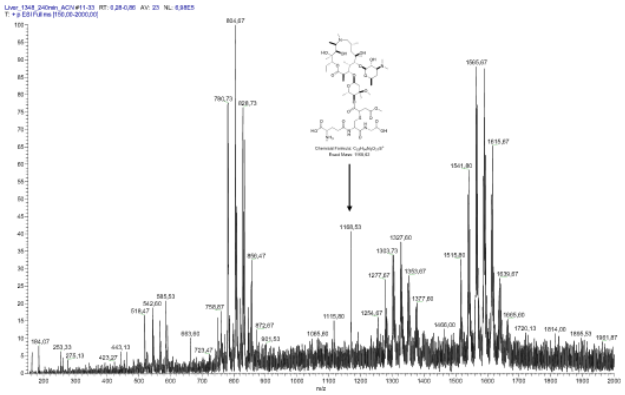

Figure 5 Mass spectra of compound 2 (20 µM) 4 h after incubation at 37 °C in liver homogenate

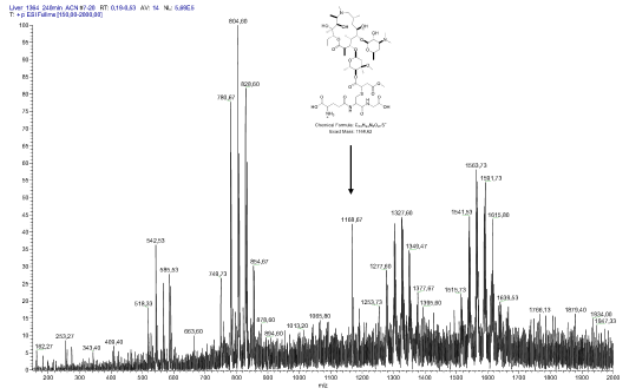

Figure 6 Mass spectra of compound 3 (20 µM) 4 h after incubation at 37 °C in liver homogenate

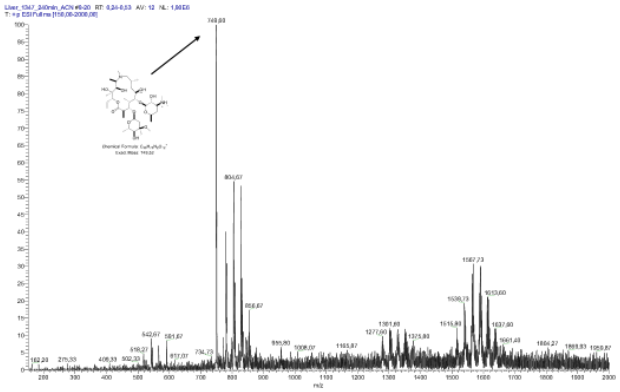

Figure 7 Mass spectra of compound **1** (20 µM) 4 h after incubation at 37 °C in liver homogenate

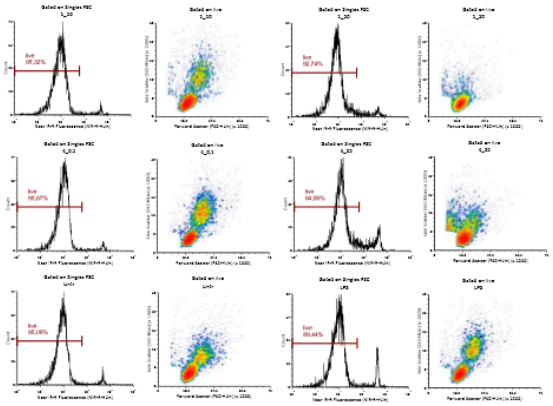

Figure 8 Scatter and live/dead staining of substances. No. 1 is DMF, no. 4 is compound **3**

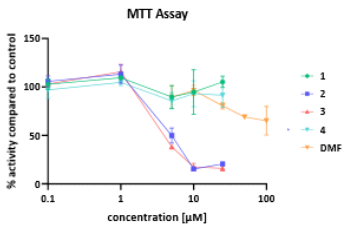

Figure 9 3-(4,5-Dimethyl-2-thiazolyl)-2,5-diphenyltetrazolium bromide (MTT) assay of compounds **1-4** and DMF at different concentrations, incubated for 1 h

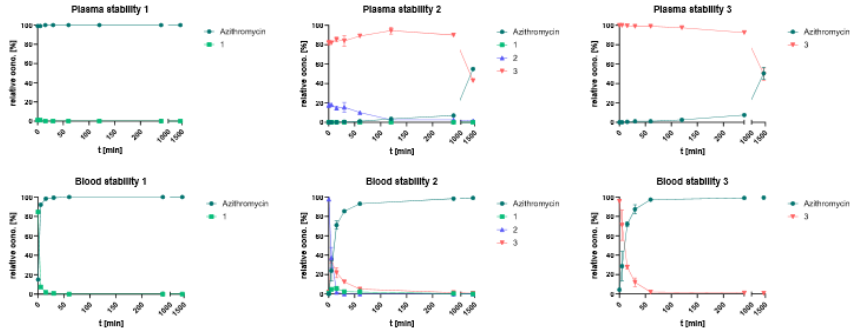

Figure 10 Stability assays of compounds **1-3** perfomed in human whole blood and plasma incubated at 37 °C over 24 h

Table 5 Measured concentrations of compounds **1** to **3** and azithromycin in uptake assay of human buffy coat. Samples were collected after 0 and 30 min and analysed via HPLC-MS/MS. Accumulation factor is calculated by division of pellet at t30 and pellet at t0 of total measured analytes

Cpd	Timepoint [min]	Matrix	Azi [nm]	1 [nm]	2 [nm]	3 [nm]	Sum [nm]	Accumulation factor
1	0	Pellet	4182	5			4187	14
1	30	Pellet	58140	14			58154	
1	0	SN	33834	18			33852	
1	30	SN	31503	1			31505	
2	0	Pellet	18	0	10547	622	11187	6
2	30	Pellet	382	0	63800	2612	66794	
2	0	SN	395	0	25428	2880	28703	
2	30	SN	276	1	10734	336	11346	
3	0	Pellet	9		9317		9325	8
3	30	Pellet	556		72001		72557	
3	0	SN	377		33586		33963	
3	30	SN	610		19707		20317	

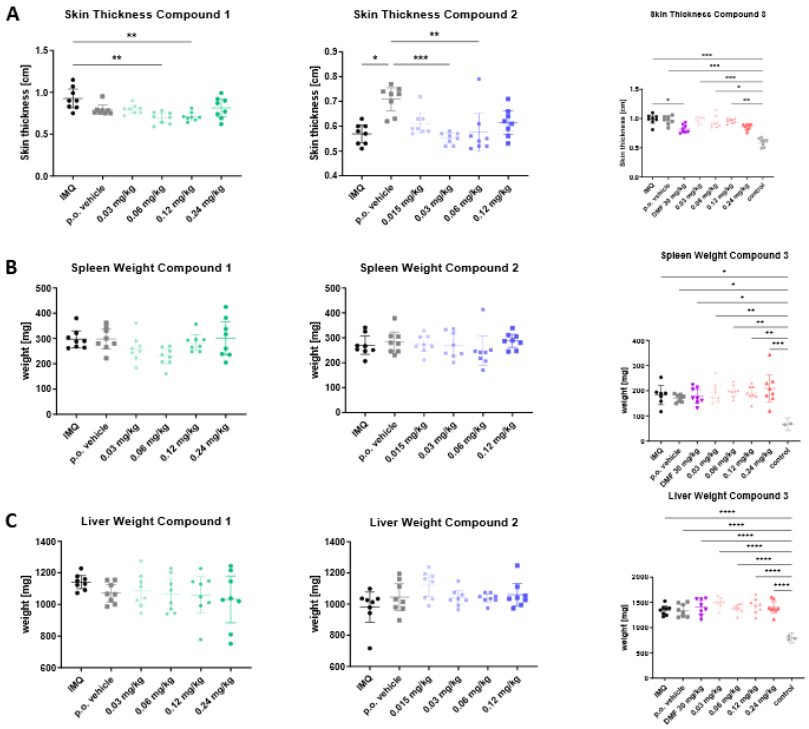

Figure 11 Skin thickness, spleen and liver masses for dose respones studies

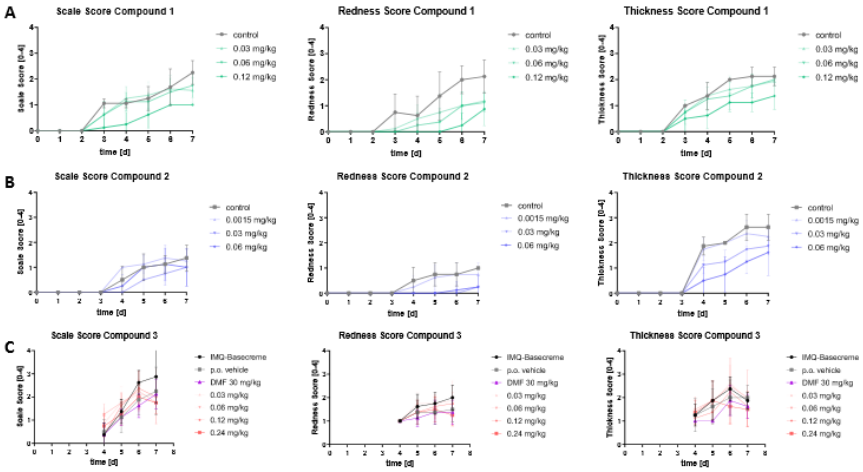

Figure 12 Scaling, redness and thickness scores for compounds 1 to 3 in psoriasis dose response studies

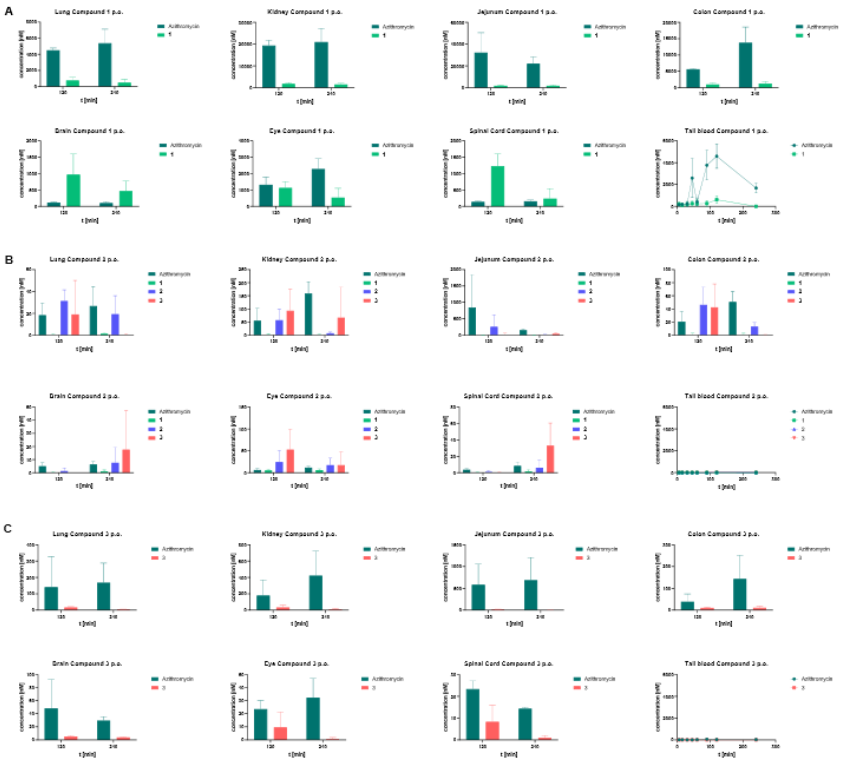

Figure 13 Comparison of pharmacokinetic data (BALB/c mice, female, 8 weeks old, n = 3) of lead substances 1-3 in different organs via oral route (12 µmol/kg)

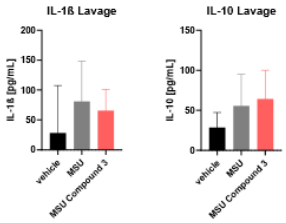

Figure 14 Cytokine concentrations in peritoneal lavage sampled from mice treated with PBS (vehicle and MSU group) or Compound 3 (0.1 mg/kg) and terminated 4 h after administration of MSU crystals

14.3. *Supporting Information* für "*Imidazoquinolines with improved pharmacokinetic properties induce a high IFNα to TNFα ratio in vitro and in vivo*"

frontiers

1. **Synthesis**

Compound S1.2 3-nitroquinoline-2,4-diol, ^{1}H NMR (300 MHz, DMSO) δ 11.98 (s, 1H), 11.36 (s, 1H), 8.01 (d, J = 8.1 Hz, 1H), 7.61 (t, J = 7.7 Hz, 1H), 7.32 (d, J = 8.2 Hz, 1H), 7.24 (t, J = 7.6 Hz, 1H), ^{13}C NMR (75 MHz, DMSO) δ 156.49, 155.91, 138.24, 133.39, 133.14, 127.29, 124.69, 124.46, 122.56, 122.33, 116.11, 115.86, 114.07, yellow solid, yield 37.1 g (72.6%), MS $(M+H)^+$ calcd *m/z* 207.04, found *m/z* 207.20. Synthesis of intermediate S1.2 was done following Shukla *et al.* (J. Med. Chem, 2010). Briefly, quinoline-2,4-diol (TCI D1753, 40 g, 0,248 mol) was dissolved in nitric acid (53%, 300 mL) and stirred at RT for 10 min. The mixture was then heated to 75 °C for 15 min. After cool down to RT the solution was poured into ice/water mixture to form solid yellow precipitate (S1.2). Precipitate was filtered off and dried to yield 37.1 g. and used without further purification.

Compound S1.3 2,4-dichloro-3-nitroquinoline, ^{1}H NMR (300 MHz, $CDCl_3$) δ 8.16 (d, J = 8.4 Hz, 1H), 8.00 (d, J = 8.4 Hz, 1H), 7.88 (t, J = 7.6 Hz, 1H), 7.74 (t, J = 7.6 Hz, 1H), ^{13}C NMR (75 MHz, $CDCl_3$) δ 146.50, 139.59, 135.62, 133.39, 129.72, 129.05, 125.24, 125.04, 124.33, 77.58, 77.16, 76.74, 49.55, 49.27, 48.98, greyish solid, yield 10.7 g (96.9%). Synthesis of intermediate S1.3 was done following Shukla *et al.* (J. Med. Chem, 2010). Briefly, compound S1.2 (9.4 g, 45.6 mmol) was dissolved in 60 mL of phenylphosphonyl dichloride (VWR A13777) and heated to 135 °C for 3 h. Solution was transferred into ice/water mixture and stirred vigorously. Formed precipitate was filtered off and dried to yield 10.7 g of S1.3 and used without further purification.

Compound S1.4-A1 tert-butyl 4-(2-((2-chloro-3-nitroquinolin-4-yl)amino)ethyl)piperidine-1-carboxylate, white solid, yield 3.1 g (57.6%), MS $(M+H)^+$ calcd *m/z* 435.18, found *m/z* 435.13. Compound S1.3 (3 g, 12.4 mmol) was dissolved in anhydrous dichloromethane with triethylamine (2.59 mL, 1.5 eq). To this solution tert-butyl 4-(2-aminoethyl)piperidine-1-carboxylate (ChemPur BD31964-5, 3.4 g, 14.9 mmol) was added. The reaction mixture was heated to 45°C for 45 min. Reaction progress was monitored via TLC (ethyl acetate/acetone/cyclohexane 2:1:3 with 0.5% triethylamine). Solvents were removed under vacuum, residue washed with water and dried. Crude product was then purified via column chromatography on silica gel (400 g) with a mixture of cyclohexane and ethyl acetate, eluted with a with a gradient of solvents to obtain 3.1 g of S1.4-A1.

Compound S1.5-A1 tert-butyl 4-(2-((3-amino-2-chloroquinolin-4-yl)amino)ethyl)piperidine-1-carboxylate, yellow solid, yield 1.06 g (>99%), MS $(M+H)^+$ calcd *m/z* 405.21, found *m/z* 405.27. Compound S1.4-A1 (1.15 g, 2.65 mmol) was dissolved in water/ethyl acetate (1:1). Subsequently 3.34 g of sodium dithionite (Fisher S/3800/63) was added and solution was heated to 55 °C. After 2 min MS analysis showed full conversion to product. Product was extracted with liquid-liquid extraction (three times with dichloromethane). Organic phases were combined, dried with sodium sulphate and solvent was evaporated under vacuum to yield 1.06 g of S1.5-A1 and used without further purification.

Compound S1.6-A1 tert-butyl 4-(2-(2-butyl-4-chloro-1H-imidazo[4,5-c]quinolin-1-yl)ethyl)piperidine-1-carboxylate, white solid, yield 1.12 g (50%), MS $(M+H)^+$ calcd *m/z* 471.25, found *m/z* 471.40. Compound S1.5-A1 (1.94 g, 4.8 mmol) was dissolved in 5 mL trimethyl orthovalerate (VWR L20377.22) and solution was heated to 135 °C over three days (heating was stopped during nights). Reaction solution was poured into cyclohexane and formed precipitate was filtered of and dried to obtain 1.12 g of S1.6-A1 and used without further purification.

Compound S1.7-A1 tert-butyl 4-(2-(2-butyl-4-hydrazineyl-1H-imidazo[4,5-c]quinolin-1-yl)ethyl)piperidine-1-carboxylate, MS $(M+H)^+$ calcd *m/z* 467.31, found *m/z* 467.33. Compound S1.6-A1 (640 mg, 1.36 mmol) was dissolved in 25 mL of ethanol, subsequently hydrazine hydrate (Sigma-Aldrich 225819-500ML, 1.5 mL, 47 mmol) was added. Solution was refluxed overnight. MS analysis showed full conversion. Product S1.7-A1 was directly used for next reaction step

Compound S1.8-A1 (also A1-Boc) tert-butyl 4-(2-(4-amino-2-butyl-1H-imidazo[4,5-c]quinolin-1-yl)ethyl)piperidine-1-carboxylate, ^{1}H NMR (300 MHz, $CDCl_3$) δ 7.84 (dd, *J* = 13.6, 8.2 Hz, 2H), 7.48 (t, *J* = 7.5 Hz, 1H), 7.31 (t, *J* = 7.5 Hz, 1H), 5.80 (s, 2H), 4.46 – 4.35 (m, 2H), 4.15 (d, *J* = 9.9 Hz, 2H), 2.89 – 2.80 (m, 2H), 2.75 (t, *J* = 12.4 Hz, 2H), 1.93 – 1.77 (m, 5H), 1.74 (s, 1H), 1.71 – 1.59 (m, 1H), 1.51 (dt, *J* = 9.8, 4.8 Hz, 2H), 1.46 (s, 9H), 1.28 (dt, *J* = 19.7, 6.1 Hz, 2H), 1.00 (t, *J* = 7.3 Hz, 3H), ^{13}C NMR (75 MHz, $CDCl_3$) δ 154.87, 153.30, 151.26, 144.07, 133.28, 127.17, 126.84, 126.80, 122.48, 119.38, 115.31, 79.71, 43.61, 36.95, 34.31, 32.07, 30.25, 28.57, 27.24, 27.02, 22.76, 13.97, white solid, yield 294 mg (48% over two steps of synthesis), purity >99% via HPLC-ELSD, MS $(M+H)^+$ calcd *m/z* 452.30, found *m/z* 452.40. Compound S1.7-A1 dissolved in 10 mL of acetic acid and subsequently three spatula tips of Zn powder were added. Reaction progress was controlled via MS. After 48 h another spatula tip of Zn powder and 1 mL of acetic acid was added. Next day full conversion was observed. The reaction mixture was diluted with water and underlayered with dichloromethane. Mixture was vigorously stirred and potassium hydroxide added until Zn formed a soluble complex. Product was extracted with liquid-liquid extraction (three times with dichloromethane). Organic phases were combined, dried with sodium sulphate and solvent was evaporated under vacuum to obtain 632 mg of crude product. To purify substance flash chromatography was performed with a gradient of cyclohexane and isopropanol (with 0.25% triethylamine each) to obtain 294 mg of compound S1.8-A1.

Compound A1 2-butyl-1-(2-(piperidin-4-yl)ethyl)-1H-imidazo[4,5-c]quinolin-4-amine, ^{1}H NMR (400 MHz, $CDCl_3$) δ 7.94 – 7.85 (m, 1H), 7.81 (dd, *J* = 8.3, 0.8 Hz, 1H), 7.53 – 7.40 (m, 1H), 7.33 – 7.27 (m, 1H), 5.40 (d, *J* = 92.9 Hz, 1H), 4.46 – 4.35 (m, 2H), 3.14 (d, *J* = 12.1 Hz, 2H), 2.89 – 2.82 (m, 2H), 2.67 (td, *J* = 12.0, 2.0 Hz, 2H), 1.95 – 1.71 (m, 6H), 1.71 – 1.56 (m, 1H), 1.50 (dq, *J* = 14.7, 7.4 Hz, 2H), 1.32 (ddd, *J* = 15.7, 12.3, 3.9 Hz, 2H), 1.00 (t, *J* = 7.4 Hz, 3H), ^{13}C NMR (101 MHz, $CDCl_3$) δ 153.22, 151.33, 144.82, 133.32, 127.42, 126.99, 122.30, 119.49, 115.63, 46.61, 43.61, 37.56, 34.56, 33.35, 30.35, 27.28, 22.78, 13.95, yellowish white solid, yield 82 mg (>99%), purity 97.5% via HPLC-ELSD, MS $(M+H)^+$ calcd *m/z* 352.25, found *m/z* 352.67. Compound S1.8-A1 (100 mg, 0.22 mmol) was dissolved in a mixture of dichloromethane and trifluoroacetic acid (10:1, 10 mL) and stirred at RT. Reaction progress was controlled via MS. To neutralize solution sodium carbonate was added after reaction was complete. Product was extracted with liquid-liquid extraction (three times with dichloromethane). Organic phases were combined, dried with sodium sulphate and solvent was evaporated under vacuum to obtain 82 mg of product A1.

Compound S1.4-A2 tert-butyl 4-(((2-chloro-3-nitroquinolin-4-yl)amino)methyl)piperidine-1-carboxylate, white solid, yield 2.3 g (46%), MS $(M+H)^+$ calcd *m/z* 421.16, found *m/z* 421.20. Compound S1.3 (2.9 g, 12.0 mmol) was dissolved in 30 mL of anhydrous dichloromethane with triethylamine (2.5 mL, 1.5 eq). To this solution tert-butyl 4-(aminomethyl)piperidine-1-carboxylate (ChemPur 11389, 3.1 g, 14.5 mmol) was added. The reaction mixture was heated to 45 °C for 45 min. Reaction progress was monitored via TLC (ethyl acetate/acetone/cyclohexane 4:1:2 with 0.5% triethylamine). Solvents were removed under vacuum, residue washed with water and dried. Crude product was then purified via column chromatography on silica gel (300 g) with a mixture of cyclohexane, ethyl acetate and acetone, eluted with a gradient of solvents to obtain 2.3 g of S1.4-A2.

Compound S1.5-A2 tert-butyl 4-(2-((3-amino-2-chloroquinolin-4-yl)amino)ethyl)piperidine-1-carboxylate, white solid, yield 1.66 g (>99%), MS $(M+H)^+$ calcd *m/z* 391.19, found *m/z* 391.27. Compound S1.4-A1 (1.78 g, 4.24 mmol) was dissolved in water/ethyl acetate (1:1). Subsequently 5.34 g of sodium dithionite (Fisher S/3800/63) was added and solution was heated to 75 °C. After 20 min MS analysis showed full conversion to product. Product was extracted with liquid-liquid extraction (three times with dichloromethane). Organic phases were combined, dried with sodium sulphate and solvent was evaporated under vacuum to yield 1.66 g of S1.5-A1 and used without further purification.

Compound S1.6-A2 tert-butyl 4-((2-butyl-4-chloro-1H-imidazo[4,5-c]quinolin-1-yl)methyl)piperidine-1-carboxylate, ^{1}H NMR (300 MHz, $CDCl_3$) δ 8.18 – 8.03 (m, 1H), 8.02 – 7.91 (m, 1H), 7.59 (dq, *J* = 7.0, 5.5 Hz, 2H), 4.36 (d, *J* = 6.9 Hz, 2H), 4.12 (d, *J* = 10.0 Hz, 2H), 2.90 (dd, *J* = 22.0, 13.9 Hz, 2H), 2.53 (t, *J* = 12.3 Hz, 2H), 2.09 (t, *J* = 9.3 Hz, 1H), 1.87 (dt, *J* = 15.6, 7.7 Hz, 2H), 1.63 – 1.45 (m, 4H), 1.39 (d, *J* = 12.5 Hz, 9H), 1.35 – 1.23 (m, 2H), 0.95 (dd, *J* = 14.2, 6.9 Hz, 3H), ^{13}C NMR (75 MHz, $CDCl_3$) δ 156.28, 154.61, 143.95, 143.79, 134.72, 133.95, 130.33, 127.48, 126.74, 119.57, 117.60, 79.86, 77.58, 77.16, 76.74, 51.17, 37.24, 30.30, 29.70, 28.44, 27.76, 22.75, 13.88, white solid, yield 2.71 g (86%), MS $(M+H)^+$ calcd *m/z* 457.24, found *m/z* 457.40. Compound S1.5-A2 (2.69 g, 6.9 mmol) was dissolved in 10 mL of dimethylformamide. To this 5 mL trimethyl orthovalerate (VWR L20377.22) were added and solution was heated to 135 °C overnight. The next day 1 mL trimethyl orthovalerate was added and solution was heated over weekend. MS analysis showed complete reaction. Crude product was purified via column chromatography on silica gel (300 g) with a mixture of cyclohexane and diethyl ether, eluted with a gradient of solvents to obtain 2.71 g of S1.6-A2.

Compound S1.7-A2 tert-butyl 4-(2-(2-butyl-4-hydrazineyl-1H-imidazo[4,5-c]quinolin-1-yl)methyl)piperidine-1-carboxylate, MS $(M+H)^+$ calcd *m/z* 453.30, found *m/z* 453.33. Compound S1.6-A2 (2.7 g, 5.92 mmol) was dissolved in 50 mL of ethanol, subsequently hydrazine hydrate (Sigma-Aldrich 225819-500ML, 4 mL, 126 mmol) was added. Solution was refluxed over two days. MS analysis showed full conversion. Product S1.7-A2 was directly used for next reaction step.

Compound S1.8-A2 (also A2-Boc) tert-butyl 4-((4-amino-2-butyl-1H-imidazo[4,5-c]quinolin-1-yl)methyl)piperidine-1-carboxylate, ^{1}H NMR (300 MHz, $CDCl_3$) δ 7.83 (t, *J* = 7.0 Hz, 2H), 7.50 (dd, *J* = 11.3, 4.2 Hz, 1H), 7.30 (dd, *J* = 11.6, 4.6 Hz, 1H), 5.51 (s, 2H), 4.31 (d, *J* = 6.9 Hz, 2H), 4.14 (d, *J* = 8.1 Hz, 2H), 2.91 – 2.83 (m, 2H), 2.56 (t, *J* = 12.4 Hz, 3H), 2.26 – 2.04 (m, 1H), 1.86 (dt, *J* = 15.4, 7.6 Hz, 2H), 1.51 (dd, *J* = 15.1, 7.6 Hz, 3H), 1.44 (s, 9H), 1.20 (d, *J* = 6.1 Hz, 1H), 0.99 (t, *J* = 7.3 Hz, 4H), ^{13}C NMR (75 MHz, $CDCl_3$) δ 154.75, 153.92, 151.36, 144.99, 133.30, 127.58, 127.15, 127.00, 122.30, 119.50, 115.71, 79.85, 50.95, 43.54, 37.31, 30.25, 29.81, 28.54, 27.64, 25.51, 22.74, 13.99, white solid, yield 332 mg (13% over two steps of synthesis), purity 96% via HPLC-ELSD, MS $(M+H)^+$ calcd *m/z* 438.29, found *m/z* 438.37. Compound S1.7-A2 dissolved in 15 mL of acetic acid and subsequently three spatula tips of Zn powder were added. Reaction progress was controlled via MS. After 48 h acetic acid was diluted with 100 mL water and underlayered with 200 mL dichloromethane. Mixture was vigorously stirred and potassium hydroxide added until Zn formed a soluble complex. Product was extracted with liquid-liquid extraction (three times with dichloromethane). Organic phases were combined, washed with water and brine, dried with sodium sulphate and solvent was evaporated under vacuum to obtain 2.56 g of crude product. To purify substance flash chromatography was performed with a gradient of cyclohexane, dichloromethane and isopropanol (with 0.25% triethylamine each) to obtain 332 mg of compound S1.8-A2.

Compound A2 2-butyl-1-(2-(piperidin-4-yl)methyl)-1H-imidazo[4,5-c]quinolin-4-amine, ^{1}H NMR (400 MHz, $CDCl_3$) δ 7.86 (dt, *J* = 6.7, 3.3 Hz, 1H), 7.82 (dd, *J* = 8.4, 0.9 Hz, 1H), 7.52 – 7.45 (m, 1H), 7.34 – 7.27 (m, 1H), 5.56 (s, 2H), 4.30 (d, *J* = 7.1 Hz, 2H), 3.09 (d, *J* = 12.1 Hz, 2H), 2.91 – 2.85 (m, 2H), 2.50 (t, *J* = 11.2 Hz, 2H), 2.19 – 2.05 (m, 1H), 1.86 (dt, *J* = 15.5, 7.6 Hz, 2H), 1.61 (d, *J* = 11.5 Hz, 2H), 1.48 (td, *J* = 14.8, 7.3 Hz, 2H), 1.43 – 1.31 (m, 2H), 1.28 – 1.15 (m, 1H), 1.02 – 0.96 (m, 3H), ^{13}C NMR (101 MHz, $CDCl_3$) δ 154.12, 151.36, 144.81, 133.45, 127.42, 127.14, 126.97, 122.30, 119.70, 115.80, 51.44, 46.18, 37.37, 30.83, 30.25, 27.64, 22.76, 13.96, yellowish white solid, yield 127 mg (75%), purity 98.5% via HPLC-ELSD, MS $(M+H)^+$ calcd *m/z* 338.23, found *m/z* 338.56. Compound S1.8-A2 (205 mg, 0.47 mmol) was dissolved in a mixture of dichloromethane and trifluoroacetic acid (10:1, 20 mL) and stirred at RT. After 30 min reaction was completed. Solution was poured into water and neutralized with potassium hydroxide. Product was extracted with liquid-liquid extraction (three times with dichloromethane). Organic phases were combined, washed with water and brine, dried with sodium sulphate and solvent was evaporated under vacuum to obtain 127 mg of A2.

Compound S1.4-A3 tert-butyl (2-(2-(2-((2-chloro-3-nitroquinolin-4-yl)amino)ethoxy)ethoxy)ethyl)carbamate, ^{1}H NMR (300 MHz, $CDCl_3$) δ 7.89 (d, *J* = 8.1 Hz, 1H), 7.82 (d, *J* = 8.4 Hz, 1H), 7.67 (dd, *J* = 8.2, 7.1 Hz, 1H), 7.48 (t, *J* = 7.7 Hz, 1H), 6.44 (s, 1H), 4.98 (s, 1H), 3.68 (dd, *J* = 9.6, 4.6 Hz, 2H), 3.63 (s, 3H), 3.57 – 3.45 (m, 4H), 3.28 (d, *J* = 5.1 Hz, 2H), 2.11 (s, 1H), 1.37 (s, 9H), ^{13}C NMR (75 MHz, $CDCl_3$) δ 156.03, 146.15, 144.66, 142.16, 132.05, 129.32, 127.79, 126.83, 126.56, 121.52, 119.32, 79.37, 77.58, 77.16, 76.74, 70.33, 68.78, 43.74, 40.30, 28.42, 28.36, white solid, yield 1.23 g (80%), MS $(M+H)^+$ calcd *m/z* 455.17, found *m/z* 455.13. Compound S1.3 (813 mg, 3.37 mmol) was dissolved in 10 mL of anhydrous dichloromethane with triethylamine (697 µL, 1.5 eq). To another 5 mL of anhydrous dichloromethane 1 g of tert-butyl (2-(2-(2-aminoethoxy)ethoxy)ethyl)carbamate (ABCR AB165344) was added. Both solutions were combined and heated to 45 °C for 3 h. Solvents were removed under vacuum. Crude product was then purified via column chromatography on silica gel (300 g) with a mixture of cyclohexane, ethyl acetate (with 0.5% of triethylamine) eluted with a gradient of solvents to obtain 1.23 g of S1.4-A3.

Compound S1.5-A3 tert-butyl (2-(2-(2-((3-amino-2-chloroquinolin-4-yl)amino)ethoxy)ethoxy)ethyl)carbamate, white solid, yield 879 mg (76%), MS $(M+H)^+$ calcd *m/z* 425.20, found *m/z* 425.27. Compound S1.4-A3 (1.23 g) was dissolved in ethyl acetate in a closed vessel. Vessel was flushed with Ar (evaporated and flushed three times). To solution a spatula of sodium sulphate and 500 mg of Pt/C (5% Pt, Sigma-Aldrich 205931-1G). The vessel was again flushed three times with Ar. Subsequently the vessel was flushed with H_2 (Air Liquide 130415). After two days of stirring reaction was completed, solution filtered through celite and solvent removed under vacuum to yield 879 mg of S1.5-A3 and used without further purification.

Compound S1.6-A3 tert-butyl (2-(2-(2-(2-butyl-4-chloro-1H-imidazo[4,5-c]quinolin-1-yl)ethoxy)ethoxy)ethyl)carbamate, white solid, yield 7.4 g (99%), MS $(M+H)^+$ calcd *m/z* 491.24, found *m/z* 491.33. Compound S1.5-A3 (6.5 g, 15.3 mmol) was dissolved in 10 mL trimethyl orthovalerate (VWR L20377.22) and solution was heated to 135 °C over three days. Residues of trimethyl orthovalerate were removed under vacuum (approx. 80 mbar) at 100 °C to yield 7.4 g of S1.6-A3.

Compound S1.7-A3 tert-butyl (2-(2-(2-(2-butyl-4-hydrazineyl-1H-imidazo[4,5-c]quinolin-1-yl)ethoxy)ethoxy)ethyl)carbamate, MS $(M+H)^+$ calcd *m/z* 487.30, found *m/z* 487.40. Compound S1.6-A3 (7.4 g, 15.1 mmol) was dissolved in 35 mL of ethanol, subsequently hydrazine hydrate

(Sigma-Aldrich 225819-500ML, 5 mL, 158 mmol) was added. Solution was refluxed over two days. MS analysis showed full conversion. Product S1.7-A3 was directly used for next reaction step.

Compound S1.8-A3 tert-butyl (2-(2-(2-(4-amino-2-butyl-1H-imidazo[4,5-c]quinolin-1-yl)ethoxy)ethoxy)ethyl)carbamate, ^{1}H NMR (300 MHz, $CDCl_3$) δ 7.90 (d, *J* = 8.1 Hz, 1H), 7.81 (d, *J* = 8.3 Hz, 1H), 7.48 (t, *J* = 7.7 Hz, 1H), 7.29 (t, *J* = 6.3 Hz, 1H), 5.51 (s, 2H), 5.02 (s, 1H), 4.66 (t, *J* = 5.6 Hz, 2H), 3.94 (t, *J* = 5.6 Hz, 2H), 3.45 (s, 4H), 3.38 (t, *J* = 5.0 Hz, 2H), 2.99 – 2.91 (m, 2H), 1.97 – 1.76 (m, 2H), 1.58 – 1.45 (m, 2H), 1.43 (s, 9H), 0.99 (t, *J* = 7.3 Hz, 3H), ^{13}C NMR (75 MHz, $CDCl_3$) δ 154.64, 151.33, 144.87, 133.27, 127.44, 127.02, 126.95, 122.26, 119.50, 115.61, 77.58, 77.36, 77.16, 76.74, 71.16, 70.45, 70.28, 69.68, 64.42, 45.70, 30.11, 28.55, 27.32, 25.51, 22.78, 14.01, white solid, yield 2.3 g (32% over two steps of synthesis), MS $(M+H)^+$ calcd *m/z* 472.33, found *m/z* 472.29. Compound S1.7-A3 dissolved in 5 mL of acetic acid and subsequently a spatula tip of Zn powder was added. The next day, another spatula tip of Zn powder and 5 mL of acetic acid were added. The day after 7 mL of acetic acid, 40 mL of water and 1 spatula of Zn powder. On the fourth day another spatula of Zn powder was added, followed by 4 mL acetic acid and 2 spatula of Zn powder on fifth day. Reaction was completed on fifth day, diluted with 100 mL water and underlayered with 200 mL dichloromethane. Mixture was vigorously stirred, cooled with ice and potassium hydroxide added until Zn formed a soluble complex. Product was extracted with liquid-liquid extraction (three times with dichloromethane). Organic phases were combined, washed with water and brine, dried with sodium sulphate and solvent was evaporated under vacuum to obtain 7 g of crude product. To purify substance flash chromatography was performed with a gradient of cyclohexane and isopropanol (with 0.25% triethylamine each) to obtain 2.3 g of compound S1.8-A3.

Compound A3 1-(2-(2-(2-aminoethoxy)ethoxy)ethyl)-2-butyl-1H-imidazo[4,5-c]quinolin-4-amine, ^{1}H NMR (300 MHz, $CDCl_3$) δ 7.89 (d, *J* = 8.2 Hz, 1H), 7.79 (d, *J* = 7.7 Hz, 1H), 7.50 – 7.42 (m, 1H), 7.34 – 7.20 (m, 1H), 5.87 – 5.10 (m, 2H), 4.64 (t, *J* = 5.6 Hz, 2H), 3.94 (dd, *J* = 10.2, 4.6 Hz, 2H), 3.33 (t, *J* = 5.2 Hz, 2H), 2.94 (dd, *J* = 9.9, 5.9 Hz, 2H), 2.80 – 2.68 (m, 2H), 2.14 (s, 2H), 1.85 (dt, *J* = 15.5, 7.6 Hz, 3H), 1.48 (tq, *J* = 13.9, 6.9 Hz, 4H), 0.98 (t, *J* = 7.3 Hz, 4H), ^{13}C NMR (75 MHz, $CDCl_3$) δ 154.53, 151.28, 144.76, 127.33, 126.97, 122.22, 119.52, 115.56, 73.60, 71.12, 70.35, 69.68, 64.27, 45.68, 41.78, 30.08, 27.27, 25.48, 22.76, 13.98, white solid, yield 1 g (98%), purity 97% via HPLC-ELSD, MS $(M+H)^+$ calcd *m/z* 372.24, found *m/z* 372.67. Compound S1.8-A3 (1.29 g, 2.75 mmol) was dissolved in a mixture of dichloromethane and trifluoroacetic acid (10:1, 10 mL) and stirred at RT. After 30 min reaction was completed. Solution was poured into water and neutralized with potassium hydroxide. Product was extracted with liquid-liquid extraction (three times with dichloromethane). Organic phases were combined, washed with water and brine, dried with sodium sulphate and solvent was evaporated under vacuum to obtain 1 g of A3.

Compound S1.4-A4 2-(2-(2-((2-chloro-3-nitroquinolin-4-yl)amino)ethoxy)ethoxy)ethan-1-ol, white solid, yield 2.5 g (57%), MS $(M+H)^+$ calcd *m/z* 356.10, found *m/z* 356.33. Compound S1.3 (3 g, 12.4 mmol) was dissolved in 10 mL of anhydrous dichloromethane with triethylamine (2.57 mL, 1.5 eq). To another 5 mL of anhydrous dichloromethane 2.22 g of tert-butyl (2-(2-(2-aminoethoxy)ethoxy)ethyl)carbamate (SynInnova SI-551) was added. Both solutions were combined and heated to 45 °C for 3 days. Solvents were removed under vacuum. Crude product was then purified via column chromatography on silica gel (300 g) with a gradient of cyclohexane and acetone (with 0.2% of triethylamine each) to obtain 2.5 g of S1.4-A4.

Compound S1.5-A4 2-(2-(2-((3-amino-2-chloroquinolin-4-yl)amino)ethoxy)ethoxy)ethan-1-ol, white solid, yield 2.2 g (96%), MS $(M+H)^+$ calcd *m/z* 326.13, found *m/z* 326.40. Compound S1.4-A4 (2.5 g) was dissolved in ethyl acetate in a closed vessel. Vessel was flushed with Ar (evaporated and

flushed three times three times). To solution a spatula of sodium sulphate and 500 mg of Pt/C (5% Pt, Sigma-Aldrich 205931-1G). The vessel was again flushed three times with Ar. Subsequently the vessel was flushed with H_2 (Air Liquide 130415). After five days reaction was completed, solution filtered through celite and solvent removed under vacuum to yield 2.2 g of S1.5-A4 and used without further purification.

Compound S1.6-A4 2-(2-(2-(2-butyl-4-chloro-1H-imidazo[4,5-c]quinolin-1-yl)ethoxy)ethoxy)ethyl pentanoate, brown oil, yield 2.1 g (65%), MS $(M+H)^+$ calcd *m/z* 476.23, found *m/z* 476.47. Compound S1.5-A4 (2.2 g, 6.77 mmol) was dissolved in 5 mL trimethyl orthovalerate (VWR L20377.22) and solution was heated to 135 °C. After two hours, the starting material was completely depleted. The product and a methoxy by-product (m/z = 508) were formed. Methoxy group and trimethyl orthovalerate residues were removed under vacuum (approx. 80 mbar) at 140 °C to yield 2.1 g of S1.6-A4.

Compound S1.7-A4 2-(2-(2-(2-butyl-4-hydrazineyl-1H-imidazo[4,5-c]quinolin-1-yl)ethoxy)ethoxy)ethan-1-ol, MS $(M+H)^+$ calcd *m/z* 388.23, found *m/z* 388.47. Compound S1.6-A4 (2.1 g, 4.42 mmol) was dissolved in 10 mL of ethanol, subsequently hydrazine (Sigma-Aldrich 225819-500ML, 2 mL, 63 mmol) was added. Solution was refluxed overnight. MS analysis showed full conversion. Product S1.7-A4 was directly used for next reaction step.

Compound A4 2-(2-(2-(4-amino-2-butyl-1H-imidazo[4,5-c]quinolin-1-yl)ethoxy)ethoxy)ethan-1-ol, ^{1}H NMR (300 MHz, $CDCl_3$) δ 7.83 (dd, *J* = 18.0, 8.3 Hz, 2H), 7.46 (t, *J* = 7.7 Hz, 1H), 7.26 (dd, *J* = 8.8, 6.4 Hz, 1H), 5.68 (s, 2H), 4.62 (t, *J* = 5.5 Hz, 2H), 3.91 (t, *J* = 5.5 Hz, 2H), 3.69 – 3.61 (m, 2H), 3.50 – 3.39 (m, 6H), 2.97 – 2.88 (m, 2H), 1.83 (dt, *J* = 15.6, 7.6 Hz, 2H), 1.47 (dq, *J* = 14.6, 7.3 Hz, 2H), 0.97 (t, *J* = 7.3 Hz, 3H), ^{13}C NMR (75 MHz, $CDCl_3$) δ 154.92, 151.31, 144.63, 133.24, 127.19, 127.03, 126.79, 122.25, 119.49, 115.46, 72.87, 71.25, 70.40, 69.59, 61.58, 45.70, 30.01, 27.29, 22.74, 13.98, white solid, yield 967 mg (59% over two steps of synthesis), purity >99% via HPLC-ELSD, MS $(M+H)^+$ calcd *m/z* 373.22, found *m/z* 373.53. Compound S1.7-A4 dissolved in 10 mL of acetic acid and 10 mL of water and cooled with ice. Subsequently two spatula tips of Zn powder were added. After 30 min another spatula tip of Zn powder was added. After 4 h 10 mL of acetic acid, 10 mL of water and one spatula tip of Zn were added. The next day, reaction was completed. Solution was diluted with 100 mL water and underlayered with 200 mL dichloromethane. Mixture was vigorously stirred, cooled with ice and potassium hydroxide added. Product was extracted with liquid-liquid extraction (three times with dichloromethane). Organic phases were combined, washed with water and brine, dried with sodium sulphate and solvent was evaporated under vacuum to obtain 1.67 g of crude product. To purify substance flash chromatography was performed (Interchim puriFlash 5.020 with Interchim PF-15SIHP-F0040 column) with a gradient of cyclohexane, dichloromethane and ethanol to obtain 967 mg of compound A4.

Compound P1 (2R,3S,4R,5R,8R,10R,11R,12S,13S,14R)-2-ethyl-3,4,10-trihydroxy-13-(((2R,4R,5S,6S)-5-hydroxy-4-methoxy-4,6-dimethyltetrahydro-2H-pyran-2-yl)oxy)-11-(((2S,3R,4S,6R)-3-hydroxy-6-methyl-4-(methylamino)tetrahydro-2H-pyran-2-yl)oxy)-3,5,6,8,10,12,14-heptamethyl-1-oxa-6-azacyclopentadecan-15-one, ^{1}H NMR (400 MHz, MeOD) δ 5.07 (d, *J* = 4.8 Hz, 1H), 4.92 (dd, *J* = 10.3, 2.4 Hz, 1H), 4.55 (d, *J* = 7.6 Hz, 1H), 4.26 (ddd, *J* = 15.6, 8.2, 3.9 Hz, 2H), 3.88 – 3.78 (m, 1H), 3.70 (d, *J* = 7.1 Hz, 1H), 3.59 (d, *J* = 4.1 Hz, 1H), 3.40 (s, 3H), 3.34 (dt, *J* = 3.3, 1.6 Hz, 1H), 3.14 – 3.04 (m, 2H), 2.89 – 2.77 (m, 2H), 2.60 (ddd, *J* = 10.1, 9.4, 3.4 Hz, 2H), 2.45 (d, *J* = 10.5 Hz, 1H), 2.41 (s, 3H), 2.34 (s, 3H), 2.19 (t, *J* = 11.7 Hz, 1H), 2.09 – 1.96 (m, 3H), 1.94 – 1.84 (m, 1H), 1.80 (d, *J* = 14.7 Hz, 1H), 1.63 (dd, *J* = 15.1, 5.0 Hz, 1H), 1.57 – 1.46 (m, 1H), 1.45 – 1.37 (m, 1H), 1.36 (s, 2H), 1.33 (d, *J* = 6.2 Hz, 3H), 1.29 (s, 3H), 1.25 (d, *J* =

7.5 Hz, 3H), 1.21 (d, J = 6.0 Hz, 3H), 1.15 – 1.06 (m, 9H), 0.93 (dd, J = 13.0, 7.1 Hz, 5H), ^{13}C NMR (101 MHz, MeOD) δ 180.08, 103.24, 96.28, 84.24, 79.48, 79.45, 78.15, 76.00, 75.57, 75.48, 75.12, 74.36, 70.88, 68.76, 66.49, 63.61, 61.28, 50.04, 46.82, 43.61, 43.39, 38.03, 36.80, 35.91, 33.18, 28.14, 27.76, 22.33, 22.18, 21.92, 21.68, 19.04, 17.36, 15.46, 11.49, 9.78, 7.65, colorless solid crystals, yield 10 g (51%), MS $(M+H)^+$ calcd m/z 735.50, found m/z 735.80. P1 was described earlier in WO 03/070173 A2 (Burnet et al.). Briefly, Azithromycin (Atomaxchemicals AM83905015, 20 g, 26.7 mmol) and sodium hydrogen carbonate (6 g, 71.5 mmol) were dissolved in 120 mL of Methanol in a 500 mL Erlenmeyer flask. Potassium carbonate (12 g, 87 mmol) was dissolved in 80 mL of water. The potassium carbonate solution and the iodine (6.3 g, 24.8 mmol) were added, and the mixture was stirred vigorously at RT, until the dark color has disappeared. A second batch of iodine (6.3 g, 24.8 mmol) and solid potassium carbonate (4.2 g, 30.4 mmol) were added. This procedure was repeated once, until MS shows full conversion ($[M+H]^+$ = 735). Sodium bisulfite (Fisher 10474511, 1 g, 10 mmol) was added to remove excess oxidants, and all volatiles were evaporated. The solid residue is finely ground and extensively extracted by Soxhlet extraction with acetonitrile. The extract is concentrated to approx. 75ml and left standing at RT at least for 1 day, following another day in the fridge. All solids were collected and recrystallized from methanol with addition of ca. 1-2 mL of water. Crystallization proceeded for about 3 days in an open vessel to yield 10 g (51%) of large crystals and used without further purification.

Compound P2 N-(2-(((2S,3R,4S,6R)-2-(((2R,3S,4R,5R,8R,10R,11R,12S,13S,14R)-2-ethyl-3,4,10-trihydroxy-13-(((2R,4R,5S,6S)-5-hydroxy-4-methoxy-4,6-dimethyltetrahydro-2H-pyran-2-yl)oxy)-3,5,6,8,10,12,14-heptamethyl-15-oxo-1-oxa-6-azacyclopentadecan-11-yl)oxy)-3-hydroxy-6-methyltetrahydro-2H-pyran-4-yl)(methyl)amino)-2-oxoethyl)-N-methylglycine, ^{1}H NMR (400 MHz, DMSO) δ 4.85 (s, 1H), 4.76 (d, J = 8.1 Hz, 1H), 4.45 (d, J = 6.9 Hz, 1H), 4.38 (s, 1H), 4.14 (s, 1H), 4.11 – 4.00 (m, 1H), 3.75 (d, J = 14.4 Hz, 1H), 3.63 (d, J = 14.7 Hz, 1H), 3.49 (dd, J = 16.0, 10.9 Hz, 3H), 3.38 (dd, J = 14.0, 7.0 Hz, 1H), 3.31 – 3.21 (m, 5H), 3.22 – 3.07 (m, 1H), 2.98 – 2.88 (m, 1H), 2.85 (s, 1H), 2.75 (dd, J = 20.7, 13.9 Hz, 1H), 2.70 (s, 2H), 2.61 (s, 1H), 2.50 (s, 1H), 2.43 (d, J = 13.6 Hz, 3H), 2.26 (s, 4H), 1.90 (s, 2H), 1.78 (dd, J = 11.6, 7.4 Hz, 1H), 1.67 (d, J = 8.3 Hz, 1H), 1.51 (dd, J = 22.3, 11.9 Hz, 2H), 1.36 (d, J = 8.0 Hz, 3H), 1.16 (dd, J = 18.5, 10.9 Hz, 9H), 1.09 (dd, J = 6.1, 3.9 Hz, 7H), 1.01 (d, J = 7.2 Hz, 3H), 1.00 – 0.91 (m, 5H), 0.86 (d, J = 6.1 Hz, 3H), 0.79 (t, J = 7.3 Hz, 3H). ^{13}C NMR (101 MHz, DMSO) δ 177.03, 102.14, 94.46, 77.35, 76.27, 73.63, 72.78, 72.69, 69.65, 66.57, 64.83, 64.74, 58.22, 58.07, 48.92, 48.75, 44.78, 44.63, 42.00, 41.88, 41.66, 41.58, 40.14, 39.94, 39.73, 39.52, 39.31, 39.10, 38.90, 35.76, 34.56, 27.07, 26.40, 25.93, 22.01, 21.07, 20.98, 20.94, 18.43, 18.33, 17.63, 15.07, 14.74, 14.65, 10.88, 9.03, 6.83, colorless solid, yield 1.89 g (80%), MS $(M+H)^+$ calcd m/z 864.54, found m/z 864.73. Compound P1 (2.00 g, 2.72 mmol) and 4-Methylmorpholine-2,6-dione (Sigma-Aldrich 734217-1G, 369 mg, 2.86 mmol) were solved in DMF (25 mL). Reaction showed full conversion via MS and TLC (acetone with 7% triethylamine) after 15 min. Polystyrene-NH_2 (Iris Biotech SR-1132, 78 mg) was added to remove the excess of 4-Methylmorpholine-2,6-dione and stirred for 30 min. Polystyrene was then filtered off, solvents removed under vacuum to yield 1.89 g of P2 and used without further purification.

Compound A1-Mac 2-((2-(4-(2-(4-amino-2-butyl-1H-imidazo[4,5-c]quinolin-1-yl)ethyl)piperidin-1-yl)-2-oxoethyl)(methyl)amino)-N-((2S,3R,4S,6R)-2-(((2R,3S,4R,5R,8R,10R,11R,12S,13S,14R)-2-ethyl-3,4,10-trihydroxy-13-(((2R,4R,5S,6S)-5-hydroxy-4-methoxy-4,6-dimethyltetrahydro-2H-pyran-2-yl)oxy)-3,5,6,8,10,12,14-heptamethyl-15-oxo-1-oxa-6-azacyclopentadecan-11-yl)oxy)-3-hydroxy-6-methyltetrahydro-2H-pyran-4-yl)-N-methylacetamide, ^{1}H NMR (400 MHz, $CDCl_3$) δ 7.82 (t, J = 7.6 Hz, 2H), 7.48 (t, J = 7.7 Hz, 1H), 7.30 (t, J = 7.5 Hz, 1H), 5.84 (s, 1H), 5.29 – 5.00 (m, 2H), 4.74 – 4.55 (m, 3H), 4.48 (t, J = 7.7 Hz, 1H), 4.43 – 4.32 (m, 2H), 4.19 (t, J = 6.4 Hz, 1H), 4.14 – 3.97 (m, 2H), 3.64 (dd, J = 18.2, 12.6 Hz, 4H), 3.55 (dd, J = 14.6, 7.2 Hz, 1H), 3.44 – 3.36 (m,

3H), 3.36 – 3.32 (m, 4H), 3.32 – 3.23 (m, 3H), 3.11 – 2.99 (m, 3H), 2.94 (d, *J* = 3.6 Hz, 2H), 2.86 – 2.80 (m, 3H), 2.67 (d, *J* = 7.1 Hz, 2H), 2.53 (d, *J* = 9.9 Hz, 1H), 2.42 (t, *J* = 7.9 Hz, 3H), 2.30 (s, 4H), 2.04 – 1.94 (m, 3H), 1.83 (dt, *J* = 17.8, 8.2 Hz, 7H), 1.69 (d, *J* = 14.4 Hz, 2H), 1.52 – 1.37 (m, 5H), 1.33 (s, 2H), 1.31 (d, *J* = 4.2 Hz, 5H), 1.24 – 1.19 (m, 7H), 1.16 (ddd, *J* = 11.9, 6.9, 3.6 Hz, 6H), 1.07 (d, *J* = 6.1 Hz, 6H), 1.02 – 0.94 (m, 7H), 0.89 (d, *J* = 6.6 Hz, 3H), 0.85 (d, *J* = 7.5 Hz, 3H), ^{13}C NMR (101 MHz, $CDCl_3$) δ 178.65, 171.03, 168.62, 153.41, 151.13, 133.38, 127.30, 126.74, 122.60, 119.34, 115.19, 78.23, 77.71, 77.48, 77.16, 76.84, 74.42, 73.81, 73.69, 73.25, 71.54, 71.27, 70.17, 68.47, 65.93, 65.84, 62.55, 54.42, 53.21, 49.62, 49.55, 45.32, 43.60, 43.36, 42.55, 41.99, 36.97, 36.81, 36.44, 35.82, 34.99, 34.37, 31.90, 30.16, 29.25, 27.47, 27.21, 27.10, 26.86, 22.71, 22.07, 21.74, 21.35, 21.14, 21.08, 18.47, 18.33, 16.37, 15.03, 13.96, 11.29, 9.58, 8.19, 7.53, white solid, yield 162 mg (35%), purity 96.1% via HPLC-ELSD, MS $(M+H)^+$ calcd *m/z* 1197.77, found *m/z* 1197.67, HRMS $(M+H)^+$ calcd *m/z* 1197.77448, found *m/z* 1197.77511, $(M+Na)^+$ calcd *m/z* 1219.75642, found *m/z* 1219.75708. Starting from A1 (135 mg, 0.385 mmol) the coupling with P2 (350 mg, 1.05 eq) using (1-[Bis(dimethylamino)methylene]-1H-1,2,3-triazolo[4,5-b]pyridinium 3-oxide hexafluorophosphate (HATU, Fluorochem 50215, 161 mg, 1.1 eq) and triethylamine (80 µL, 1.5 eq) was carried out in dichloromethane. Reaction was complete after 3 h (reaction progress checked via MS). Solvents were evaporated and crude product was purified via flash chromatography with a gradient of cyclohexane, isopropanol and dichloromethane to yield 162 mg of A1-Mac.

Compound A2-Mac 2-((2-(4-(2-(4-amino-2-butyl-1H-imidazo[4,5-c]quinolin-1-yl)ethyl)piperidin-1-yl)-2-oxoethyl)(methyl)amino)-N-((2S,3R,4S,6R)-2-(((2R,3S,4R,5R,8R,10R,11R,12S,13S,14R)-2-ethyl-3,4,10-trihydroxy-13-(((2R,4R,5S,6S)-5-hydroxy-4-methoxy-4,6-dimethyltetrahydro-2H-pyran-2-yl)oxy)-3,5,6,8,10,12,14-heptamethyl-15-oxo-1-oxa-6-azacyclopentadecan-11-yl)oxy)-3-hydroxy-6-methyltetrahydro-2H-pyran-4-yl)-N-methylacetamide, ^{1}H NMR (400 MHz, $CDCl_3$) δ 7.82 (t, *J* = 6.2 Hz, 2H), 7.50 (t, *J* = 7.6 Hz, 1H), 7.31 (t, *J* = 7.6 Hz, 1H), 5.86 (s, 1H), 5.10 (s, 2H), 4.73 – 4.66 (m, 1H), 4.63 (d, *J* = 10.8 Hz, 2H), 4.51 – 4.42 (m, 1H), 4.29 (s, 2H), 4.20 (s, 1H), 4.06 (s, 2H), 3.66 (d, *J* = 18.9 Hz, 4H), 3.56 (dd, *J* = 14.6, 7.3 Hz, 2H), 3.37 – 3.30 (m, 7H), 3.03 (d, *J* = 6.9 Hz, 2H), 2.92 (s, 2H), 2.88 – 2.81 (m, 4H), 2.75 – 2.62 (m, 3H), 2.53 (d, *J* = 9.7 Hz, 2H), 2.44 – 2.37 (m, 4H), 2.31 (s, 4H), 1.85 (dt, *J* = 15.6, 7.7 Hz, 3H), 1.74 – 1.66 (m, 2H), 1.46 (dt, *J* = 20.3, 7.3 Hz, 6H), 1.32 (d, *J* = 7.8 Hz, 9H), 1.25 – 1.19 (m, 10H), 1.07 (s, 5H), 0.98 (t, *J* = 7.5 Hz, 7H), 0.90 (d, *J* = 5.6 Hz, 4H), 0.86 (t, *J* = 7.4 Hz, 6H), ^{13}C NMR (101 MHz, $CDCl_3$) δ 178.64, 171.01, 170.49, 168.66, 154.06, 151.34, 133.39, 127.23, 127.06, 122.49, 119.46, 115.45, 78.21, 77.73, 77.48, 77.16, 76.84, 74.42, 73.80, 73.69, 73.27, 71.57, 70.23, 68.52, 65.96, 65.82, 62.54, 59.35, 54.42, 53.19, 50.80, 49.54, 45.31, 43.34, 42.56, 41.69, 37.40, 36.46, 35.81, 34.97, 30.15, 29.79, 29.75, 29.45, 29.24, 27.61, 27.46, 27.09, 26.87, 22.70, 22.08, 21.73, 21.33, 21.09, 18.47, 18.33, 16.36, 15.06, 13.98, 11.30, 9.59, 8.20, 7.52, white solid, yield 143 mg (32%), purity >99% via HPLC-ELSD, MS $(M+H)^+$ calcd *m/z* 1183.76, found *m/z* 1184.07, HRMS $(M+H)^+$ calcd *m/z* 1183.75883, found *m/z* 1183.75812, $(M+Na)^+$ calcd *m/z* 1205.74077, found *m/z* 1205.74005. Starting from A2 (127 mg, 0.377 mmol) the coupling with P2 (376 mg, 1.1 eq) using HATU (Fluorochem 50215, 158 mg, 1.1 eq) and triethylamine (78 µL, 1.5 eq) was carried out in dichloromethane. Reaction was complete after 5 h (reaction progress checked via MS). Solvents were evaporated and crude product was purified via flash with a gradient of cyclohexane, isopropanol and dichloromethane to yield 143 mg of A2-Mac.

2. HPLC-MS/MS

Table S1. Specific detection parameters of substances in HPLC-MS/MS. A1-mac and A2-mac were analyzed as their double charged ion $(M+2H)^{2+}$. Terbuthylazine was used as internal standard for calibration of HPLC-MS/MS.

Substance	Q1 mass	Q3 mass	DP (V)	CE (V)	CXP (V)
RSQ	315	197	106	43	36
IMQ	241	185	96	33	36
A1	352	241	56	35	14
A1-mac	600	521	91	31	34
A2-mac	592	421	116	49	26
Terbuthylazine	230	174	61	23	10

FIGURE S1 | Reagents and conditions: (1) HNO_3, (2) $PhP(=O)Cl_2$, (3) H_2N-R', 45°C, (4) H_2/Pd or Na_2S2O_4, (5) $C_4H_9C(OCH_3)_3$, Δ, (6) N_2H_4/H_2O, Δ, (7) Zn/TFA/EtOH, (7a) DCM/TFA; deprotection of Boc group, if present. R can be 2-(4-piperidinyl)ethyl (for compound A1) and (4-piperidinyl)methyl (for compound A2), 2-[2-(2-aminoethoxy)ethoxy]ethyl (for compound A3). For compound A4 R' is 2-[2-(2-hydroxyethoxy)ethoxy]ethyl (in steps S14 to S.7 as pentanoate).

FIGURE S2 | Reagents and conditions: (1) Iodine, K_2CO_3, (2) 4-Methylmorpholine-2,6-dione, (3) HATU, triethylamine; R''' can be A1 or A2.

FIGURE S3 | Dose response of compounds in HEK Blue hTLR7. Circles represent normalized replicate measurements pooled from 3 experiments. Lines represent non-linear functions fit to the data to calculate compound-specific EC50, values in grey have been excluded before fitting.

FIGURE S4 | Dose response of compounds in HEK Blue hTLR8. Circles represent normalized replicate measurements pooled from 3 experiments. Lines represent non-linear functions fit to the data to calculate compound-specific EC50, values in grey have been excluded before fitting.

FIGURE S5 | A Relationship between serum concentration, signal to noise ratio and compound toxicity at high doses in the HEK Blue hTLR7/8 reporter assay **B** Variance in maximal cytokine secretion between donors in the full blood stimulation assay. Each point represents the maximal concentration of a given cytokine observed for a donor (for TNFα (right axis) generally samples treated with 10 µM RSQ, for IFNα (left axis) samples treated with either 10 µM RSQ or A1-mac), n=8

379 **FIGURE S6 |** Cytokine profile in peripheral blood over time after 3, 6 and 12 µmol/kg s.c.
380 compound administration in 8-week-old, female C57BL/6 mice (n=3 mice per group). IFNβ, IFNγ,
381 IL6, IL10 levels in tail plasma over time were determined via cytometric bead array. At each
382 sampling timepoint the plasma of mice in one treatment group **(A)** RSQ **(B)** A1 **(C)** A1-mac was
383 pooled.

384 **FIGURE S7 |** Compound concentration after repeated applications of A1, A1-mac compared to RSQ
385 and IMQ. Samples were collected 4 h, 28 h and 52 h after s.c. treatment. Skin samples were sampled
386 at time points 4 h and 52 h. Compound concentrations were analyzed by HPLC-MS/MS, data
387 presented as mean ± SD

388

Reaction Scheme I

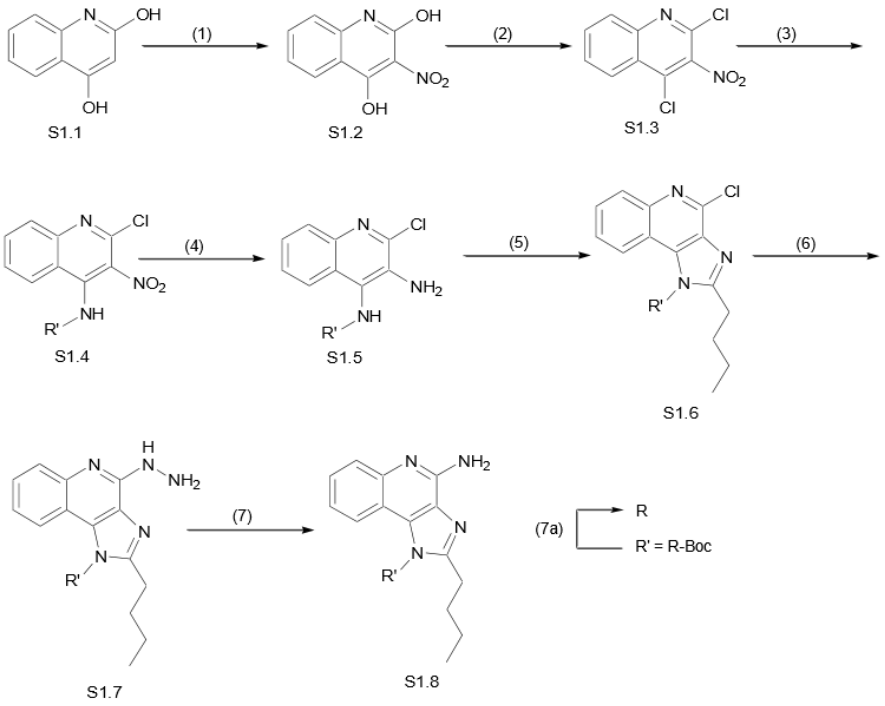

FIGURE S1 | Reagents and conditions: (1) HNO3, (2) PhP(=O)Cl2, (3) H2N-R', 45°C, (4) H2/Pd or Na2S2O4, (5) C4H9C(OCH3)3, D, (6) N2H4/H2O, D, (7) Zn/TFA/EtOH, (7a) deprotection of Boc group, if present. R can be 2-(4-piperidinyl)ethyl (for compound A1) and (4-piperidinyl)methyl (for compound A2), 2-[2-(2-aminoethoxy)ethoxy]ethyl (for compound A3). For compound A4 R' is 2-[2-(2-hydroxyethoxy)ethoxy]ethyl (in steps S14 to S.7 as pentanoate).

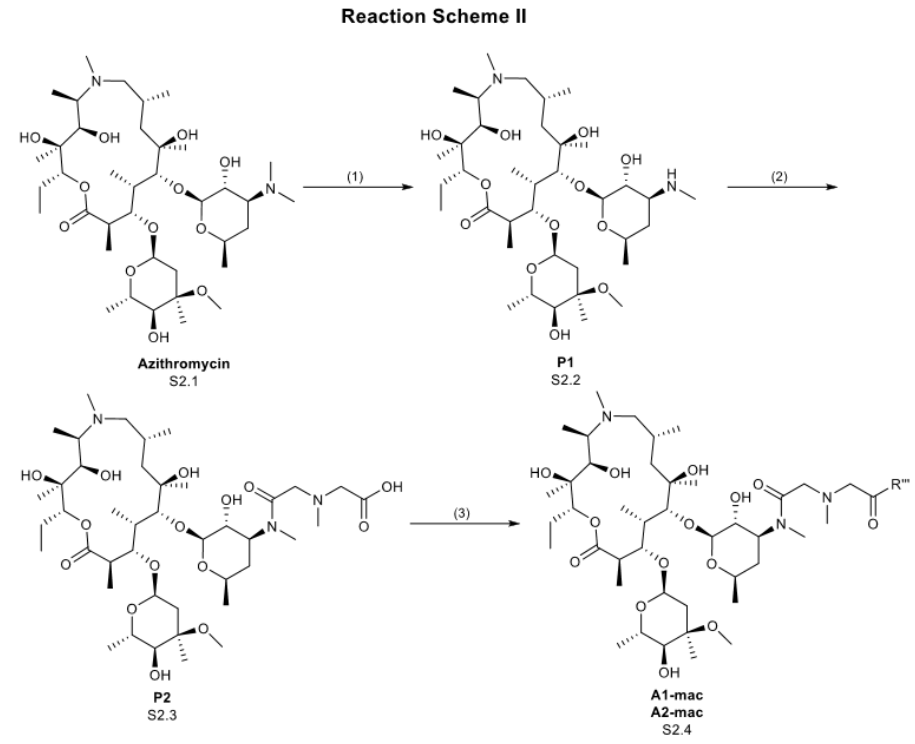

FIGURE S2 | Reagents and conditions: (1) Iodine, (2) 4-Methylmorpholine-2,6-dione, (3) R''' can be A1 or A2.

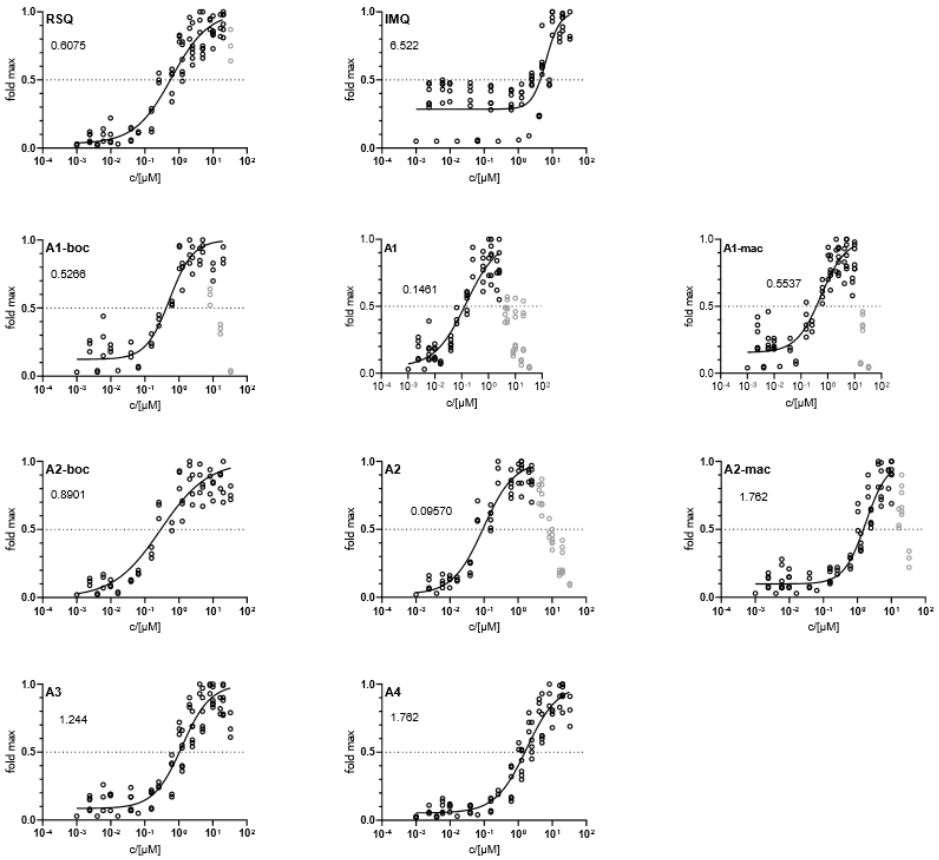

FIGURE S3 | dose response of compounds in HEK Blue hTLR7. Circles represent normalized replicate measurements pooled from 3 experiments. Lines represent non-linear functions fit to the data to calculate compound-specific EC50, values in grey have been excluded before fitting.

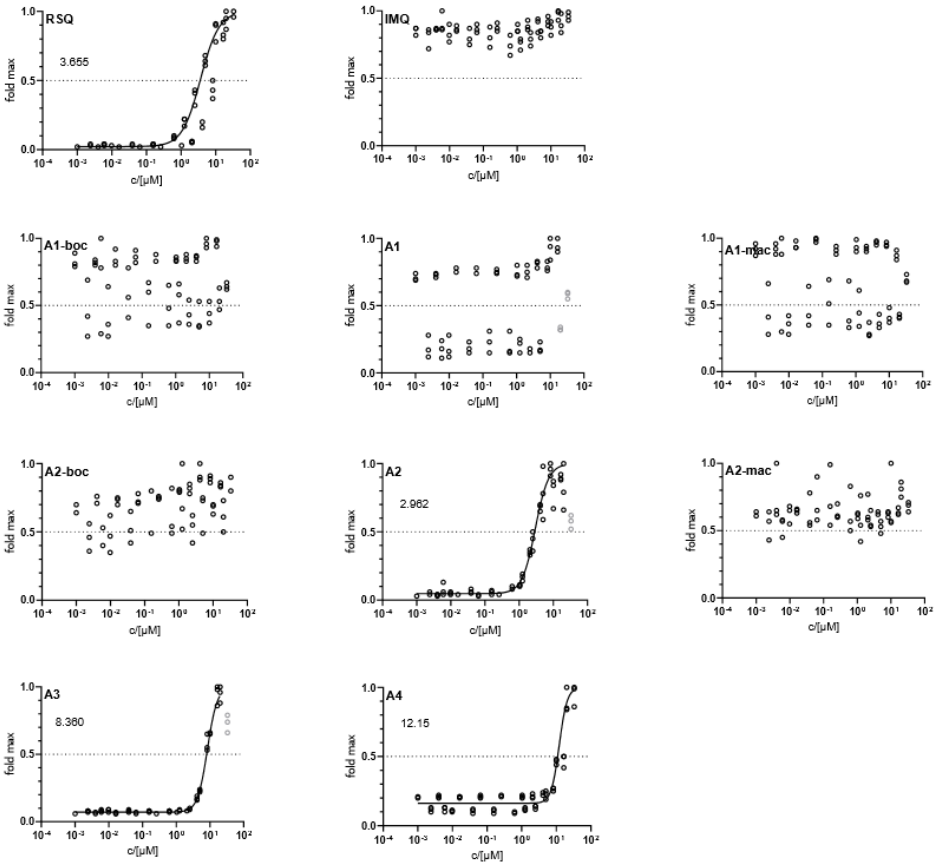

FIGURE S4 | dose response of compounds in HEK Blue hTLR8. Circles represent normalized replicate measurements pooled from 3 experiments. Lines represent non-linear functions fit to the data to calculate compound-specific EC50, values in grey have been excluded before fitting.

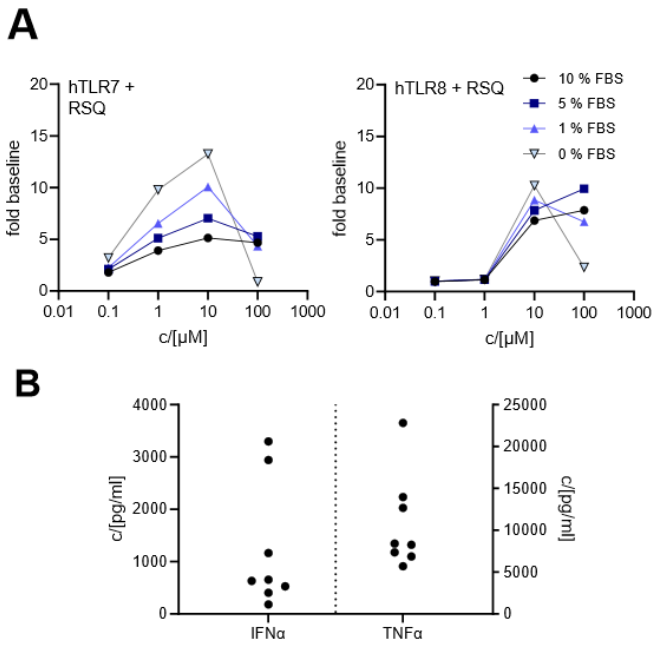

FIGURE S5 | A Relationship between serum concentration, signal to noise ratio and compound toxicity at high doses in the HEK Blue hTLR7/8 reporter assay **B** Variance in maximal cytokine secretion between donors in the full blood stimulation assay. Each point represents the maximal concentration of a given cytokine observed for a donor (for TNFα generally samples treated with 10 µM RSQ, for IFNα samples treated with either 10 µM RSQ or A1-mac), n=8

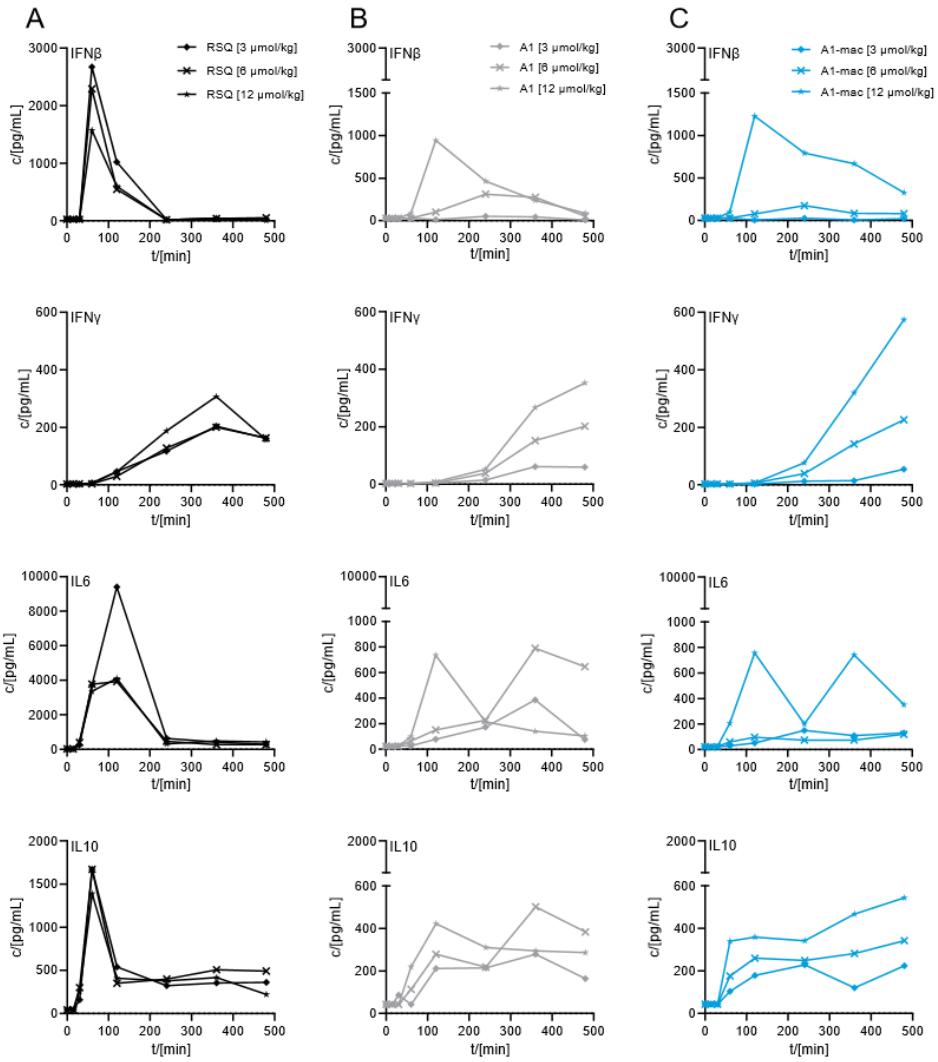

FIGURE S6 | Cytokine profile in peripheral blood over time after 3, 6 and 12 µmol/kg s.c. compound administration in 8 old, female C57BL/6 mice (n=3 mice per group). IFNβ, IFNγ, IL6, IL10 levels in tail plasma over time were determined via cytometric bead array. At each sampling timepoint the plasma of mice in one treatment group **(A)** RSQ **(B)** A1 **(C)** A1-mac was pooled.

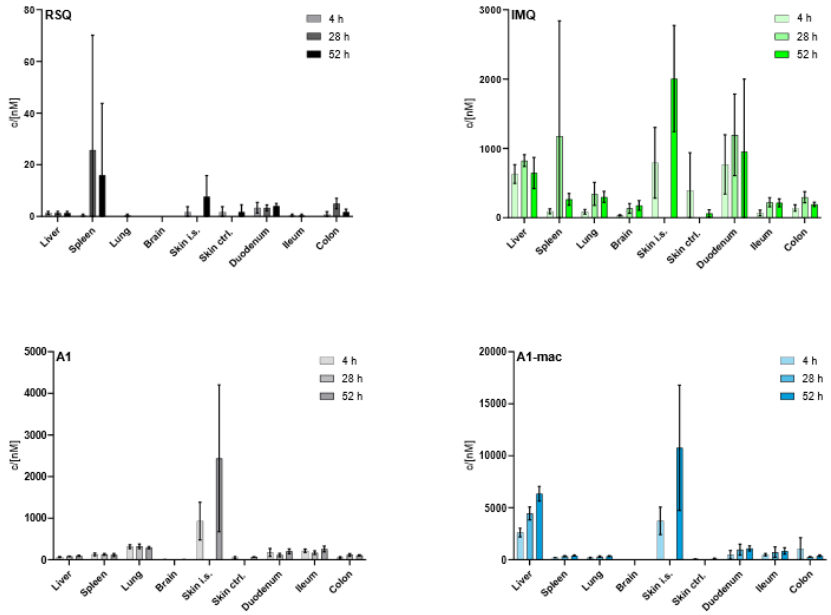

FIGURE S7 | compound concentration after repeated applications of A1, A1-mac compared to RSQ and IMQ. Samples were collected 4 h, 28 h and 52 h after s.c. treatment. Skin samples were only sampled at time points 4 h and 52 h. Compound concentrations were analyzed by HPLC-MS/MS, data presented as mean ± SD

Table S1 | Specific detection parameters of substances in HPLC-MS/MS. A1-mac and A2-mac were analysed as their double charged ion (M+2H)2+. Terbuthylazine was used as internal standard for calibration of HPLC-MS/MS.

Substance	Q1 mass	Q3 mass	DP (V)	CE (V)	CXP (V)
RSQ	315	197	106	43	36
IMQ	241	185	96	33	36
A1	352	241	56	35	14
A1-mac	600	521	91	31	34
A2-mac	592	421	116	49	26
Terbuthylazine	230	174	61	23	10